Multivariable Control of Fixed Wing Aircrafts

by

Kaustav Mondal

A Thesis Presented in Partial Fulfillment
of the Requirements for the Degree
Master of Science

Approved April 2015 by the
Graduate Supervisory Committee:

Armando Rodriguez, Chair
Konstantinos S. Tsakalis
Jennie Si

ARIZONA STATE UNIVERSITY

May 2015

ABSTRACT

This thesis addresses control design for fixed-wing air-breathing aircraft. Four aircraft with distinct dynamical properties are considered: a scram-jet powered hypersonic (100foot long, X-43 like, wedge shaped) aircraft with flexible modes operating near Mach 8, 85k ft, a NASA HiMAT (Highly Maneuverable Aircraft Technology) F-18 aircraft, a McDonnell Douglas AV-8A Harrier aircraft, and a Vought F-8 Crusader aircraft. A two-input two-output (TITO) longitudinal LTI (linear time invariant) dynamical model is used for each aircraft. Control design trade studies are conducted for each of the aircraft. Emphasis is placed on the hypersonic vehicle because of its complex nonlinear (unstable, non-minimum phase, flexible) dynamics and uncertainty associated with hypersonic flight (Mach > 5, shocks and high temperatures on leading edges). Two plume models are used for the hypersonic vehicle an old plume model and a new plume model. The old plume model is simple and assumes a typical decaying pressure distribution for aft nozzle. The new plume model uses Newtonian impact theory and a nonlinear solver to compute the aft nozzle pressure distribution. Multivariable controllers were generated using standard weighted H_{inf} mixed-sensitivity optimization as well as a new input disturbance weighted mixed-sensitivity framework that attempts to achieve good multivariable properties at both the controls (plant inputs) as well as the errors (plant outputs). Classical inner-outer (PD-PI) structures (partially centralized and decentralized) were also used. It is shown that while these classical (sometimes partially centralized PD-PI) structures could be used to generate comparable results to the multivariable controllers (e.g. for the hypersonic vehicle, Harrier, F-8), considerable tuning (iterative optimization) is often essential. This is especially true for the highly coupled hypersonic vehicle thus justifying the need for a good multivariable control design tool. Fundamental control design tradeoffs for each aircraft are presented comprehensively for the hypersonic aircraft. In short, the thesis attempts to shed light on when complex controllers are essential and when simple structures are sufficient for achieving control designs with good multivariable loop properties at both the errors (plant outputs) and the controls (plant inputs).

DEDICATION

Dedicated to my mother, sister and the loving memory of my father.

ACKNOWLEDGEMENTS

Foremost, I would like to express my sincere gratitude to my thesis adviser Dr. Armando Rodriguez for showing confidence in my work, for his patience,motivation, enthusiasm and immense knowledge.

Besides my thesis adviser, I would like to thank the rest of my thesis committee: Dr.Kostas Tsakalis and Dr.Jennie Si.

I would also like to acknowledge the support of my fellow research mates Justin Echols, Karan Puttaniah and Aniket Shirsat for their tremendous support and for the stimulating discussions we had about my research which kept me motivated to complete my Masters thesis.

Last but not the least, I would like to thank my family: my mother Keya Mondal, my sister Kritika Mondal and my father late Kallol Mondal for their love and support.

TABLE OF CONTENTS

CHAPTER Page

CHAPTER Page

CHAPTER Page

LIST OF TABLES

Table Page

LIST OF FIGURES

Figure Page

Figure Page

Figure Page

Figure Page

Figure Page

Figure Page

Figure Page

Figure Page

Figure Page

Figure Page

Chapter 1

INTRODUCTION AND OVERVIEW

1.1 Fundamental Questions Being Addressed

This thesis attempts to shed light on several fundamental questions for fixed-wing aircraft. These fundamental questions are as follows:

1. When is a decentralized (single-input single-output diagonal) controller possible?
2. When is a centralized (multivariable) controller essential?
3. How can hierarchical (inner-outer loop) control be exploited in each of the above?
4. How can a control system designer systematically obtain good feedback control properties at distinct breaking points such as the plant output (or error signal) and input?
5. What are some of the fundamental tradeoffs observed as bandwidth is varied?

Within this thesis, some insights/answers are provided to each of these questions. Future work will seek more precise answers to the fundamental questions being addressed.

Four aircraft are used to focus all developments within the thesis. These aircraft are as follows:

1. Hypersonic (100 foot long, X-43 like, wedge shaped) vehicle operating near Mach 8, 85k ft
2. NASA HiMAT (Highly Maneuverable Aircraft Technology) F-18 Aircraft
3. McDonnell Douglas Av-8A Harrier Aircraft
4. Vought F-8 Crusader Aircraft

A longitudinal two-input two-output (TITO) dynamical LTI (linear time invariant) model is used for each aircraft to conduct all studies.

1.2 Literature Survey

Each of the following topics are relevant to the work in this thesis.

Modeling and Control of Aircraft. The following references address modeling and control of aircraft: Echols *et al.* (2015), Dickeson *et al.* (2009).

1. Within Echols *et al.* (2015), the authors discuss a non-standard input-disturbance weighted H_∞ mixed sensitivity control framework. It is applied the hypersonic vehicle addressed within this thesis. The authors specifically design multivariable controllers which offer good properties at both loop breaking points (errors, controls). The design of hierarchical (inner-outer) PI-PD decentralized controllers is also discussed within the paper.

2. Within Dickeson *et al.* (2009), the author addresses designing hierarchical (inner-outer loop) decentralized PI-PD controllers for the hypersonic aircraft considered within this thesis. Trade studies are performed to study the effect of varying the bandwidth at different loop breaking points.

Decentralized and Classical Single-Input Single-Output (SISO) Theory. The following references address classical control theory Ogata (1998), Franklin *et al.* (2006).

The following references address the feasibility/applicability of decentralized control Gahinet and Apkarian (2011a),Messner *et al.* (2007)

1. Within Gahinet and Apkarian (2011a), a MATLAB-based tool named HINFSTRUCT is presented for designing (optimizing) structured controller architectures (PI, PD, PI-PD, PID) with multiple feedback loops. HINFSTRUCT uses specialized nonsmooth optimization technique for solving structured H_∞ synthesis problems.

2. Within Messner *et al.* (2007), the authors discuss the design of real and complex lead-lag controllers. Complex lead-lag controllers are used to when tighter magnitude-phase tradeoffs are required. They also discuss the benefits of designing a cascaded lead-lag network over a single lead-lag network.

Multiple-Input Multiple-Output (MIMO) Control Theory. The following reference addresses MIMO control theory Skogestad and Postlethwaite (2007). Within Skogestad and Postlethwaite (2007), the authors offer a rather comprehensive discourse on multivariable control system analysis. The authors H_∞ design in some detail. The text also addresses limitations of performance (for both SISO and MIMO systems) imposed by time delays, RHP zeros, RHP poles and uncertainty.

Multi-objective Control Design. The following references address multi-objective control design :

1. Within Scherer *et al.* (1997), multi-objective synthesis for dynamic output feedback controllers is conducted via LMI optimization. The paper also addresses how design objectives like passivity, closed loop pole placement constraints and time-domain constraints can be expressed in the form of an LMI.

2. Within Puttannaiah (2013), the authors discusses a new generalized weighted mixed-sensitivity framework that can be used to directly tradeoff multivariable control properties at distinct loop breaking points (e.g. error, control). The method introduced can be used to obtain what the authors refer to as "equilibrated designs; i.e. designs with comparable properties at the error and the controls.

Fundamental Control-Theoretic Tradeoffs. The following reference addresses fundamental control-theoretic tradeoffs :

Within Freudenberg and Looze (1986), the author discusses the relation between properties at distinct loop breaking points for a multivariable plant; i.e. input (controls) and output (error). The paper points out how difficult it can be to obtain good properties at both loop breaking points for a multivariable plant possessing a high condition number.

While the above references provide a solid foundation for the work pursued in this thesis, the fundamental questions posed in Section 1.1 remain, to a large extent, unanswered. This provides motivation for the work pursued within this thesis.

1.3 Contributions and Overview of Main Results

The paramount contribution of the thesis (besides providing partial insights/answers to the fundamental questions posed in Section 1.1), is illustrating the importance of multivariable design tools for systematically achieving complex design objectives. Four aircraft - with distinct dynamical properties - are used to conduct all studies. Because the aircraft possess distinct dynamical properties, they provide a diverse set of case studies. As such, this will help shed light on the fundamental questions being asked (see Section 1.1),).

A longitudinal two-input two-output (TITO) dynamical LTI (linear time invariant) model is used for each aircraft to conduct all studies. Specific contributions of the thesis are as follows.

1. **Four Distinct Aircraft.** Four different air-breathing aircraft of varying complexity (and distinct dynamical properties) were examined throughout the thesis. The four aircraft are as

follows:

(a) Hypersonic (100 foot long, X-43 like, wedge shaped) vehicle operating near Mach 8, 85k ft,

(b) NASA HiMAT (Highly Maneuverable Aircraft Technology) F-18 Aircraft,

(c) McDonnell Douglas Av-8A Harrier Aircraft, and

(d) Vought F-8 Crusader Aircraft.

2. **New Mixed-Sensitivity Design Method for Addressing Design Specifications at the Controls.** A new non-standard weighted H_∞ mixed-sensitivity design methodology has been developed. This method weights the input disturbance as well as the traditionally used reference in an effort to obtain multivariable control designs with good properties at both loop breaking points (i.e. error and control). While the method is very useful, it is not as easy to use as one which directly weights the functions of interest (see convex optimization approach within Puttannaiah (2013)).

3. **Control Design Trade Studies.** Control design trade studies were conducted for each of the four aircraft being considered. For each aircraft, the new (input disturbance weighted) mixed-sensitivity design method was applied to obtain an inner-outer loop multivariable control system. Classical decentralized SISO theory was also applied to each aircraft. For the hypersonic aircraft, a more centralized classical inner-outer loop (centralized PD-PI) structure was also investigated. More focus was placed on the scramjet-powered hypersonic vehicle because it is a very complex vehicle (see below) and because hypersonic vehicles represent the next key to achieving NASAs longstanding low cost, reliable two-stage-to-orbit vision.

The following is an overview of the main results for each of the four targeted aircraft. A fixed sensitivity bandwidth at the error was used to compare distinct control system designs.

Hypersonic Vehicle. For this vehicle, two LTI models are examined at Mach 8, 85kft, each corresponding to a different plume model. This vehicle is characterized by an instability, a non-minimum phase zero (elevator to flight path angle), and a considerable multivariable coupling. The inputs are fuel and elevator. The outputs are speed and flight path angle. Two plume models are examined Dickeson (2012). While simple SISO control structures can be used to achieve desirable multivariable properties (comparable to that of a multivariable controller),

they are very difficult to design; i.e. they may require extensive brute force optimization. The benefit of a good multivariable design methodology is clearly demonstrated in this chapter since the design of a good hierarchical fully populated PI-PD controller is very time consuming. Hence, for this vehicle, a good multivariable control design tool is very important in order to help systematize the design process. For this vehicle, a partially centralized SISO (inner-outer PD-PI) controller was found to achieve performance comparable to that of a multivariable controller found using the new input disturbance weighted mixed-sensitivity framework. The later multivariable controller achieved a peak sensitivity of 4.97 db at the error and 7.61 db at the controls for new (Newtonian) plume model and a peak sensitivity of 4.15 db at the error and 4.56 db at the controls for the old plume model. The former partially centralized controller achieved the following comparable performance: Peak error sensitivity - 0.19 db better for new (Newtonian) plume model, 0.49 dB worse for old plume model; Peak control sensitivity - 2.02 dB better for new plume, 0.15 db better for old plume.

HiMAT F-18 Aircraft. This vehicle is characterized by an instability and multivariable coupling. The inputs are elevator and canard. The outputs are flight path angle and pitch. For this vehicle, it is difficult to obtain an equilibrated design using a multivariable controller based on non-standard H_∞ control methodology. Hence, there is a need to explore generalized weighted mixed-sensitivity control methodology (Puttannaiah (2013)) to design a multivariable controller which could offers good properties at both loop breaking points. A decentralized SISO controller achieved comparable performance to that of a multivariable controller at the error but not at controls. The multivariable controller achieved a peak sensitivity of 1.82 db at the error and 12.79 db at the controls. The decentralized SISO controller achieved the following performance at the error : Peak error sensitivity -0.26 db better. At the controls, decentralized SISO controller achieved the the following performance: -2.21 db better.

McDonnell Douglas AV-8A Harrier Aircraft. This vehicle is characterized by a non-minimum phase zero and multivariable coupling. The inputs are throttle and stick. The outputs are velocity and flight path angle. For this vehicle, SISO decentralized ideas work well but a multivariable controller was found to yield better performance. The multivariable controller achieved a peak sensitivity of 4.39 db at the error and 6.06 db at the controls. The decentralized SISO controller achieved the following performance at the error : Peak error sensitivity 2.49 db worse. At the controls, decentralized SISO controller achieved the the

following performance: 1.15 db better.

Vought F-8 Crusader Aircraft. This vehicle is stable and minimum phase. It possesses multivariable coupling. The inputs are elevon and flaperon. The outputs are flight path angle and pitch. For this vehicle, SISO decentralized ideas work really well performing comparably to the multivariable controllers examined. The multivariable controller achieved a peak sensitivity of 7.41 db at the error and 6.03 db at the controls. The decentralized SISO controller achieved the following performance at the error : Peak error sensitivity 3.5 db better. At the controls, decentralized SISO controller achieved the the following performance: 1.22 db worse.

Some general (qualitative) insights into the fundamental questions addressed are as follows:

When is a decentralized (single-input single-output diagonal) controller possible? Decentralized control can be very effective even for a coupled system. Why? While it is obvious that high gain control in each control channel can be used to reduce the sensitivity at low frequencies arbitrarily, a price is paid at higher frequencies. In general, a multivariable controller is expected to resolve multivariable tradeoffs better when the plant is very coupled and the specifications are demanding.

When is a centralized (multivariable) controller essential? When the vehicle is complex and/or the specifications are very demanding, a multivariable controller should be required.

How can hierarchical (inner-outer loop) control be exploited in each of the above? Hierarchical inner-outer loop control is the norm for aircraft. The purpose of the fast inner loop (generally speaking) is to alleviate the workload for the outer loop. More fundamentally, inner-outer architecture can be used to tradeoff properties at the error for properties at the control.

How can a control system designer systematically obtain good feedback control properties at distinct breaking points such as the plant output (or error signal) and input?While the new input disturbance weighted mixed sensitivity method helps, the convex optimization approach presented within Puttannaiah (2013) is much more powerful and direct for achieving input-output (control-error) tradeoffs.

What are some of the fundamental tradeoffs observed as bandwidth is varied? It is well known that right half plane poles place a lower limit on the bandwidth at the controls (input). Aircraft longitudinal (“pitch up) instability is generally associated with an unstable short period mode

due to the center of gravity lying aft of the center of pressure. Similarly, right half plane zeros place an upper bound on the achievable bandwidth at the error (input). Aircraft often exhibit this non-minimum phase (inverse response) characteristic in the elevator to flight path angle transfer function.

1.4 Organization of Thesis

The remainder of this thesis is organized as follows.

Chapter 2 addresses modeling and control for the hypersonic vehicle.

Chapter 3 addresses modeling and control for the HiMAT F-18 aircraft.

Chapter 4 addresses modeling and control for the McDonnell Douglas AV-8A Harrier aircraft.

Chapter 5 addresses modeling and control for the Vought F-8 Crusader aircraft.

Chapter 6 summarizes the thesis and presents directions for future research.

Appendix 1 contains system-theoretic results.

Appendix 2 contains all MATLAB code (and data) that was used to generate the results within the thesis.

1.5 Summary and Conclusions

Supported by a relevant literature survey, this chapter describes the fundamental questions to be addressed within this thesis. These questions are to be addressed (in part) for four fixed-wing aircraft:

Chapter 2

HYPERSONIC AIRCRAFT

2.1 Overview

In this chapter, we briefly discuss the longitudinal dynamics of the hypersonic aircraft. In the following sections we design a dynamic output feedback controller using Linear Matrix Inequality. We also discuss the inner outer loop control structure and how it is implemented on the rigid model of hypersonic aircraft. Finally we attempt to design a PI-PD controller which would similar closed loop properties as the dynamic output feedback controller.

The Hypersonic aircraft is 100 ft long with weight 6154 lb per foot of length and has a bending mode at about 21 rads/sec. The controls inclue : elevator, stoichiometrically normalized fuel equivalency ratio (FER), diffuser area ratio(not considered in the model) and a canard(not considered in the model). The vehicle may be visualized as shown in Figure 2.1 (Rodriguez *et al.* (2008),Soloway *et al.* (2009))

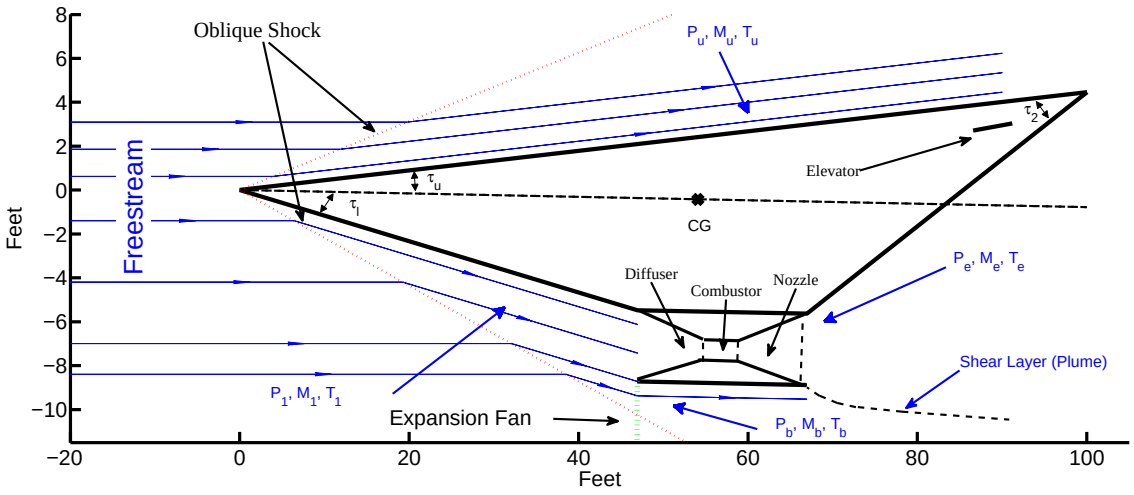

Figure 2.1: Schematic of Hypersonic Scramjet Vehicle

2.2 Longitudinal Dynamics.

The equations of motion for the 3DOF flexible vehicle are given as follows(Rodriguez *et al.* (2009),Rodriguez *et al.* (2008)):

$$\dot{v} = \left[\frac{Tcos(\alpha) - D}{m}\right] - gsin(\gamma) \tag{2.1a}$$

$$\dot{\alpha} = -\left[\frac{L + Tsin(\alpha)}{mv}\right] + q + \left[\frac{g}{v} - \frac{v}{R_E + h}\right] cos(\gamma) \tag{2.1b}$$

$$\dot{q} = \frac{\mathcal{M}}{I_{yy}} \tag{2.1c}$$

$$\dot{\theta} = q \tag{2.1d}$$

$$\ddot{n_i} = -2\zeta\omega_i\dot{\eta_i} - \omega_i^2\eta_i + N_i \; i = 1, 2, 3 \tag{2.1e}$$

$$\gamma = \theta - \alpha \tag{2.1f}$$

$$g = g_o\left[\frac{R_E}{R_E + h}\right]^2 \tag{2.1g}$$

where L denotes lift,T denotes engine thrust,D denotes drag,$\mathcal{M}$ is the pitching moment,N_i denotes generalized forces,ζ denotes flexible mode damping factor,ω_i denotes flexible mode undamped natural frequencies,m denotes the vehicle's total mass,I_{yy} is the pitch axis moment of inertia, g_o is the acceleration due to gravity at sea level and R_E is the radius of the earth.

1. **States.** The states consist of five classical rigid body states and six flexible modes states: the rigid body states are velocity v, FPA γ, altitude h, pitch rate q , pitch angle θ and the flexible body states η_1,$\dot{\eta_1}$,η_2,$\dot{\eta_2}$,η_3,$\dot{\eta_3}$. These eleven(11) states are summarized in Table 2.1.

2. **Controls.** The vehicle has 3 control inputs: a forward situated canard δ_c(not considered), a rearward situated elevator δ_e and stoichometrically normalized fuel equivalence ration(FER). These control inputs are summarized in Table 2.2. While designing control system, we would consider elevator and FER,i.e. the canard has been removed. The FER is the engine control. While FER is primarily governs the velocity, its impact on FPA is significant. Thrust is linearly related to FER for all expected FER values. For large FER values, the thrust levels off. In practice,when FER¿1, it results in decreased thrust. Since this phenomena is not captured in the model on which the linearized plant is based on, it imposes a control constraint $FER \leq 1$. Minor violations of this constraint has been allowed in this study.

Table 2.1: States for Hypersonic Vehicle Model

	Symbol	Description	Units
1	v	speed	kft/sec
2	γ	flight path angle	deg
3	α	angle-of-attack(AOA)	deg
4	q	pitch rate	deg/sec
5	h	altitude	ft
6	η_1	1_{st} flex mode	–
7	$\dot{\eta_1}$	1_{st} flex mode rate	sec^{-1}
8	η_2	2_{nd} flex mode	–
9	$\dot{\eta_2}$	2_{nd} flex mode rate	sec^{-1}
10	η_3	3_{rd} flex mode	–
11	$\dot{\eta_3}$	3_{rd} flex mode rate	sec^{-1}

Table 2.2: Controls for Hypersonic Vehicle Model

	Symbol	Description	Units
1	FER	Stoichometrically normalized fuel equivalence ratio	–
2	δ_e	Elevator deflection	deg
3	δ_c	Canard deflection	deg

We now consider the nominal plant which has been linearized at Mach 8, 85 kft. The pole-zero map for the HSV model is shown in Table 2.3

table 2.2

The poles of the linearized model are shown in Table 2.3.The short period mode consists of a stable and an unstable pole. This unstable pole is due to the long lower forebody of a typical hypersonic vehicles combined with a rearward shifted center-of-gravity(CG) which results in a pitch-up instability. Hence we need a minimum bandwidth for stabilization(Sridharan (2010),Page 94).The flexible modes are lightly damped which also limits the bandwidth(Sridharan (2010),Page 94).

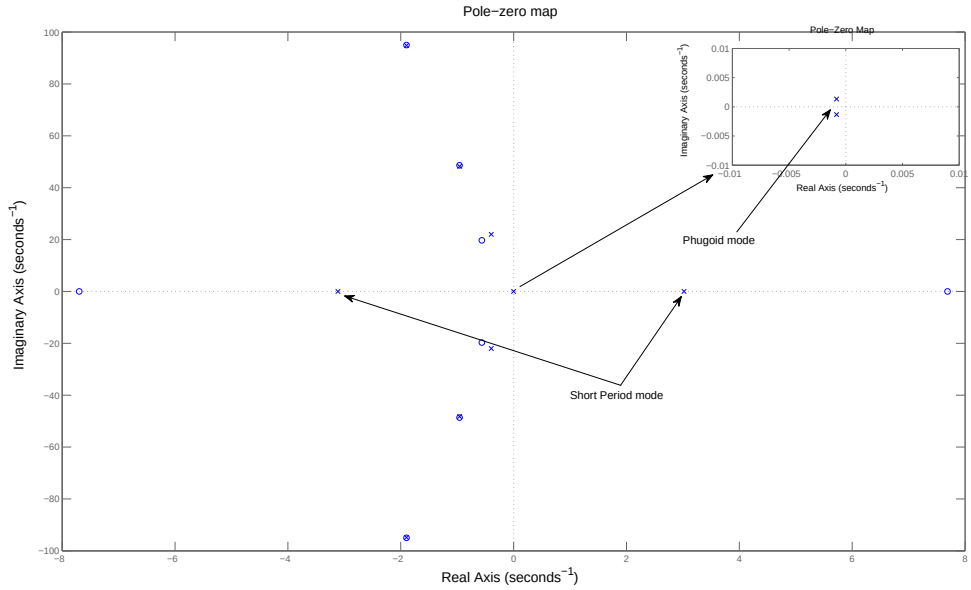

Figure 2.2: Pole-Zero Map of Hypersonic Vehicle

The zeros of the linearized model are shown in Table 2.4. We see that the plant is non-minimum phase. This is a common characteristic for tail-controlled aircrafts, unless a canard is used(Sridharan (2010),Page 94). It is well known that any canard approach would face severe structural and heating issues.

Table 2.3: Poles at Mach 8,885kft : Level Flight,Flexible Vehicle

Pole	Damping	Freq.(rad/sec)	Mode name
-8.15e-004 ± 1.34e-003i	5.20e-001	1.57e-003	Phugoid Mode
3.02e+000	-1.00e+000	3.02e+000	Unstable Short Period
-3.11e+000	1.00e+000	3.11e+000	Stable Short Period
-3.96e-001 ± 2.20e+001i	1.80e-002	2.20e+001	1_{st} Flex
-9.57e-001 ± 4.82e+001i	1.98e-002	4.83e+001	2_{nd} Flex
-1.90e+000 ± 9.48e+001i	2.00e-002	9.48e+001	3_{rd} Flex

Table 2.4: Zeros at Mach 8,885kft : Level Flight,Flexible Vehicle

Pole	Damping	Freq.(rad/sec)
7.69e+000	-1.00e+000	7.69e+000
-7.70e+000	1.00e+000	7.70e+000
-5.63e-001 ± 1.97e+001i	2.86e-002	1.97e+001
-9.58e-001 ± 4.86e+001i	1.97e-002	4.86e+001
-1.90e+000 ± 9.50e+001i	2.00e-002	9.50e+001

In the following sections we consider two different models of the hypersonic aircraft which uses two different plume models. The New Engine Old Plume(NEOP) model uses the "'Old Plume" using a simple plume calculation as described in Chavez and Schmidt (1994). The New Engine New Plume(NEOP) model uses the "'New Plume" which is an approximation of a numerical discretization as described in Chavez and Schmidt (1992) and proposed in Sridharan *et al.* (2011).

Plant Singular Values. The plant singular values is plotted in Figure 2.3.In the plot, we notice that the minimum singular values are near 0db for the New Engine New Plume model and the singular values are wide spread at low frequencies.This suggests that the resulting controller will have to compensate for low plant gain in the minimum singular value direction i.e. in the elevator channel. Hence we expect that significant elevator activity will be required to achieve a loop with low frequency disturbance attenuation(e.g. $\sigma_{min}[PK] > 20$ db at low frequencies) and desirable low frequency command following. The singular values of the New Engine Old Plume model are high at low frequencies. Therefore we should be able to attain good low frequency input disturbance attenuation and command following with ease.

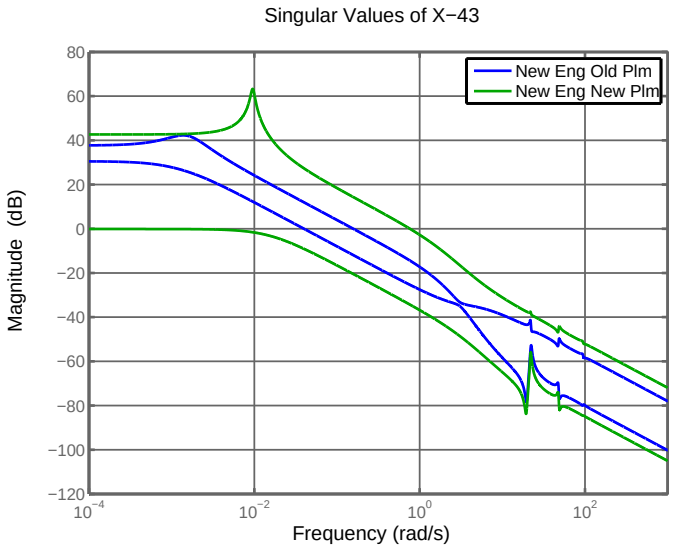

Figure 2.3: Singular Values-TITO Hypersonic Aircraft Longitudinal Dynamics

The frequency response bode plots for each of the 4 system transfer functions for both the models is given in Figure 2.4-2.7.

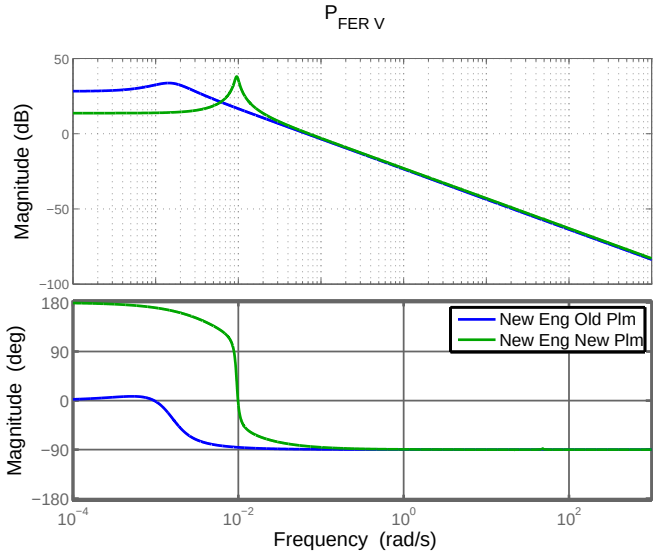

Figure 2.4: $P_{FER \rightarrow Vel}$: Hypersonic

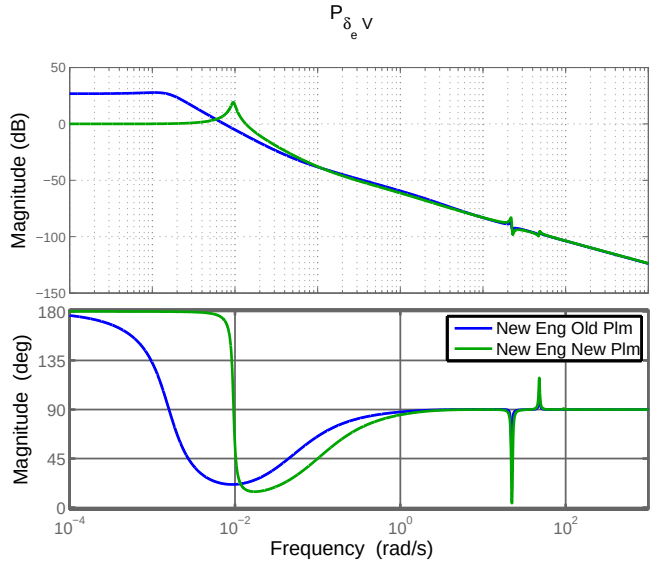

Figure 2.5: $P_{\delta_e \rightarrow Vel}$: Hypersonic

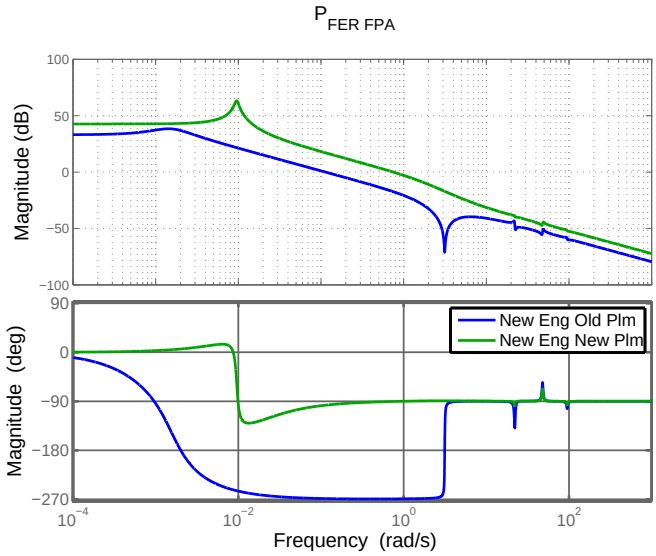

Figure 2.6: $P_{FER \to \gamma}$: Hypersonic

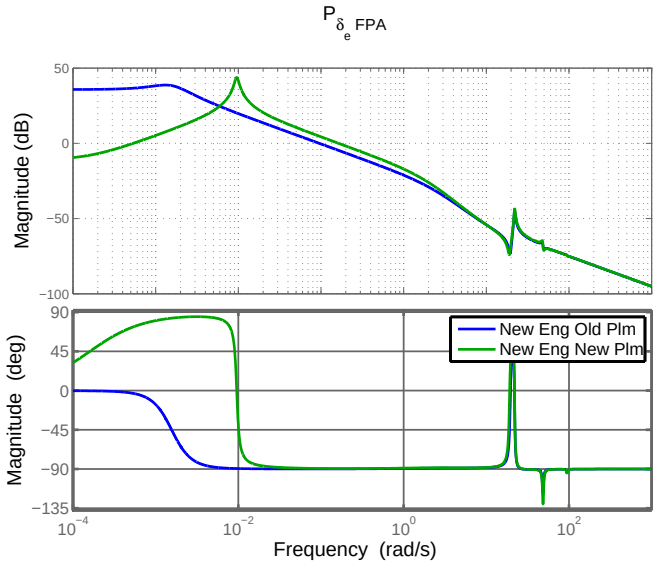

Figure 2.7: $P_{\delta_e \to \gamma}$: Hypersonic

Singular Value Decomposition. Let us analyze the singular value decomposition of both the models at DC.

From the SVD plots we can notice the following:

1. In the New Engine Old Plume model of Hypersonic aircraft, the elevator has greater impact on the FPA as compared to the Velocity and hence it should be primarily used to control the FPA. The FER is associated with the minimum singular value and it is primarily used to control Velocity.

2. In the New Engine New plume model of Hypersonic aircraft, we notice that FER has more impact on the FPA as compared to the Velocity and it is associated with the maximum singular value. Also the Elevator has more impact on the velocity as compared to the FPA. This means that the New Engine New Plume model has significant coupling.

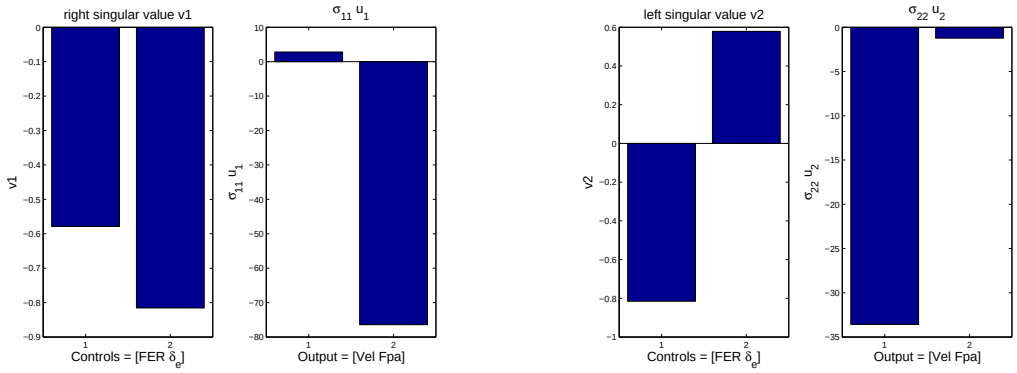

Figure 2.8: Singular Value Decomposition of New Engine Old Plume At DC

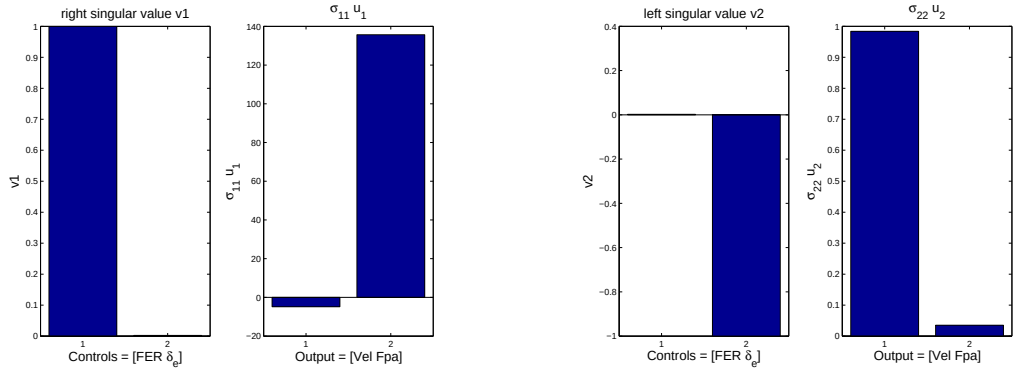

Figure 2.9: Singular Value Decomposition of New Engine New Plume At DC

Control Challenges. Some of the key control challenges associated with the linearized model are:

1. RHP pole - The long lower forebody of a hypersonic aircraft along with a rearward shifted center of gravity(CG) results in a pitch-up instability. The linearized plant is therefore unstable and this instability requires a minimum bandwidth for stability(Echols *et al.* (2015)).

2. RHP zero - The elevator to flight-path-angle(FPA) element of the plant is associated with a RHP zero which makes the plant non-minimum phase. This is a characteristic of tail-controlled vehicles.The RHP zero limits the maximum achievable bandwidth(Echols *et al.* (2015),Sridharan and Rodriguez (2012)).

3. Lightly damped flexible modes - If the flexible modes are excited , the output and the control of the aircraft are affected. Structural flexing impacts the bow shock which in turn affects the scramjet's inlet properties, aft body forces, thrust generated and the vehicle's attitude. Therefore we should be careful that the lightly damped flexible modes are not excited. The flexible modes limits the maximum achievable bandwidth(Echols *et al.* (2015)).

   We now consider the design of a control system for the longitudinal dynamics of Hypersonic aircraft for both new engine old plume and new engine new plume. The nonlinear model has been linearized about Mach 8, 85kft.

   The TITO model for the longitudinal dynamics is as follows:

$$\dot{x} = Ax + Bu \tag{2.2}$$

$$y = Cx + Du \tag{2.3}$$

   where

$$x = \begin{bmatrix} \theta & \text{Velocity} & \text{kft/sec} \\ q & \text{Flight Path Angle} & \text{deg} \\ \gamma & \text{Pitch Attitude} & \text{deg} \\ v & \text{Pitch rate} & \text{ft/sec} \\ \eta_1 & \text{1st flex mode} & \\ \dot{\eta_1} & \text{1st flex mode rate} & \\ \eta_2 & \text{2nd flex mode} & \\ \dot{\eta_2} & \text{2nd flex mode rate} & \\ \eta_3 & \text{3rd flex mode} & \\ \dot{\eta_3} & \text{3rd flex mode state} & \end{bmatrix}$$

$$u = \begin{bmatrix} FER & \text{Fuel Efficiency Ratio} \\ \delta_e & \text{Elevator Deflection} \end{bmatrix}$$

$$y = \begin{bmatrix} v & \text{Velocity} & \text{deg} \\ \gamma & \text{Flight path angle} & \text{deg} \end{bmatrix}$$

Bandwidth Design Specification. Let us aim for the following bandwidths for New Engine New Plume and New Engine Old Plume models of the Hypersonic aircraft aircraft.

1. **New Engine Old Plume.** Based on the presence of RHP-pole at $s = 3.02$ and the 1st flexible mode at 22 rads/sec, we sought an open loop bandwidth greater than 6 rads/sec ($\omega_B^* > 2p$) at the input loop breaking point. Based on the presence of RHP-zero at $s = 7.6892$, we sought an open loop bandwidth of $\omega_B^* < 0.5z$ at the output loop breaking point (Skogestad and Postlethwaite (2007),Page 186,235).

2. **New Engine New Plume.** Based on the presence of RHP-pole at $s = 2.3$ and and the 1st flexible mode at 22 rads/sec, we sought an open loop bandwidth of about 10 ¿ $\omega_B^* > 2p$ at the input loop breaking point. Based on the presence of RHP-zero at $s = 7.7146$, we sought an open loop bandwidth of $\omega_B^* < 0.5z$ at the output loop breaking point (Skogestad and Postlethwaite (2007),Page 186,235).

2.3 Inner-Outer Loop Feedback Loop Control Design Methodology

In the section,we discuss the design methodology for Inner-Outer loop control design for the longitudinal control system. An inner-outer loop structure is mainly used to circumvent the limitations imposed by the small RHP zero-pole ratio(Echols *et al.* (2015),Sridharan (2010)).

The following assumptions have been made for the linearized plant in order to develop a nominal control design procedure:

1. Linearized at Mach 8,85kft
2. Altitude state removed(to provide observability;included in all nonlinear simulations)
3. Flexible mode states are not available to control system i.e. not directly measured.
4. Small RHP zero to RHP pole ratio necessitates an Inner-Outer Loop feedback structure as shown below:

The nominal linear model contains 10 states after the removal of the altitude state and it is not suitable for designing a decentralized controller. Therefore the flexible states are removed so that the control design methodology does not treat them as measured signals. The rigid model has the following form (Sridharan (2010)):

$$\begin{bmatrix} \dot{V}_t \\ \dot{\gamma} \\ \dot{\theta} \\ \dot{Q} \end{bmatrix} = \begin{bmatrix} a_{11} & a_{12} & a_{13} & a_{14} \\ a_{21} & a_{22} & a_{23} & a_{24} \\ 0 & 0 & 0 & 1 \\ a_{41} & a_{42} & a_{43} & a_{44} \end{bmatrix} \begin{bmatrix} V_t \\ \gamma \\ \theta \\ Q \end{bmatrix} + \begin{bmatrix} b_{11} & b_{12} \\ b_{21} & b_{22} \\ 0 & 0 \\ b_{41} & b_{42} \end{bmatrix} \begin{bmatrix} FER \\ \delta e \end{bmatrix}$$

The system in above equation represents the coupled longitudinal dynamics associated with the aircraft. To simplify the model, the following assumptions have been made (Sridharan (2010)).

1. The velocity mode is affected by the FER only. Hence a_{12}, a_{13}, a_{14} and b_{12} can be considered as zero.
2. Elevator-to-FPA is decoupled from FER-to-velocity. Hence a_{21}, a_{41}, b_{21} and b_{41} can be considered as zero.
3. From the nonlinear Equations of Motion , we can see that $\dot{\gamma}$ and $\dot{Q}$ are not affected by Q. This can be changed due to unsteady aerodynamic forces but since we are working at trim,

the effect can be neglected.Since at trim $\dot{x} - \epsilon < 0$, hence the a_{24} and a_{44} terms are small and hence they are set to zero.

Also we take advantage of the following facts:

1. $a_{22} = -a_{23}$
2. $a_{42} = -a_{43}$

The decentralized system is now written in the following form:

$$\begin{bmatrix} \dot{V}_t \\ \dot{\gamma} \\ \dot{\theta} \\ \dot{Q} \end{bmatrix} = \begin{bmatrix} a_{11} & 0 & 0 & 0 \\ 0 & -a_{23} & a_{23} & 0 \\ 0 & 0 & 0 & 1 \\ 0 & -a_{43} & a_{43} & 0 \end{bmatrix} \begin{bmatrix} V_t \\ \gamma \\ \theta \\ Q \end{bmatrix} + \begin{bmatrix} b_{11} & 0 \\ 0 & b_{22} \\ 0 & 0 \\ 0 & b_{42} \end{bmatrix} \begin{bmatrix} FER \\ \delta e \end{bmatrix} \tag{2.4}$$

The system in above equation is the decoupled system consisting of the following (Sridharan (2010)):

1. The system from FER to velocity is expressed as a first order system

$$P_{FER\ v}(s) = \frac{c_1}{s + a_{11}} \tag{2.5}$$

2. The system from Elevator to Flight Path Angle is expressed as a 3rd order system containing a RHP pole and a RHP zero.

$$P_{\delta_e\ \gamma}(s) = \frac{c_2(s - z)(s + z)}{s(s - p_1)(s + p_2)} \tag{2.6}$$

where

$$c_1 = b_{11} \tag{2.7}$$

$$c_2 = b_{22} \tag{2.8}$$

$$p_1 = -\frac{a_{23}}{2} + \frac{\sqrt{a_{23}^2 + 4a_{43}}}{2} \tag{2.9}$$

$$p_2 = -\frac{a_{23}}{2} - \frac{\sqrt{a_{23}^2 + 4a_{43}}}{2} \tag{2.10}$$

$$z = \sqrt{a_{23}\frac{b_{42}}{b_{22}} - a_{43}} \tag{2.11}$$

The inner-outer controller structure for the rigid model consists of $K_i(s)$ in the inner loop and $K_o(s)$ in the outer loop.

$K_i(s)$ is written as :

$$K_i(s) = \frac{\delta_e}{\theta(s)} = g_{i_2}(s + z_{i_2}) \tag{2.12}$$

We augment $K_i(s)$ with a high frequency roll off term so as to ensure high frequency input noise attenuation. Hence $K_i(s)$ becomes

$$K_i(s) = g_{i_2}(s + z_{i_2}) \left[\frac{100}{(s + 100)}\right]^2 \tag{2.13}$$

In what follows, we shall omit the roll-off for convenience.

Now let us consider $P_{delta_e \to \gamma}$. This can be written as $P_{delta_e \to \gamma} = P_{delta_e \to \theta} P_{\theta \to \gamma}$

where

$$P_{delta_e \to \theta} = \frac{g_\theta(s + z_\theta)}{s(s - p_1)(s - +p_2)} \tag{2.14}$$

$$P_{\theta \to \gamma} = \frac{g_\gamma(s - z)(s + z)}{g_\theta(s + z_\theta)} \tag{2.15}$$

The open loop transfer function for the inner loop is given by

$$L_{mod} = P_{delta_e \to \theta} K_i(s) = \frac{g_\theta g_i(s + z_\theta)(s + z_i)}{s(s - p_1)(s + p_2)} \tag{2.16}$$

The final modified plant after the inclusion of the inner loop is

$$P_{mod} = \frac{P_{\delta_e \to \theta}}{1 + L_{mod}} \frac{\gamma(s)}{\theta(s)} \tag{2.17}$$

$$= \frac{g_\gamma(s - z)(s + z)}{s^3 + (p_2 - p_1 + g_i g_\theta)s^2 + (g_i g_\theta z_i + g_i g_\theta z_\theta - p_1 p_2)s + g_i g_\theta z_i z_\theta} \tag{2.18}$$

RHP pole/zero Limitations The hypersonic model is characterized by a small RHP pole/zero ratio. Using SISO ideas(Sridharan (2010)), this leads to higher $||S||_\infty$ and $||T||_\infty$ as shown :

$$\bar{\sigma}[S], \bar{\sigma}[T] \geq \frac{|z+p|}{|z-p|} \tag{2.19}$$

For the elevator to FPA system this means :

$$\bar{\sigma}[S], \bar{\sigma}[T] \geq 6.5db \tag{2.20}$$

But this rule does not apply to the inner-outer loop structure(Sridharan (2010)). Hence it is advantageous to use inner-outer loop structure for designing control systems.

Bandwidth Constraints

1. We aim for a $BW < 1/10 * z_{rhp}$ at the output loop breaking point. Hence $BW < 0.7 rads/sec$ for both New Engine Old Plume and New Engine New plume model

2. At the controls, the bandwidth is constrained by RHP pole and the 1st lightly damped flexible mode. We aim for $2 * p_{rhp} < BW < \frac{1}{2} * \omega_{n_1}$(1st flexible mode frequency). Considering $p_{rhp} = 2.3$ and $\omega_{n_1} = 22$ rads/sec for New Engine New Plume, we aim for $5 rads/sec < BW < 10 rads/sec$. Considering $p_{rhp} = 3.02$ and $\omega_{n_1} = 22$ rads/sec for New Engine Old Plume, we aim for $6 rads/sec < BW < 10 rads/sec$.

The inner outer loop structure of the following form has been used in the control system design.

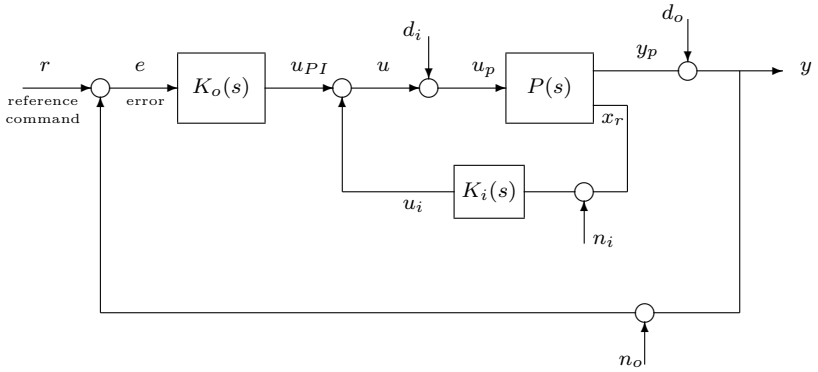

Figure 2.10: Inner Outer Feedback Loop : Hypersonic

where

1. Output vector: $y = [y1\ y2]^\top = [v\ \gamma]^\top$
2. Control vector: $u = [u1\ u2]^\top = [FER\ \delta_e]^\top$
3. State : $x_r = [\theta]$; $x = [V\ \gamma\ \theta\ q\ \eta_1\ \dot{\eta_1}\ \eta_2\ \dot{\eta_2}\ \eta_3\ \dot{\eta_3}]$
4. The inner controller $K_i(s)$ has 4 parameters (g_{i_1},z_{i_1},g_{i_2},z_{i_2}) associated with it.
5. The outer controller $K_o(s)$ has 8 parameters (g_{o_1},z_{o_1},g_{o_2},z_{o_2},g_{o_3},z_{o_3},g_{o_4},z_{o_4}) associated with it.

The nominal controllers $K_i(s)$ and $K_o(s)$ are of the following form. Roll-off terms have been used to ensure good noise attenuation.

$$K_i(s) = \begin{bmatrix} g_{i_1}\,(s + z_{i_1})\left(\frac{60}{s+60}\right)^3 \\ g_{i_2}\,(s + z_{i_2})\left(\frac{60}{s+60}\right)^3 \end{bmatrix}$$

$$K_o(s) = \begin{bmatrix} g_{o_1}\left(\frac{s+z_{o_1}}{s}\right)\left(\frac{10}{s+10}\right)^2 & g_{o_2}\left(\frac{s+z_{o_2}}{s}\right)\left(\frac{10}{s+10}\right)^2 \\ g_{o_3}\left(\frac{s+z_{o_3}}{s}\right)\left(\frac{10}{s+10}\right)^2 & g_{o_4}\left(\frac{s+z_{o_4}}{s}\right)\left(\frac{10}{s+10}\right)^2 \end{bmatrix} \tag{2.21}$$

Let us consider the New Engine Old Plume model of the hypersonic aircraft. The decentralized representation of the New Engine Old Plume model is as follows:

1. The transfer function from FER to velocity is expressed as

$$P_{FER\to v}(s) = \frac{0.06951}{s + 0.0008568} \tag{2.22}$$

2. The transfer function from Elevator to Flight Path Angle is expressed as a

$$P_{\delta_e\to\gamma}(s) = \frac{0.017543(s + 7.979)(s - 7.967)}{(s + 3.114)(s - 3.02)(s + 0.00107)} \tag{2.23}$$

Let us design a PI controller for $P_{FER\to v}(s)$. Since $P_{FER\to v}(s)$ is a first order stable transfer function, it is easy to control. Let $K_{o_1} = \frac{g_{o_1}(s+z_{o_1})}{s}$. In the rootlocus plot as shown in Figure 2.11, we see that as we increase g_{o_1}, the damping of the closed loop poles improves. We select $g_{o_1} = 0.7$ and $z_{o_1} = 0.02$ so that closed loop poles have a damping of $\zeta = 0.7$.

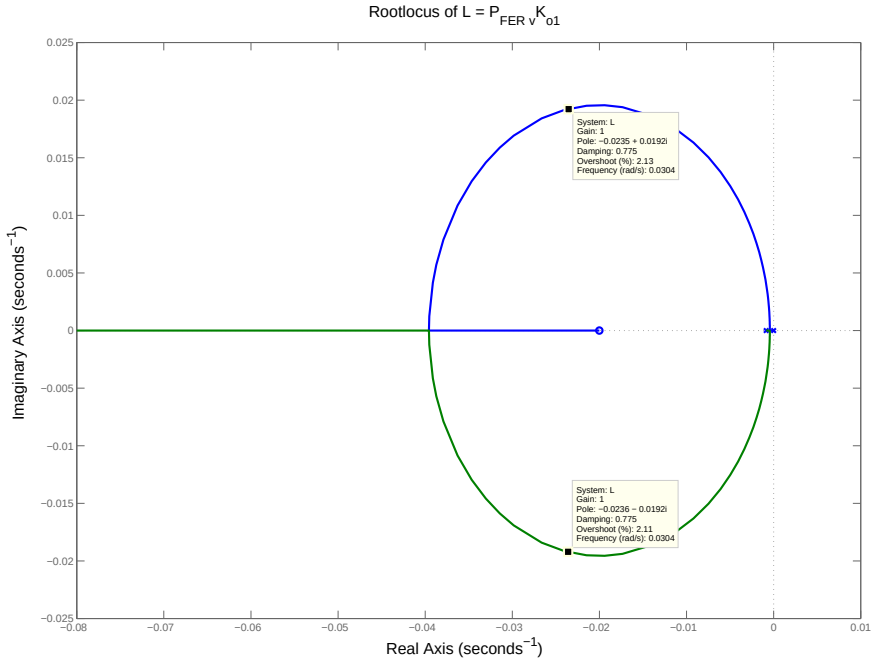

Figure 2.11: Rootlocus of $L = P_{FER\to v}K_{o1}$:Hypersonic

Let us now consider the transfer function of $P_{\delta_e\to\gamma}(s)$. The presence of an instability at $s = 3.02$ and RHP zero at $s = 7.967$ makes $P_{\delta_e\to\gamma}(s)$ difficult to control. Due to the small RHP zero to pole

ratio, a combination of state and output feedback will be used to control this system. Let us consider $P_{\delta_e \to \theta}(s)$ and $P_{\theta \to \gamma}(s)$ such that $P_{\delta_e \to \gamma}(s) = P_{\delta_e \to \theta}(s) P_{\theta \to \gamma}(s)$. To design the flight control system for FPA, let us consider the following inner-outer closed loop system as shown in Figure 5.11.

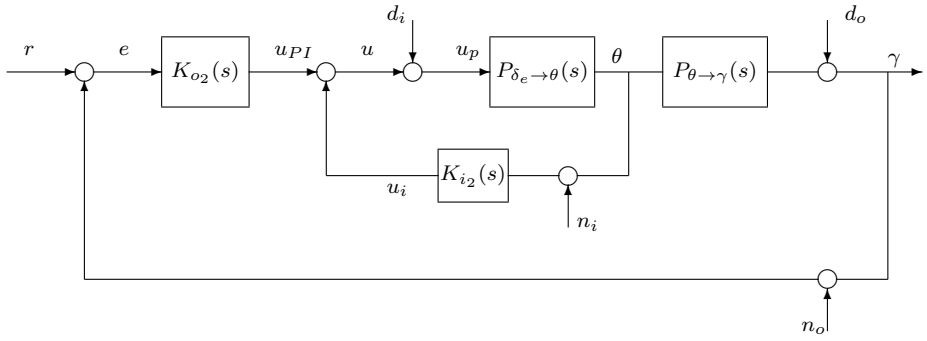

Figure 2.12: Inner Outer Feedback Loop : Hypersonic

As a rule of thumb, we always consider the inner loop as a negative feedback loop. From the transfer function matrix of the plant we obtain

$$P_{\delta_e \to \theta}(s) = \frac{-9.4888}{(s + 3.114)(s - 3.02)} \tag{2.24}$$

$$P_{\theta \to \gamma}(s) = \frac{-0.017543(s + 7.979)(s - 7.967)}{9.488(s + 0.00107)} \tag{2.25}$$

Since $P_{\delta_e \to \theta}(s)$ has an instability, the inner loop is used to move the unstable poles to a location in the left half plane with good damping so that the outer loop can stabilize the system. We use $K_{i_2} = -1.5(s+6)$. As seen in the root locus plot of $L_{mod} = P_{\delta_e \to \theta}(s) K_{i_2}$ in Figure 2.13 and Table **??**, the instability is moved in the left half plane to a location $s = -7.16 \pm 4.97i$ having $\zeta = 0.822$.

Table 2.5: Closed Loop Poles : $T_{mod} = \left(\frac{P_{\delta_e \to \theta}}{1+P_{\delta_e \to \theta} K_{i2}}\right)$: New Engine Old Plume

Pole	Damping	Frequency(rad/sec)	Time constant(sec)
-7.16e+00 + 4.97e+00i	8.22e-01	8.72e+00	1.40e-01
-7.16e+00 - 4.97e+00i	8.22e-01	8.72e+00	1.40e-01

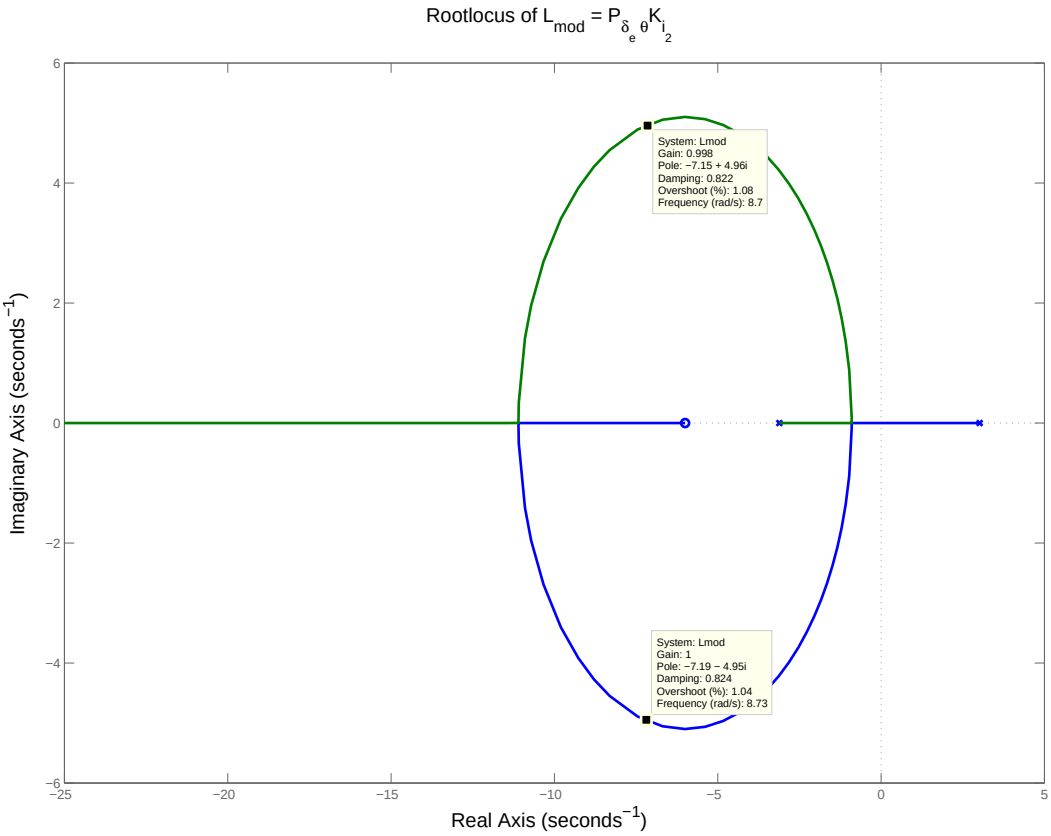

Figure 2.13: Rootlocus of $L_{mod} = P_{\delta_e \to \theta} K_{i2}$:Hypersonic

Let us now consider $P_{mod} = T_{mod} P_{\theta \to \gamma}$. From this relation we obtain

$$P_{mod} = \frac{0.017544(s + 7.979)(s - 7.967)}{(s + 0.00107)(s^2 + 14.33s + 75.99)} \tag{2.26}$$

K_{o_2} is now used to stabilize the modified plant. Let us use $K_{o_2} = \frac{-1.5(s+0.01)}{s}$.The root locus of $L = P_{mod} K_{o_2}$ is shown in Figure 2.14 and Figure 2.15. We see that the rootlocus has an upward gain margin. Hence g_{o2} can't be increased arbitrarily. As seen in Figure 2.14 and Table **??**, the closed loop poles are placed at $s = -7.14 \pm 4.97i$, $\zeta = 0.82$ and $s = -0.01 \pm 0.0934i$, $\zeta = 0.78$.

Table 2.6: Closed Loop Poles : $T = \frac{P_{mod} K_{o2}}{1 + P_{mod} K_{o2}}$:Hypersonic

Pole	Damping	Frequency(rad/sec)	Time constant(sec)
-1.16e-02 + 9.34e-03i	7.78e-01	1.49e-02	8.64e+01
-1.16e-02 - 9.34e-03i	7.78e-01	1.49e-02	8.64e+01
-7.14e+00 + 4.97e+00i	8.21e-01	8.70e+00	1.40e-01
-7.14e+00 - 4.97e+00i	8.21e-01	8.70e+00	1.40e-01

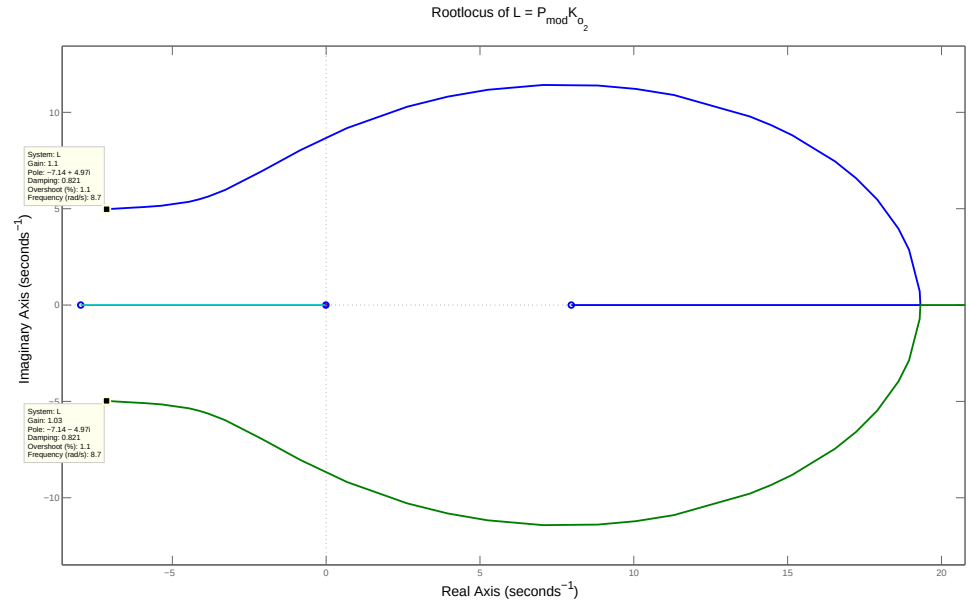

Figure 2.14: Rootlocus of $L = P_{mod}K_{o2}$: New Engine Old Plume

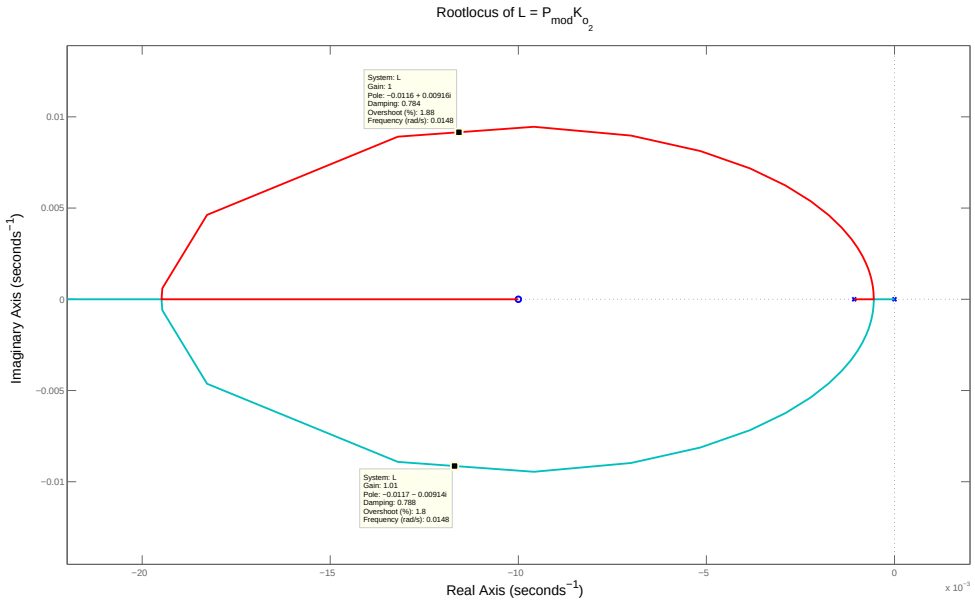

Figure 2.15: Rootlocus of $L = P_{mod}K_{o2}$ Magnified near the Origin : New Engine Old Plume

Hence we have designed a decentralized inner outer loop control system for the rigid model for New Engine Old Plume model. The controllers are as follows:

$$K_i(s) = \begin{bmatrix} 0 \\ -1.5(s+6) \end{bmatrix}$$

$$K_o(s) = \begin{bmatrix} \frac{7(s+0.01)}{s} & 0 \\ 0 & \frac{-1.5(s+0.01)}{s} \end{bmatrix} \tag{2.27}$$

The above mentioned PI-PD controller also stabilizes the rigid model of the Hypersonic NENP model.

It is seen that if Ko is allowed to have very high bandwidth i.e. the roll-off term considered for Ko is not very aggressive (for example $\left[\frac{1000}{(s+1000)}\right]^2$), then we can observe the following:

1. In the NENP model, as the parameter g_{o1} of K_{o1} is made arbitrarily large, the $||S_i||_\infty$, $||T_i||_\infty$ decreases and $||S_o||_\infty$, $||T_o||_\infty$ increases as shown in Figure 2.16 and Figure 2.17. $||PS||_\infty$ decreases which gives us good input disturbance attenuation as shown in Figure 2.18. Hence we are in a position to get equilibrated design at both the loop breaking points. But this comes at the cost of having unreasonably high KS(control-action) crossover. $||KS||_\infty$ also increases which results in saturation as the constraint $FER < 1$ is violated.

2. In the NEOP mode, as the parameter g_{o1} of K_{o1} is made arbitrarily large, the $||S_i||_\infty$, $||T_i||_\infty$ does not change much. However $||S_o||_\infty$, $||T_o||_\infty$ increases as shown in as shown in Figure 2.16 and Figure 2.17. $||PS||_\infty$ also decreases which gives us good input disturbance attenuation as shown in Figure 2.18. This also comes at the cost of unreasonably high KS(control-action) crossover and high $||KS||_\infty$ which violates the constraint $FER < 1$. Hence for the NEOP model, we are not in a position to get equilibrated designs even at the expense of unreasonably high control action and high KS(control-action) crossover.

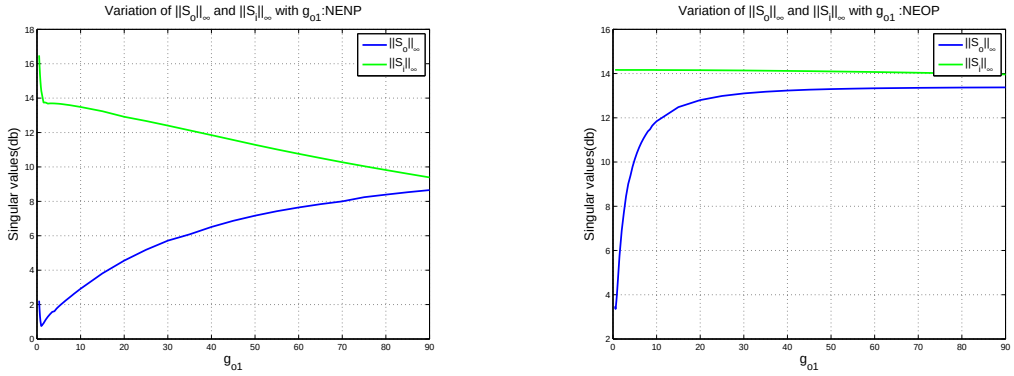

Figure 2.16: Variation of $||S||_\infty$ with g_{o1} for NEOP and NENP

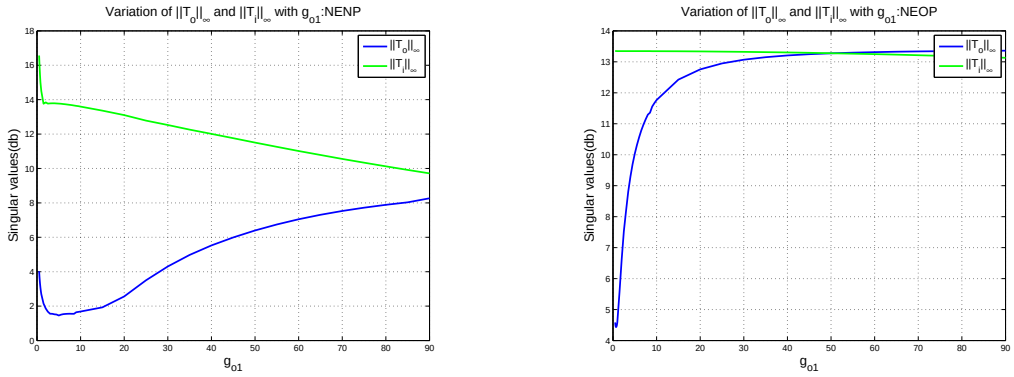

Figure 2.17: Variation of $||T||_\infty$ with g_{o1} for NEOP and NENP

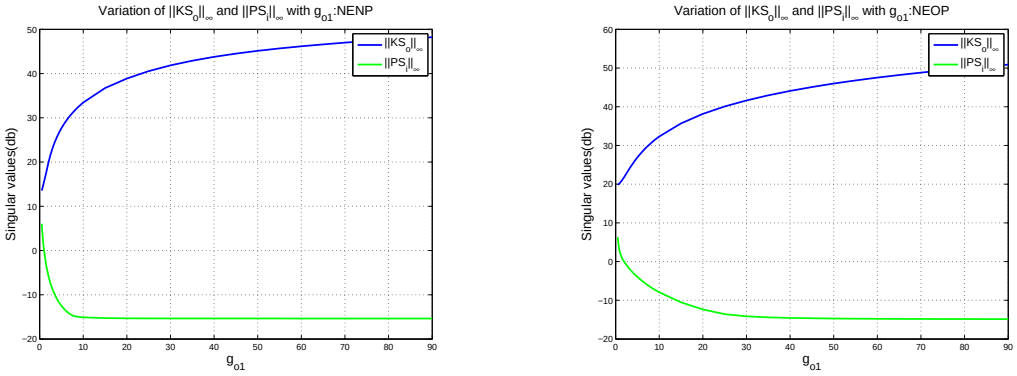

Figure 2.18: Variation of $||KS_o||_\infty$ and $||PS_i||_\infty$ with g_{o1} for NEOP and NENP

2.3.1 *Tradeoffs using Hierarchical PI-PD Controllers*

In this section, we compare the closed loop properties obtained by using different structures of PI-PD controllers for both New Engine Old Plume and New Engine New Plume(Dickeson *et al.* (2009)). The Matlab command Hinfstruct(Gahinet and Apkarian (2011a),Gahinet and Apkarian (2011b),Yang *et al.* (2013),Saussié *et al.* (2013)) was used to design the PI-PD controllers. We start with the basic decentralized structure of the form.

$$K_i(s) = \begin{bmatrix} 0 \\ g_{i_2}\left(s + z_{i_2}\right)\left(\frac{60}{s+60}\right)^3 \end{bmatrix}$$
$$K_o(s) = \begin{bmatrix} g_{o_1}\left(\frac{s+z_{o_1}}{s}\right)\left(\frac{10}{s+10}\right)^2 & 0 \\ 0 & g_{o_2}\left(\frac{s+z_{o_2}}{s}\right)\left(\frac{10}{s+10}\right)^2 \end{bmatrix} \tag{2.28}$$

The following are the closed loop properties obtained using a family of controllers for the New Engine Old Plume.

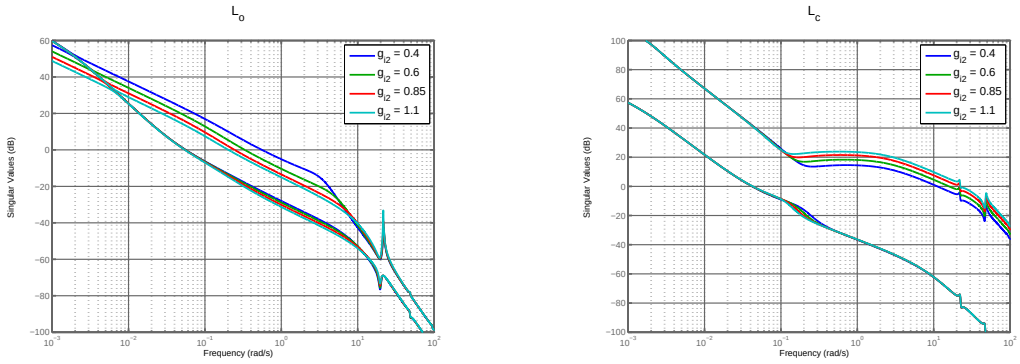

Figure 2.19: Open Loop Singular Values(Old Plume) : $K_{o_{decentralized}}, K_{i_{decentralized}}$

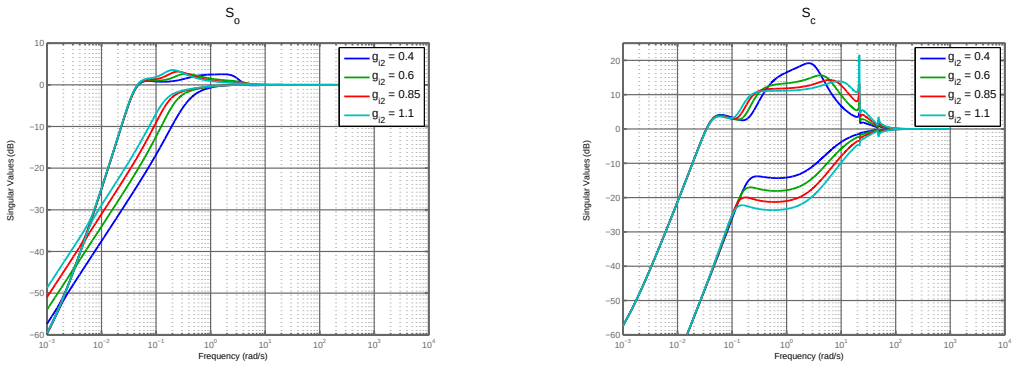

Figure 2.20: Sensitivity(Old Plume) : $K_{o_{decentralized}}, K_{i_{decentralized}}$

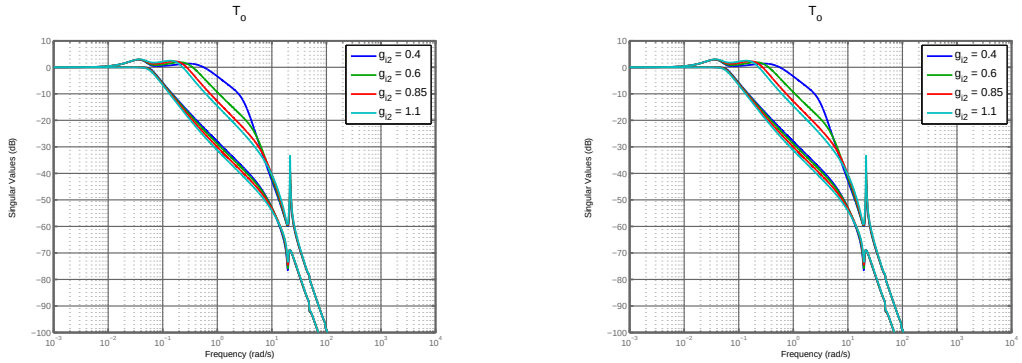

Figure 2.21: Complementary Sensitivity(Old Plume) : $K_{o_{decentralized}}, K_{i_{decentralized}}$

1. $||S_e||_\infty$ is below 5 db for all these designs. The singular values are low ($\leq$ -20 db for $\omega \leq 0.01$ rads/sec) at low frequencies which ensures good low frequency command following and output disturbance attenuation.

2. $||T_e||_\infty$ is below 5 db for all these designs. It also has good high frequency noise attenuation and good robustness to multiplicative uncertainity.

3. $||S_c||_\infty$ and $||T_c||_\infty$ is dominated by the peak near 22 rads/sec as we increase the bandwidth at the controls. This means that the flexible modes which puts an upper bound on the bandwidth are getting excited as we are increasing the bandwidth at the controls.

Control Action

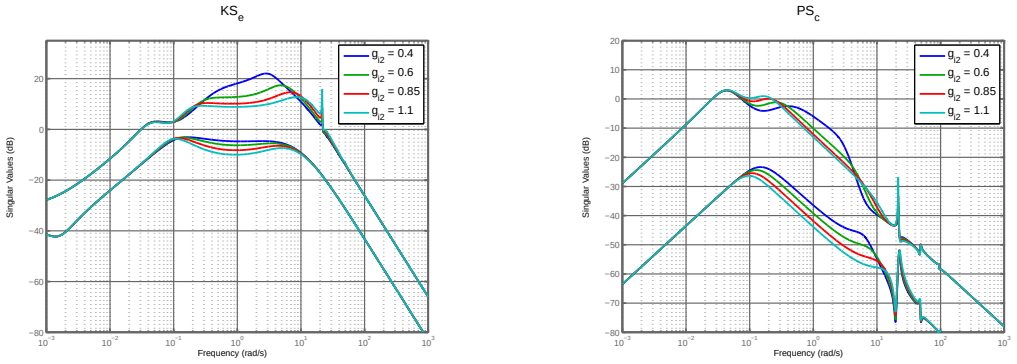

Figure 2.22: KS_e and PS_c(Old Plume) : $K_{o_{decentralized}}, K_{i_{decentralized}}$

1. It is noticed that as the control action increases, the input disturbance attenuation decreases. Hence there is a tradeoff between control action and input disturbance attenuation.

The following are the closed loop properties obtained using a family of controllers for the New Engine New Plume.

Open Loop transfer function at the Error

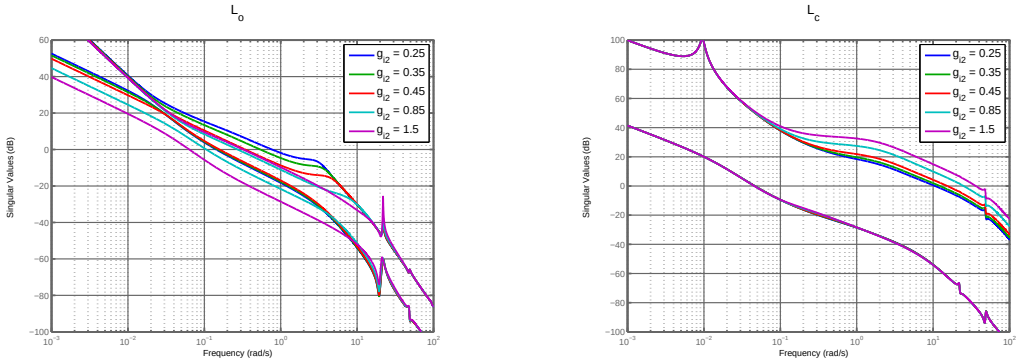

Figure 2.23: Open Loop singular values(New Plume) : $K_{o_{decentralized}}, K_{i_{decentralized}}$

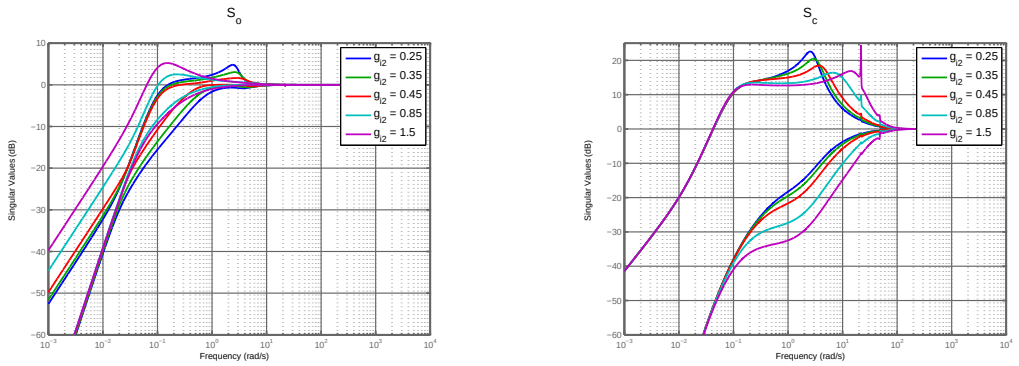

Figure 2.24: Sensitivity(New Plume) : $K_{o_{decentralized}}, K_{i_{decentralized}}$

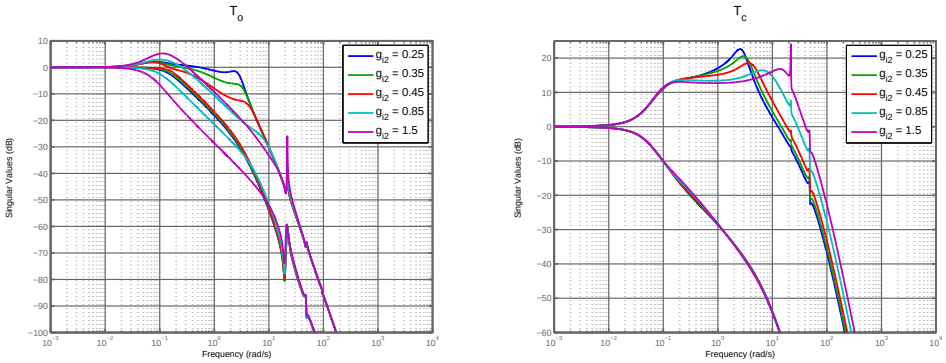

Figure 2.25: Complementary Sensitivity(New Plume) : $K_{o_{decentralized}}, K_{i_{decentralized}}$

1. $||S_e||_\infty$ and $||T_e||_\infty$ are below 5 db for all these designs. Low singular values of T_e at high frequencies ensures good noise attenuation and good robustness to multiplicative uncertainity.

2. $||S_c||_\infty$ and $||T_c||_\infty$ is dominated by the peak near 22 rads/sec as we increase the bandwidth at the controls. This means that the flexible modes which puts an upper bound on the bandwidth are getting excited as we are increasing the bandwidth at the controls.

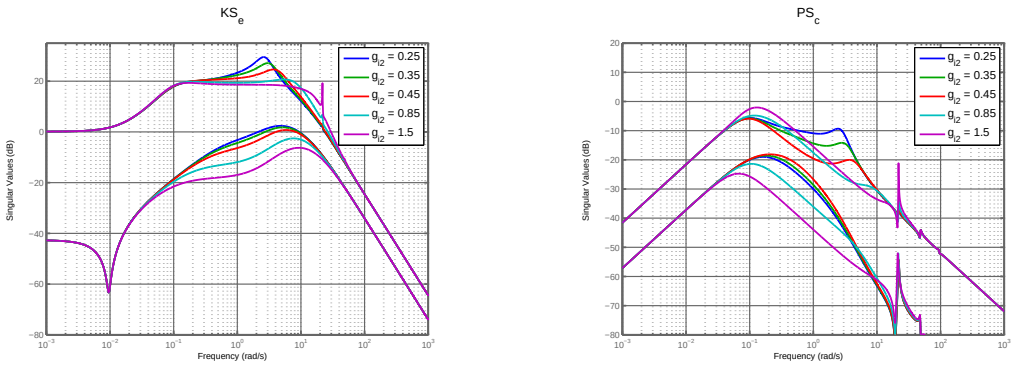

Figure 2.26: KS_e and PS_c(New Plume) : $K_{o_{decentralized}}, K_{i_{decentralized}}$

1. It is noticed that as the control action increases, the input disturbance attenuation decreases. Hence there is a tradeoff between control action and input disturbance attenuation.

We compare the best designs obtain for New Engine Old Plume and New Engine New Plume using a decentralized K_o and decentralized K_i. The controllers are for New Engine New Plume and New Engine Old Plume are as follows

New Engine Old Plume

$$K_i(s) = \begin{bmatrix} 0 \\ -0.8\,(s+5)\left(\frac{60}{s+60}\right)^3 \end{bmatrix}$$
$$K_o(s) = \begin{bmatrix} 1.25\left(\frac{s+0.04}{s}\right)\left(\frac{10}{s+10}\right)^2 & 0 \\ 0 & -9.5\left(\frac{s+0.07}{s}\right)\left(\frac{10}{s+10}\right)^2 \end{bmatrix} \tag{2.29}$$

New Engine New Plume

$$K_i(s) = \begin{bmatrix} 0 \\ -0.7\,(s+3)\left(\frac{60}{s+60}\right)^3 \end{bmatrix}$$
$$K_o(s) = \begin{bmatrix} 1.5\left(\frac{s+0.06}{s}\right)\left(\frac{10}{s+10}\right)^2 & 0 \\ 0 & -6\left(\frac{s+0.12}{s}\right)\left(\frac{10}{s+10}\right)^2 \end{bmatrix} \tag{2.30}$$

1. We see that we get slightly better closed loop properties at the controls for New Engine Old Plume than New Engine New Plume using a decentralized K_o and a decentralized K_i.

Table 2.7: Attained Closed Loop Properties($||.||_\infty$ in db) for NEOP and NENP Model

	$\|\|S_e\|\|_\infty$	$\|\|T_e\|\|_\infty$	$\|\|S_c\|\|_\infty$	$\|\|T_c\|\|_\infty$	$\|\|KS_e\|\|_\infty$	$\|\|PS_c\|\|_\infty$	v_{ts}	γ_{ts}
New Engine Old Plume	5.85	3.65	15.69	15.81	16.79	0.14	78.3	38.02
New Engine New Plume	4.78	2.77	16.53	16.46	19.57	-2.56	54.65	15.31

2. The properties at the output are better for New Engine New Plume compared to New Engine Old Plume. However it is seen that for New Engine Old Plume, the $||S_e||_\infty$ and $||T_e||_\infty$ reduces as the velocity channel is made slower i.e. v_{ts} increases.

Now let us introduce $K_i(1,1)$ element into the controller and study the closed loop properties obtained. Introduction of the $K_i(1,1)$element makes the inner loop controller θ centralized. K_o is considered decentralized in the following designs. We consider the controller of the following form.

$$K_i(s) = \begin{bmatrix} g_{i_1}\left(s+z_{i_1}\right)\left(\frac{60}{s+60}\right)^3 \\ g_{i_2}\left(s+z_{i_2}\right)\left(\frac{60}{s+60}\right)^3 \end{bmatrix}$$

$$K_o(s) = \begin{bmatrix} g_{o_1}\left(\frac{s+z_{o_1}}{s}\right)\left(\frac{10}{s+10}\right)^2 & 0 \\ 0 & g_{o_2}\left(\frac{s+z_{o_2}}{s}\right)\left(\frac{10}{s+10}\right)^2 \end{bmatrix} \tag{2.31}$$

The following are the closed loop properties obtained using a family of controllers for the New Engine Old Plume.

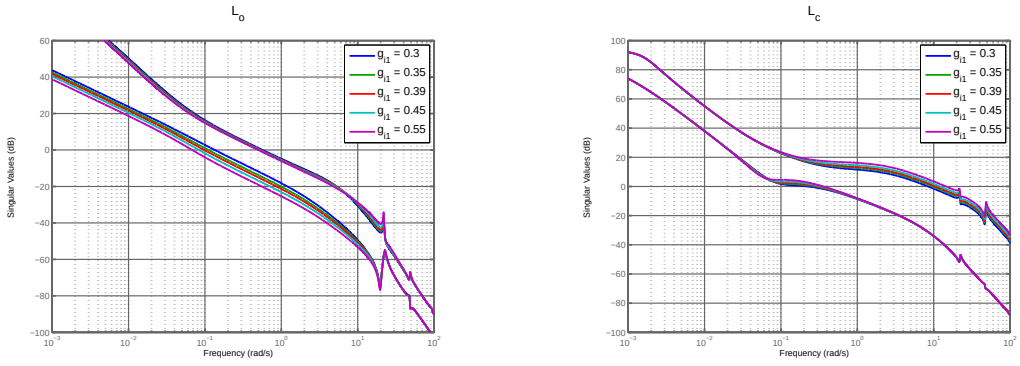

Figure 2.27: Open Loop Singular Values(Old Plume) : $K_{o_{decentralized}}, K_{i_{\theta centralized}}$

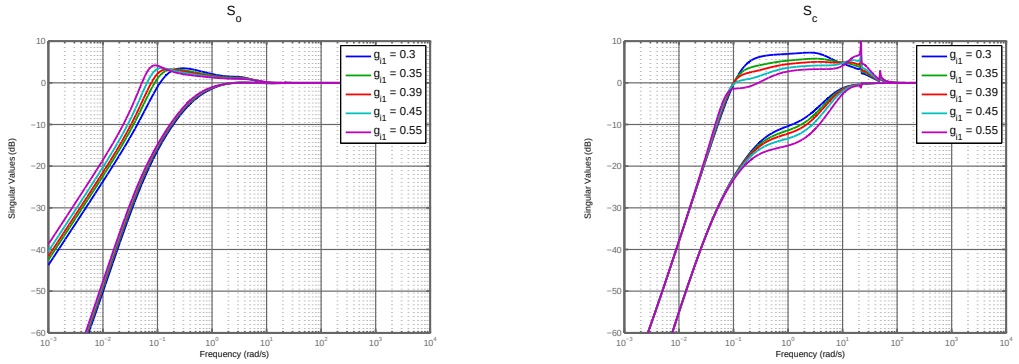

Figure 2.28: Sensitivity(Old Plume) : $K_{o_{decentralized}}, K_{i_{\theta centralized}}$

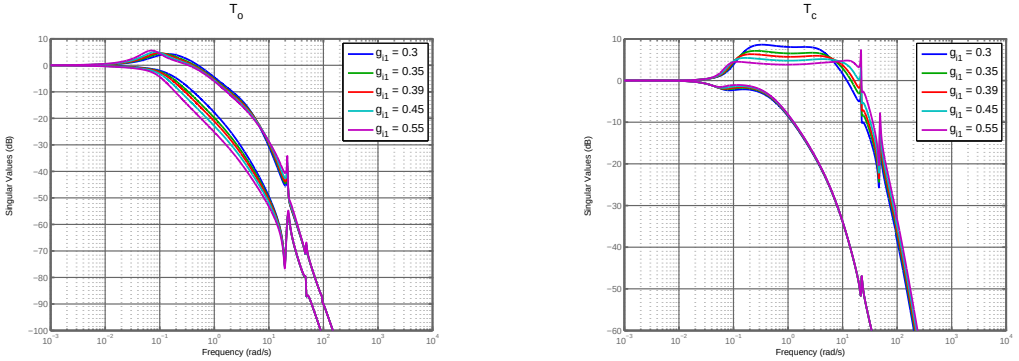

Figure 2.29: Complementary Sensitivity(Old Plume) : $K_{o_{decentralized}}, K_{i_{\theta centralized}}$

1. $||S_e||_\infty$ and $||T_e||_\infty$ are below 5 db. We have good sensor noise attenuation and robustness to additive and multiplicative uncertainity.

2. $||S_c||_\infty$ and $||T_c||_\infty$ is dominated by the peak near 22 rads/sec as we increase the bandwidth at the controls. This means that the flexible modes which puts an upper bound on the bandwidth are getting excited as we are increasing the bandwidth at the controls.

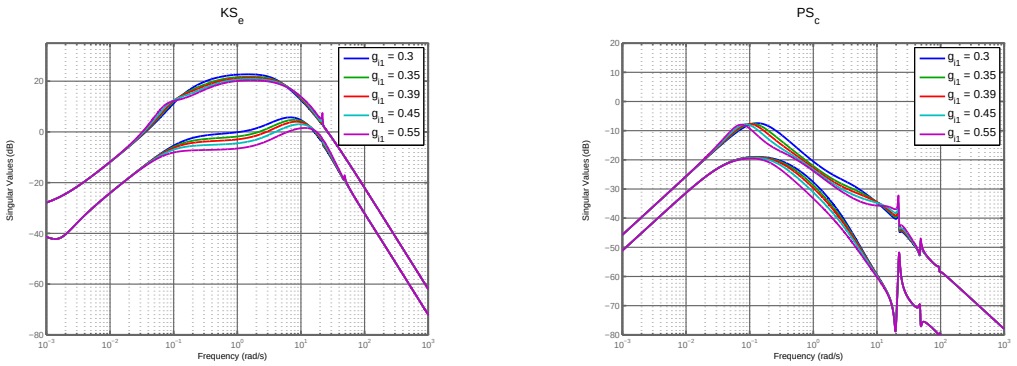

Figure 2.30: KS_e and PS_c(Old Plume) : $K_{o_{decentralized}}, K_{i_{\theta centralized}}$

The following are the closed loop properties obtained using a family of controllers for the New Engine New Plume.

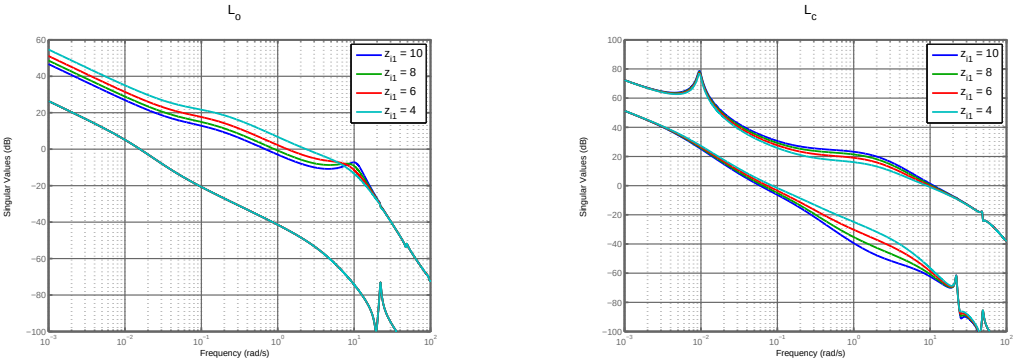

Figure 2.31: Open Loop Singular Values(New Plume) : $K_{o_{decentralized}}, K_{i_{\theta centralized}}$

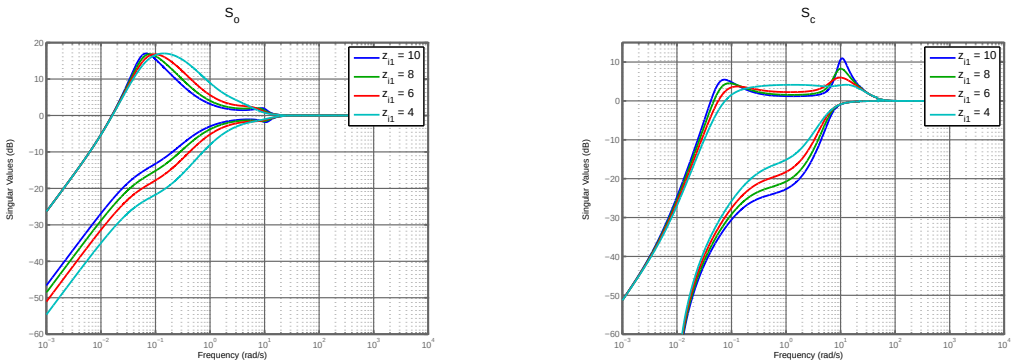

Figure 2.32: Sensitivity(New Plume) : $K_{o_{decentralized}}, K_{i_{\theta centralized}}$

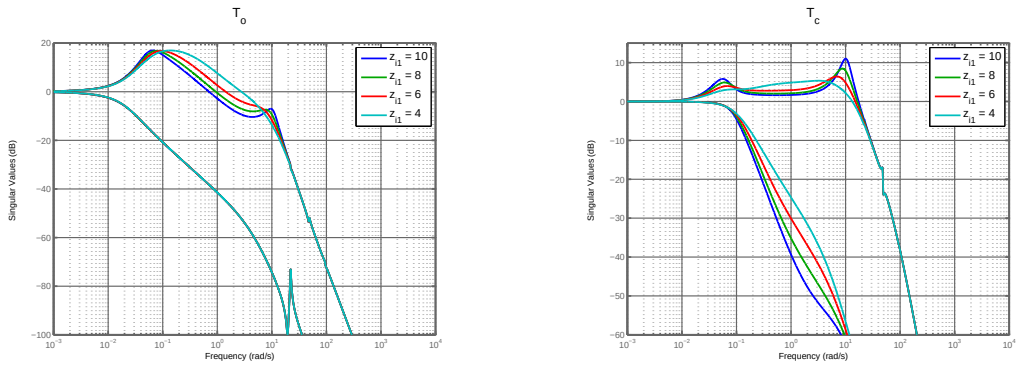

Figure 2.33: Complementary Sensitivity(New Plume) : $K_{o_{decentralized}}, K_{i_{\theta centralized}}$

1. $||S_e||_\infty$ and $||T_e||_\infty$ are less tha 5 db for these designs.

2. There is significant improvement in the closed loop properties at the controls by making K_i θ centralized. $||S_c||_\infty$ and $||T_c||_\infty$ are below 11 db for these designs.

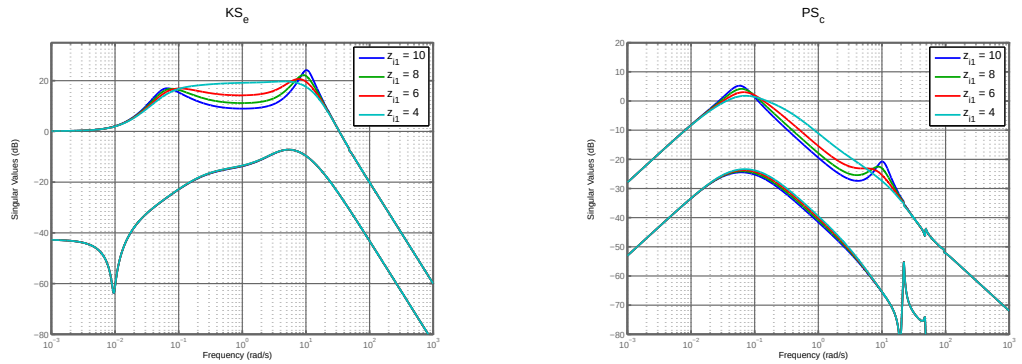

Figure 2.34: KS_e and PS_c(New Plume) : $K_{o_{decentralized}}, K_{i_{\theta centralized}}$

We compare the best designs obtain for New Engine Old Plume and New Engine New Plume using a decentralized K_o and θ centralized K_i.

New Engine Old Plume

$$K_i(s) = \begin{bmatrix} 0.39\,(s+4.02)\left(\frac{60}{s+60}\right)^3 \\ 0.06\,(s+10.73)\left(\frac{60}{s+60}\right)^3 \end{bmatrix}$$
$$K_o(s) = \begin{bmatrix} -3\left(\frac{s+0.08}{s}\right)\left(\frac{10}{s+10}\right)^2 & 0 \\ 0 & 2.5\left(\frac{s+0.05}{s}\right)\left(\frac{10}{s+10}\right)^2 \end{bmatrix} \tag{2.32}$$

New Engine New Plume

$$K_i(s) = \begin{bmatrix} -0.38\,(s+1.5)\left(\frac{60}{s+60}\right)^3 \\ -0.08\,(s+14)\left(\frac{60}{s+60}\right)^3 \end{bmatrix}$$
$$K_o(s) = \begin{bmatrix} 4\left(\frac{s+0.06}{s}\right)\left(\frac{10}{s+10}\right)^2 & 0 \\ 0 & -5\left(\frac{s+0.1}{s}\right)\left(\frac{10}{s+10}\right)^2 \end{bmatrix} \tag{2.33}$$

Table 2.8: Attained Closed Loop Properties($||.||_\infty$ in db) for NEOP and NENP Model

	$\|\|S_e\|\|_\infty$	$\|\|T_e\|\|_\infty$	$\|\|S_c\|\|_\infty$	$\|\|T_c\|\|_\infty$	$\|\|KS_e\|\|_\infty$	$\|\|PS_c\|\|_\infty$	v_{ts}	γ_{ts}
New Engine Old Plume	5.63	5.83	7.57	8.56	16.33	-3.75	62.2	36.1
New Engine New Plume	5.92	5.24	9.68	10.17	22.04	-7.98	46.8	17.65

1. There is significant improvement in the properties at the controls for both New Engine Old Plume and New Engine New Plume, when we make K_i θ centralized.

2. There is not much change in the properties at the error when we make K_i θ centralized.

Now let us keep K_i θ centralized and introduce off-diagonal elements in the K_o thus making K_o centralized. We consider the controller of the following form.

$$K_i(s) = \begin{bmatrix} g_{i_1}\left(s + z_{i_1}\right)\left(\frac{60}{s+60}\right)^3 \\ g_{i_2}\left(s + z_{i_2}\right)\left(\frac{60}{s+60}\right)^3 \end{bmatrix}$$

$$K_o(s) = \begin{bmatrix} g_{o_{11}}\left(\frac{s+z_{o_{11}}}{s}\right)\left(\frac{10}{s+10}\right)^2 & g_{o_{12}}\left(\frac{s+z_{o_{12}}}{s}\right)\left(\frac{10}{s+10}\right)^2 \\ g_{o_{21}}\left(\frac{s+z_{o_{21}}}{s}\right)\left(\frac{10}{s+10}\right)^2 & g_{o_{22}}\left(\frac{s+z_{o_{22}}}{s}\right)\left(\frac{10}{s+10}\right)^2 \end{bmatrix} \tag{2.34}$$

The following are the closed loop properties obtained using a family of controllers for the New Engine Old Plume.

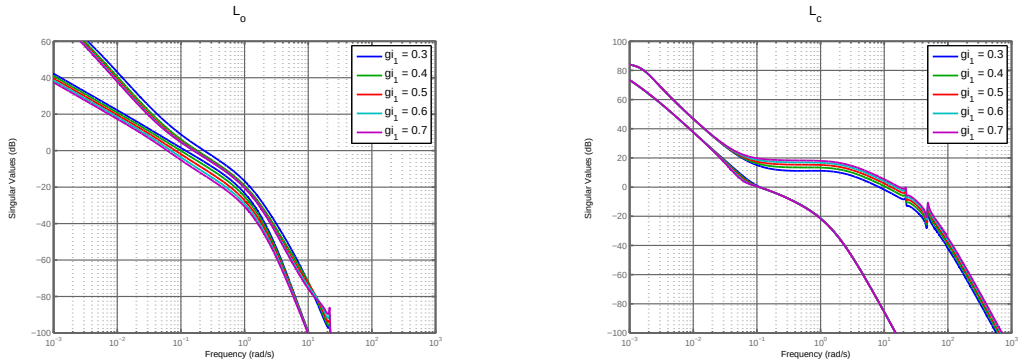

Figure 2.35: Open loop Singular Values(Old Plume) : $K_{o_{centralized}}, K_{i_{\theta centralized}}$

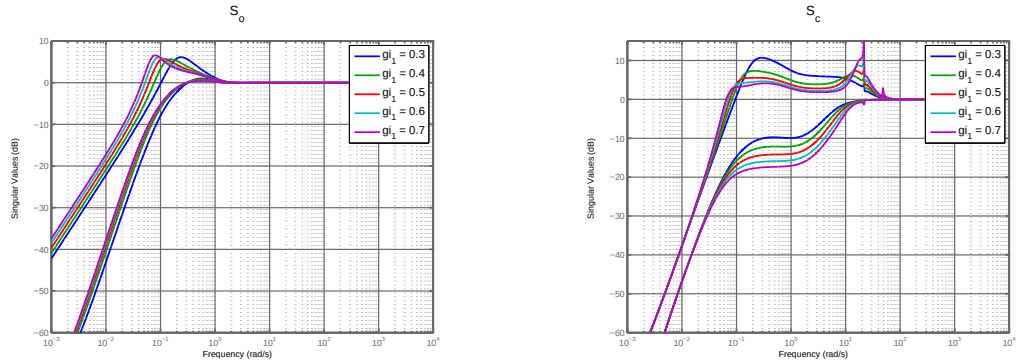

Figure 2.36: Sensitivity(Old Plume) : $K_{o_{centralized}}, K_{i_{\theta centralized}}$

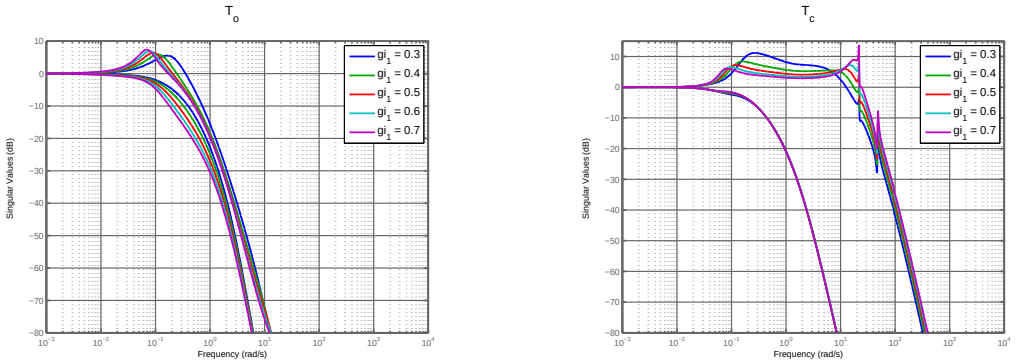

Figure 2.37: Complementary Sensitivity(Old Plume) : $K_{o_{centralized}}, K_{i_{\theta centralized}}$

1. $||S_e||_\infty$ and $||T_e||_\infty$ are below 6 db.

2. $||S_c||_\infty$ and $||T_c||_\infty$ increases as we increase the bandwidth at the controls. This means that the flexible modes which puts an upper bound on the bandwidth are getting excited as we are increasing the bandwidth at the controls.

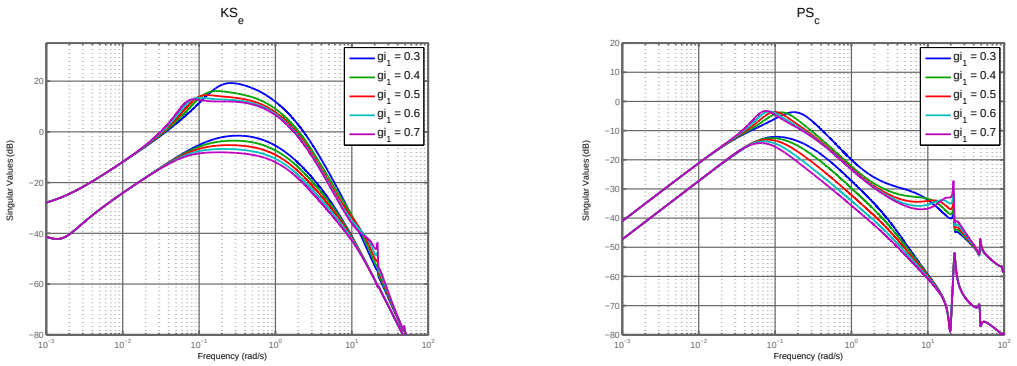

Figure 2.38: KS_e and PS_c(Old Plume) : $K_{o_{centralized}}, K_{i_{\theta centralized}}$

The following are the closed loop properties obtained using a family of controllers for the New Engine New Plume.

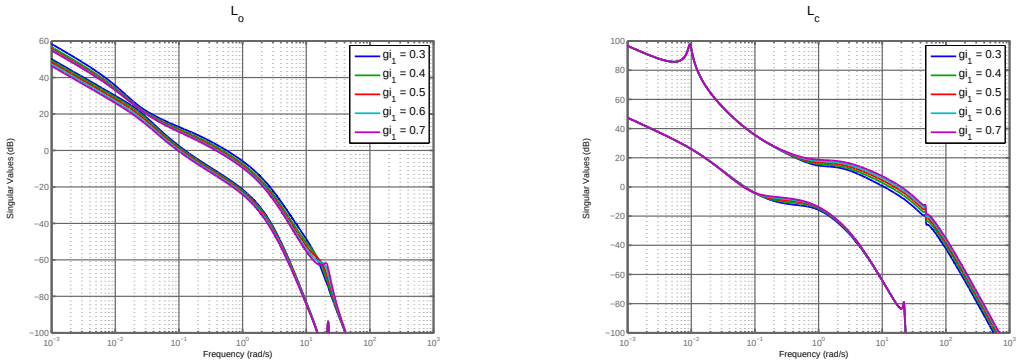

Figure 2.39: Open loop Singular Values(New Plume) : $K_{o_{centralized}}, K_{i_{\theta centralized}}$

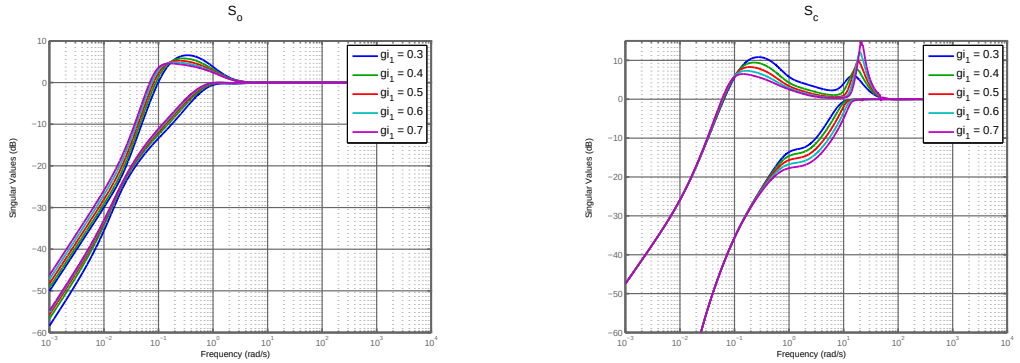

Figure 2.40: Sensitivity(New Plume) : $K_{o_{centralized}}, K_{i_{\theta centralized}}$

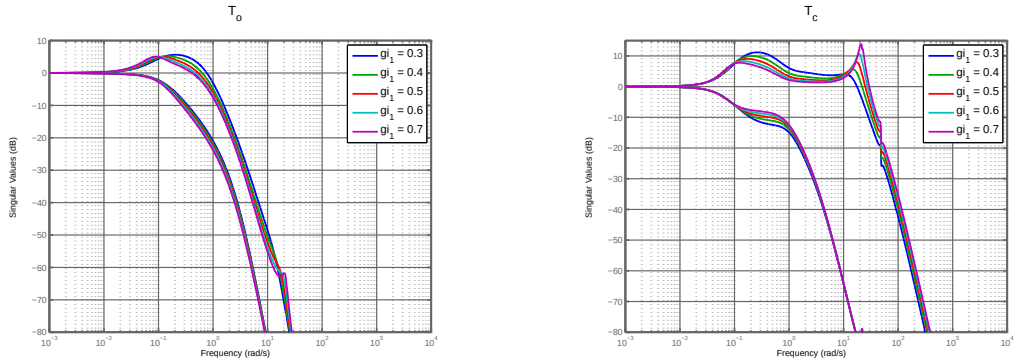

Figure 2.41: Complementary Sensitivity(New Plume) : $K_{o_{centralized}}, K_{i_{\theta centralized}}$

1. By introducing the offdiagonal elements in K_o, we see a slight improvement in the properties at the error for the New Engine New Plume.

2. $||S_e||_\infty$ and $||T_e||_\infty$ are below 5 db for these designs.

3. $||S_c||_\infty$ and $||T_c||_\infty$ increases as we increase the bandwidth at the controls. This means that the flexible modes which puts an upper bound on the bandwidth are getting excited as we are increasing the bandwidth at the controls.

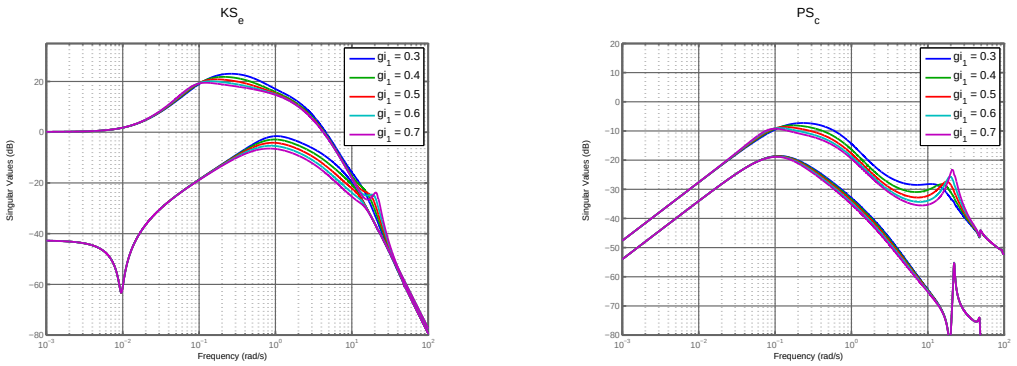

Figure 2.42: KS_e and PS_c(New Plume) : $K_{o_{centralized}}, K_{i_{\theta centralized}}$

We compare the best designs obtain for New Engine Old Plume and New Engine New Plume using a centralized K_o and θ centralized K_i.

New Engine Old Plume

$$K_i(s) = \begin{bmatrix} 0.25\,(s+3.25)\left(\frac{60}{s+60}\right)^3 \\ -0.1\,(s+4.72)\left(\frac{60}{s+60}\right)^3 \end{bmatrix}$$

$$K_o(s) = \begin{bmatrix} 0.19\left(\frac{s-0.19}{s}\right)\left(\frac{10}{s+10}\right)^2 & 2.6\left(\frac{s+0.1}{s}\right)\left(\frac{10}{s+10}\right)^2 \\ 3.5\left(\frac{s+0.08}{s}\right)\left(\frac{10}{s+10}\right)^2 & 0.48\left(\frac{s-0.06}{s}\right)\left(\frac{10}{s+10}\right)^2 \end{bmatrix} \tag{2.35}$$

New Engine New Plume

$$K_i(s) = \begin{bmatrix} -0.3\,(s+2)\left(\frac{60}{s+60}\right)^3 \\ -0.05\,(s+1.6)\left(\frac{60}{s+60}\right)^3 \end{bmatrix}$$
$$K_o(s) = \begin{bmatrix} 2\left(\frac{s-0.01}{s}\right)\left(\frac{10}{s+10}\right)^2 & -1.2\left(\frac{s+0.26}{s}\right)\left(\frac{10}{s+10}\right)^2 \\ -5\left(\frac{s+0.08}{s}\right)\left(\frac{10}{s+10}\right)^2 & -0.2\left(\frac{s+0.37}{s}\right)\left(\frac{10}{s+10}\right)^2 \end{bmatrix} \tag{2.36}$$

Table 2.9: Attained Closed Loop Properties($||.||_\infty$ in db) for NEOP and NENP Model

	$\|\|S_e\|\|_\infty$	$\|\|T_e\|\|_\infty$	$\|\|S_c\|\|_\infty$	$\|\|T_c\|\|_\infty$	$\|\|KS_e\|\|_\infty$	$\|\|PS_c\|\|_\infty$	v_{ts}	γ_{ts}
New Engine Old Plume	4.64	3.46	4.42	5.72	13.18	-6.87	61.63	15.22
New Engine New Plume	4.76	2.72	5.61	4.21	16.56	-0.77	64.14	16.67

1. After making K_o centralized we see a significant improvement in the properties at the error for New Engine New Plume.

2. There is no further improvement in the properties at the error or at the controls for New Engine Old Plume when we make K_o centralized.

Now let us feedback velocity and pitch in the inner loop. Thus we would need K_i to be a controller of dimension 2×2. K_o is considered to be centralized. We consider the controller of the following form.

$$K_i(s) = \begin{bmatrix} g_{i_{11}}\,(s+z_{i_{11}})\left(\frac{60}{s+60}\right)^3 & g_{i_{12}}\,(s+z_{i_{12}})\left(\frac{60}{s+60}\right)^3 \\ g_{i_{21}}\,(s+z_{i_{21}})\left(\frac{60}{s+60}\right)^3 & g_{i_{22}}\,(s+z_{i_{22}})\left(\frac{60}{s+60}\right)^3 \end{bmatrix}$$
$$K_o(s) = \begin{bmatrix} g_{o_{11}}\left(\frac{s+z_{o_{11}}}{s}\right)\left(\frac{10}{s+10}\right)^2 & g_{o_{12}}\left(\frac{s+z_{o_{12}}}{s}\right)\left(\frac{10}{s+10}\right)^2 \\ g_{o_{21}}\left(\frac{s+z_{o_{21}}}{s}\right)\left(\frac{10}{s+10}\right)^2 & g_{o_{22}}\left(\frac{s+z_{o_{22}}}{s}\right)\left(\frac{10}{s+10}\right)^2 \end{bmatrix} \tag{2.37}$$

The following are the closed loop properties obtained using a family of controllers for the New Engine Old Plume.

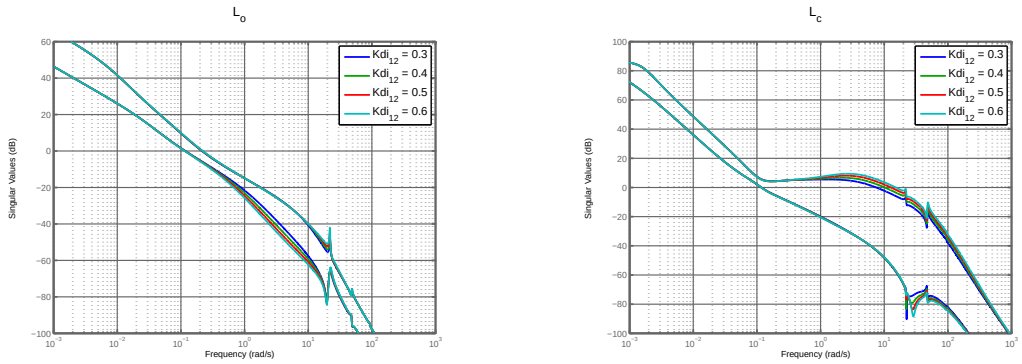

Figure 2.43: Open loop Singular Values(Old Plume) : $K_{o_{centralized}}, K_{i_{centralized}}$

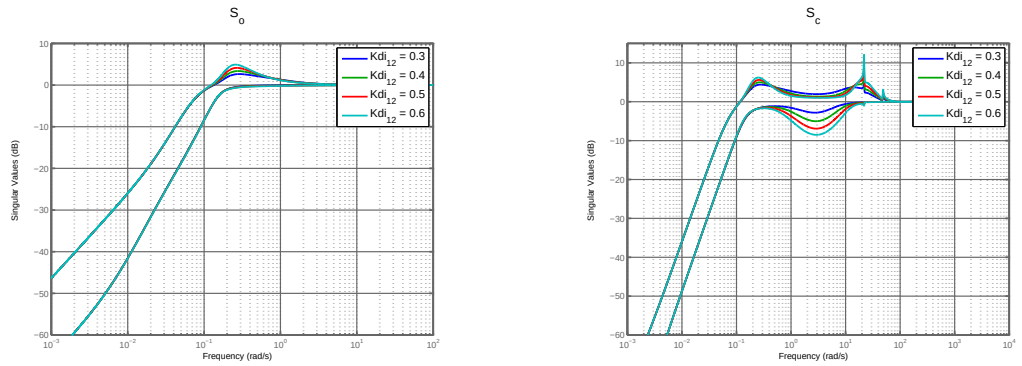

Figure 2.44: Sensitivity(Old Plume) : $K_{o_{centralized}}, K_{i_{centralized}}$

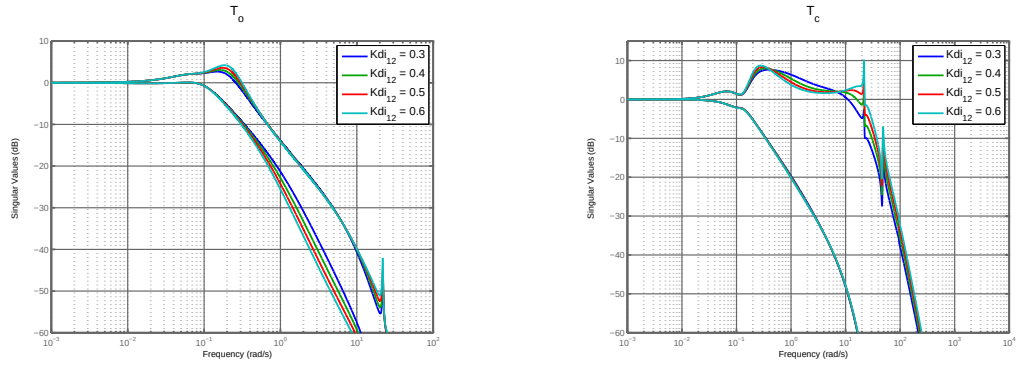

Figure 2.45: Complementary Sensitivity(Old Plume) : $K_{o_{centralized}}, K_{i_{centralized}}$

1. $||S_e||_\infty$ and $||T_e||_\infty$ are below 6 db for these designs.

2. $||S_c||_\infty$ and $||T_c||_\infty$ increases as we increase the bandwidth at the controls. This means that the flexible modes which puts an upper bound on the bandwidth are getting excited as we are increasing the bandwidth at the controls.

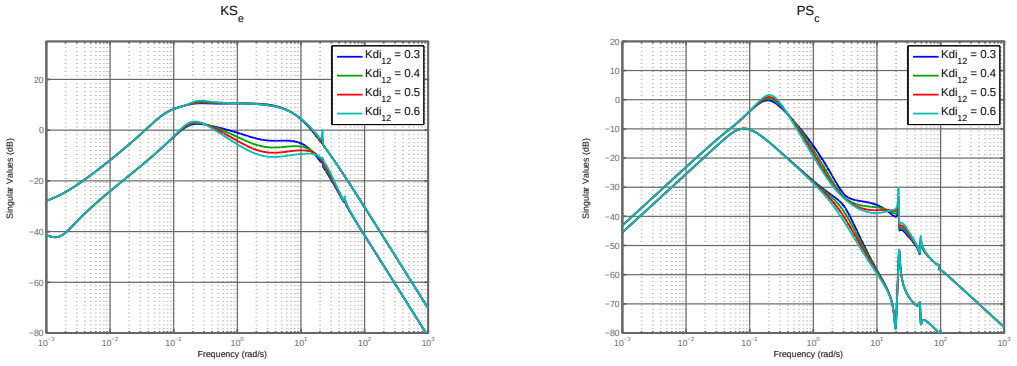

Figure 2.46: KS_e and PS_e(Old Plume) : $K_{o_{centralized}}, K_{i_{centralized}}$

The following are the closed loop properties obtained using a family of controllers for the New Engine New Plume.

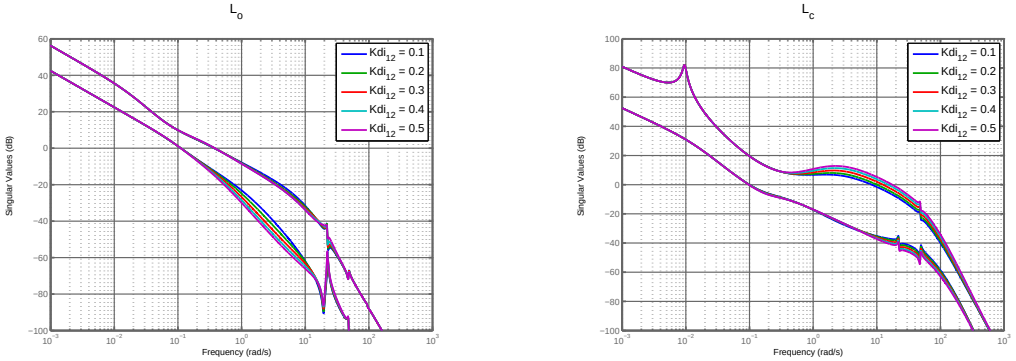

Figure 2.47: Open Loop Singular Values(New Plume) : $K_{o_{centralized}}, K_{i_{centralized}}$

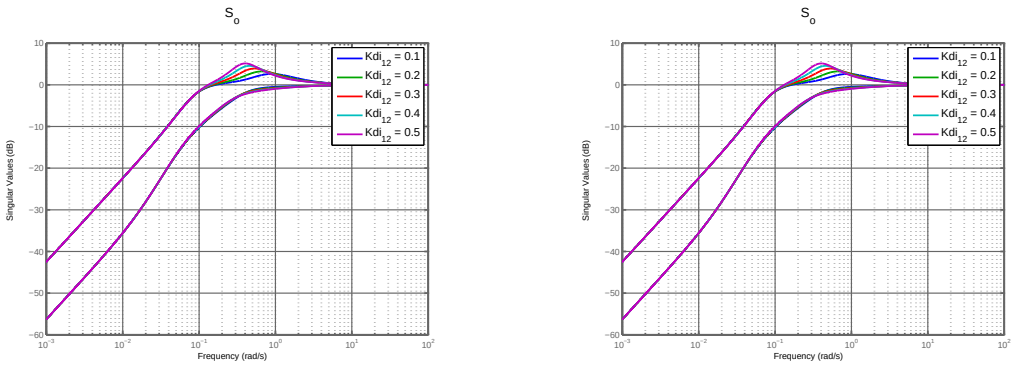

Figure 2.48: Sensitivity(New Plume) : $K_{o_{centralized}}, K_{i_{centralized}}$

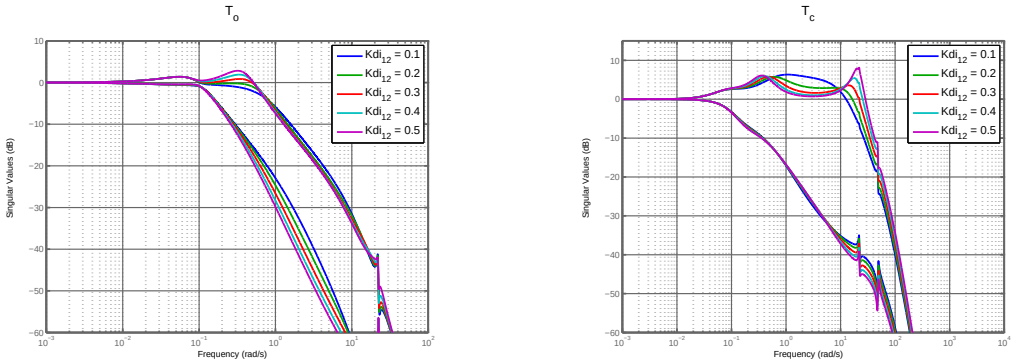

Figure 2.49: Complementary Sensitivity(New Plume) : $K_{o_{centralized}}, K_{i_{centralized}}$

1. $||S_e||_\infty$ and $||T_e||_\infty$ is below 6 db.

2. $||S_c||_\infty$ and $||T_c||_\infty$ increases as we increase the bandwidth at the controls. This means that the flexible modes which puts an upper bound on the bandwidth are getting excited as we are increasing the bandwidth at the controls.

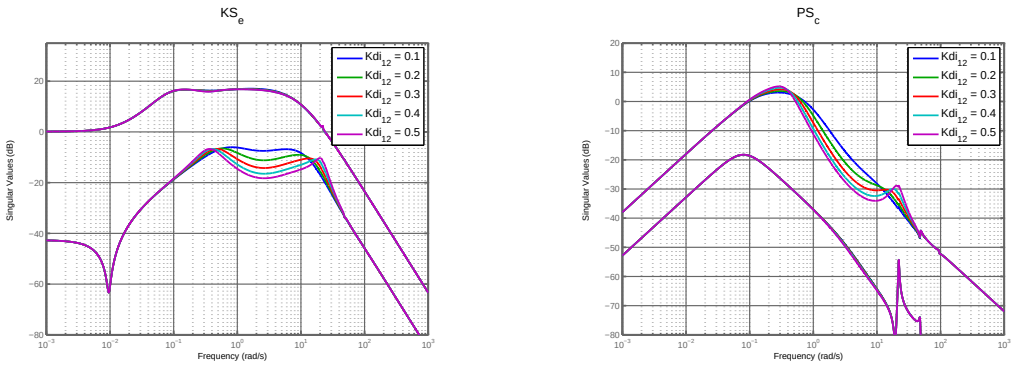

Figure 2.50: KS_e and PS_c(New Plume) : $K_{o_{centralized}}, K_{i_{centralized}}$

We compare the best designs obtain for New Engine Old Plume and New Engine New Plume using a centralized K_o and a centralized K_i.

New Engine Old Plume

$$K_i(s) = \begin{bmatrix} -0.5\,(s+0.5)\left(\frac{60}{s+60}\right)^3 & 0.3\,(s+1.9)\left(\frac{60}{s+60}\right)^3 \\ 0.013\,(s-7.81)\left(\frac{60}{s+60}\right)^3 & 0.01\,(s-26.76)\left(\frac{60}{s+60}\right)^3 \end{bmatrix}$$

$$K_o(s) = \begin{bmatrix} 0.16\left(\frac{s-0.05}{s}\right)\left(\frac{10}{s+10}\right)^2 & 0.9\left(\frac{s+0.167}{s}\right)\left(\frac{10}{s+10}\right)^2 \\ 3\left(\frac{s+0.06}{s}\right)\left(\frac{10}{s+10}\right)^2 & 0.537\left(\frac{s-0.05}{s}\right)\left(\frac{10}{s+10}\right)^2 \end{bmatrix} \tag{2.38}$$

New Engine New Plume

$$K_i(s) = \begin{bmatrix} -0.784\,(s-1.275)\left(\frac{60}{s+60}\right)^3 & -0.12\,(s+2.99)\left(\frac{60}{s+60}\right)^3 \\ 0.099\,(s-0.732)\left(\frac{60}{s+60}\right)^3 & -0.2183\,(s-0.0458)\left(\frac{60}{s+60}\right)^3 \end{bmatrix}$$

$$K_o(s) = \begin{bmatrix} 2\left(\frac{s+0.1}{s}\right)\left(\frac{10}{s+10}\right)^2 & -0.4715\left(\frac{s+0.15}{s}\right)\left(\frac{10}{s+10}\right)^2 \\ -6.5\left(\frac{s+0.06}{s}\right)\left(\frac{10}{s+10}\right)^2 & -0.2378\left(\frac{s+0.15}{s}\right)\left(\frac{10}{s+10}\right)^2 \end{bmatrix} \tag{2.39}$$

Table 2.10: Attained Closed Loop Properties($||.||_\infty$ in db) for NEOP and NENP Model

	$\|\|S_e\|\|_\infty$	$\|\|T_e\|\|_\infty$	$\|\|S_c\|\|_\infty$	$\|\|T_c\|\|_\infty$	$\|\|KS_e\|\|_\infty$	$\|\|PS_c\|\|_\infty$	v_{ts}	γ_{ts}
New Engine Old Plume	2.63	2.62	4.54	7.64	10.52	-0.23	59.3	22.6
New Engine New Plume	2.54	1.31	5.35	6.33	17.05	3.05	60.9	16.5

1. It is noticed that the properties at the controls slightly deteriorates for both New Engine Old Plume and New Engine New Plume when velocity is fed back along with the pitch in the inner loop as compared to when only pitch is fed back in the inner loop.

2. The properties at the output are decent for both New Engine Old Plume and New Engine New Plume.

After studying the closed loop properties using various structures of PI-PD controllers for New Engine Old Plume and New Engine New Plume, we come to the following conclusions.

1. A decentralized K_o and decentralized K_i ensure good properties at the error but not at the controls for both New Engine Old Plume and New Engine New Plume.

2. A decentralized K_o and a θ centralized K_i significantly improves properties at the controls for both New Engine New Plume and New Engine Old Plume. The properties at the output for New Engine Old Plume and New Engine New Plume are decent.

3. A decentralized K_o and a θ centralized K_i is sufficient to ensure good properties at both the loop breaking points for New Engine Old Plume but not New Engine New Plume.

4. A centralized K_o and a θ centralized K_i ensures good properties at both the loop breaking points for New Engine New Plume and New Engine Old Plume. However it is not necessary to use this particular PI-PD structure to get good properties for New Engine Old Plume as a decentralized K_o does the job.

5. A centralized K_o and centralized K_i ensures good properties at the error for both New Engine Old Plume and New Engine New Plume. However the properties at the controls slightly deteriorates when we feedback both velocity and pitch in the inner loop as compared to the

previous bullet where we just feedback pitch. Hence it is not a good idea to use a centralized K_i in the inner-loop.

2.3.2 H_∞ Mixed Sensitivity Control System Design for Hypersonic Longitudinal Dynamics

H_∞ Dynamic Output Feedback Controller Design. We now design the dynamic output feedback controller keeping the above mentioned bandwidth constraints in mind. Let us consider the generalized plant of the following form:

$$\begin{cases} \dot{x} = Ax + B_1 u + B_2 w \\ z = C_1 x + D_{11} u + D_{12} w \\ y = C_2 x + D_{21} u + D_{22} w \end{cases}$$

where $u = [FER\ \delta_e]^T$ is the input, $w = [r\ di]^T$ is the set of exogenous signals, $y = [Velocity\ \gamma]^T$ is the measured output and z is an output vector related to the performance of the closed loop system.

Weighted H_∞ Mixed Sensitivity Problem The standard weighted H_∞ mixed sensitivity problem is to find a finite dimensional real-rational proper internally stabilizing controller K that satisfies(Echols *et al.* (2015),Scherer *et al.* (1997))

$$K = \arg\{ \min_{K\ stabilizing} \gamma | \begin{bmatrix} W_1 S_e \\ W_2 K S_e \\ W_3 T_e \end{bmatrix}_\infty < \gamma \} \tag{2.40}$$

where S is the sensitivity transfer function, T is the complementary sensitivity transfer function of the closed loop system and KS is the control action.

The selection of exogenous signals has significant impact on the closed loop properties at the input and output loop breaking points. Selecting reference(r) to be the only reference signal will result in good properties at the output loop breaking point but not necessarily at the input loop breaking point. Similarly selecting exogenous signal to be d_i(input disturbance) will allow us to get good properties at the input loop breaking point but not necessarily at the output loop breaking point. Hence exogenous signal $w = [r\ d_i]^T$ has been used to shape closed loop maps at both the loop breaking points(Echols *et al.* (2015)).

$$K = \arg\{\min_{K \ stabilizing} \gamma | \begin{bmatrix} W_1 S_e & W_1 P S_c \\ W_2 K S_e & W_2 T_c \\ W_3 T_e & W_3 P S_c \end{bmatrix}_\infty < \gamma\} \tag{2.41}$$

Finding a internally stabilizing controller K that minimizes γ can be translated into an LMI optimization problem as shown below(Scherer *et al.* (1997),Gahinet *et al.* (1995),Gahinet (1996),Boyd *et al.* (1993),Duan and Yu (2013)):

$$\begin{aligned}
&\underset{\hat{A},\hat{B},\hat{C},\hat{D},X,Y}{\text{minimize}} \quad \gamma \\
&\text{s.t.} \quad \begin{bmatrix} AX + XA^T + B_2\hat{C} + (B_2\hat{C})^T & \hat{A}^T + (A + B_2\hat{D}C_2) & * & * \\ \hat{A} + (A + B_2\hat{D}C_2)^T & A^TY + YA + \hat{B}C + (\hat{B}C)^T & * & * \\ (B_1 + B_2\hat{D}D_{21})^T & (YB_1 + \hat{B}D_{21})^T & -\gamma I & * \\ C_1X + D_{12}\hat{C} & C_1 + D_{12}\hat{D}C_2 & D_{11} + D_{12}\hat{D}D_{21} & -\gamma I \end{bmatrix} < 0 \\
&\quad \begin{bmatrix} X & I \\ I & Y \end{bmatrix} > 0
\end{aligned}$$

After solving the optimization problem and obtaining the set of $\hat{A}$,$\hat{B}$,$\hat{C}$,$\hat{D}$,X,Y which minimizes γ, the dynamic output feedback controller is obtained as follows(Scherer *et al.* (1997)):

1. Find nonsingular matrices M,N which satisfies $MN^T = I - XY$

2. Construct the controller using

$$\begin{aligned}
D_K &= \hat{D} \\
C_K &= (\hat{C} - D_K C_2 X)M^{-T} \\
B_K &= N^{-1}(\hat{B} - YB_2D_K) \\
A_K &= N^{-1}(\hat{A} - NB_KC_2X - YB_2C_KM^T - Y(A + B_2D_KC_2)X)M^{-T}
\end{aligned} \tag{2.42}$$

Structure of Weighting functions for H_∞ Mixed Sensitivity Optimization. The structure of weighting functions which has been used to do the above optimization is shown below:

$$W_1 = \begin{bmatrix} \frac{s/M_{s_1} + \omega_{b_1}}{s + \omega_{b_1}\epsilon} & 0 & 0 \\ 0 & \frac{s/M_{s_2} + \omega_{b_2}}{s + \omega_{b_2}\epsilon} & 0 \\ 0 & 0 & 7e-05 \end{bmatrix}$$

$$W_2 = \begin{bmatrix} \frac{s+\omega_{bu_1}/M_{u_1}}{s\epsilon+\omega_{bu_1}\epsilon} & 0 \\ 0 & \frac{s+\omega_{bu_2}/M_{u_2}}{s\epsilon+\omega_{bu_2}} \end{bmatrix}$$

$$W_2 = \begin{bmatrix} \frac{s+\omega_{bc_1}/M_{y_1}}{s\epsilon+\omega_{bc_1}\epsilon} & 0 & 0 \\ 0 & \frac{s+\omega_{bc_2}/M_{y_2}}{s\epsilon+\omega_{bc_2}} & 0 \\ 0 & 0 & 7e-05 \end{bmatrix}$$

While designing the dynamic output feedback controller, the controller architecture has been selected to imitate a classical inner-outer loop structure to ensure that the designer won't have to design an inner loop controller and outer loop controller separately. The closed loop architecture has been shown in Figure 2.51 as follows(Echols *et al.* (2015)):

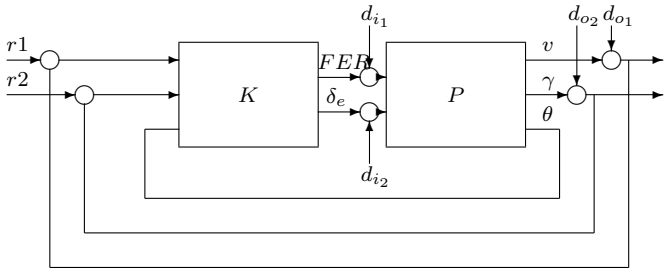

Figure 2.51: Topology of Dynamic Output Feedback Control System : Hypersonic

H_∞ Controller Synthesis

1. Augment the velocity and γ output channels of the plant with integrators so as to ensure integral action at low frequencies which would lead to zero steady state error to a step reference input.

2. In order to prevent cancellation of the lightly damped phugoid modes and integrator states by the H_∞ controller synthesis methodology, use bilinear transformation to shift the system slightly to the right half plane(Tsai *et al.* (1990),Folly (2007)). We use the following Bilinear transformation parameters for NEOP and NENP models of Hypersonic aircraft.

   The bilinear transformation parameters for both NEOP and NENP model are selected are as

follows:

$$p_1 = -0.0097 \tag{2.43}$$

$$p_2 = -10^{20} \tag{2.44}$$

The selection results in

Transform:

$$s = \frac{\hat{s} + p_1}{\frac{\hat{s}}{p_2} + 1} = \frac{\hat{s} - 0.0097}{\frac{\hat{s}}{-10^20} + 1} \approx \hat{s} - 0.0097 \tag{2.45}$$

Inverse Transform:

$$\tilde{s} \approx s + 0.0097 \tag{2.46}$$

3. Choose W1 to shape sensitivity transfer function to have good integral action at low frequencies and ensure that $||S||_\infty$ is below 8db. Choose W2 to shape the KS transfer function such that $||KS||_\infty$ is not too high which would prevent control signal saturation. Also ensure that KS rolls off at higher frequencies. Choose W3 so that $||T||_\infty$ is below 8 db and T rolls off at higher frequencies to ensure sensor noise attenuation at higher frequencies.

4. Create a generalized plant using $w = [r\ d_i]$ as the set of exogenous signals so that we get good properties at both input and output loop breaking points.

5. Minimize gamma by solving LMI. We use YALMIP(Lofberg (2004),Löfberg (2008))for solving the LMI. The parameter $\epsilon = 10^{-13}$ has been used while running the optimization.

6. Obtain the controller from the parameters returned by the optimization. Do inverse bilinear transformation to shift the controller to the left half plane so that it corresponds to the original untransformed plant.

7. Shift the integrators from the plant output to the controller input. In other words, augment the controller at the input with integrators.

8. Feed the θ state into the controller as the 3rd input as shown in Figure 2.51. This serves as the inner loop feedback as seen in a standard inner-outer feedback control architecture. Obtain the closed loop system using the final controller containing 3 inputs and 2 outputs and the original plant.

2.3.3 PI-PD Controller vs Dynamic Output Feedback Controller

In this subsection we compare the performance of a PI-PD controller to a dynamic output feedback controller. The following 3 cases are considered. To design a dynamic output feedback controller, the weighting functions W_1,W_2 and W_3 are designed to ensure good command following, good output disturbance and noise attenuation. W_2 is designed to limit the control action and the bandwidth of the controller so that the controller does not saturate. Bilinear transformation ($p_1 = -0.0097$,$p_2 = -10^{20}$)is used as mentioned in the previous subsection to avoid the cancellation of the phugoid modes. The H_∞ controller synthesis procedure is followed to obtain the dynamic output feedback controller.

Table 2.11: Weighting Function Parameters for New Engine Old Plume model

	W1	W2	W3
M1	5	0.01	5
M2	5	0.01	5
ω_1	0.01	200	50
ω_2	0.01	200	50
ϵ_1	0.001	0.0001	0.001
ϵ_2	0.001	0.0001	0.001

Table 2.12: Weighting Function Parameters for New Engine New Plume model

	W1	W2	W3
M1	1	0.1	5
M2	1	0.01	5
ω_1	0.04	100	50
ω_2	0.04	100	50
ϵ_1	0.001	0.001	0.001
ϵ_2	0.001	0.001	0.001

HINFSTRUCT command extends the classical H_∞ synthesis to fixed structure classical control systems. It uses specialized nonsmooth programming technique for solving structured H_∞ synthesis problems. HINFSTRUCT features a multi-start mode that automatically runs the optimization from multiple randomly selected initial points. This is not guaranteed to give us a global optimium. But it is observed that a few runs is enough to find a satisfactory design if it exists(Gahinet and Apkarian (2011a),Gahinet and Apkarian (2011b),Saussié *et al.* (2013),Yang *et al.* (2013))

HINFSTRUCT has been used to design 3 initial fixed structure PI-PD inner outer loop controllers . After obtaining the initial controllers, an exhaustive search is performed in the neighborhood of the previously obtained PI-PD parameters in order to obtain a set of values which would stabilize the closed loop system. While doing this search via brute force, we minimize $||S_{e1} - S_{e2}||_\infty$ (where S_{e1} corresponds to Output feedback controller and S_{e2} corresponds to PI-PD controller) in the low frequency range 0.0001 rads/sec to 0.01 rads/sec in order to ensure that we obtain the best PI-PD controller which gives us similar properties at the output loop breaking point when compared to the dynamic output feedback controller at low frequencies.The roll-off terms have been selected in a way so that the KS crossover frequency corresponding to the dynamic output feedback based closed loop system and the PI-PD based closed loop system is the same. This is done in order to ensure that we are in a position to compare two designs. For convenience, we use the following notations for the 3 PI-PD controllers.

1. K_o decentralized , K_i decentralized : $PI - PD_1$
2. K_o decentralized , K_i theta centralized : $PI - PD_2$
3. K_o centralized , K_i theta centralized : $PI - PD_3$

After exhaustive enumeration, the following PI-PD controllers were obtained.

$PI - PD_1$

1. New Engine Old plume :

$$K_i(s) = \begin{bmatrix} 0 \\ -1(s+3)\left[\frac{50}{(s+50)}\right]^3 \end{bmatrix}$$
$$K_o(s) = \begin{bmatrix} \frac{0.5(s+0.02)}{s}\left[\frac{0.5}{(s+0.5)}\right]^2 & 0 \\ 0 & \frac{-3(s+0.1)}{s}\left[\frac{0.5}{(s+0.5)}\right]^2 \end{bmatrix} \tag{2.47}$$

2. New Engine New Plume:

$$K_i(s) = \begin{bmatrix} 0 \\ -0.85(s+5)\left[\frac{60}{(s+60)}\right]^3 \end{bmatrix}$$
$$K_o(s) = \begin{bmatrix} \frac{2(s+0.02)}{s}\left[\frac{2}{(s+2)}\right]^3 & 0 \\ 0 & \frac{-6(s+0.12)}{s}\left[\frac{2}{(s+2)}\right]^3 \end{bmatrix} \tag{2.48}$$

$PI - PD_2$

1. New Engine Old Plume

$$K_i(s) = \begin{bmatrix} 0.25\,(s+3.25)\left(\frac{60}{s+60}\right)^3 \\ -0.1\,(s+4.715)\left(\frac{60}{s+60}\right)^3 \end{bmatrix}$$
$$K_o(s) = \begin{bmatrix} 0.19\left(\frac{s-0.194}{s}\right)\left(\frac{2}{s+2}\right)^3 & 2.6\left(\frac{s+0.1}{s}\right)\left(\frac{2}{s+2}\right)^3 \\ 3.5\left(\frac{s+0.075}{s}\right)\left(\frac{2}{s+2}\right)^3 & 0.48\left(\frac{s-0.0574}{s}\right)\left(\frac{2}{s+2}\right)^3 \end{bmatrix} \tag{2.49}$$

2. New Engine New Plume

$$K_i(s) = \begin{bmatrix} -0.3\,(s+2)\left(\frac{60}{s+60}\right)^3 \\ -0.05\,(s+1.6)\left(\frac{60}{s+60}\right)^3 \end{bmatrix}$$
$$K_o(s) = \begin{bmatrix} 2\left(\frac{s-0.01}{s}\right)\left(\frac{3}{s+3}\right)^3 & 0 \\ 0 & -0.2\left(\frac{s+0.37}{s}\right)\left(\frac{3}{s+3}\right)^3 \end{bmatrix} \tag{2.50}$$

$PI - PD_3$

1. New Engine Old Plume

$$K_i(s) = \begin{bmatrix} 0.25\,(s+3.25)\left(\frac{60}{s+60}\right)^3 \\ -0.1\,(s+4.715)\left(\frac{60}{s+60}\right)^3 \end{bmatrix}$$
$$K_o(s) = \begin{bmatrix} 0.19\left(\frac{s-0.194}{s}\right)\left(\frac{2}{s+2}\right)^3 & 2.6\left(\frac{s+0.1}{s}\right)\left(\frac{2}{s+2}\right)^3 \\ 3.5\left(\frac{s+0.075}{s}\right)\left(\frac{2}{s+2}\right)^3 & 0.48\left(\frac{s-0.0574}{s}\right)\left(\frac{2}{s+2}\right)^3 \end{bmatrix} \tag{2.51}$$

2. New Engine New Plume

$$K_i(s) = \begin{bmatrix} -0.3\,(s+2)\left(\frac{60}{s+60}\right)^3 \\ -0.05\,(s+1.6)\left(\frac{60}{s+60}\right)^3 \end{bmatrix}$$

$$K_o(s) = \begin{bmatrix} 2\left(\frac{s-0.01}{s}\right)\left(\frac{3}{s+3}\right)^3 & -1.2\left(\frac{s+0.26}{s}\right)\left(\frac{3}{s+3}\right)^3 \\ -5\left(\frac{s+0.08}{s}\right)\left(\frac{3}{s+3}\right)^3 & -0.2\left(\frac{s+0.37}{s}\right)\left(\frac{3}{s+3}\right)^3 \end{bmatrix} \tag{2.52}$$

Closed loop properties

Table 2.13: Attained Closed Loop Properties($||.||_\infty$ in db) for PI-PD and Dynamic Output Feedback Controller:New Engine Old Plume

	$\|\|S_e\|\|_\infty$	$\|\|T_e\|\|_\infty$	$\|\|S_c\|\|_\infty$	$\|\|T_c\|\|_\infty$	$\|\|KS_e\|\|_\infty$	$\|\|PS_c\|\|_\infty$	v_{ts}	γ_{ts}
Dynamic Controller	4.15	3.10	4.56	5.94	13.36	-6.07	55.21	34.39
$PI-PD_1$	5.85	3.65	15.69	15.71	16.79	0.14	78.63	38.02
$PI-PD_2$	5.64	5.84	7.51	8.56	16.33	-3.75	62.26	36.09
$PI-PD_3$	4.64	3.51	4.41	5.72	13.14	-6.87	61.63	15.21

Table 2.14: Attained Closed Loop Properties($||.||_\infty$ in db) for PI-PD and Dynamic Output Feedback Controller:New Engine New Plume

	$\|\|S_e\|\|_\infty$	$\|\|T_e\|\|_\infty$	$\|\|S_c\|\|_\infty$	$\|\|T_c\|\|_\infty$	$\|\|KS_e\|\|_\infty$	$\|\|PS_c\|\|_\infty$	v_{ts}	γ_{ts}
Dynamic Controller	4.97	3.02	7.61	7.12	19.86	-0.22	59.82	12.07
$PI-PD_1$	4.78	2.77	16.53	16.46	19.57	-2.56	54.65	15.31
$PI-PD_2$	5.2	4.97	9.67	9.02	20.81	-8.63	50.03	21.48
$PI-PD_3$	4.78	2.72	5.59	4.21	16.54	-0.764	64.15	16.67

From the above tables, we observe the following

1. $PI - PD_1$ offers better properties at the output loop breaking point for New Engine New Plume that New Engine Old Plume.

2. $PI - PD_1$ offers bad properties at the control for both New Engine Old Plume and New Engine New Plume. However the properties at the controls are worse for New Engine New Plume than New Engine Old Plume.

3. By introducing $K_i(1,1)$ element in $PI - PD_2$, we notice a significant improvement in the properties at the controls for both New Engine Old Plume and New Engine New Plume. However the properties at the controls are slightly worse for New Engine New Plume than New Engine Old Plume.

4. By making K_o centralized in PI_PD_3 while keeping K_i theta centralized, the close loop properties improve at the both the loop breaking points for New Engine Old Plume and New Engine New Plume.

Let us now compare the $|Se1 - Se2|$ and $|Sc1 - Sc2|$ plots of both the models where S_{e1} and S_{c1} corresponds to Dynamic output feedback controller and S_{e2} and S_{c2} corresponds to PI-PD controller as shown in the following figures.

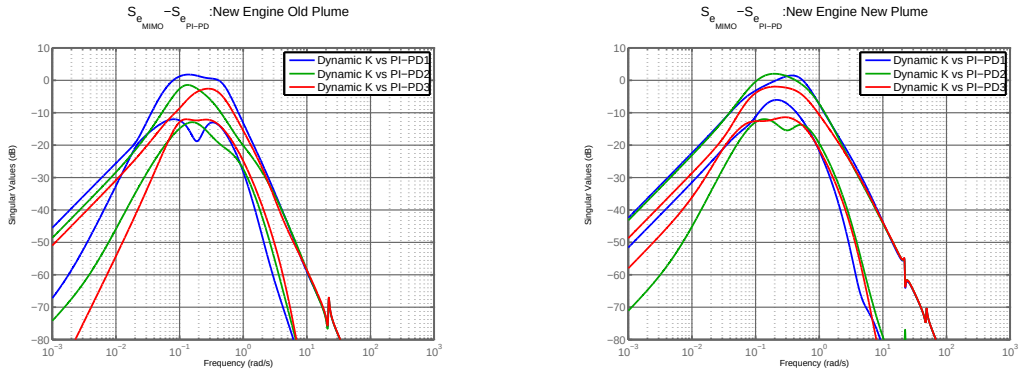

Figure 2.52: $|S_{e_{MIMO}} - S_{e_{PI-PD}}|$

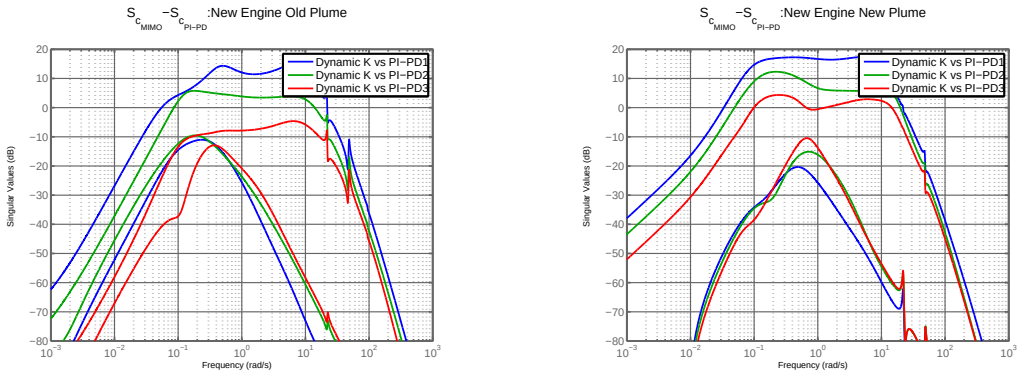

Figure 2.53: $|S_{c_{MIMO}} - S_{c_{PI-PD}}|$

From these plots we make the following observations.

1. $||S_{e_{MIMO}} - S_{e_{PI-PD}}||_\infty$ and the singular value at 0.01 rads/sec decreases as we increase the order of the PI-PD controller. This means that as we increase the order of the PI-PD controller, we can obtain similar closed loop properties at the output loop breaking point as obtained using a higher order dynamic output feedback controller. This is true for both New Engine Old Plume and New Engine New Plume.

2. $|S_{c_{MIMO}} - S_{c_{PI-PD}}|$ has very low singular values at low frequencies(-40 db at 0.01 rads/sec) which means that both the controllers would give similar properties at the input loop breaking point for New Engine Old Plume and New Engine New Plume when we are working at low frequencies. However at higher frequencies, $||S_{c_{MIMO}} - S_{c_{PI-PD}}||_\infty$ is greater than zero for New Engine New Plume. Hence the dynamic feedback controller would not approximate the PI-PD controller at the controls when working at higher frequencies. Also we can better approximate the closed loop properties of dynamic output feedback controller at the controls using a PI-PD controller if we increase the order of the PI-PD controller.

In the following figures we compare the frequency domain and time domain plots of various closed loop properties for both PI-PD and dynamic output feedback controller based closed loop system for New Engine Old Plume and the New Engine New Plume model of the hypersonic vehicle.

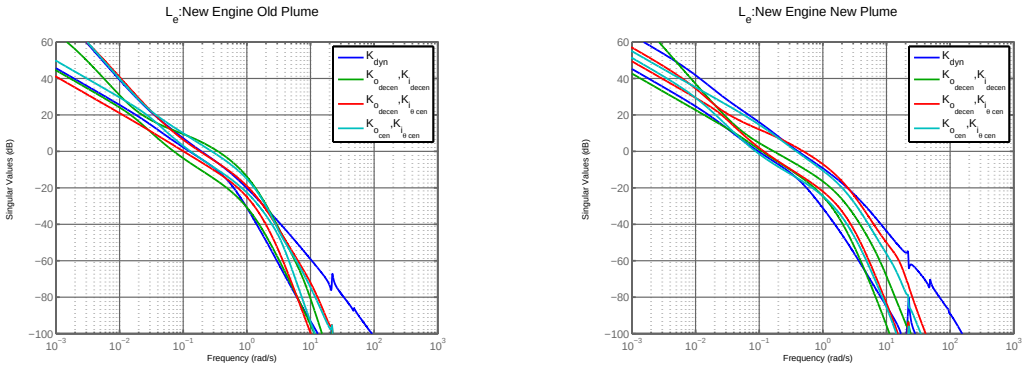

Figure 2.54: Open Loop Singular Values at Error

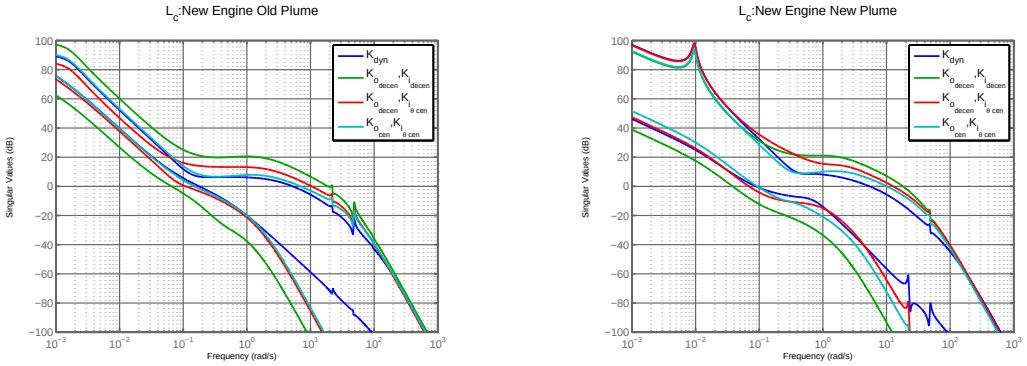

Figure 2.55: Open Loop Singular Values at Control

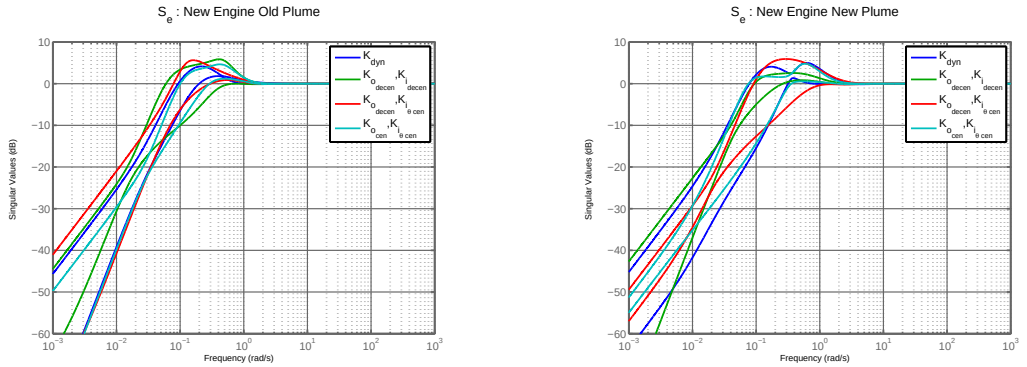

Figure 2.56: Sensitivity at Error

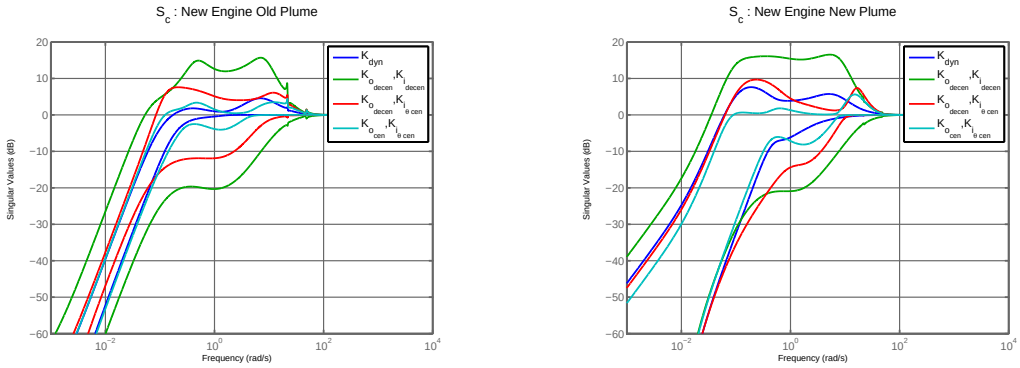

Figure 2.57: Sensitivity at Control

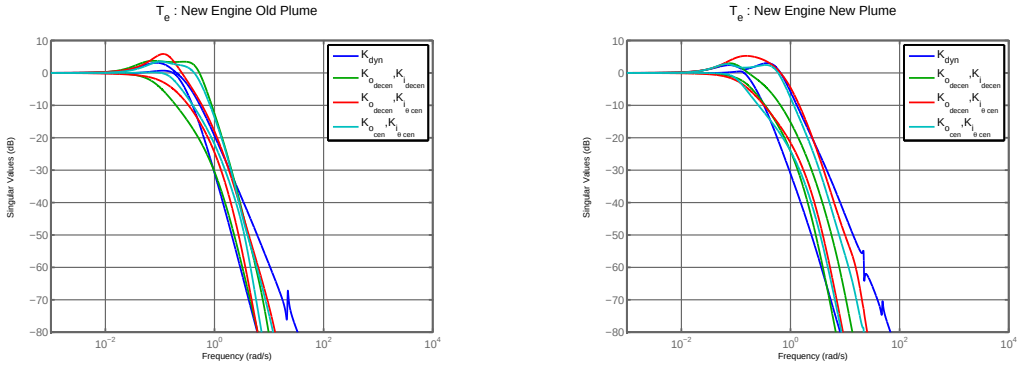

Figure 2.58: Complementary Sensitivity at Error

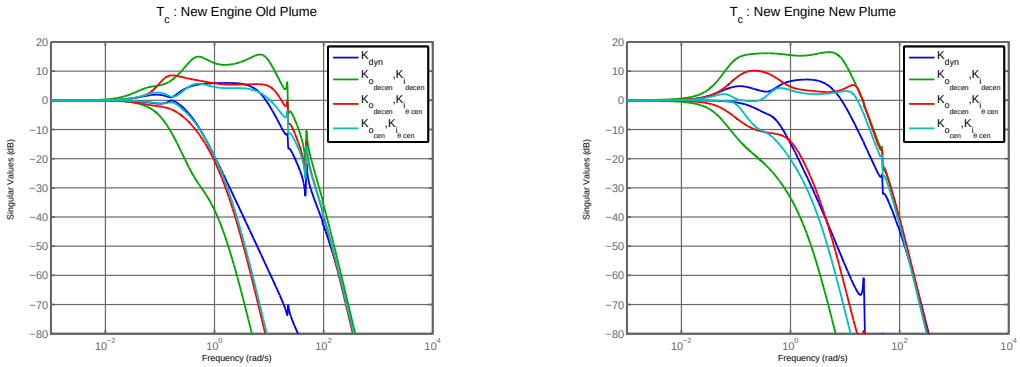

Figure 2.59: Complementary Sensitivity at Control

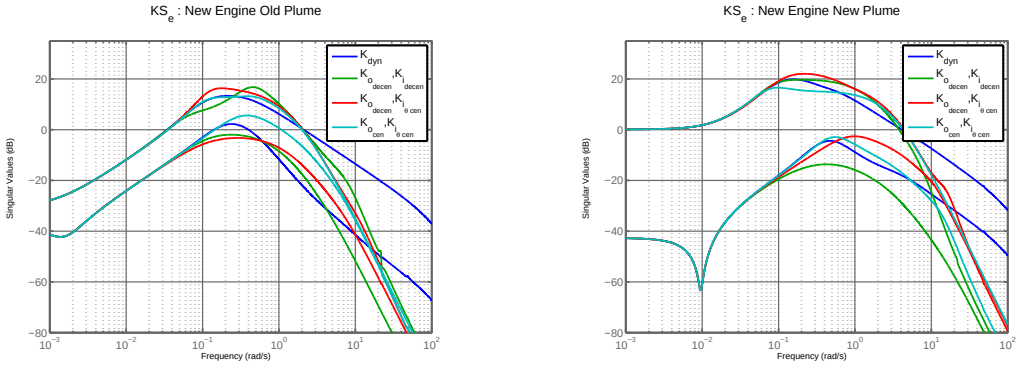

Figure 2.60: Control Action

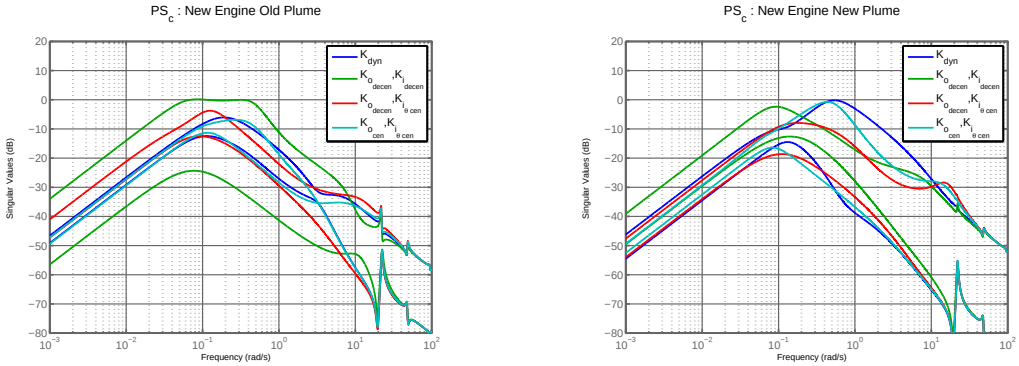

Figure 2.61: Input Disturbance Attenuation

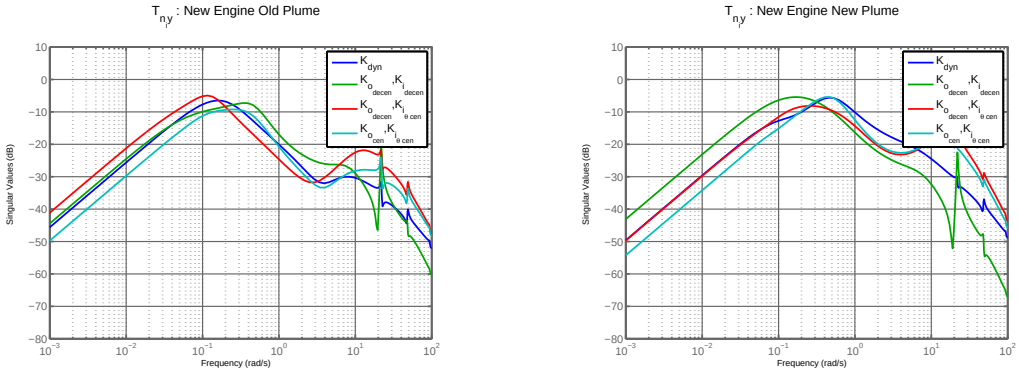

Figure 2.62: $T_{n_i \to y}$

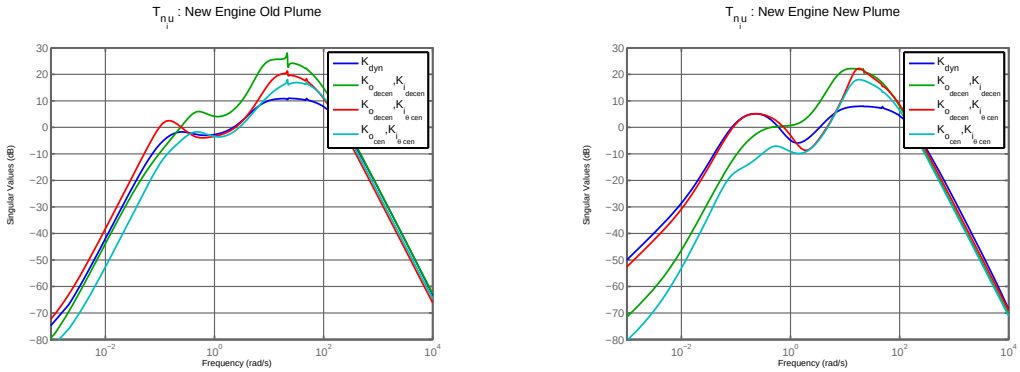

Figure 2.63: $T_{n_i \to u_p}$

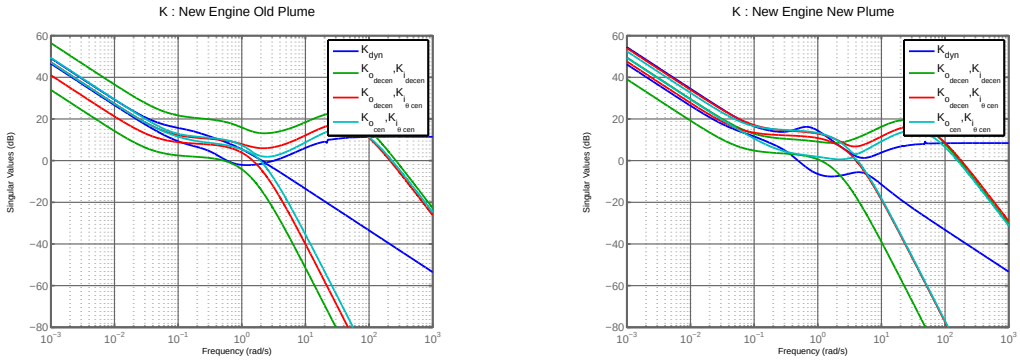

Figure 2.64: Controller Singular Values

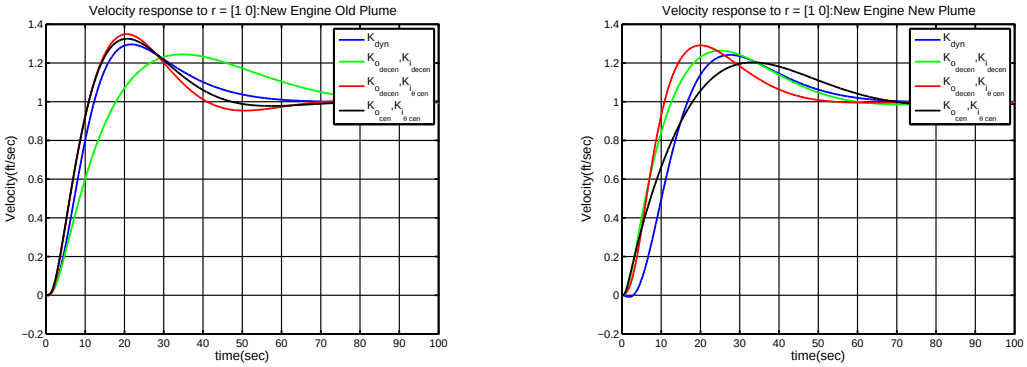

Figure 2.65: Velocity Response to $r = [1\ 0]$

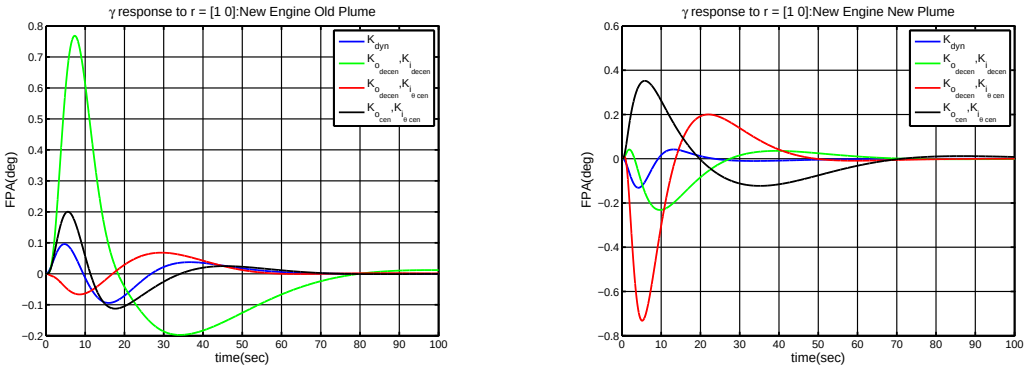

Figure 2.66: FPA Response to $r = [1\ 0]$

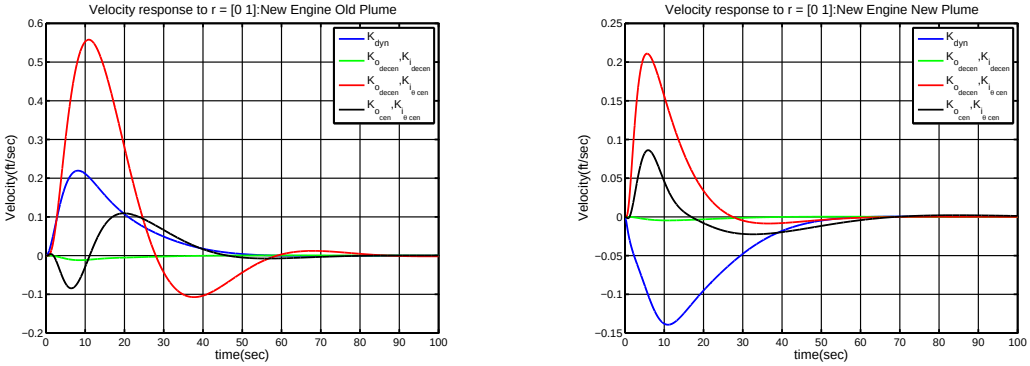

Figure 2.67: Velocity Response to $r = [0\ 1]$

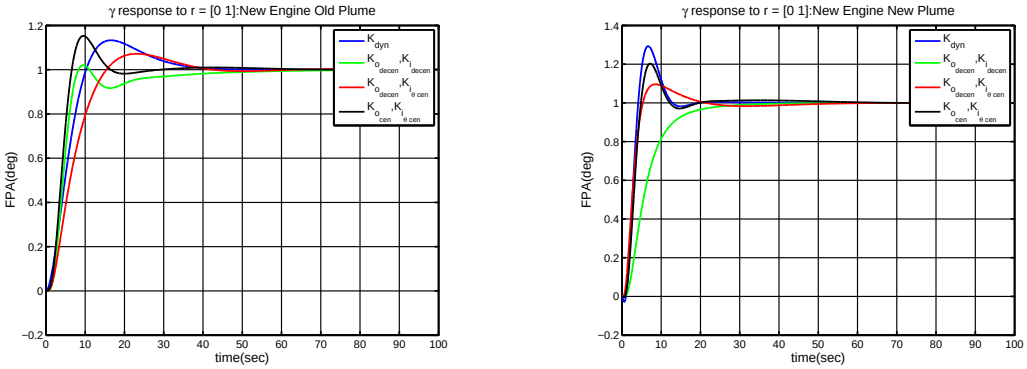

Figure 2.68: FPA Response to $r = [0\ 1]$

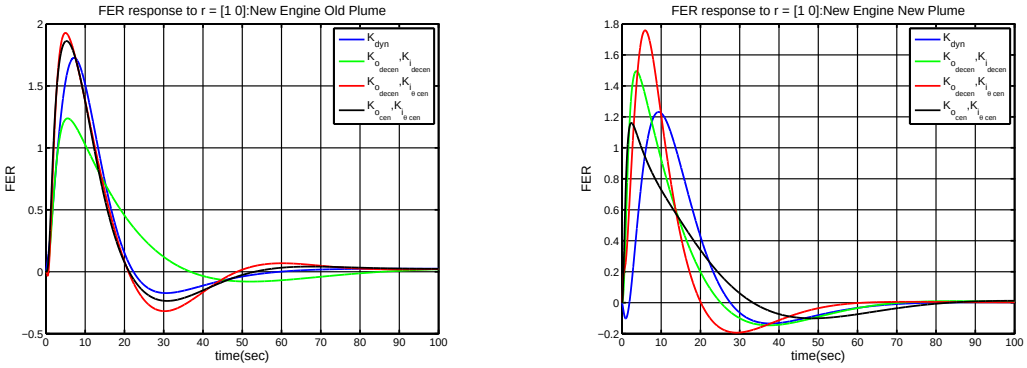

Figure 2.69: FER Response to $r = [1\ 0]$

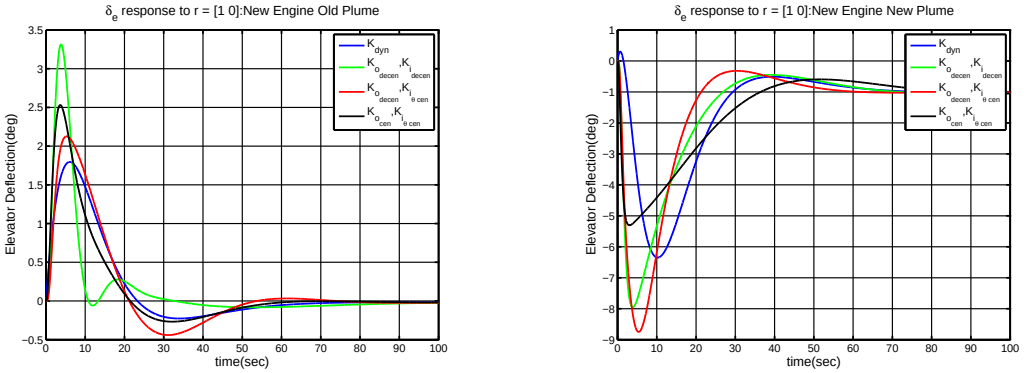

Figure 2.70: Elevator Response to $r = [1\ 0]$

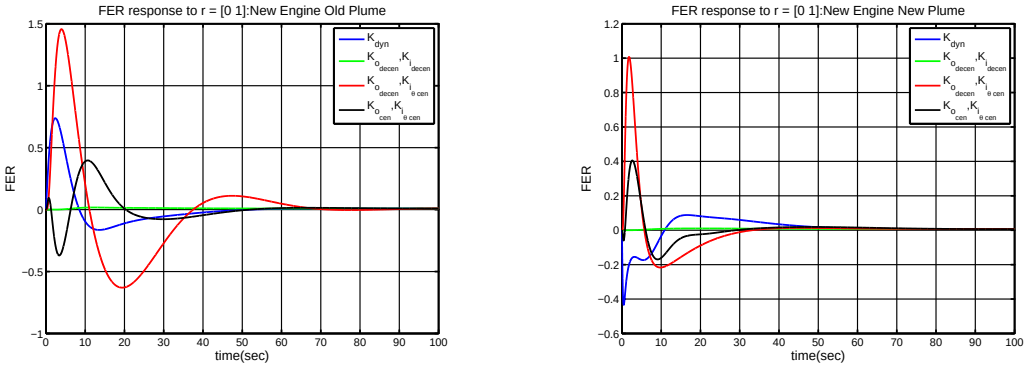

Figure 2.71: FER Response to $r = [0\ 1]$

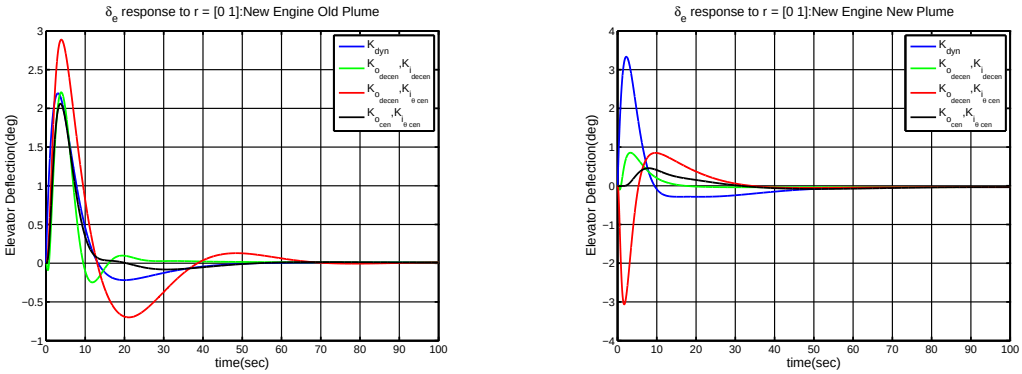

Figure 2.72: Elevator Response to $r = [0\ 1]$

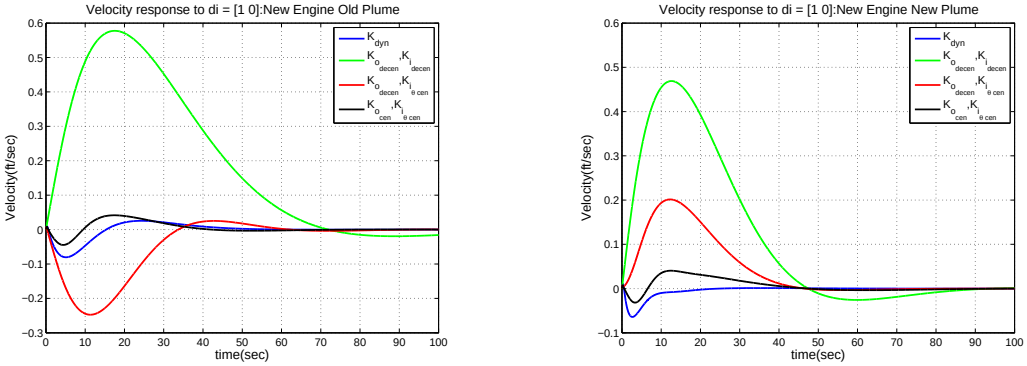

Figure 2.73: Velocity Response to $di = [1\ 0]$

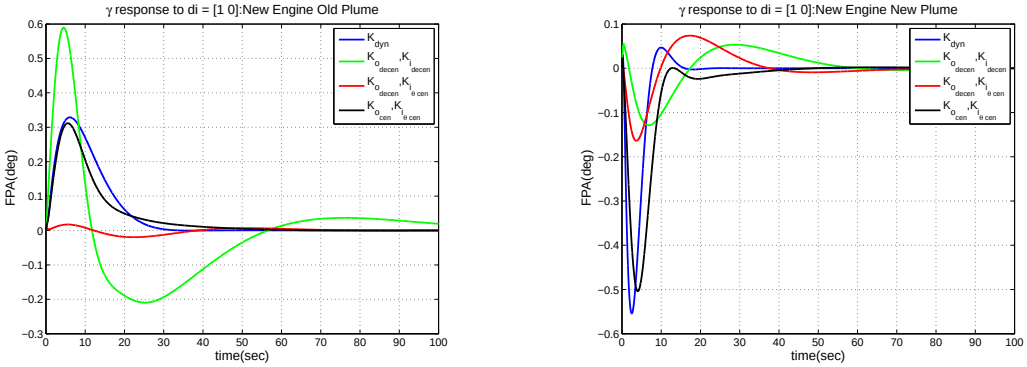

Figure 2.74: FPA Response to $di = [1\ 0]$

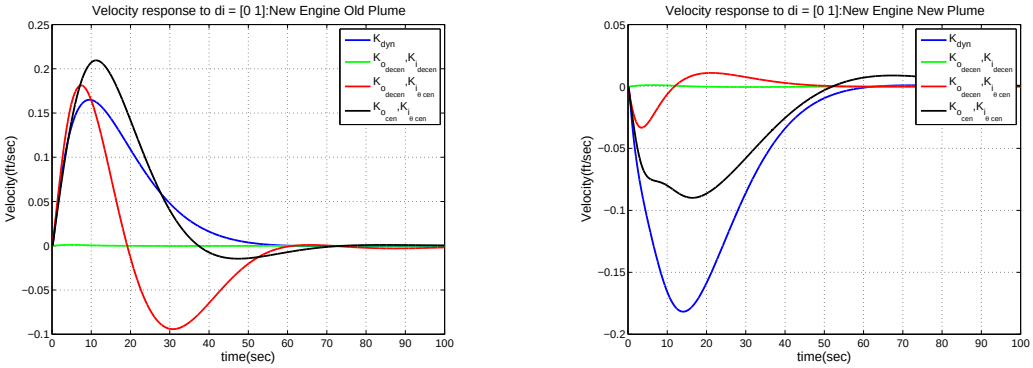

Figure 2.75: Velocity Response to $di = [0\ 1]$

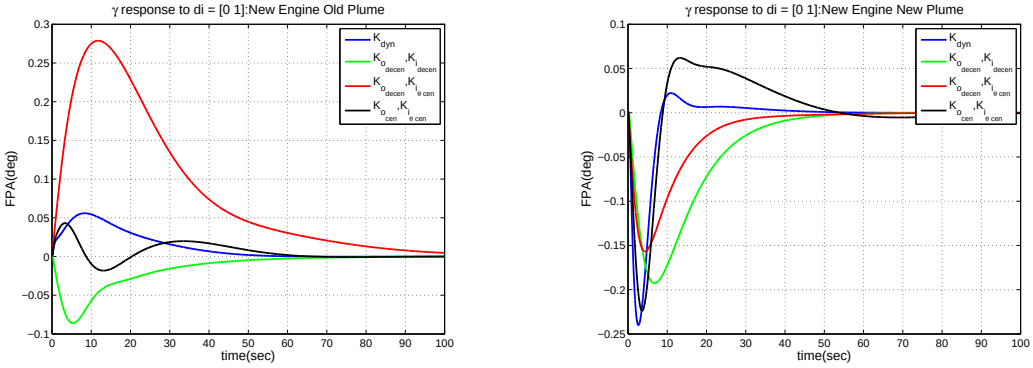

Figure 2.76: FPA Response to $di = [0\ 1]$

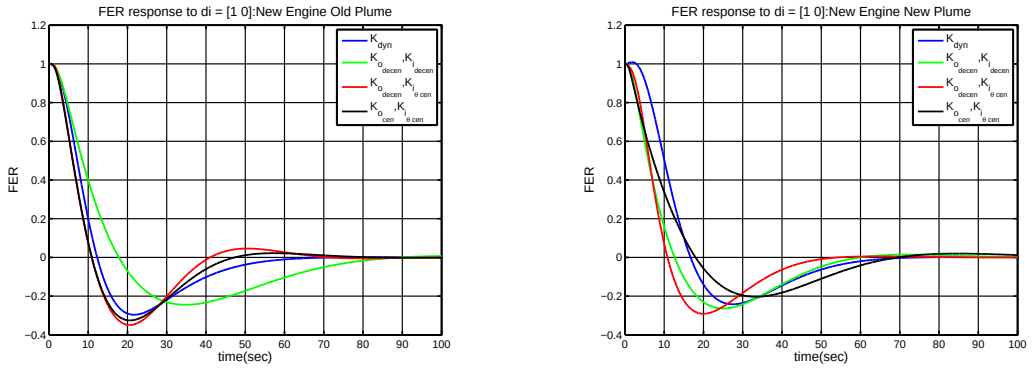

Figure 2.77: FER Response to $di = [1\ 0]$

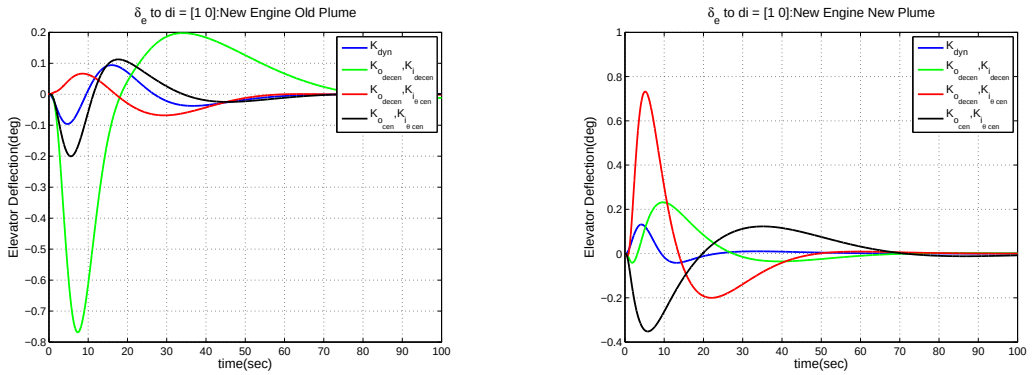

Figure 2.78: Elevator Response to $di = [1\ 0]$

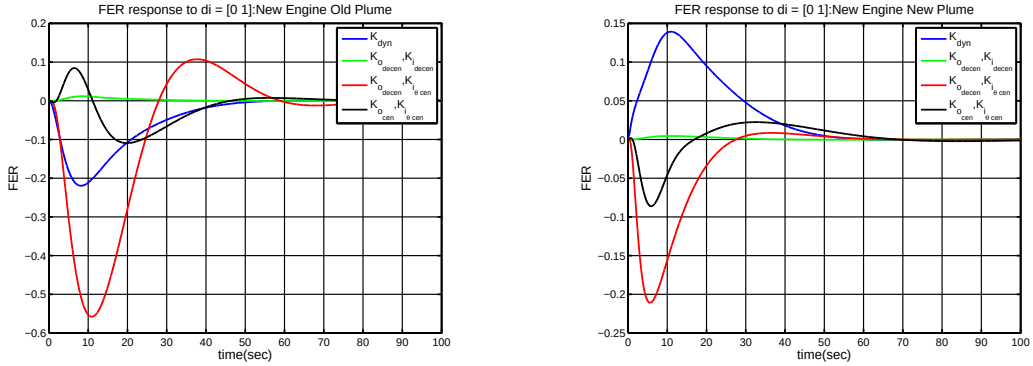

Figure 2.79: FER Response to $di = [0\ 1]$

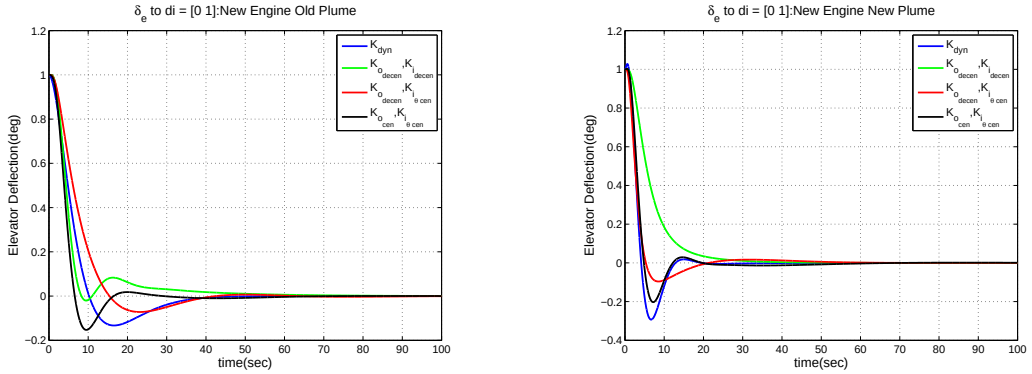

Figure 2.80: Elevator Response to $di = [0\ 1]$

2.4 Lead and Lag Compensator with Real/Complex Poles and Zeros

In the section,we discuss the design methodology for Inner-Outer loop control design using complex/real lead lag compensators. These compensators are cascaded to modify the gain and phase properties of the open loop frequency response to achieve closed loop performance specifications for command following, noise attenuation, disturbance attenuation etc.

2.4.1 Real Lead/Lag Compensator

Lead networks are the systems which contribute phase lead to compensate the phase lag associated with many physical systems. Lead systems are typically used to increase the phase margin at the 0 db crossover frequency.For a phase lead greater than 90 deg, multiple leads may be cascaded together. Cascaded lead networks may also be used to introduce a phase lead less than 90 deg because the gain of a single lead network with a phase lead greater than 60 deg is large as compared to the gain of n cascaded lead networks, each contributing $\frac{1}{n}$ of the desired phase lead. The lead network is of the form (Messner *et al.* (2007)):

$$K(s) = \alpha \left(\frac{s+z}{s+\alpha z} \right), \alpha > 1 \tag{2.53}$$

$$\angle K(j\omega) = \tan \frac{\omega}{z} - \tan \frac{\omega}{\alpha z} \tag{2.54}$$

The zero at $s = -z$ is closer to the origin than the pole at $s = -\alpha z$, so the angle of the numerator is greater than equal to that of the denominator. Hence $\angle K(j\omega) \geq 0$ for all ω. The lead network can also be considered as a high pass system.The frequency of maximum phase lead is $\omega_m = \sqrt{\alpha} z$

Lag networks are used to increase the loop gain to improve low frequency(steady state) command following and disturbance attenuation or decrease the high frequency loop gain for improved sensor noise attenuation while maintaining a set of desirable closed loop poles without introducing too much lag. The lag network is of the form(Messner *et al.* (2007)):

$$K(s) = \frac{1}{\alpha} \left(\frac{s+\alpha p}{s+p} \right), \alpha > 1 \tag{2.55}$$

$$\angle K(j\omega) = \tan \frac{\omega}{\alpha p} - \tan \frac{\omega}{p} \tag{2.56}$$

The pole at $s = -p$ is closer to the origin than the zero at $s = -\alpha p$, so the angle of the denominator is greater than or equal to the numerator . Hence $\angle K(j\omega) \leq 0$ for all ω. Since lag systems are used to alter the magnitude properties of the loop, it is their magnitude characteristic that is most exploited. Lag network can also be considered as a low pass system. The frequency of maximum phase lag is $\omega_m = \sqrt{\alpha}p$.

2.4.2 Complex Lead/Lag compensators

The simplest cascade of a lead network is the square of a lead network. This is called a double lead compensator which has a maximum phase lead of $2\phi_m$. It is of the form (Messner *et al.* (2007))

$$K^2(s) = \alpha^2 \left(\frac{s+z}{s+\alpha z} \right)^2 = \frac{\omega_d}{\omega_n} \left(\frac{s^2 + 2\zeta_n \omega_n s + \omega_n^2}{s^2 + 2\zeta_d \omega_d s + \omega_d^2} \right) \tag{2.57}$$

The complex lead/lag compensator is a type of double lead/lag compensator in which the poles and zeros are complex conjugates with the same damping ratio. The equal damping ratio ζ provides symmetry to the phase peak.

$$K_{complex}(s) = \frac{\omega_p}{\omega_z} \left(\frac{s^2 + 2\zeta \omega_z s + \omega_z^2}{s^2 + 2\zeta \omega_p s + \omega_p^2} \right) \tag{2.58}$$

The maximum phase lead/lag offered by the complex lead/lag compensator is $2\phi_m$ at frequency $\omega_m = \sqrt{\omega_p \omega_z}$. The frequency of the maximum phase lead/lag is the geometric mean of the natural frequencies of the zeros and poles. This is analogous to ω_m for real lead/lag compensator. While designing the compensator, we have two parameters ζ and ϕ_m to form the complex lead/lag compensator. The expressions of ω_p and ω_z are as follows :

$$\omega_p = \omega_m(\zeta \tan \phi_m + \sqrt{\zeta^2 \tan^2 \phi_m + 1})$$

$$\omega_z = \omega_m(-\zeta \tan \phi_m + \sqrt{\zeta^2 \tan^2 \phi_m + 1})$$

2.4.3 Inner Outer Control Design Using Real Lead Networks

In this subsection we discuss the inner-outer loop control system design for the SISO plant (δ_e to FPA) of the New Engine Old Plume and New Engine New Plume models. A real lead network has been designed for the inner loop and a lead network multiplied by an integrator has been designed for the outer loop. The following is the steps followed to design the lead networks.

For the inner loop,a lead network has been designed to satisfy the following specifications

1. Phase Margin of 60 deg for L_i

2. Gain crossover frequency ω_{g_i} of L_i/L_c to be between 6 rads and 10 rads/sec.

For the lead network in the inner loop we propose the following lead structure.

$$K_{inner} = g\left(\frac{s+z}{s+\alpha z}\right)^n \alpha > 1 \tag{2.59}$$

This lead network provides a maximum phase lead at the frequency that we desire (Gain crossover frequency of L_i) and ensures robustness at the input by increasing the phase margin.

The following steps are followed to obtain the compensator

1. Choose the gain crossover frequency($6 <= \omega_{g_i} <= 10$) of L_i.

2. Calculate the maximum phase (ϕ_m) which the lead network should provide to ensure a $PM = 60\,\text{deg}$ at the desired crossover frequency ω_{g_i} of L_i using the phase of P_1 (elevator to theta) at ω_{g_i}

3. Choose n = number of desired cascaded lead networks to be used for the design.

4. Calculate $\alpha = \frac{1+\sin\frac{\phi_m}{n}}{1-\sin\frac{\phi_m}{n}}$ and $z = \frac{w_{g_i}}{\sqrt{\alpha}}$

5. Calculate K using the parameters in the previous steps.

6. Calculate $L_{nominal}(initial) = P_1 * (K)^n$

7. Calculate $g = \frac{1}{|L_{nominal}(jwg)|}$

8. Obtain the final controller $K_{inner} = g\left(\frac{s+z}{s+\alpha z}\right)^n$.

After the controller has been designed for the inner loop, we use the modified plant $P_{mod} = \frac{P_1}{1+P_1K_{inner}}P_2$ to design the lead network for the outer loop.The compensator for the outer loop has been designed to satisfy the following specifications

1. Zero steady state tracking for step reference commands.

2. Phase Margin of 60 deg at the output loop breaking point.

3. Gain crossover frequency ω_{g_o} of $L_o <= 0.7$ rads/sec

For the compensator in the outer loop, we propose the following structure of the lead network

$$K = \frac{g}{s}\left(\frac{s+z}{s+\alpha z}\right)^n = K_o K_{lead}, \alpha > 1 \tag{2.60}$$

The integrator in K ensures zero steady state error to step reference commands. The lead network provides the phase lead at the desired frequency (Gain crossover frequency ω_{g_i} of L_o). The following steps are followed to obtain the compensator

1. Choose the desired gain crossover frequency($\omega_{g_o} <= 0.7$) of L_o.
2. Calculate the maximum phase (ϕ_m) which the lead network should provide to ensure a $PM =$ 60 deg at the desired crossover frequency w_{g_o} of L_o using the phase of $P_{mod}P_2$ at ω_{g_o}.
3. Choose $n =$ number of desired cascaded lead networks to be used for the design.
4. Calculate $\alpha = \frac{1+\sin\frac{\phi_m}{n}}{1-\sin\frac{\phi_m}{n}}$ and $z = \frac{\omega_{g_o}}{\sqrt{\alpha}}$
5. Calculate K using the parameters in the previous steps.
6. Calculate $L_{nominal}(initial) = P_{mod}P_2 * (K)^n$
7. Calculate $g = \frac{1}{|L_{nominal}(j\omega_{g_o})|}$
8. Obtain the final controller $K = \frac{g}{s}\left(\frac{s+z}{s+\alpha z}\right)^n$.

2.4.4 Inner Outer Control Design Using Complex Lead Networks

In this subsection we discuss the inner-outer loop control system design for the SISO plant (δ_e to FPA) of the New Engine Old Plume and New Engine New Plume models using complex lead networks. A complex lead network has been designed for the inner loop and a complex lead network multiplied by an integrator has been designed for the outer loop. The following is the steps followed to design the complex lead networks.

Two complex lead networks are proposed for the inner loop and the outer loop respectively. The compensator for the inner loop has been designed to satisfy the following specifications

1. Phase Margin of 60 deg for L_i
2. Gain crossover frequency ω_{g_i} of L_i/L_c to be between 6 rads and 10 rads/sec.

For the compensator in the inner loop we propose the following lead structure.

$$K_{inner} = g\left(\frac{s^2 + 2\zeta\omega_z s + \omega_z^2}{s^2 + 2\zeta\omega_p s + \omega_p^2}\right)^n \tag{2.61}$$

This lead network provides a maximum phase lead $2\phi_m$ at the frequency that we desire and ensures robustness at the input by increasing the PM.The following steps are followed to obtain the compensator.

1. Choose the gain crossover frequency ($6 <= wg <= 10$) of Li and damping factor ζ of the poles/zeros of the lead network.
2. Calculate the maximum phase (ϕ_m) which the lead network should provide to ensure a $PM = 60$ at the desired crossover frequency ω_{g_i} of L_i. using the phase of P_1 (δ_e to θ) at ω_{g_i}.
3. Choose n = number of desired cascaded lead networks to be used for the design.
4. Calculate $w_p = w_{g_i}\left(\zeta tan(\frac{\phi_m}{2n}) + \sqrt{\zeta^2 tan(\frac{\phi_m}{2n})^2 + 1}\right)$.
5. Calculate $w_z = w_{g_i}\left(-\zeta tan(\frac{\phi_m}{2n}) + \sqrt{\zeta^2 tan(\frac{\phi_m}{2n})^2 + 1}\right)$.
6. Obtain $K = \left(\frac{s^2+2\zeta\omega_z s+\omega_z^2}{s^2+2\zeta\omega_p s+\omega_p^2}\right)$.
7. Calculate $L_{nominal}(initial) = P1 * (K)^n$.
8. Calculate $g = \frac{1}{|L_{nominal}(jwg)|}$.
9. Obtain the final controller $K = g\left(\frac{s^2+2\zeta\omega_z s+\omega_z^2)}{s^2+2\zeta\omega_p s+\omega_p^2}\right)^n$.

After the controller has been designed for the inner loop, we use the modified plant $P_{mod} = \frac{P_1}{1+P_1 K_{inner}} P_2$ to design the lead network for the outer loop.The compensator for the outer loop has been designed to satisfy the following specifications.

1. Zero steady state tracking for step reference commands
2. Phase margin of 60 deg at the output.
3. Gain crossover frequency ω_{g_o} of $L_o <= 0.7$ rads/sec

For the compensator in the outer loop, we propose the following structure of the lead network

$$K = \frac{g}{s}\left(\frac{s^2 + 2\zeta\omega_z s + \omega_z^2)}{s^2 + 2\zeta\omega_p s + \omega_p^2}\right)^n \tag{2.62}$$

The integrator in K ensures zero steady state error to step reference commands. The lead network provides the phase lead at the desired frequency.The following steps are followed to obtain the compensator.

1. Choose the gain crossover frequency($\omega_{g_o} <= 0.7$) of L_o and damping factor ζ of the poles/zeros of the lead network.
2. Calculate the maximum phase (ϕ_m) which the lead network should provide to ensure a $PM = 60\,\text{deg}$ at the desired crossover frequency ω_{g_o} of L_o using the phase of P_{mod} at ω_{g_o}.
3. Choose n = number of desired cascaded lead networks to be used for the design.
4. Calculate $w_p = w_{g_o}\left(\zeta tan(\frac{\phi_m}{2n}) + \sqrt{\zeta^2 tan(\frac{\phi_m}{2n})^2 + 1}\right)$.
5. Calculate $w_z = w_{g_o}\left(-\zeta tan(\frac{\phi_m}{2n}) + \sqrt{\zeta^2 tan(\frac{\phi_m}{2n})^2 + 1}\right)$.
6. Obtain $K = \left(\frac{s^2+2\zeta\omega_z s+\omega_z^2}{s^2+2\zeta\omega_p s+\omega_p^2}\right)$.
7. Calculate $L_{nominal}(initial) = P1 * (K)^n$.
8. Calculate $g = \frac{1}{|L_{nominal}(jwg)|}$.
9. Obtain the final controller $K = \frac{g}{s}\left(\frac{s^2+2\zeta\omega_z s+\omega_z^2)}{s^2+2\zeta\omega_p s+\omega_p^2}\right)^n$.

2.4.5 Surgical Insertion of Lead-Lag Networks

In the following subsection, real lead-lag elements have been surgically inserted in the hierarchical inner outer PI-PD control structure to further improve the closed loop properties at both the loop breaking points. A real lead-lag network of the following structures are considered :

1. **Lead Network**

$$K(s) = \alpha\left(\frac{s+z}{s+\alpha z}\right), \alpha > 1 \tag{2.63}$$

$$\angle K(j\omega) = \tan\frac{\omega}{z} - \tan\frac{\omega}{\alpha z} \tag{2.64}$$

The frequency of maximum phase lead is $\omega_m = \sqrt{\alpha}z$

2. **Lag Network**

$$K(s) = \frac{1}{\alpha}\left(\frac{s+\alpha p}{s+p}\right), \alpha > 1 \tag{2.65}$$

$$\angle K(j\omega) = \tan\frac{\omega}{\alpha p} - \tan\frac{\omega}{p} \tag{2.66}$$

The frequency of maximum phase lag is $\omega_m = \sqrt{\alpha}p$.

First, let us consider $K_{o_{decentralized}}$, $K_{i_{\theta centralized}}$. In this controller we have the option of adding lead-lag networks at 4 different positions i.e. 2 in K_i and 2 in K_o. Using brute force enumeration, lead networks were added to elements of K_i to add phase lead at specific frequencies to improve the closed loop properties. Similarly lag networks were added to K_o at specific frequencies to further improve the properties.

Step 1

In the initial step, a lead network $\frac{1.8s+0.1342}{s+0.1342}$ was introduced in the $K_i(2,2)$ position to introduce phase lead $\phi_m = 17\,\text{deg}$ at $\omega = 0.1$ rads/sec. This leads to the following change in the closed loop properties.

1. $||S_e||_\infty$ decreases (5.9db $\rightarrow$ 3.6db)
2. $||S_c||_\infty$ decreases (9.7db $\rightarrow$ 8.3db)
3. $||KS_e||_\infty$ decreases (22db $\rightarrow$ 20db)
4. $||PS_c||_\infty$ decreases (-8db $\rightarrow$ -9.4db)
5. $t_{sett_{pitch}}$ increases (17sec $\rightarrow$ 28sec)

Step 2

In step 2, a lead network $\frac{2s+18.38}{s+18.38}$ was added in $K_i(1,1)$ position to introduce phase lead $\phi_m = 19.5\,\text{deg}$ at $\omega = 13$ rads/sec. This leads to increase in the unity crossover frequency of L_c from 12.5 rads/sec to 18.5 rads/sec without any deterioration of the closed loop properties at both the loop breaking points. This shows that as we increases the order and complexity of the controller, we can push bandwidth higher without much deterioration of the closed loop properties even though the flexible modes put a upper bound on the achievable bandwidth.

Step 3

In step 3, a lead network $\frac{3s+1.732}{s+1.732}$ was added in $K_o(1,1)$ position to introduce phase lead $\phi_m = 30\,\text{deg}$ at $\omega = 1$ rads/sec. This leads to the following change in the closed loop properties.

1. $||S_e||_\infty$ decreases (3.7db $\rightarrow$ 2.8db)
2. $||KS_e||_\infty$ increases (20db $\rightarrow$ 22db)
3. $||PS_c||_\infty$ decreases (-9.4db $\rightarrow$ -10.4db)
4. $t_{sett_{vel}}$ increases (48sec $\rightarrow$ 52 sec)

Step 4

In step 4, a lead network $\frac{5s+15.65}{s+15.65}$ was added in $K_o(2,2)$ position to introduce a phase lead $\phi_m = 42\,\text{deg}$ at $\omega = 7$ rads/sec. This leads to the following change in the closed loop properties.

1. $||S_e||_\infty \downarrow$ (2.8db $\rightarrow$ 2.3db)

$K_{o_{decen}}, K_{i_{\theta cen}}$ **with surgically inserted lead networks :**

$$K_i(s) = \begin{bmatrix} -0.38\,(s+1.5)\left(\frac{2s+18.38}{s+18.38}\right) \\ -0.08\,(s+14)\left(\frac{1.8s+0.13}{s+0.13}\right) \end{bmatrix} K_o(s) = \begin{bmatrix} 4\left(\frac{s+0.06}{s}\right)\left(\frac{3s+1.73}{s+1.73}\right) & 0 \\ 0 & -5\left(\frac{s+0.1}{s}\right)\left(\frac{5s+15.65}{s+15.65}\right) \end{bmatrix} \tag{2.67}$$

Table 2.15: Comparison of Closed Loop Properties($||.||_\infty$ in db) for $K_{o_{decentralized}}$,$K_{i_{\theta centralized}}$ and Surgical Insertion of Leads : New Engine New Plume

	$\|\|S_e\|\|_\infty$	$\|\|T_e\|\|_\infty$	$\|\|S_c\|\|_\infty$	$\|\|T_c\|\|_\infty$	$\|\|KS_e\|\|_\infty$	$\|\|PS_c\|\|_\infty$	v_{ts}	γ_{ts}
$K_{o_{decen}}, K_{i_{\theta cen}}$	5.89	5.25	9.66	10.16	22.04	-7.97	46.80	17.65
Surgical Insertion	2.31	3.71	8.28	7.86	22.68	-10.47	51.89	28.78

Now let us consider $K_{o_{cen}}$, $K_{i_{\theta cen}}$. In this controller we have the option of adding lead-lag networks at 6 different positions i.e. 2 in K_i and 4 in K_o. Using brute force enumeration, it was realized that insertion of lead networks leads to deterioration in the properties irrespective of the frequency where the phase lead may be inserted. However, it was seen that insertion of lag network

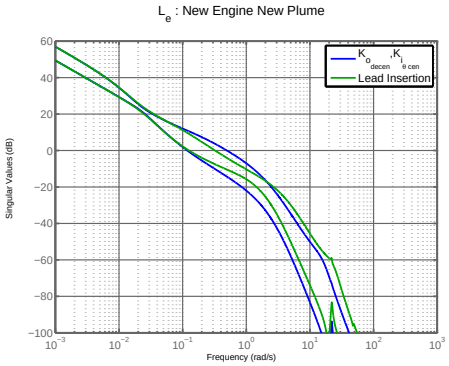

Figure 2.81: L_e : Lead Insertion

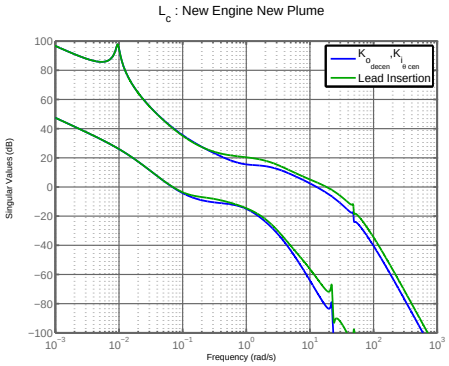

Figure 2.82: L_c : Lead Insertion

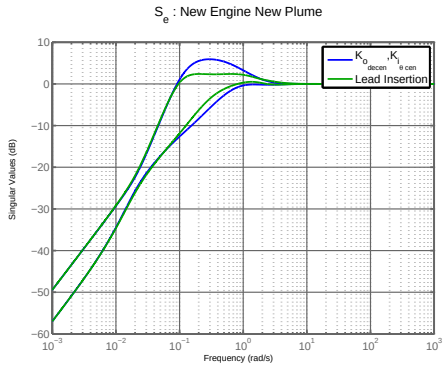

Figure 2.83: S_e : Lead Insertion

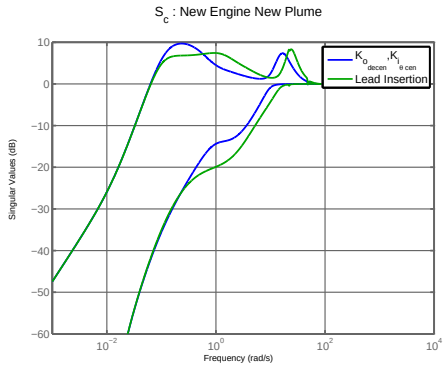

Figure 2.84: S_c : Lead Insertion

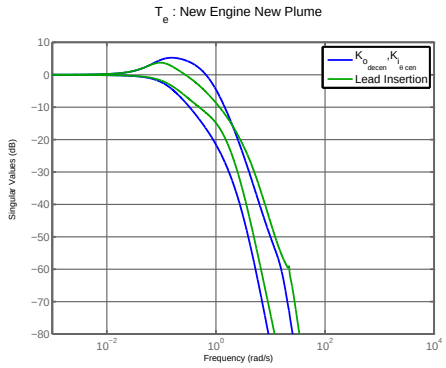

Figure 2.85: T_e : Lead Insertion

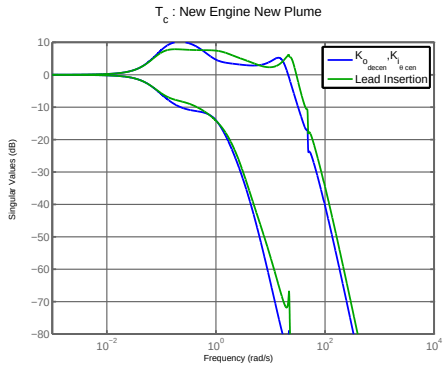

Figure 2.86: T_c : Lead Insertion

did help in improving the closed loop properties at both the loop breaking points. A lag network $\left(\frac{0.5s+0.71}{s+0.71}\right)$ was added in the $K_i(1,1)$ position to introduce a phase lag of $\phi_m = 20\,\text{deg}$ at $\omega = 1$ rads/sec.

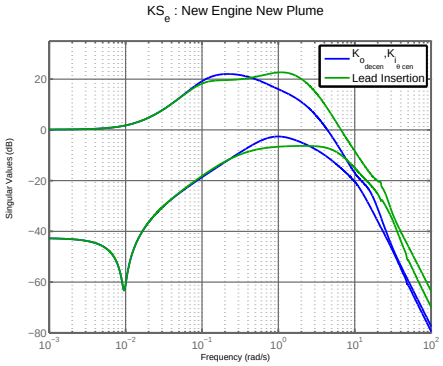

Figure 2.87: KS_e : Lead Insertion

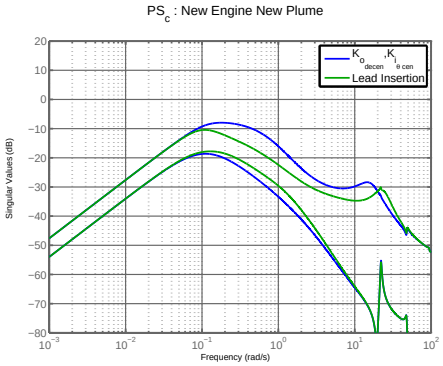

Figure 2.88: PS_c : Lead Insertion

$$K_i(s) = \begin{bmatrix} -0.3\,(s+2)\left(\frac{0.5s+0.71}{s+0.71}\right) \\ -0.05\,(s+1.6) \end{bmatrix} K_o(s) = \begin{bmatrix} 2\left(\frac{s-0.01}{s}\right) & -1.2\left(\frac{s+0.26}{s}\right) \\ -5\left(\frac{s+0.08}{s}\right) & -0.2\left(\frac{s+0.37}{s}\right) \end{bmatrix} \tag{2.68}$$

Table 2.16: Comparison of Closed Loop Properties($||.||_\infty$ in db) for $K_{o_{centralized}}$,$K_{i_{\theta centralized}}$ and Surgical Insertion of Lags : New Engine New Plume

	$\|\|S_e\|\|_\infty$	$\|\|T_e\|\|_\infty$	$\|\|S_c\|\|_\infty$	$\|\|T_c\|\|_\infty$	$\|\|KS_e\|\|_\infty$	$\|\|PS_c\|\|_\infty$	v_{ts}	γ_{ts}
$K_{o_{decen}}, K_{i_{\theta cen}}$	4.78	2.72	5.59	4.21	16.54	-0.76	64.14	16.67
Surgical Insertion	4.33	2.71	3.61	6.32	16.51	-2.71	64.28	11.32

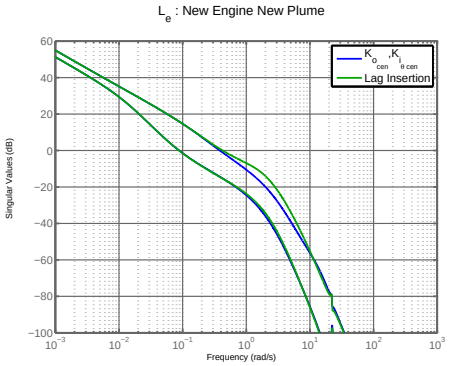

Figure 2.89: L_e : Lag Insertion

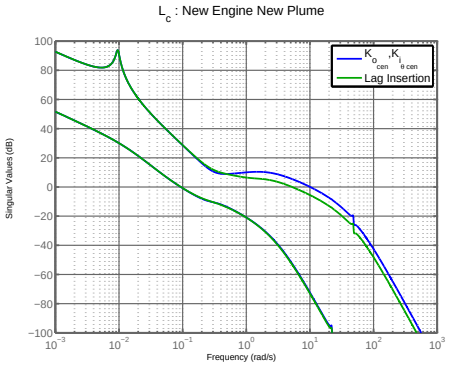

Figure 2.90: L_c : Lag Insertion

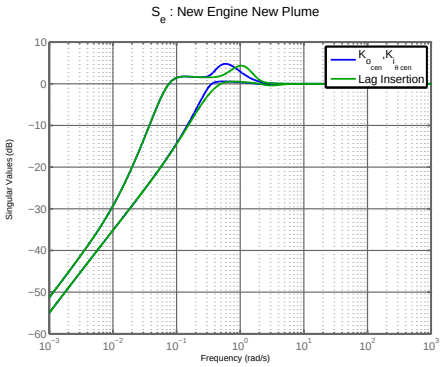

Figure 2.91: S_e : Lag Insertion

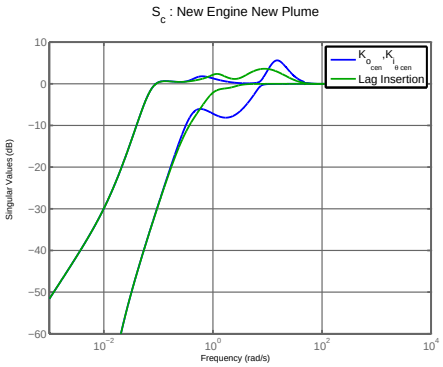

Figure 2.92: S_c : Lag Insertion

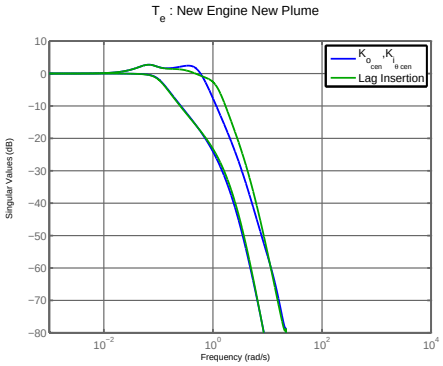

Figure 2.93: T_e : Lag Insertion

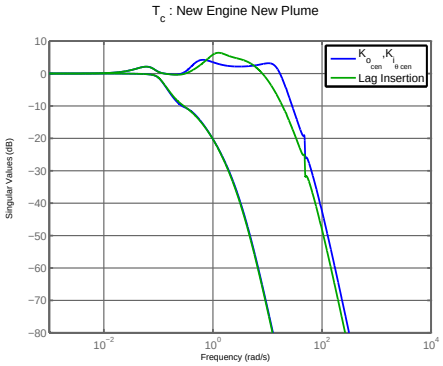

Figure 2.94: T_c : Lag Insertion

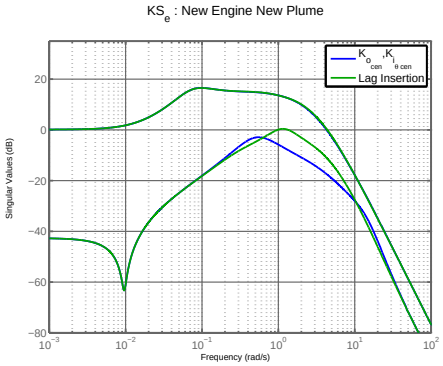

Figure 2.95: KS_e : Lag Insertion

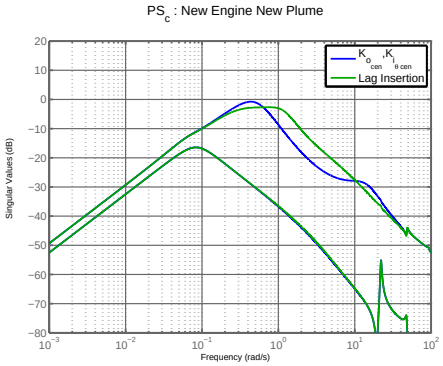

Figure 2.96: PS_c : Lag Insertion

2.4.6 Comparison of Real Lead-Lag and Complex Lead-Lag Controllers

In the following plots we compare the two designs obtained from the real lead-lag controller and complex lead-lag controller respectively. A family of 2500 controllers were designed by varying the parameters ω_{g_i} and ω_{g_o} over a range of frequencies. It is to be noted that a double cascaded structure was used for the inner loop controller and a single lead network was used for the outer loop controller. For the complex lead network $\zeta = 0.7$ was chosen since it offered the best set of closed loop properties.

Sensitivity at the Output

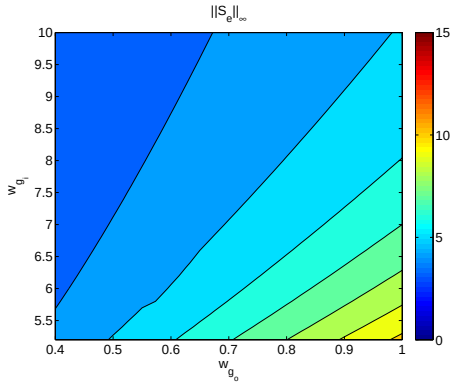

Figure 2.97: S_e : NENP using Complex leadlag

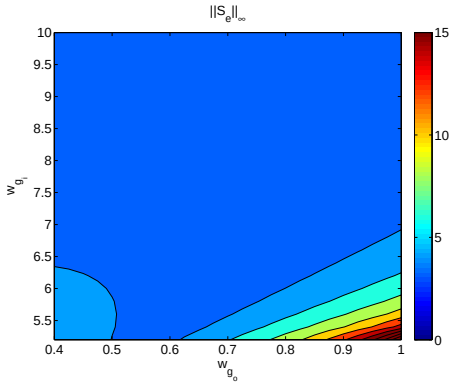

Figure 2.98: S_e : NENP using Real leadlag

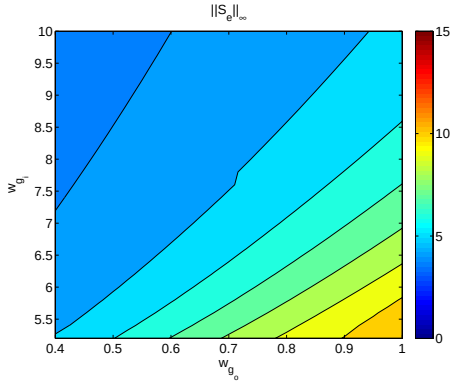

Figure 2.99: S_e : NEOP using Complex leadlag

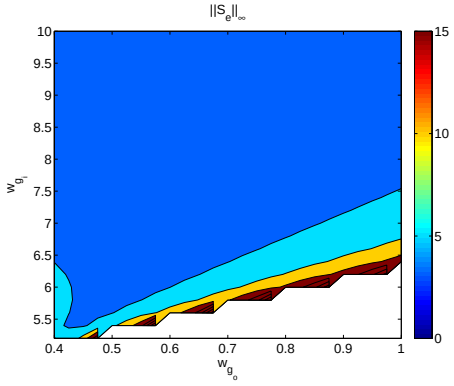

Figure 2.100: S_e : NEOP using Real leadlag

1. The family of Real lead-lag controllers give better properties at the output loop breaking point as compared to real lead-lag controllers for New Engine Old Plume and New Engine New Plume.

2. The $||S_e||_\infty$ increases as $\omega_{g_o} > 0.7$ due to the presence of a RHP zero at $s = 7.7$ which puts an upper bound on the bandwidth at the output loop breaking point.

3. For New Engine Old Plume, system becomes unstable as the ω_{g_o} is pushed towards 0.7 rads/sec. However using a more complicated controller like the complex lead-lag controller, we can push the bandwidth at the output close to 1 rads/sec without destabilizing the closed loop system.

4. The flexible modes don't affect the properties at the output loop breaking point.

Complementary Sensitivity at the Output

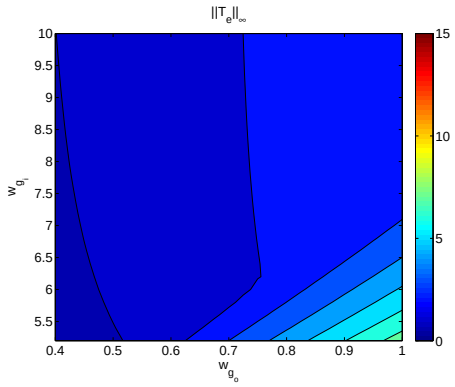

Figure 2.101: T_e : NENP Using Complex Leadlag

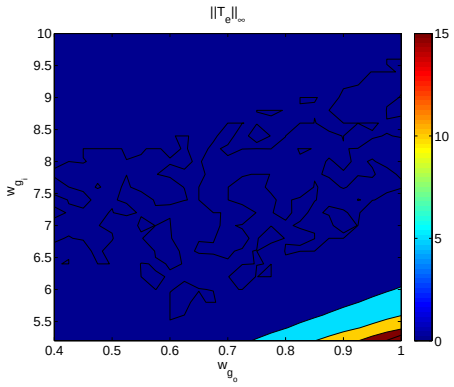

Figure 2.102: T_e : NENP Using Real Leadlag

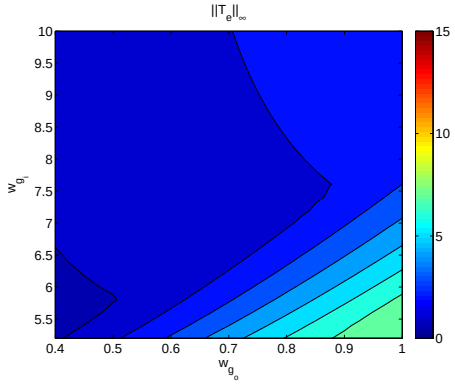

Figure 2.103: T_e : NEOP Using Complex Leadlag

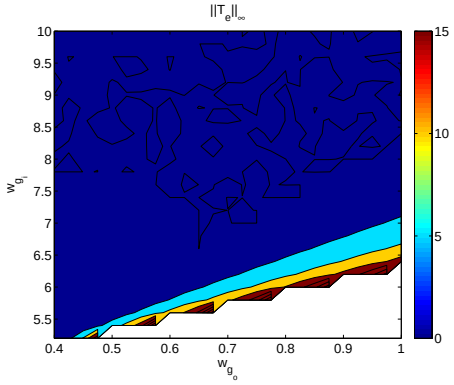

Figure 2.104: T_e : NEOP Using Real Leadlag

We see similar trends as we saw while comparing $||S_e||_\infty$ variation for New Engine Old Plume and New Engine New Plume.

Sensitivity at the Controls

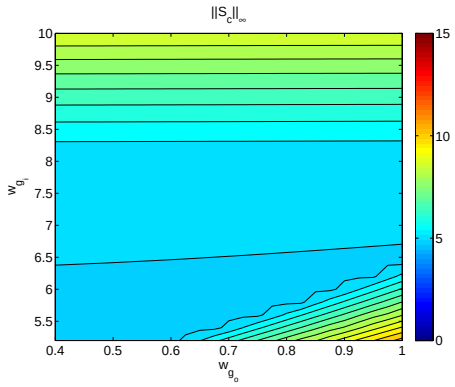

Figure 2.105: S_c : NENP Using Complex leadlag

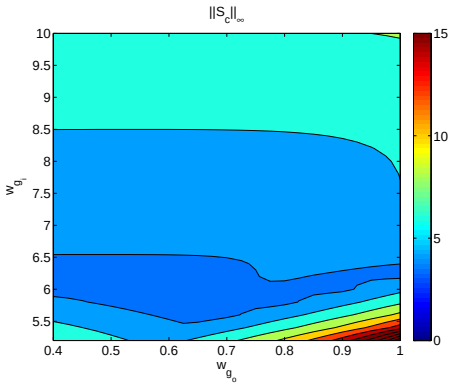

Figure 2.106: S_c : NENP Using Real leadlag

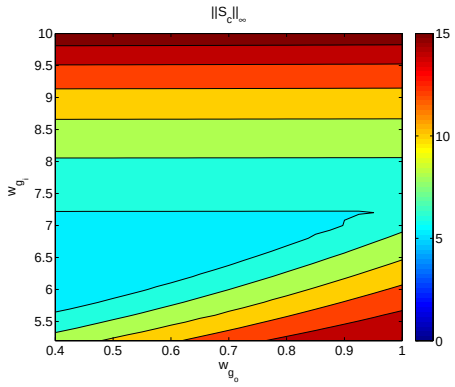

Figure 2.107: S_c : NEOP Using Complex leadlag

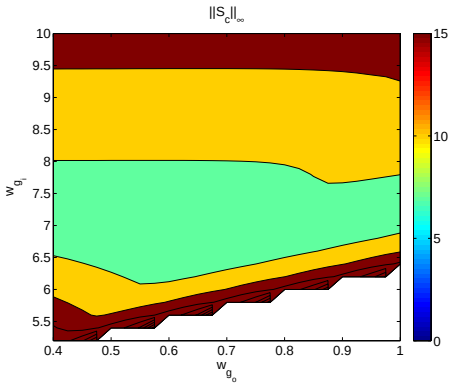

Figure 2.108: S_c : NEOP Using Real leadlag

1. $||S_c||_\infty$ increases as ω_{g_i} approaches 10 rads/sec because the flexible modes at 22 rads/sec gets excited and deteriorates the properties at the controls. Hence the flexible modes put a upper bound on the achievable bandwidth at the controls.

2. $||S_c||_\infty$ increases as ω_{g_i} approaches 6 rads/sec because the RHP pole at $s = 3.1$for the New Engine Old Plume puts a lower bound on the achievable bandwidth at the controls.

3. The New Engine New Plume as RHP pole at $s = 2.3$ as compared to New Engine Old Plume having a RHP pole at $s = 3.1$. Hence we have a smaller lower bound on the achievable bandwidth at the controls for New Engine New Plume compared to New Engine Old Plume. Hence, New Engine New Plume has better properties at the controls compared to New Engine Old Plume.

4. The complex-leadlag controller gives us better properties at the controls compared to a real leadlag controller for both New Engine New Plume and New Engine Old Plume.

Nyquist plots

In the following plots, a family of nyquist plot of L_c for both the rigid and the flexible plant has been plotted by keeping ω_e(bandwidth at error) fixed at 0.65 rads/sec and varying ω_c(bandwidth at control) from 5 rads/sec to 10 rads/sec. This analysis has been done for both New Engine Old Plume and New Engine New Plume.

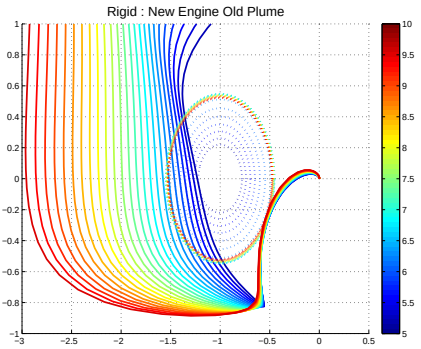

Figure 2.109: New Engine Old Plume : Rigid

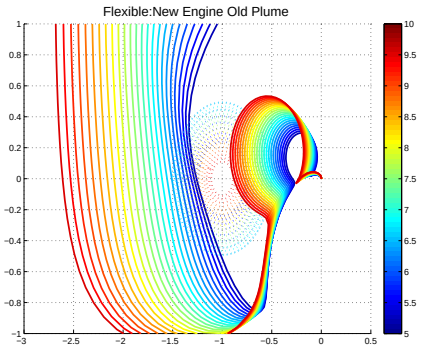

Figure 2.110: New Engine Old Plume : Flexible

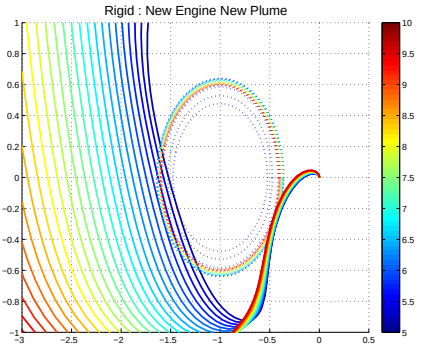

Figure 2.111: New Engine New Plume : Rigid

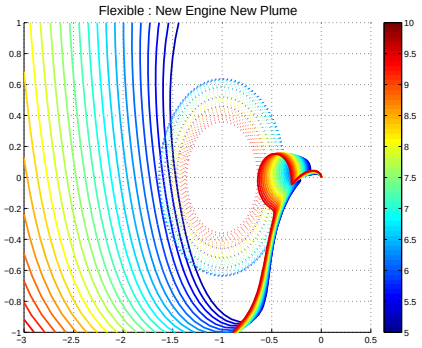

Figure 2.112: New Engine New Plume : Flexible

1. The rigid model nyquist plots for both Old Plume and New Plume show that as we decrease the bandwidth at the control to below 5 rads/sec, the nyquist plot gets closed to the (-1,0) point which means that the $||S_c||_\infty \uparrow$ and robustness decreases. This is due to the fact that the RHP pole at $s = 2 - 3$ puts a lower bound on the bandwidth at the controls. However increasing the bandwidth does not deteriorate the properties since the rigid body does not

have an flexible mode to put an upper bound on the bandwidth.

2. The flexible model nyquist plots for both Old and New Plume shows the same trend of deterioration in properties when we decrease the bandwidth at controls. This is due to the presence of RHP pole. However as we increase the bandwidth close to 10 rads/sec, we see that the nyquist plot gets closer to the (-1,0) point which means that$||S_c||_\infty \uparrow$ and robustness decreases. This means that the flexible modes put an upper bound on the bandwidth at the controls.

3. The nyquist plot of the flexible model for both Old Plume and New Plume shows that the $P_{\delta_e \to \gamma}$ for New Plume is easier to control than the Old Plume since the family of Nyquist plot is farther away from the (-1,0) point for New Plume as compared to the Old Plume.

Complementary Sensitivity at the Controls

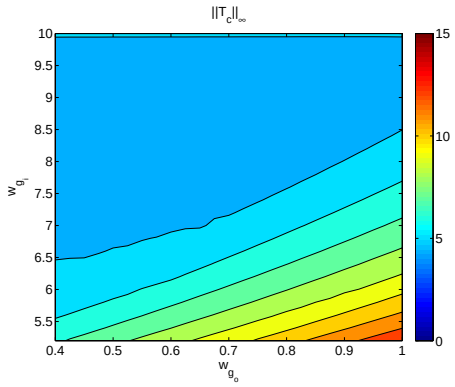

Figure 2.113: T_c : NENP Using Complex Leadlag

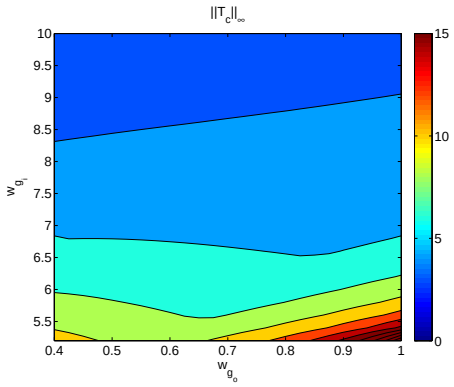

Figure 2.114: T_c : NENP Using Real Leadlag

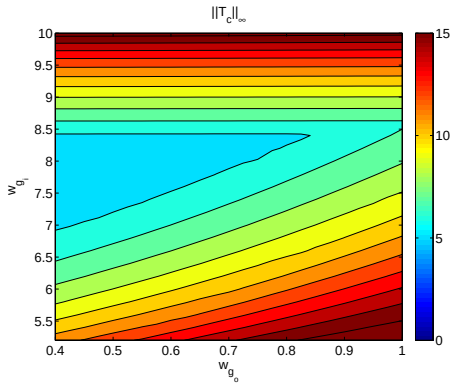

Figure 2.115: T_c : NEOP Using Complex Leadlag

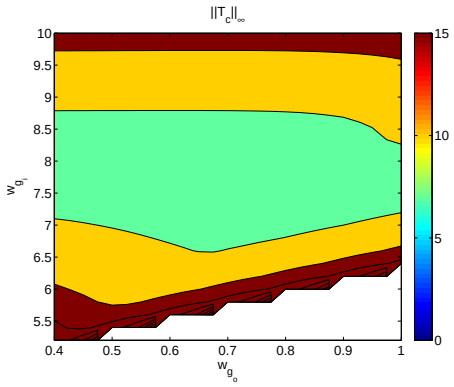

Figure 2.116: T_c : NEOP Using Real Leadlag

1. We see similar trends as we saw while comparing $||S_c||_\infty$ variation for New Engine Old Plume and New Engine New Plume.

2. $||T_c||_\infty$ increases as we increase ω_{g_i} to 10 rads/sec or decrease it to 6 rads/sec. Hence we would like to operate in a band of frequencies between 6 and 10 rads/sec.

3. $||T_c||_\infty$ also increases as we increase ω_{g_o} close to 0.7 rads/sec. Hence RHP zero affects the properties at the controls as well.

↓GM at the controls

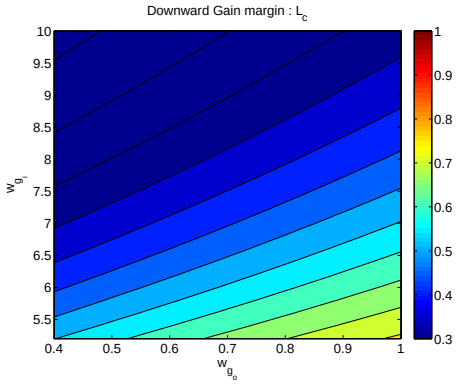

Figure 2.117: ↓GM : NENP Using Complex Lead-lag

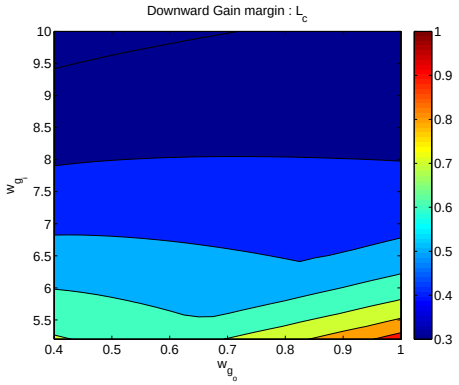

Figure 2.118: ↓GM : NENP Using Real Leadlag

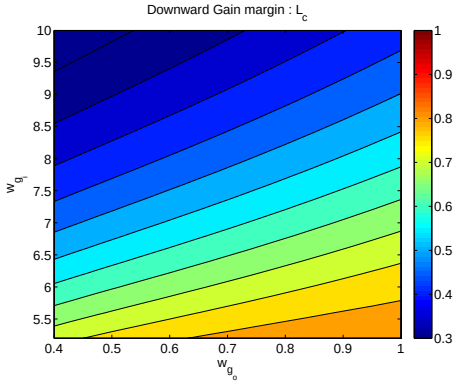

Figure 2.119: ↓GM : NEOP Using Complex Lead-lag

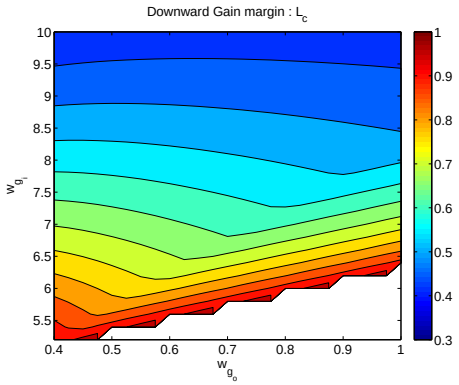

Figure 2.120: ↓GM : NEOP Using Real Leadlag

1. While comparing the ↓GM at controls of the real lead-lag and complex lead-lag designs for New Engine Old Plume and New Engine New Plume respectively, we notice that the average ↓GM for the real lead-lag design is much higher than that for complex lead-lag design. Hence Complex lead-lag controller gives us better closed loop properties than a real lead-lag controller.

2. While comparing the ↓GM for the real lead-lag designs for New Engine Old Plume and New Engine New Plume, we notice that the average ↓GM for the New Engine New Plume is lower than that of New Engine Old Plume. We notice similar trend for the complex lead-lag designs.

This is due to the fact that the RHP pole for New Engine New Plume is at $s = 2.3$ compared to the RHP pole of New Engine Old Plume which is located at $s = 3.1$.

↑GM at the Controls

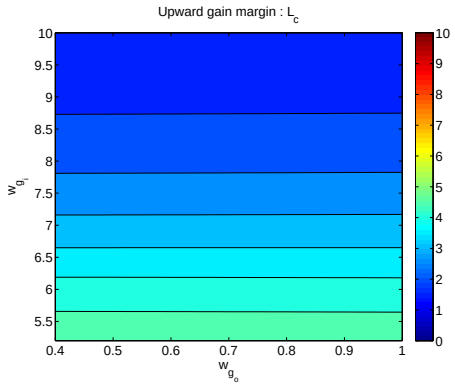

Figure 2.121: ↑GM : NENP Using Complex Lead-lag

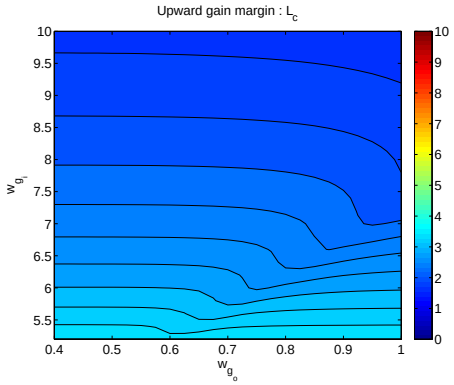

Figure 2.122: ↑GM : NENP Using Real Leadlag

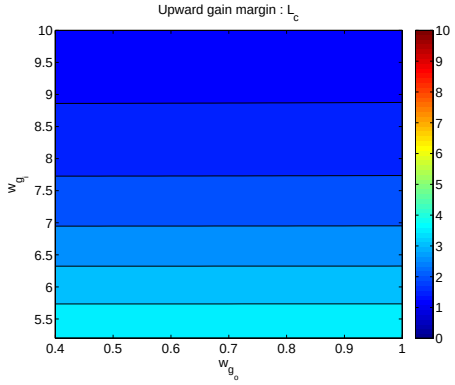

Figure 2.123: ↑GM : NEOP Using Complex Lead-lag

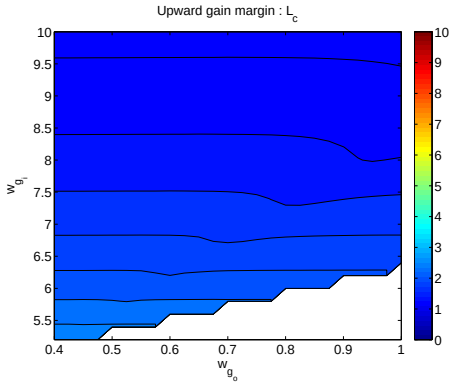

Figure 2.124: ↑GM : NEOP Using Real Leadlag

1. While comparing the ↑GM at the controls of the real lead-lag and complex lead-lag designs for New Engine Old Plume and New Engine New Plume respectively, we notice that the average ↑GM for the family of real lead-lag designs is much lower than that for complex lead-lag designs. Hence the complex lead-lag controller gives us better closed loop properties than a real lead-lag controller.

2. While comparing the ↑GM for the real lead-lag designs for New Engine Old plume and New Engine New Plume, we notice that the average ↑GM for the New Engine New Plume is higher

than that of New Engine Old Plume. We notice a similar trend for the complex-lead lag designs.

Phase Margin at the output

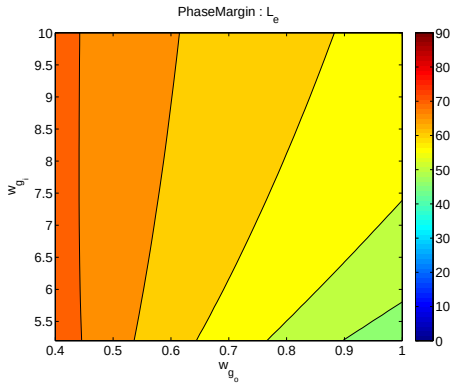

Figure 2.125: PM : NENP Using Complex Leadlag

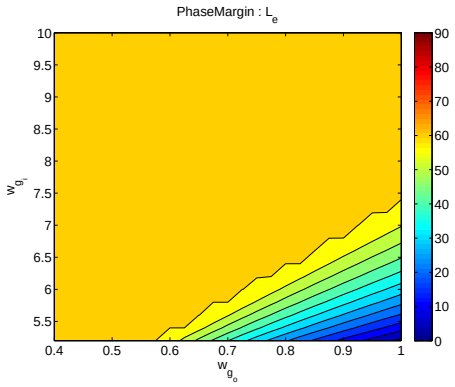

Figure 2.126: PM : NENP Using Real Leadlag

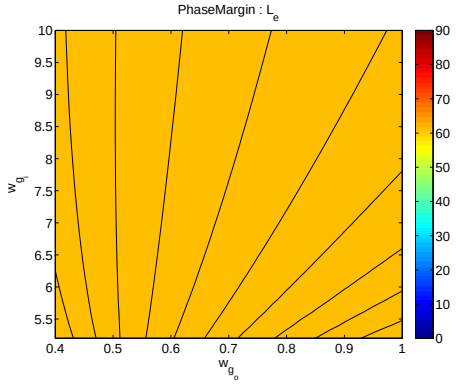

Figure 2.127: PM : NEOP Using Complex Leadlag

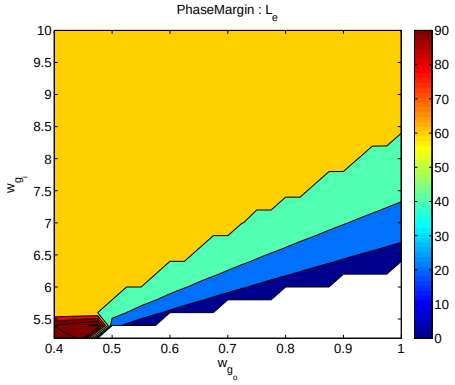

Figure 2.128: PM : NEOP Using Real Leadlag

While comparing the Phase margin at the output, of the real lead-lag and complex lead-lag designs for the New Engine Old Plume , we notice that the PM decreases as the ω_{g_o} increases and approaches 0.7 rads/sec. However the PM of the complex-lead lag designs are close 60 deg. We see a similar trend for New Engine New Plume. Hence complex lead-lag controllers offer better robustness at the output loop breaking point as compared to real lead-lag controllers.

Phase Margin at the Controls

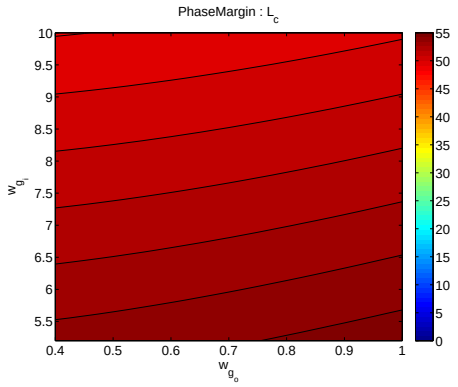

Figure 2.129: PM : NENP Using Complex Leadlag

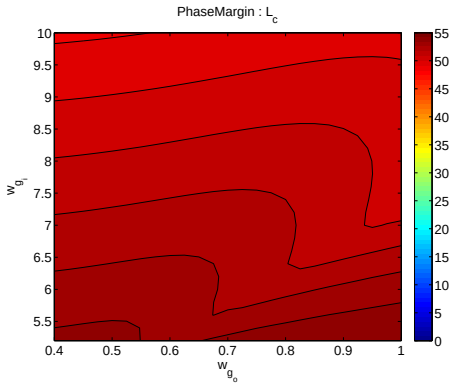

Figure 2.130: PM : NENP Using Real Leadlag

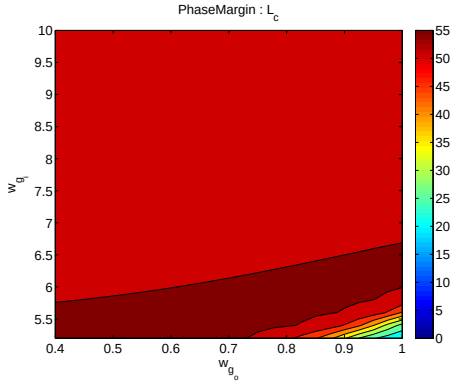

Figure 2.131: PM : NEOP Using Complex Leadlag

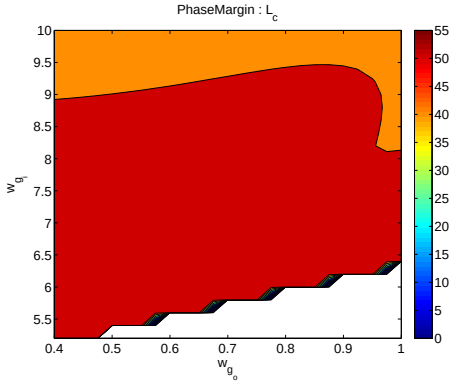

Figure 2.132: PM : NEOP Using Real Leadlag

1. While comparing the Phase margin at the controls, of the real lead-lag and complex lead-lag designs for New Engine Old Plume, we notice a similar trend in the variation of PM.

2. The average phase margin at the controls of the real lead-lag and complex lead-lag designs for New Engine New Plume are greater than the respective real lead-lag and complex lead-lag designs for New Engine Old Plume.

By studying these plots, we conclude that the δ_e to FPA transfer function of the New Engine New Plume is easier to control that the δ_e to FPA transfer function of the New Engine Old Plume.

Now let us design controllers for the MIMO plant of New Engine New Plume using complex lead networks. In the following designs, we design controllers of the following form.

$$K_i(s) = \begin{bmatrix} 0 \\ g_{i_2}\left(\frac{s^2+2\zeta_1\omega_{z1}s+\omega_{z1}^2}{s^2+2\zeta_1\omega_{p1}s+\omega_{p1}^2}\right)^{n_1} \end{bmatrix}$$

$$K_o(s) = \begin{bmatrix} g_{o_1}\frac{s+z_{o_1}}{s} & 0 \\ 0 & \frac{g_{o_2}}{s}\left(\frac{s^2+2\zeta_2\omega_{z2}s+\omega_{z2}^2}{s^2+2\zeta_2\omega_{p2}s+\omega_{p2}^2}\right)^{n_2} \end{bmatrix} \tag{2.69}$$

Since the P_{11} element i.e. the transfer function from FER to velocity is approximately a first order transfer function, a basic PI controller has been used in the outer loop controller. For the P_{22} element i.e. the transfer function from δ_e to FPA , a lead network multiplied by an integrator, has been used to ensure zero steady state error. In the inner loop , θ is fed back and a complex lead network has been used. The steps to be followed for designing the complex lead networks has been covered while discussing the SISO case. The PI controller is designed separately followed by the design of the lead networks keeping the PI parameters fixed. Ko_{11} was selected to be $3\frac{s+0.06}{s}$ to ensure a settling time of 50 sec for the step response of velocity.

A family of 1600 controllers were designed by varying the parameters ω_{g_i} and ω_{g_o} over a range of frequencies keeping the following specifications in mind. It is to be noted that a double cascaded structure was used for the inner loop lead network and a single lead network was used for the outer loop controller. After playing around with the ζ_1 and ζ_2 values, it was seen that $\zeta_1 = \zeta_2 = 0.7$ gives the best set of closed loop properties.

1. Phase Margin of 60 deg at the output loop breaking point for the P_{22} element (δ_e to FPA).
2. Phase Margin of 60 deg at the input loop breaking point for the P_{22} element(δ_e to FPA).
3. Zero steady state error due to step reference commands.

The corresponding closed loop properties were studied as shown in the following plots.

Variation of $||S_e||_\infty$

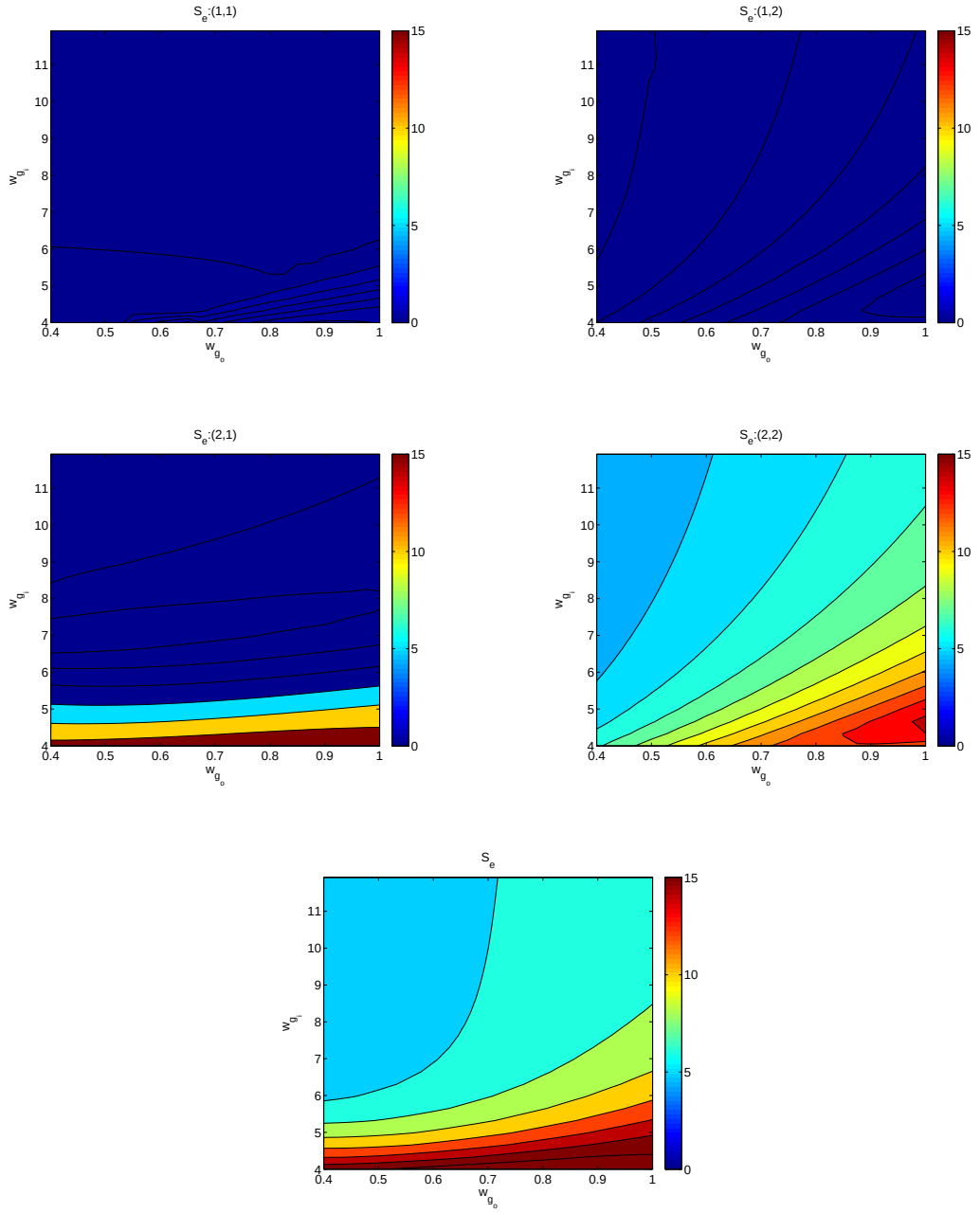

1. $||S_e||_\infty$(Singular Values) increases as gain crossover frequency of L_c (breaking the loop at the elevator) is decreased below 4.5 rads/sec due to the presence of RHP pole at $s = 2.3$ which puts a lower bound on bandwidth.

2. $||S_e(2,2)||_\infty$ increases as the gain crossover frequency of L_e (breaking the loop at error(velocity)) is increased above 0.7 rads/sec because the RHP zero at $s = 7.7$ which puts an upper bound on

bandwidth.

Variation of $||T_e||_\infty$

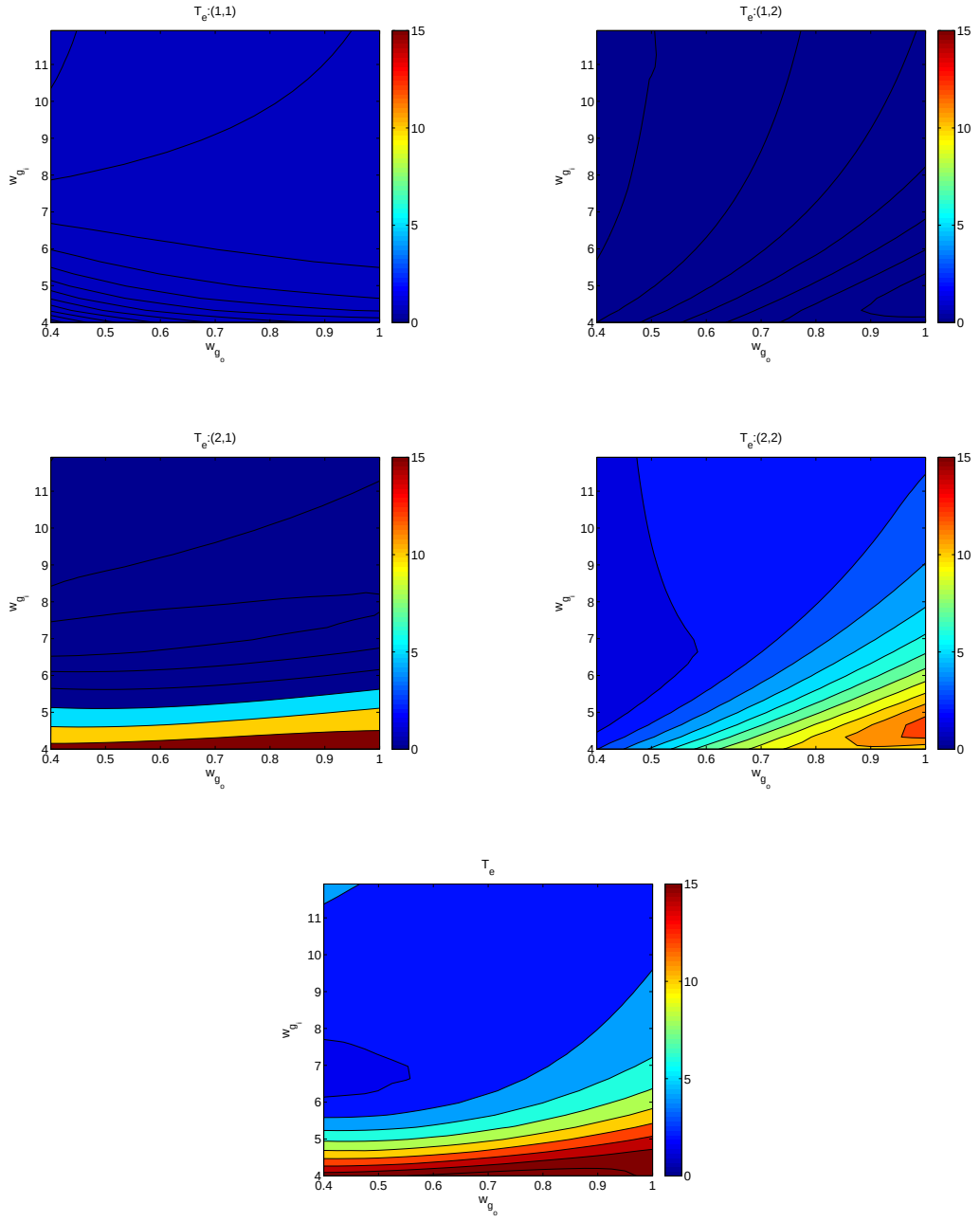

$||T_e||_\infty$(singular values) show a similar trend as the variation of $||S_e||_\infty$ due to the presence of RHP zero at $s = 7.7$ and RHP pole at $s = 2.3$ which puts an upper bound and a lower bound on the bandwidth respectively.

Variation of $||S_c||_\infty$

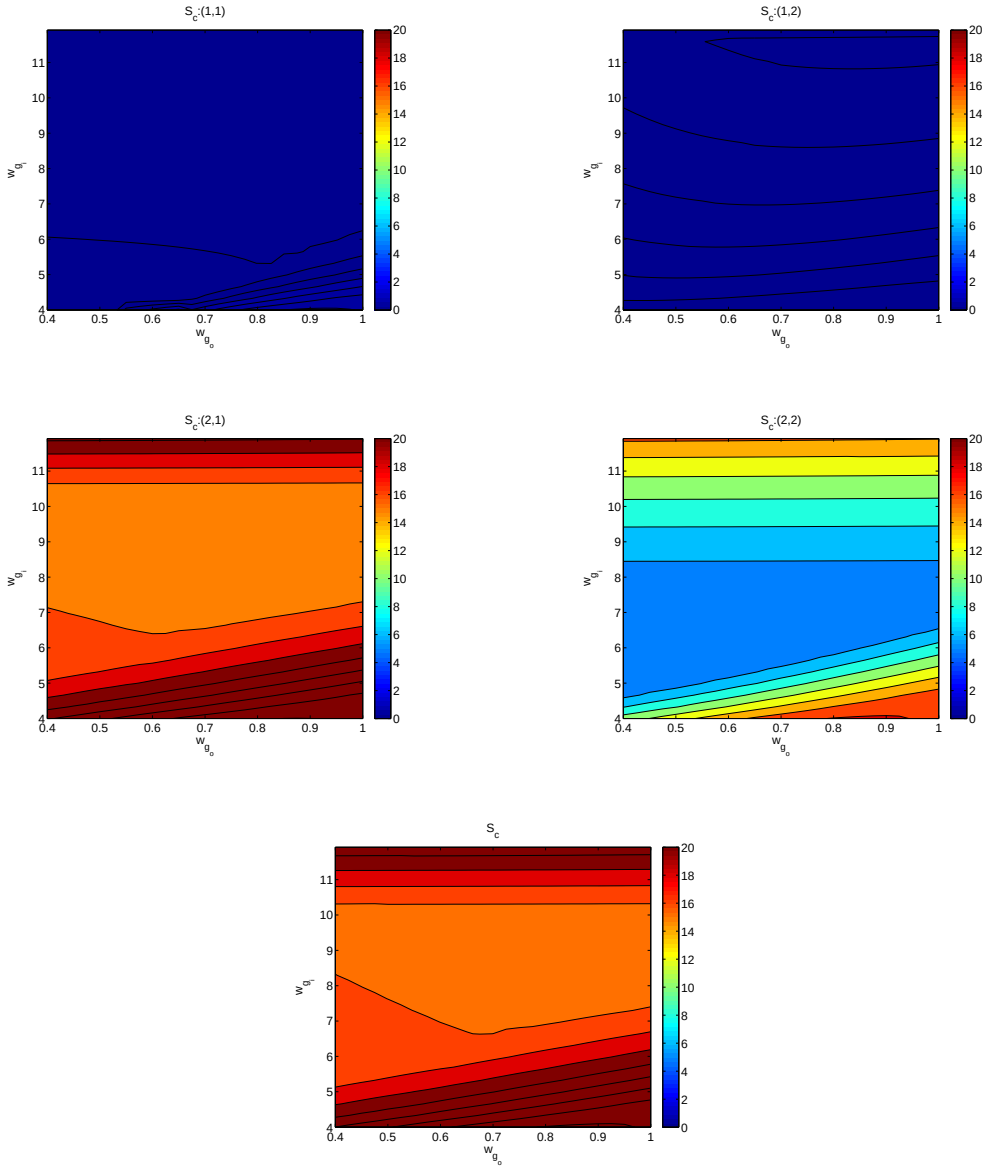

1. $||S_c||_\infty$ in the elevator channel and the net $||S_c||_\infty$(singular value) increases as the ω_{g_i} of L_c(breaking the loop at the elevator) increases beyond 9 rads/sec because the flexible modes at 22 rads/sec are getting excited. $||S_c||_\infty$ also increases as the ω_{g_i} decreases below 4 rads/sec because the RHP pole at $s = 2.3$ puts a lower bound on bandwidth.

2. $||S_c(2,1)||_\infty$ is larger than the other three elements because the coupling from FER to γ is large. This leads to a large peak S_c because the (2,1) element overshadows all the other 3 elements which have lower peaks.

Variation of $||T_c||_\infty$

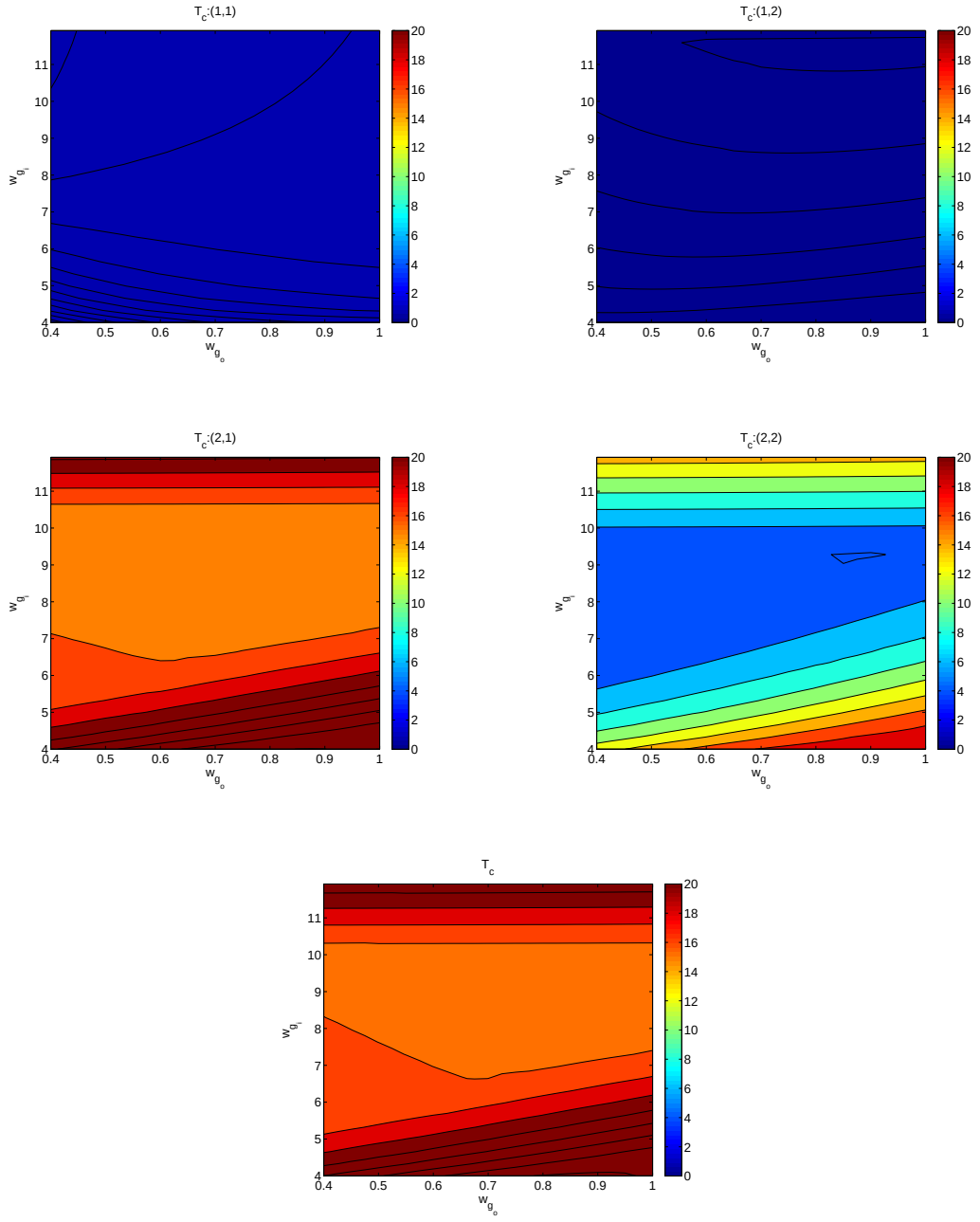

$||T_c||_\infty$(singular values) show a similar trend as the variation of $||S_c||_\infty$ due to the presence of RHP zero at $s = 7.7$ and RHP pole at $s = 2.3$ which puts an upper bound and a lower bound on the bandwidth respectively.

Variation of $||KS_e||_\infty$

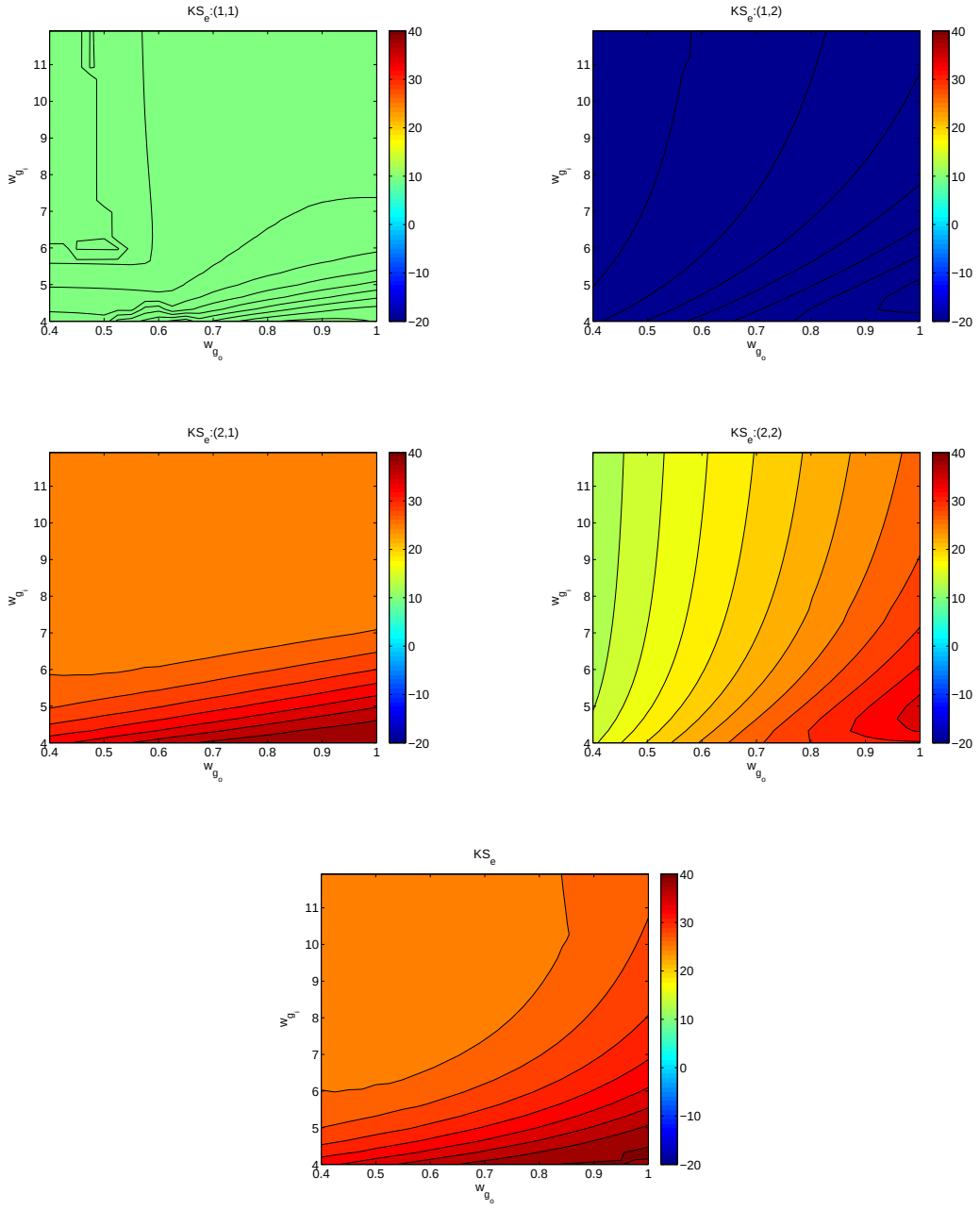

1. Control Action increases as ω_{g_i} of L_c(breaking the loop at the elevator) decreases beyond 4 rads/sec due to the presence of RHP pole which puts a lower bound on bandwidth.

2. Control Action increases as ω_{g_o} of L_e(breaking the loop at the error(velocity)) increases beyond 0.7 rads/sec because the RHP zero puts an upper bound on the bandwidth.

Variation of $||PS_c||_\infty$

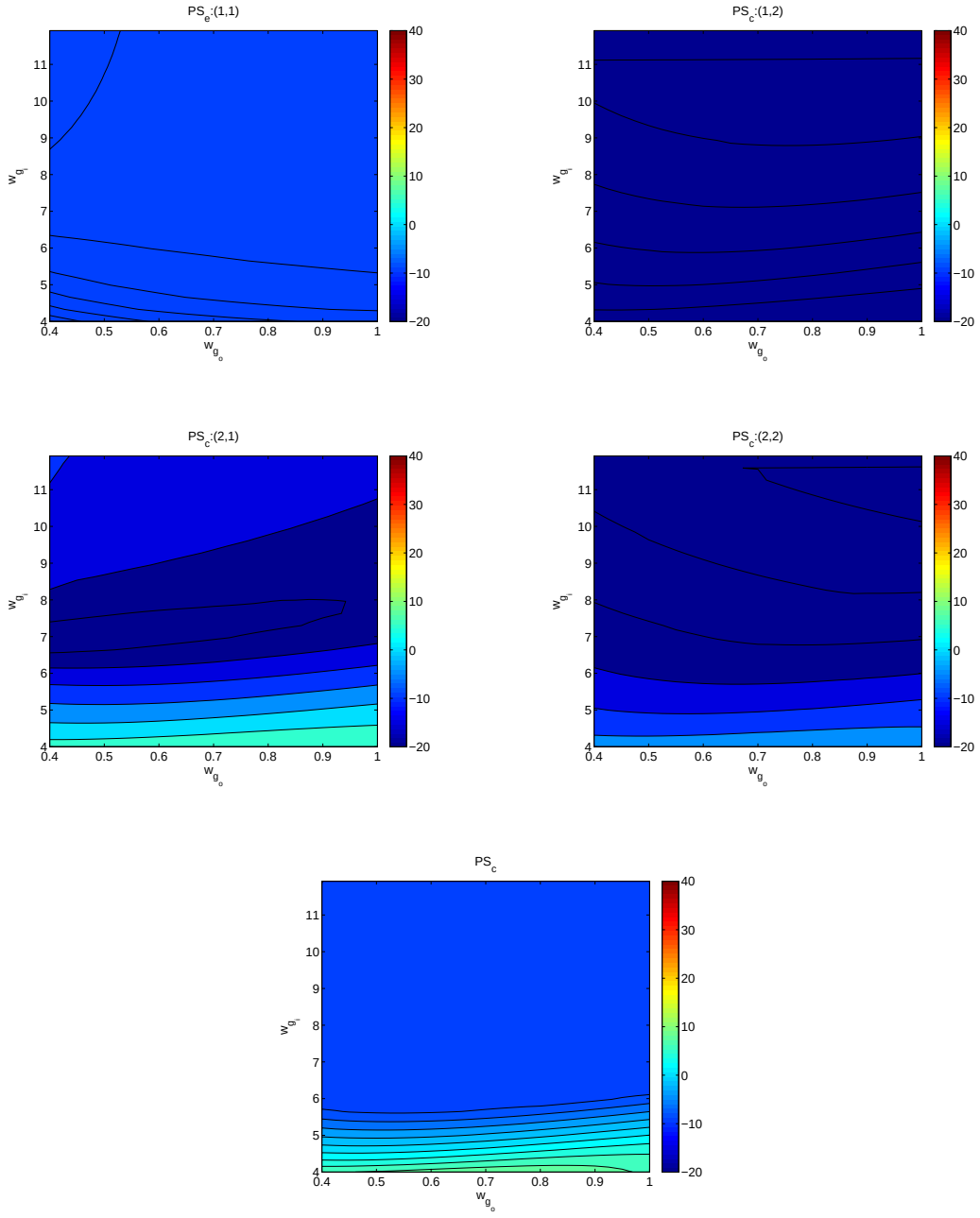

Input disturbance attenuation increases as ω_{g_i} of L_c(breaking the loop at the elevator) is decreased below 6 rads/sec.

Variation of Overshoot

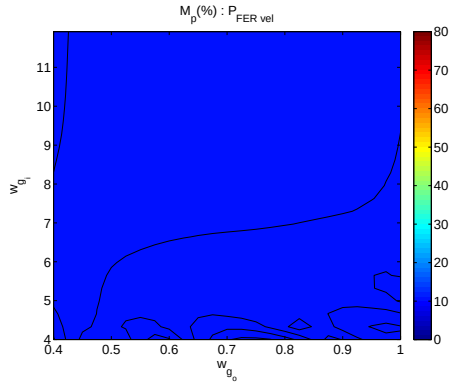

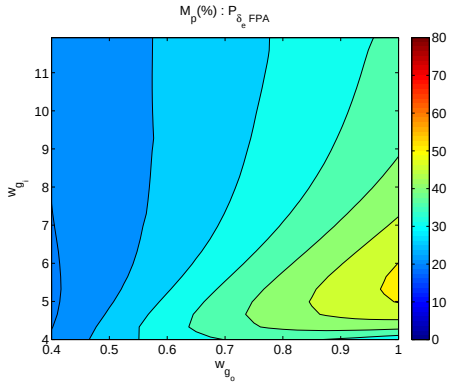

Variation of Settling Time

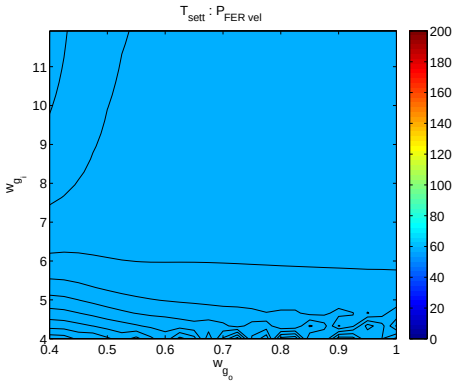

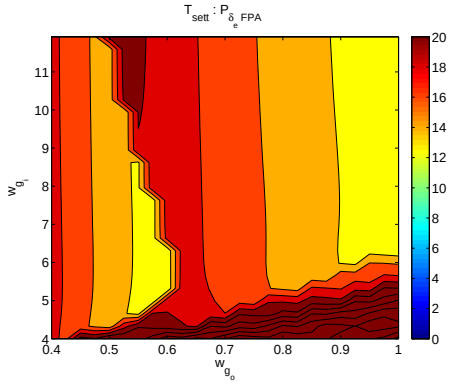

Overshoot of the step response of γ increases as ω_{g_o} of L_e(breaking the loop at the error(velocity)) increases. This is due to the RHP zero at $s = 7.7$.

2.5 Comparison of Centralized and Decentralized Controllers

Let us compare the best dynamic output feedback controller for Standard and Non-standard Mixed Sensitivity:

1. **Standard Mixed Sensitivity**

Design	$\overline{S_e}$	$\overline{T_e}$	$\overline{S_c}$	$\overline{T_c}$	$\overline{KS_e}$	$\overline{PS_c}$	v_{ts}	γ_{ts}
Old Plume								
1	3.70	2.81	11.92	12.38	15.14	-5.1	46.34	39.26
New Plume								
1	2.52	2.07	20.88	20.87	17.12	7.78	39.12	27.03

Table 2.17: Closed Loop Properties(Hypersonic) : Standard Mixed Sensitivity

2. **Non-Standard Mixed Sensitivity**

Design	$\overline{S_e}$	$\overline{T_e}$	$\overline{S_c}$	$\overline{T_c}$	$\overline{KS_e}$	$\overline{PS_c}$	v_{ts}	γ_{ts}
Old Plume								
1	4.15	3.11	4.56	5.94	13.36	-6.07	55.21	34.39
New Plume								
1	4.97	3.02	7.62	7.13	19.86	-0.23	59.82	12.08

Table 2.18: Closed Loop Properties(Hypersonic) : Non-Standard Mixed Sensitivity

K_{MIMO} designed using H_∞ standard mixed sensitivity gives good properties at the output but bad properties at the input loop breaking point.However K_{MIMO} designed using H_∞ non-standard mixed sensitivity gives good properties at output and input loop breaking points.

Standard Mixed Sensitivity Plots

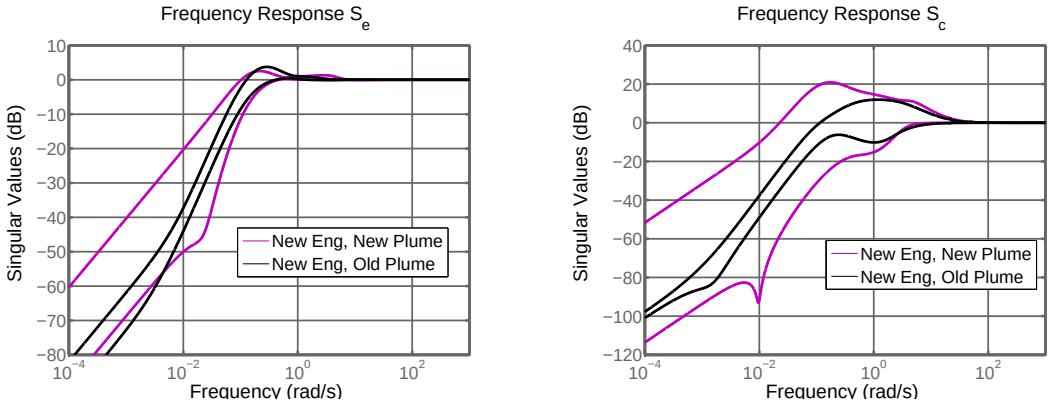

Figure 2.133: Sensitivity

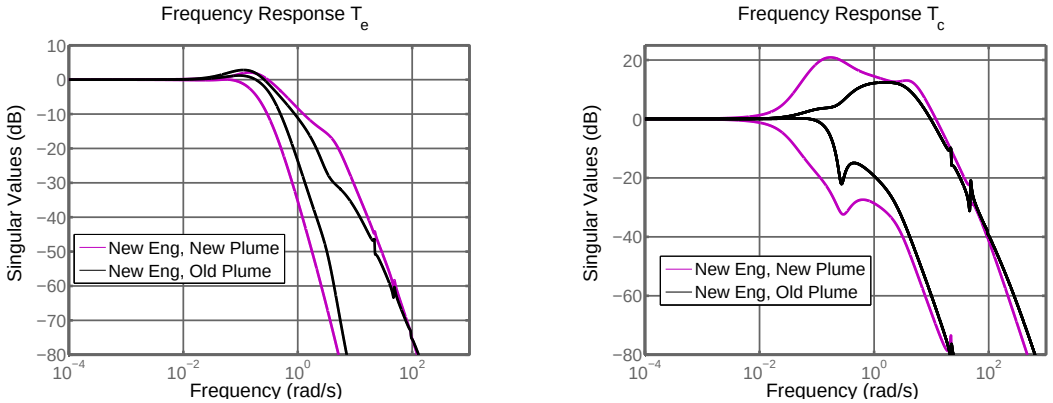

Figure 2.134: Complementary Sensitivity

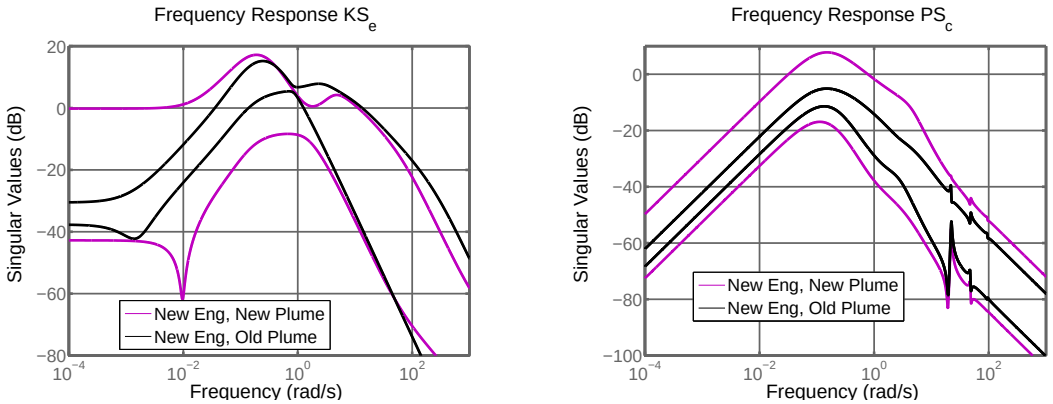

Figure 2.135: KS_e and PS_c

Non-Standard Mixed Sensitivity Plots

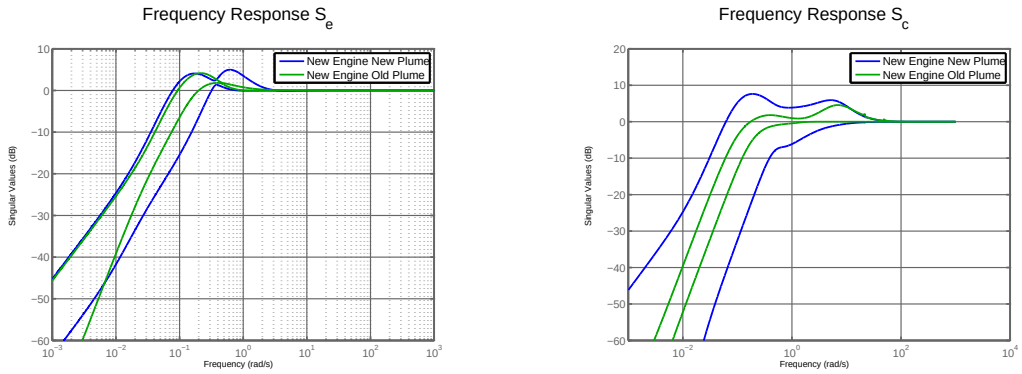

Figure 2.136: Sensitivity

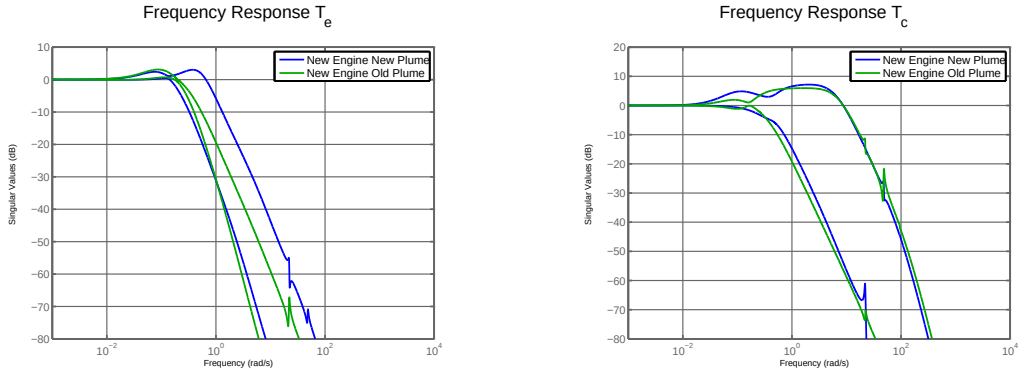

Figure 2.137: Complementary Sensitivity

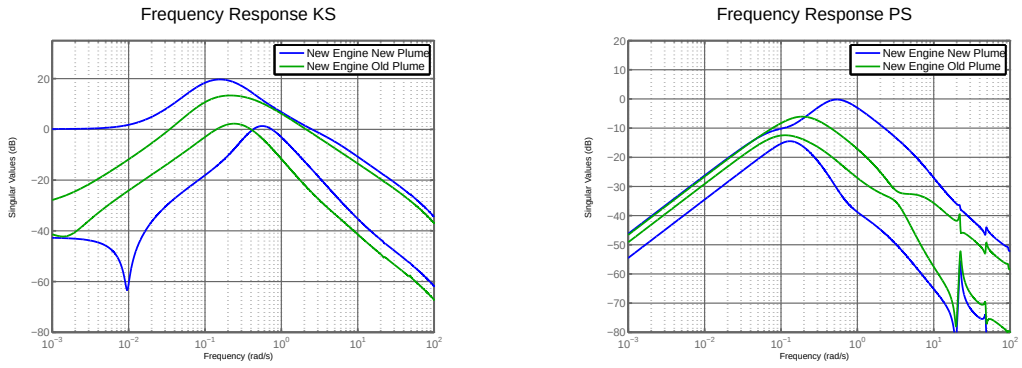

Figure 2.138: KS_e and PS_c

Let us now compare the performance of a decentralized complex lead-lag controller and a PI-PD controller with K_o decentralized, K_i decentralized for New Engine Old Plume

1. $K_{o_{decentralized}}, K_{i_{decentralized}}$

$$K_i(s) = \begin{bmatrix} 0 \\ -0.8\,(s+5) \end{bmatrix} K_o(s) = \begin{bmatrix} 1.25\left(\frac{s+0.04}{s}\right) & 0 \\ 0 & -9.5\left(\frac{s+0.07}{s}\right) \end{bmatrix} \tag{2.70}$$

2. **Lead-Lag**

$$K_i(s) = \begin{bmatrix} 0 \\ 18.78\left(\frac{s^2+12.98s+65.82}{s^2+17.8s+123.7}\right)^2 \end{bmatrix} K_o(s) = \begin{bmatrix} 1.4\left(\frac{s+0.06}{s}\right) & 0 \\ 0 & \frac{-167.99(s+0.97)(s+0.07)}{s(s+7.03)(s+0.50)} \end{bmatrix} \tag{2.71}$$

Table 2.19: Comparison of Closed Loop Properties for $K_{o_{decen}}$,$K_{i_{decen}}$ and Surgical Insertion of Leads : New Engine Old Plume

	$\overline{S_e}$	$\overline{T_e}$	$\overline{S_c}$	$\overline{T_c}$	$\overline{KS_e}$	$\overline{PS_c}$	v_{ts}	γ_{ts}
$K_{o_{decen}}, K_{i_{\theta cen}}$	5.85	3.65	15.69	15.70	16.79	0.14	78.63	38.02
Complex lead-lag	3.15	2.55	14.89	15.06	25.31	-2.87	64.06	11.65

For the New Engine Old Plume, the decentrazlied Complex lead-lag controller offers better properties than the decentralized PI-PD controller at both the loop breaking points.

Plots

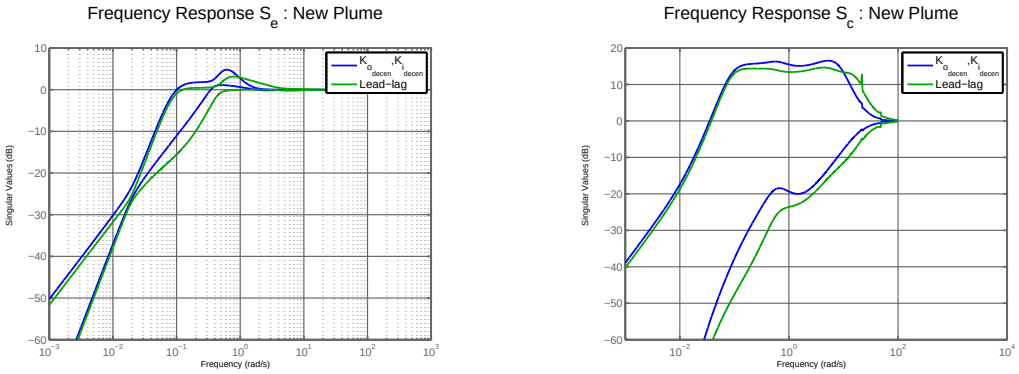

Figure 2.139: Sensitivity(New Engine New Plume)

Let us now compare the performance of a decentralized complex lead-lag controller and a PI-PD controller with K_o decentralized, K_i decentralized for New Engine New Plume

1. $K_{o_{decentralized}}, K_{i_{decentralized}}$

$$K_i(s) = \begin{bmatrix} 0 \\ -0.7\,(s+3) \end{bmatrix} K_o(s) = \begin{bmatrix} 1.5\left(\frac{s+0.06}{s}\right) & 0 \\ 0 & -6\left(\frac{s+0.12}{s}\right) \end{bmatrix} \tag{2.72}$$

2. Lead-Lag

$$K_i(s) = \begin{bmatrix} 0 \\ 26.91\left(\frac{s^2+14.05s+54.68}{s^2+23.19s+149}\right)^2 \end{bmatrix} K_o(s) = \begin{bmatrix} 1.5\left(\frac{s+0.07}{s}\right) & 0 \\ 0 & \frac{-48.73(s+0.77)(s+0.05)}{s(s+4.54)(s+0.33)} \end{bmatrix} \tag{2.73}$$

Table 2.20: Comparison of Closed Loop Properties for $K_{o_{decen}}$,$K_{i_{decen}}$ and Surgical Insertion of Leads : New Engine New Plume

	$\overline{S_e}$	$\overline{T_e}$	$\overline{S_c}$	$\overline{T_c}$	$\overline{KS_e}$	$\overline{PS_c}$	v_{ts}	γ_{ts}
$K_{o_{decen}}, K_{i_{\theta cen}}$	4.78	2.77	16.53	16.46	19.57	2.56	54.65	15.31
Complex lead-lag	3.11	2.53	14.59	14.74	19.15	-3.42	53.69	23.34

For the New Engine New Plume, the complex lead-lag controller offers better properties than the PI-PD controller at both loop breaking points.

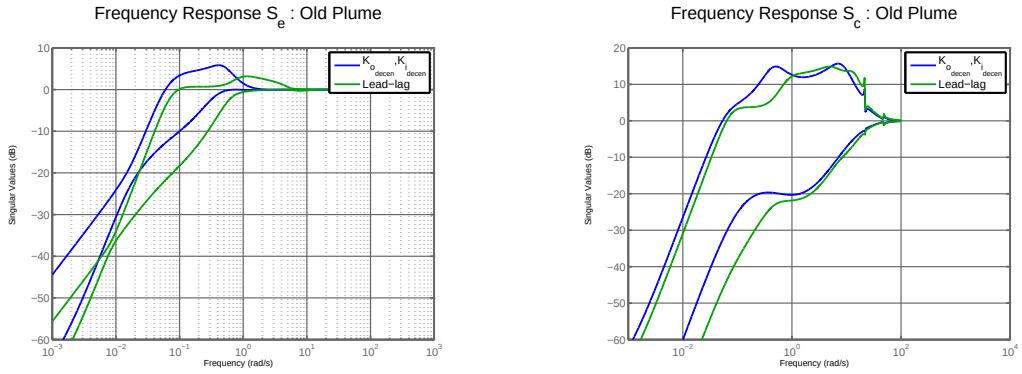

Figure 2.140: Sensitivity(New Engine Old Plume)

2.6 Summary & Conclusion

In this chapter we have studied the design of dynamic output feedback controllers using Standard and Non-Standard Mixed Sensitivity Design on New Engine Old Plume and New Engine New Plume models of the Hypersonic aircraft. We have also designed 3 types of hierarchical PI-PD controllers and surgically inserted lead-lag networks to these controllers to improve the closed loop properties further. Decentralized Lead-lag networks were also designed for both the models of the Hypersonic Aircraft.

The dynamic controller obtained using non-standard mixed sensitivity control gives better properties at the input loop breaking point as compared to the dynamic controller designed using standard mixed sensitivity. Both the controllers give good properties at the output loop breaking point.

As the complexity of PI-PD controllers increases i.e. as PI-PD controllers become more populated, the closed loop properties at both the loop breaking points improve. The fully populated $(K_{o_{centralized}}, K_{i_{\theta centralized}})$ gives better closed loop properties at both the loop breaking points than the dynamic controller using H_∞ mixed sensitivity. However the PI-PD controllers have been designed via brute force enumeration which takes a lot of time. Therefore we require a multivariable controller can be designed in minimal time using LMI optimization but still give good properties at both the loop breaking points.

The decentralized complex lead-lag controllers performs better than the decentralized real lead-lag controllers. It also performs better than the decentralized PI-PD controllers. So we see that as the complexity of the controller increases, the closed loop properties improve as well.

Chapter 3

ROCKWELL RPRV-870 HIMAT

3.1 Overview

In this chapter, we briefly discuss the longitudinal dynamics of the NASA-HiMAT aircraft. In the following sections we design a dynamic output feedback controller using Linear Matrix Inequality. We also discuss the inner outer loop control structure and design a PI-PD controller for the longitudinal dynamics. Finally we attempt to design a PI-PD controller which would similar closed loop properties as the dynamic output feedback controller.

Background. The Rockwell RPRV-870 HiMAT(Highly Maneuverable Aircraft technology) was a NASA project($1979 - 1983$) to develop high performance fighter technologies like close coupled-canards,fully digital flight control,remotely piloted aircrafts etc, which would be used in future fighter aircrafts. The aircraft was half the size of an F-16 and it had twice the fighter's turning capability. The HiMAT plane's rear-mounter swept wings and forward controllable canard made the plane's turn radius twice as tight as that of the conventional places. Traveling at the speed of sound and an altitude of 25000 feet, the aircraft could sustain an 8-G turn compared to an F-16's maximum sustained turning capability of about 4.5 Gs. One of the HiMAT project's important contribution was the use of new composite materials in structural design such as fibreglass and graphite to strengthen the plane to allow it to withstand high G- force conditions encountered during flight tests. The X-29 used many of the technologies developed from the HiMAT research like the successful use of forward canard and rear-mounted swept-wing developed from light-weight composite materials.

Figure 3.1: NASA-HiMAT(Highly Maneuverable Aircraft Technology)

3.2 NASA Himat Longitudinal Dynamics

In this section, we examine the longitudinal dynamics for the NASA Himat aircraft.

Aircraft Characteristics. We examine the aircraft during a straight and level powered approach.The flight conditions are as follows:

1. Altitude of 25,000 ft
2. Speed of Mach 0.9 (1004.8 fts/sec)

The TITO model for the longitudinal dynamics at the above flight conditions is as follows:

$$\dot{x} = Ax + Bu \tag{3.1}$$

$$y = Cx + Du \tag{3.2}$$

where

$$A = \begin{bmatrix} -0.022567 & -36.617 & -18.897 & -32.090 & 3.2509 & -0.76257 \\ 0.000092 & -1.8997 & 0.98312 & -0.00072 & -0.17080 & -0.00496 \\ 0.012338 & 11.720 & -2.6316 & 0.00087 & -31.604 & 22.396 \\ 0 & 0 & 1 & 0 & 0 & 0 \\ 0 & 0 & 0 & 0 & -30 & 0 \\ 0 & 0 & 0 & 0 & 0 & -30 \end{bmatrix}$$

$$B = \begin{bmatrix} 0 & 0 \\ 0 & 0 \\ 0 & 0 \\ 0 & 0 \\ 30 & 0 \\ 0 & 30 \end{bmatrix}$$

$$C = \begin{bmatrix} 0 & 1 & 0 & 0 & 0 & 0 \\ 0 & -1 & 0 & 1 & 0 & 0 \end{bmatrix}$$

$$D = \begin{bmatrix} 0 & 0 \\ 0 & 0 \end{bmatrix}$$

$$x = \begin{bmatrix} v & \text{Velocity} & \text{ft/sec} \\ \alpha & \text{angle of attack} & \text{deg} \\ q & \text{pitch rate} & \text{deg/sec} \\ \theta & \text{pitch angle} & \text{deg} \\ x_5 & \text{elevon actuator state} & \text{deg} \\ x_6 & \text{canard actuator state} & \text{deg} \end{bmatrix}$$

$$u = \begin{bmatrix} \delta_e & \text{Elevon deflection} \\ \delta_c & \text{Canard deflection} \end{bmatrix}$$

$$y = \begin{bmatrix} \theta & \text{Pitch Angle} \\ \gamma & \text{Flight Path Angle} \end{bmatrix}$$

The aircraft's two control surfaces are as follows :

1. Elevon - Situated on the wings

2. Canard - Forward situated control surface

Poles and Zeros. The aircraft has two stable poles at $s = -5.6757$ and $s = -0.2578$, two instabilities at $s = 0.6898 \pm j0.2488(\zeta = -0.941, w_n = 0.744)$, two actuater poles at $s = -30, -30$. It also has a transmission zero at $s = -0.0210$.

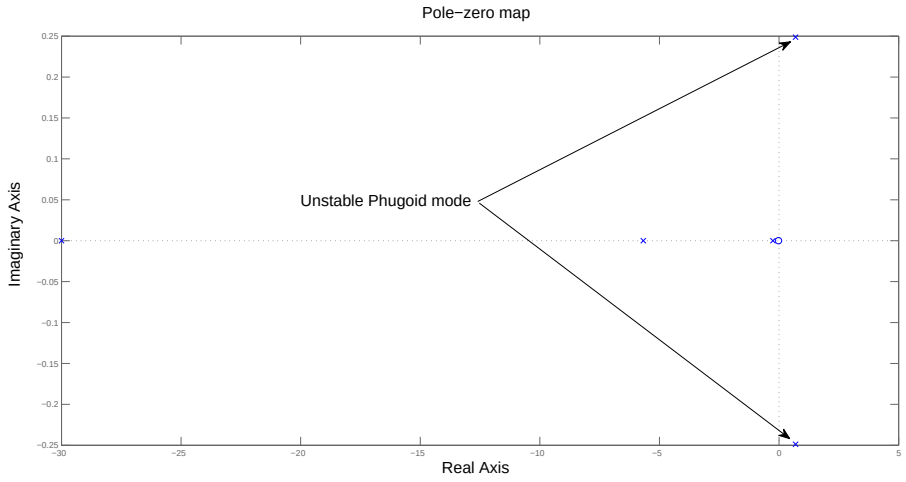

Figure 3.2: Pole Zero Map of NASA-HiMAT Aircraft

Table 3.1: Poles of NASA HiMAT Longitudinal Dynamics

Pole	Damping	Frequency(rad/sec)	Mode name
-0.258	1	0.258	Damping mode
0.69 ± j0.249	-0.94	0.733	Unstable Phugoid Mode
-5.68	1	5.68	Damping mode
-30	1	30	Damping mode
-30	1	30	Damping mode

Transfer Function Matrix. The system transfer function matrix from u to y is given by

$$G(s) = C(sI - A)^{-1}B + D = \begin{bmatrix} G_{\delta_e\theta} & G_{\delta_c\theta} \\ G_{\delta_e\gamma} & G_{\delta_c\gamma} \end{bmatrix}$$

where

$$G_{\delta_e\theta} = \frac{-948.12(s+0.02177)(s+1.963)}{(s+5.676)(s+30)(s+0.2578)(s^2-1.38s+0.5377)}$$

$$G_{\delta_c\gamma} = \frac{0.14896(s+0.02555)(s^2+78.78s+8568)}{(s+5.676)(s+30)(s+0.2578)(s^2-1.38s+0.5377)}$$

$$G_{\delta_e\gamma} = \frac{5.124(s-19.31)(s+18.82)(s+0.02218)}{(s+5.676)(s+30)(s+0.2578)(s^2-1.38s+0.5377)}$$

$$G_{\delta_c\theta} = \frac{671.88(s+0.02399)(s+1.895)}{(s+5.676)(s+30)(s+0.2578)(s^2-1.38s+0.5377)}$$

The individual transfer functions show the presence of unstable phugoid modes at $s = 0.6898 \pm j0.2488(\zeta = -0.941, w_n = 0.744)$ and damping modes at $s = -30$,$s = -5.6757$ and $s = -0.2578$.The transfer functions $G_{\delta_e\gamma}$ shows the presence of right half plane pole at $s = 19.31$. It is not a transmission zero but it makes the NASA HiMAT difficult to control.

DC Gain Analysis. Singular Value Decomposition. While analyzing the NASA HiMAT model at DC, we get the following matrix of DC gains:

$$\begin{bmatrix} \theta \\ \gamma \end{bmatrix} = \begin{bmatrix} -1.7162 & 1.2942 \\ -1.7502 & 1.3817 \end{bmatrix} \begin{bmatrix} \delta_e \\ \delta_c \end{bmatrix}$$

A singular value decomposition at DC yields the following:

$$G(j0) = C(-A)^{-1}B + D = U\Sigma V^{\top} = \begin{bmatrix} -1.7162 & 1.2942 \\ -1.7502 & 1.3817 \end{bmatrix}$$

$$U = \begin{bmatrix} -0.6940 & -0.7200 \\ -0.7200 & 0.6940 \end{bmatrix}; \Sigma = \begin{bmatrix} 3.0971 & 000.0343 \end{bmatrix}; V = \begin{bmatrix} 0.7915 & 0.6112 \\ -0.6112 & 0.7915 \end{bmatrix}$$

From the singular value decomposition, conclusions can be drawn about the steady state input output coupling.

1. Examination of the first columns of V,Σ and U shows that elevon has almost an equal impact on the pitch angle and flight path angle of the aircraft.This may be visualized as shown in Figure **??**. Elevator channel is associated with the maximum singular value.

2. Examination of the second columns of V,Σ and U shows that canard also has an equal impact on the pitch angle and flight path angle of the aircraft. This may be visualized as shown in Figure **??**. Canard channel is associated with the minimum singular value. The Singular values decomposition shows that NASA-HiMAT is coupled at DC.

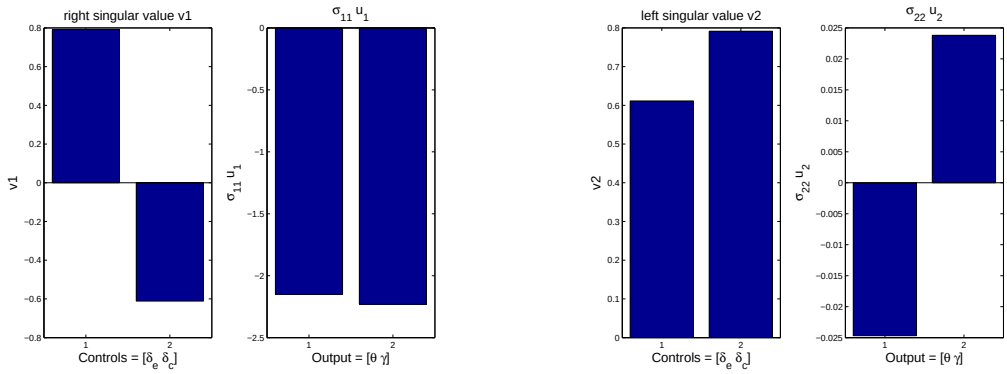

Figure 3.3: NASA-HiMAT Singular Value Decomposition at DC

Plant Singular Values. The plant singular values is plotted in Figure 3.4.We notice that the minimum singular values are below 0db and the singular values are wide spread at low frequencies.This suggests that the resulting controller will have to compensate for low plant gain in the minimum singular value direction i.e. in the canard channel. Hence we expect that significant canard activity will be required to achieve a loop with low frequency disturbance attenuation(e.g. $\sigma_{min}[PK] > 20$ db at low frequencies) and desirable low frequency command following.

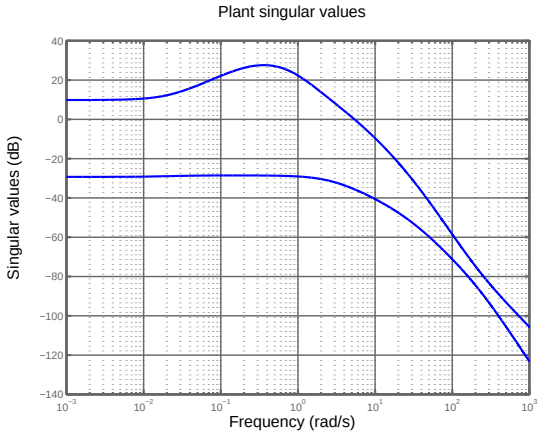

Figure 3.4: Singular Values-TITO NASA Longitudinal Dynamics

The frequency response bode plots for each of the 4 system transfer functions are given in Figure 3.5-3.8

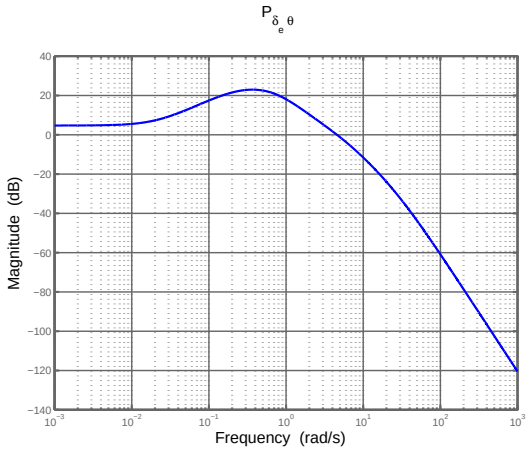

Figure 3.5: $P_{\delta_e \to \theta}$

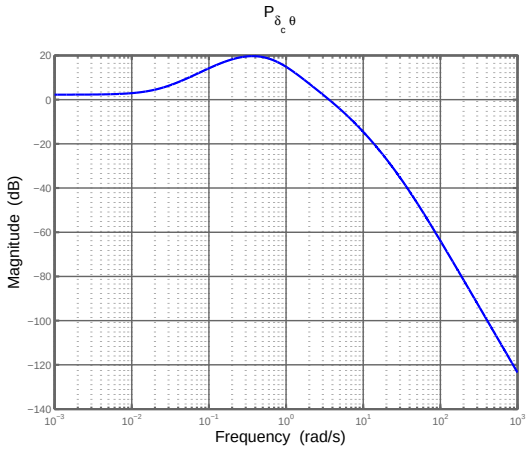

Figure 3.6: $P_{\delta_c \to \theta}$

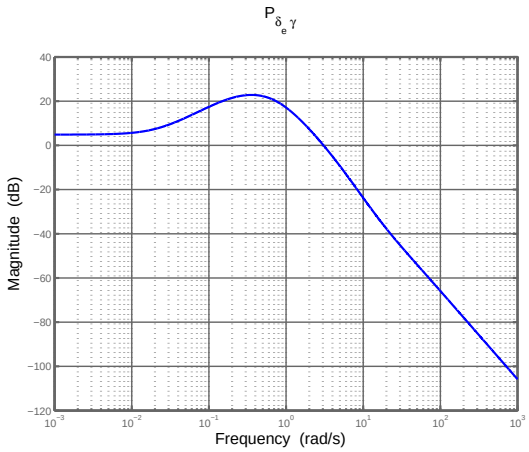

Figure 3.7: $P_{\delta_e \to \gamma}$

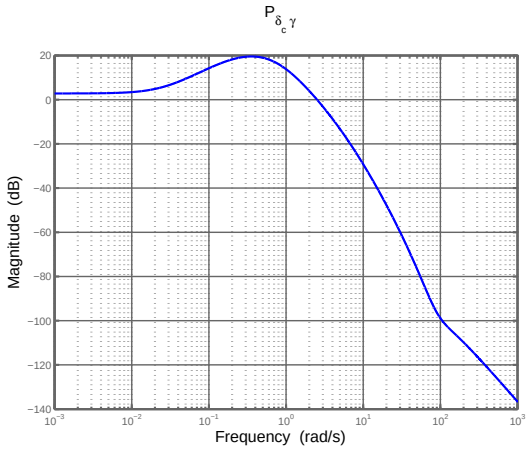

Figure 3.8: $P_{\delta_c \to \gamma}$

3.3 H_∞ Mixed Sensitivity Control System Design for NASA-HiMAT Longitudinal Dynamics

In this section , we consider the design of a control system for the longitudinal dynamics of NASA-HiMAT.

The TITO model for the longitudinal dynamics is as follows:

$$\dot{x} = Ax + Bu \tag{3.3}$$

$$y = Cx + Du \tag{3.4}$$

where

$$x = \begin{bmatrix} v & \text{speed} & \text{ft/sec} \\ \alpha & \text{angle of attack} & \text{deg} \\ q & \text{pitch rate} & \text{deg/sec} \\ \theta & \text{pitch angle} & \text{deg} \\ x_5 & \text{elevon actuator state} & \text{deg} \\ x_6 & \text{canard actuator state} & \text{deg} \end{bmatrix}$$

$$u = \begin{bmatrix} \delta_e & \text{Elevon deflection} \\ \delta_c & \text{Canard deflection} \end{bmatrix}$$

$$y = \begin{bmatrix} \alpha & \text{Pitch Angle} \\ \theta & \text{Flight Path Angle} \end{bmatrix}$$

Bandwidth Design Specification. Based on the presence of RHP-poles at at $s = 0.6898 \pm j0.2488 (\zeta = -0.941, w_n = 0.744)$, we sought an close loop loop bandwidth of about $\omega_B^* > 2Re(p)$ at the input loop breaking point.(Skogestad and Postlethwaite (2007), Page 186,235). Since the plant does not have any RHP-zero, there is no upper bound on the open loop bandwidth at the output loop breaking point. However we can't arbitrarily increases the bandwidth because there would always be high frequency unmodelled actuator dynamics, parasitic dynamics which would render the system unstable if excited.

H_∞ Dynamic Output Feedback Controller Design. We now design the dynamic output feedback controller keeping the above mentioned bandwidth constraints in mind. Let us consider

the generalized plant of the following form:

$$\begin{cases} \dot{x} = Ax + B_1 u + B_2 w \\ z = C_1 x + D_{11} u + D_{12} w \\ y = C_2 x + D_{21} u + D_{22} w \end{cases}$$

where $u = [\delta_e \ \delta_t]^T$ is the input, $w = [r \ di]^T$ is the set of exogenous signals, $y = [\theta \ \gamma]^T$ is the measured output and z is an output vector related to the performance of the closed loop system.

Weighted H_∞ Mixed Sensitivity Problem The standard weighted H_∞ mixed sensitivity problem is to find a finite dimensional real-rational proper internally stabilizing controller K that satisfies(Echols *et al.* (2015)) :

$$K = \arg\{ \min_{K \ stabilizing} \gamma | \left[\begin{array}{c} W_1 S_e \\ W_2 K S_e \\ W_3 T_e \end{array} \right]_\infty < \gamma \} \tag{3.5}$$

where S is the sensitivity transfer function, T is the complementary sensitivity transfer function of the closed loop system and KS is the control action.

However we would use $w = [r \ d_i]$ as the set of exogenous signals in order to get good properties at both input and output loop breaking points.So we do a slightly modified weighted mixed sensitivity problem to find a finite dimensional real-rational proper internally stabilizing controller K that satisfies(Echols *et al.* (2015)):

$$K = \arg\{ \min_{K \ stabilizing} \gamma | \left[\begin{array}{cc} W_1 S_e & W_1 P S_c \\ W_2 K S_e & W_2 T_c \\ W_3 T_e & W_3 P S_c \end{array} \right]_\infty < \gamma \} \tag{3.6}$$

Finding a internally stabilizing controller K that minimizes γ can be translated into an LMI optimization problem as shown below(Scherer *et al.* (1997)):

$$\underset{\hat{A},\hat{B},\hat{C},\hat{D},X,Y}{\text{minimize}} \quad \gamma$$

$$\text{s.t.} \quad \begin{bmatrix} AX + XA^T + B_2\hat{C} + (B_2\hat{C})^T & \hat{A}^T + (A + B_2\hat{D}C_2) & * & * \\ \hat{A} + (A + B_2\hat{D}C_2)^T & A^TY + YA + \hat{B}C + (\hat{B}C)^T & * & * \\ (B_1 + B_2\hat{D}D_{21})^T & (YB_1 + \hat{B}D_{21})^T & -\gamma I & * \\ C_1X + D_{12}\hat{C} & C_1 + D_{12}\hat{D}C_2 & D_{11} + D_{12}\hat{D}D_{21} & -\gamma I \end{bmatrix} < 0$$

$$\begin{bmatrix} X & I \\ I & Y \end{bmatrix} > 0$$

After solving the optimization problem and obtaining the set of $\hat{A}$,$\hat{B}$,$\hat{C}$,$\hat{D}$,X,Y which minimizes γ, the dynamic output feedback controller is obtained as follows(Scherer *et al.* (1997)):

1. Find nonsingular matrices M,N which satisfies $MN^T = I - XY$

2. Construct the controller using

$$\begin{aligned} D_K &= \hat{D} \\ C_K &= (\hat{C} - D_K C_2 X)M^{-T} \\ B_K &= N^{-1}(\hat{B} - YB_2D_K) \\ A_K &= N^{-1}(\hat{A} - NB_KC_2X - YB_2C_KM^T - Y(A + B_2D_KC_2)X)M^{-T} \end{aligned} \tag{3.7}$$

Structure of Weighting functions for H_∞ Mixed Sensitivity Optimization. The structure of weighting functions which has been used to do the above optimization is shown below:

$$W_1 = \begin{bmatrix} \frac{s/M_{s_1} + \omega_{b_1}}{s + \omega_{b_1}\epsilon} & 0 & 0 \\ 0 & \frac{s/M_{s_2} + \omega_{b_2}}{s + \omega_{b_2}\epsilon} & 0 \\ 0 & 0 & 7e-05 \end{bmatrix}$$

$$W_2 = \begin{bmatrix} \frac{s + \omega_{bu_1}/M_{u_1}}{s\epsilon + \omega_{bu_1}\epsilon} & 0 \\ 0 & \frac{s + \omega_{bu_2}/M_{u_2}}{s\epsilon + \omega_{bu_2}} \end{bmatrix}$$

$$W_2 = \begin{bmatrix} \frac{s + \omega_{bc_1}/M_{y_1}}{s\epsilon + \omega_{bc_1}\epsilon} & 0 & 0 \\ 0 & \frac{s + \omega_{bc_2}/M_{y_2}}{s\epsilon + \omega_{bc_2}} & 0 \\ 0 & 0 & 7e-05 \end{bmatrix}$$

	W1	W2	W3
M1	0.1	6	5
M2	0.1	6	5
ω_1	0.5	500	5
ω_2	0.5	500	5
ϵ_1	0.001	0.009	0.05
ϵ_2	0.001	0.009	0.05

Table 3.2: Weighting Function Parameters for NASA-HiMAT

While designing the dynamic output feedback controller, the controller architecture has been considered to imitate a classical inner-outer loop structure to ensure that the designer won't have to design an inner loop controller and outer loop controller separately. The controller architecture has been shown in Figure 3.9.

H_∞ Controller Synthesis

1. Augment the θ and γ output channels of the plant with integrators so as to ensure integral action at low frequencies which would lead to zero steady state error to a step reference input.

2. In order to prevent cancellation integrator states by the H_∞ controller synthesis methodology, use bilinear transformation(Tsai *et al.* (1990),Folly (2007))to shift the system slightly to the right half plane. We use the following Bilinear transformation parameters for NASA-HiMAT longitudinal dynamics model.

   The bilinear transformation parameters for NASA HiMAT model are selected are as follows:

$$p_1 = -0.005 \tag{3.8}$$

$$p_2 = -10^{20} \tag{3.9}$$

   The selection results in

   Transform:

$$s = \frac{\hat{s} + p_1}{\frac{\hat{s}}{p_2} + 1} = \frac{\hat{s} - 0.005}{\frac{\hat{s}}{-10^{20}} + 1} \approx \hat{s} - 0.005 \tag{3.10}$$

Inverse Transform:

$$\tilde{s} \approx s + 0.005 \tag{3.11}$$

3. Choose W1 to shape sensitivity transfer function to have good integral action at low frequencies and ensure that $||S||_\infty$ is below 8db. Choose W2 to shape the KS transfer function such that $||KS||_\infty$ is not too high which would prevent control signal saturation. Also ensure that KS rolls off at higher frequencies. Choose W3 so that $||T||_\infty$ is below 8 db and T rolls off at higher frequencies to ensure sensor noise attenuation at higher frequencies.

4. Create a generalized plant using $w = [rd_i]$ as the set of exogenous signals so that we get good properties at both input and output loop breaking points.

5. Minimize gamma by solving LMI. We use YALMIP(Lofberg (2004),Löfberg (2008)) for solving the LMI.

6. Obtain the controller from the parameters returned by the optimization. Do inverse bilinear transformation to shift the controller to the left half plane so that it corresponds to the original untransformed plant.

7. Shift the integrators from the plant output to the controller input. In other words, augment the controller at the input with integrators.

8. Feed the θ state into the controller as the 3rd input.. This serves as the inner loop feedback as seen in a standard inner-outer feedback control architecture in Figure 3.9. Obtain the closed loop system using the final controller containing 3 inputs and 2 outputs and the original plant.

After performing the optimization, the closed loop poles obtained are as follows:

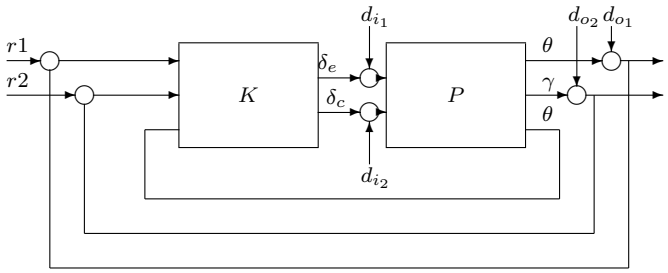

Figure 3.9: Topology of Dynamic Output Feedback Control System

Table 3.3: NASA HiMAT: Closed Loop Poles Using Dynamic Output Feedback

Pole	Damping	Frequency(rad/sec)	Time Constant(sec)
-1.57e-02	1.00e+00	1.57e-02	6.39e+01
-2.18e-02	1.00e+00	2.18e-02	4.59e+01
-3.96e-02	1.00e+00	3.96e-02	2.52e+01
-4.98e-02	1.00e+00	4.98e-02	2.01e+01
-7.61e-02	1.00e+00	7.61e-02	1.31e+01
-1.85e+00 + 7.27e-01i	9.30e-01	1.98e+00	5.42e-01
-1.85e+00 - 7.27e-01i	9.30e-01	1.98e+00	5.42e-01
-3.10e+00 + 1.39e+00i	9.13e-01	3.39e+00	3.23e-01
-3.10e+00 - 1.39e+00i	9.13e-01	3.39e+00	3.23e-01
-6.03e+00 + 2.67e+00i	9.14e-01	6.59e+00	1.66e-01
-6.03e+00 - 2.67e+00i	9.14e-01	6.59e+00	1.66e-01
-3.77e+00 + 1.18e+01i	3.05e-01	1.24e+01	2.65e-01
-3.77e+00 - 1.18e+01i	3.05e-01	1.24e+01	2.65e-01
-2.99e+01	1.00e+00	2.99e+01	3.35e-02
-3.00e+01	1.00e+00	3.00e+01	3.34e-02
-3.00e+01	1.00e+00	3.00e+01	3.33e-02
-3.44e+01 + 2.64e+01i	7.93e-01	4.34e+01	2.91e-02
-3.44e+01 - 2.64e+01i	7.93e-01	4.34e+01	2.91e-02
-8.36e+01	1.00e+00	8.36e+01	1.20e-02
-9.90e+01 + 1.35e+01i	9.91e-01	9.99e+01	1.01e-02
-9.90e+01 - 1.35e+01i	9.91e-01	9.99e+01	1.01e-02
-9.99e+01	1.00e+00	9.99e+01	1.00e-02
-1.00e+02 + 3.13e-01i	1.00e+00	1.00e+02	1.00e-02
-1.00e+02 - 3.13e-01i	1.00e+00	1.00e+02	1.00e-02

The closed loop poles at $s = -0.000856$ and $s = -0.000993$ are the dominant poles and they have

a very large time constant. However they are related to offdiagonal terms of T_o i.e. step response of θ to $r = [0\ 1]$ and γ to $r = [1\ 0]$ as shown in Figure **??** and Figure **??** respectively. The step responses don't have a large peak. Hence the slow dominant poles won't affect the system much.

3.4 Inner-Outer Loop Feedback Loop Control Design Methodology

In the section,we discuss the design methodology for Inner-Outer loop control design for the longitudinal control system.

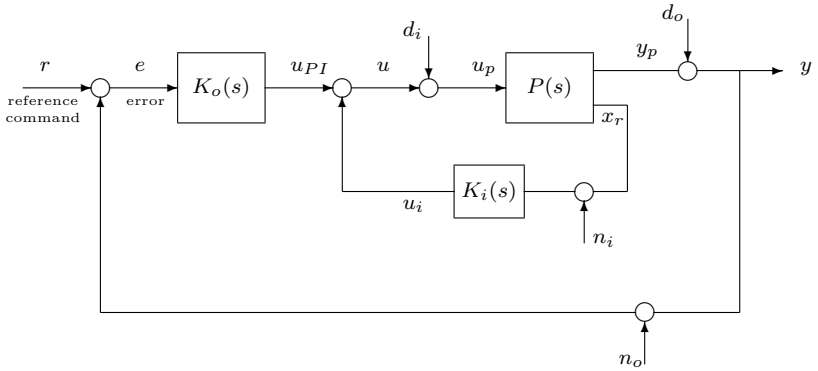

Figure 3.10: Inner Outer Feedback Loop

where

1. Output vector: $y = [y1\ y2]^\top = [\theta\ \gamma]^\top$
2. Control vector: $u = [u1\ u2]^\top = [\delta_e\ \delta_c]^\top$
3. State : $x_r = [\theta]$

Let us first design an inner-outer loop controller for the NASA-HiMAT considering only the diagonal elements of the plant transfer function matrix i.e. $P_{\delta_e \to \theta}$ and $P_{\delta_c \to \gamma}$.

Let us consider the $(1,1)$ element of the plant transfer function matrix i.e. $P_{\delta_e \to \theta}$.

$$P_{\delta_e \to \theta} = \frac{-948.12(s+1.963)(s+0.02177)}{(s+5.676)(s+30)(s+0.2578)(s^2-1.38s+0.5377)} \tag{3.12}$$

Here we use the inner-outer loop feedback control architecture in order to shift the lightly damped unstable phugoid modes of $P_{\delta_e \to \theta}$ to a location with better damping using a PD controller in the

inner loop to obtain $P_{mod} = \frac{P_{\delta_e \to \theta}}{1+L_{mod}}$ where $L_{mod} = P_{\delta_e \to \theta} K_{i1}$. This is followed by the stabilization of P_{mod} using a PI controller in the outer loop. The closed loop system architecture is shown in Figure 3.11 :

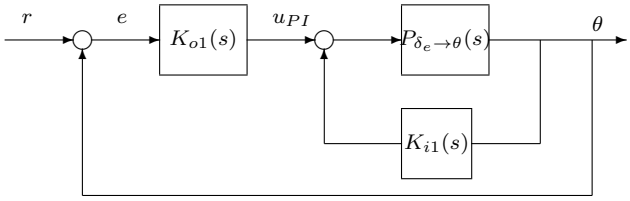

Figure 3.11: F8: Inner Outer Loop Structure for $P_{\delta_e \to \theta}(s)$

As seen in Figure 3.12, the zero of Ki1 pulls the unstable poles to the left half plane and the inner loop with $K_{i1} = -0.5(s + 0.7)$ places the unstable phugoid modes at the location $s = -11.7 + 13.6i, \zeta = 0.652$.

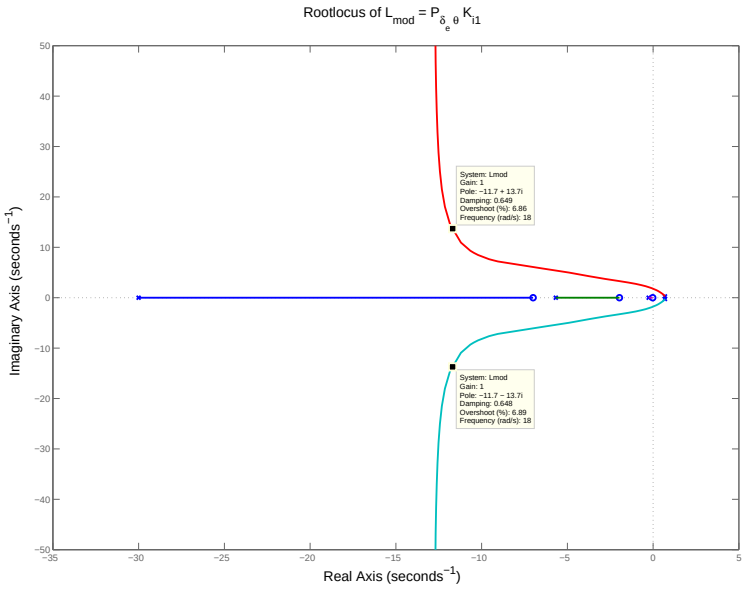

Figure 3.12: Rootlocus of $L_{mod} = P_{\delta_e \to \theta} K_i$ using PD controller

Pole	Damping	Frequency(rad/sec)	Time constant(sec)
-2.53e-02	1.00e+00	2.53e-02	3.95e+01
-2.30e+00	1.00e+00	2.30e+00	4.35e-01
-8.78e+00	1.00e+00	8.78e+00	1.14e-01
-1.17e+01 + 1.36e+01i	6.52e-01	1.80e+01	8.53e-02
-1.17e+01 - 1.36e+01i	6.52e-01	1.80e+01	8.53e-02

Table 3.4: NASA HiMAT: Closed Loop Poles of $P_{mod} = \frac{P_{\delta_e \to \theta} K_{i1}}{1 + P_{\delta_e \to \theta} K_{i1}}$

Now let us use an outer loop to stabilize $L = P_{mod} K_{o1}$ where $P_{mod} = \frac{P_{\delta_e \to \theta}}{1 + L_{mod}}$ and $L_{mod} = P_{\delta_e \to \theta} K_{i1}$. We select $K_{o1} = \frac{-0.2(s+1.5)}{s}$. The rootlocus of $L = P_{mod} K_{o1}$ is as shown in Figure 3.13.

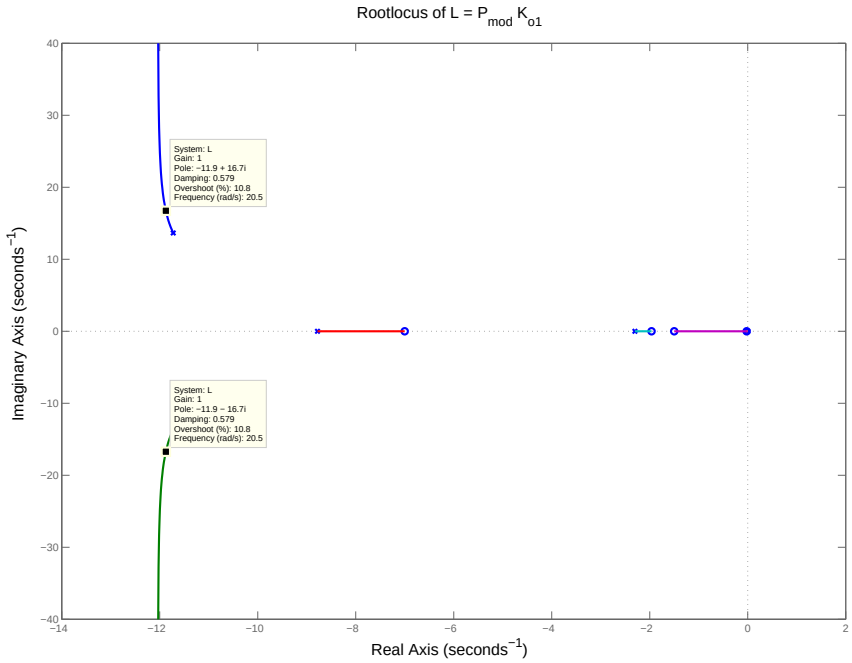

Figure 3.13: Rootlocus of $L = P_{mod} K_{o1}$

The poles of the closed loop system is as follows:

Pole	Damping	Frequency(rad/sec)
-8.15e-002	1.00e+000	8.15e-002
-2.29e+000	1.00e+000	2.29e+000
-9.66e+000	1.00e+000	9.66e+000
-1.12e+001 + 1.35e+001i	6.39e-001	1.76e+001
-1.12e+001 - 1.35e+001i	6.39e-001	1.76e+001

Table 3.5: Closed Loop Poles of $T = \frac{P_{mod}K_{o1}}{1+P_{mod}K_{o1}}$: NASA-HiMAT

Let us now consider the $(2,2)$ element of the plant transfer function matrix i.e. $P_{\delta_c \to \gamma}$.

$$P_{\delta_c \to \gamma} = \frac{0.14896(s + 0.02555)(s^2 + 78.78s + 8568)}{(s + 5.676)(s + 30)(s + 0.2578)(s^2 - 1.38s + 0.5377)} \tag{3.13}$$

Let us now consider the transfer function of $P_{\delta_c \to \gamma}(s)$. Let us consider $P_{\delta_c \to \theta}(s)$ and $P_{\theta \to \gamma}(s)$ such that $P_{\delta_c \to \gamma}(s) = P_{\delta_c \to \theta}(s)P_{\theta \to \gamma}(s)$. To design the flight control system for FPA, let us consider the inner-outer structure in Figure 3.14.

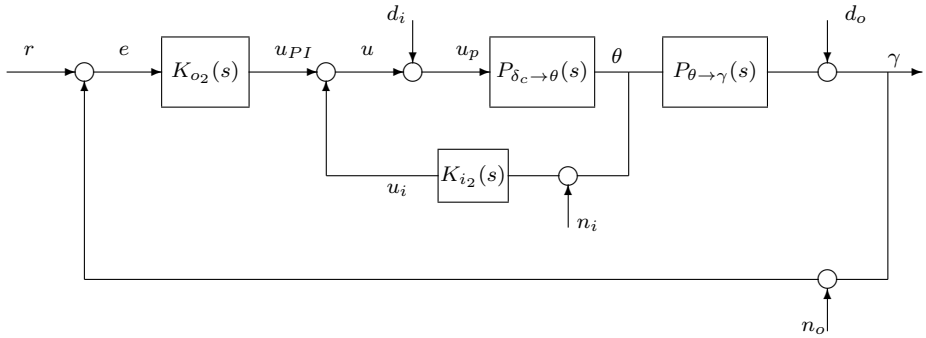

Figure 3.14: Inner Outer Feedback Loop : NASA-HiMAT

As a rule of thumb, we always consider the inner loop as a negative feedback loop. From the transfer function matrix of the plant we obtain

$$P_{\delta_c \to \theta}(s) = \frac{671.88(s + 0.02399)(s + 1.895)}{(s + 5.676)(s + 30)(s + 0.2578)(s^2 - 1.38s + 0.5377)} \tag{3.14}$$

$$P_{\theta\to\gamma}(s) = \frac{0.14896(s+0.02555)(s^2+78.78s+8568)}{671.88(s+0.02399)(s+1.895)} \tag{3.15}$$

Since $P_{\delta_c\to\theta}(s)$ has an instability, the inner loop is used to move the unstable poles of the phugoid mode to a location in the left half plane with good damping so that the outer loop can stabilize the system. We use $K_{i_2} = 0.5(s+7)$. As seen in the root locus plot of $L_{mod} = P_{\delta_c\to\theta}(s)K_{i_2}$ in Figure 3.15, the instability has been moved to the left half plane to a location $s = -9.21 \pm 7.22i$ having $\zeta = 0.78$.

Pole	Damping	Frequency(rad/sec)	Time constant(sec)
-2.91e-02	1.00e+00	2.91e-02	3.43e+01
-2.40e+00	1.00e+00	2.40e+00	4.16e-01
-9.17e+00 + 7.16e+00i	7.88e-01	1.16e+01	1.09e-01
-9.17e+00 - 7.16e+00i	7.88e-01	1.16e+01	1.09e-01
-1.38e+01	1.00e+00	1.38e+01	7.26e-02

Table 3.6: Closed Loop Poles : $T_{mod} = \left(\frac{P_{\delta_c\to\theta}}{1+P_{\delta_c\to\theta}K_{i2}}\right)$:NASA-HiMAT

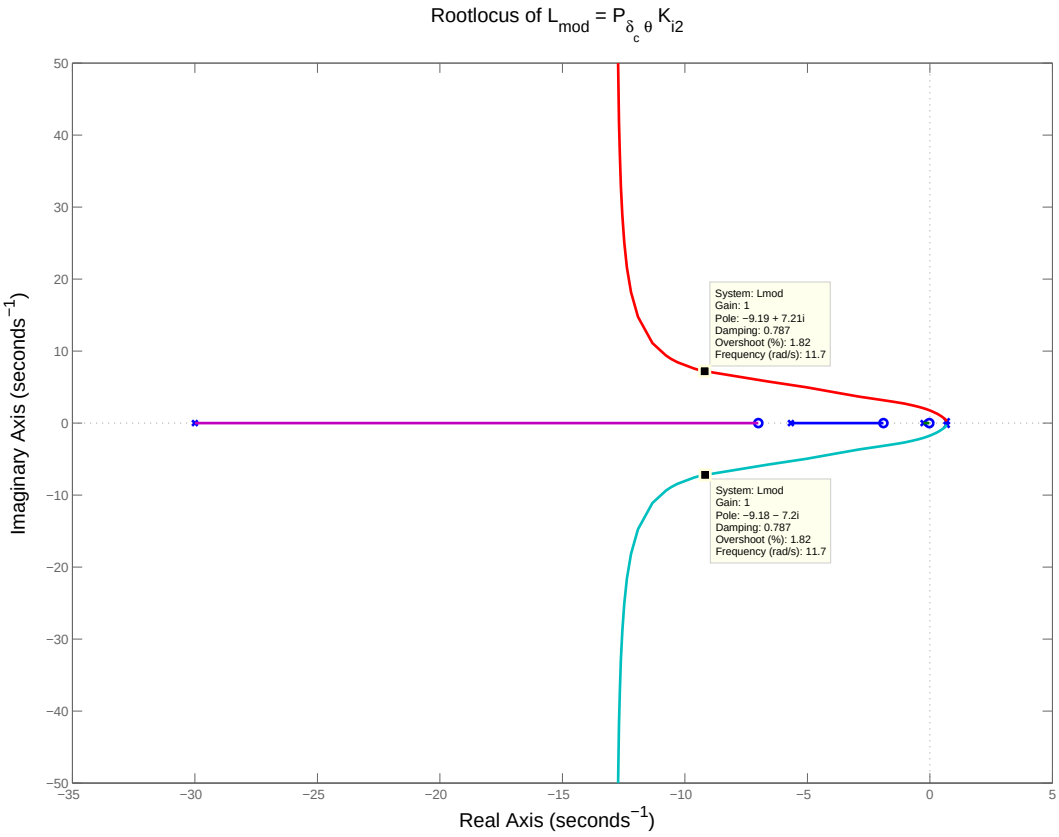

Figure 3.15: Rootlocus of $L_{mod} = P_{\delta_c \to \theta} K_{i2}$

Let us now consider $P_{mod} = T_{mod} P_{\theta \to \gamma}$. From this relation we obtain

$$P_{mod} = \frac{0.14896(s^2 + 78.78s + 8568)}{(s + 2.403)(s + 13.77)(s^2 + 18.35s + 135.5)} \tag{3.16}$$

K_{o_2} is now used to stabilize P_{mod}. Let us use $K_{o_2} = \frac{-1(s-1.5)}{s}$.The root locus of $L = P_{mod} K_{o_2}$ is shown in Figure 3.16.

Hence we have designed a decentralized inner outer loop control system for the rigid model for NASA-HiMAT. The controllers are as follows:

Pole	Damping	Frequency(rad/sec)	Time Constant(sec)
-6.46e-01 + 6.69e-01i	6.95e-01	9.30e-01	1.55e+00
-6.46e-01 - 6.69e-01i	6.95e-01	9.30e-01	1.55e+00
-9.14e+00 + 8.03e+00i	7.51e-01	1.22e+01	1.09e-01
-9.14e+00 - 8.03e+00i	7.51e-01	1.22e+01	1.09e-01
-1.49e+01	1.00e+00	1.49e+01	6.69e-02

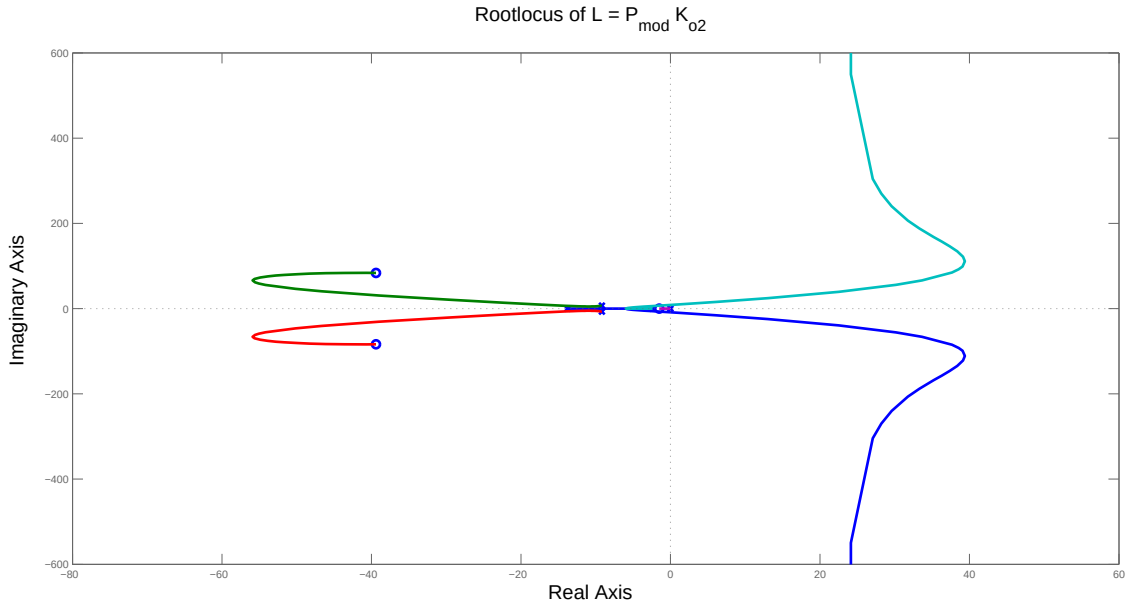

Figure 3.16: Rootlocus of $L = P_{mod}K_{o2}$

$$K_i(s) = \begin{bmatrix} -0.5(s+7) \\ 0.5(s+7) \end{bmatrix} \tag{3.17}$$

$$K_o(s) = \begin{bmatrix} \frac{-0.2(s+1.5)}{s} & 0 \\ 0 & \frac{-1(s-1.5)}{s} \end{bmatrix}$$

3.5 PI-PD controller vs Dynamic Output Feedback Controller

In the section we try to obtain a PI-PD controller which best approximates the dynamic output feedback controller obtained in the previous sections.

We have already obtained a decentralized PI-PD controller which stabilizes the plant provided only the diagonal elements are considered. The controller obtained is as follows:

$$K_i(s) = \begin{bmatrix} -0.5(s+7) \\ 0.5(s+7) \end{bmatrix}$$
$$K_o(s) = \begin{bmatrix} \frac{-0.2(s+1.5)}{s} & 0 \\ 0 & \frac{-1(s-1.5)}{s} \end{bmatrix} \tag{3.18}$$

This controller stabilizes the centralized plant. This means that the centralized system is decoupled enough to let the above PI-PD controller stabilize it.. Therefore, we do a exhaustive search in the neighborhood of the previously obtained g_{o1},z_{o1},g_{o2},z_{o2},g_{i1},z_{i1} parameters in order to obtain a set of values which would stabilize the centralized system. While doing this search, we minimize $||So1 - So2||_\infty$ (where So1 corresponds to Output feedback controller and So2 corresponds to PI-PD controller) in the low frequency range 0.0001 rads/sec to 0.01 rads/sec in order to ensure that we obtain the best PI-PD controller which gives us similar properties at the output loop breaking point when compared to the dynamic output feedback controller at low frequencies.

After doing the optimization, we obtain the following PI-PD controller which minimizes $||So1 - So2||_\infty$ in the range 0.0001 rads/sec to 0.01 rads/sec.The roll-off terms have been selected in a way so that the KS crossover frequency for the dynamic output feedback based closed loop system and the PI-PD based closed loop system is the same. This is done in order to ensure that we are in a position to compare two designs.

$$K_i(s) = \begin{bmatrix} -0.65(s+1.5)\left[\frac{100}{(s+100)}\right]^2 \\ 0.5(s+9)\left[\frac{100}{(s+100)}\right]^2 \end{bmatrix}$$

$$K_o(s) = \begin{bmatrix} \frac{-2(s+0.5)}{s}\left[\frac{5}{(s+5)}\right]^2 & 0 \\ 0 & \frac{-0.5(s-2.5)}{s}\left[\frac{50}{(s+50)}\right]^2 \end{bmatrix} \tag{3.19}$$

The damping of the closed loop system using the PI-PD controller is as follows:

Pole	Damping	Frequency(rad/sec)	Time Constant(sec)
-1.91e-02	1.00e+00	1.91e-02	5.23e+01
-4.95e-02	1.00e+00	4.95e-02	2.02e+01
-4.17e-01	1.00e+00	4.17e-01	2.40e+00
-1.56e+00	1.00e+00	1.56e+00	6.43e-01
-2.73e+00 + 3.05e+00i	6.67e-01	4.09e+00	3.66e-01
-2.73e+00 - 3.05e+00i	6.67e-01	4.09e+00	3.66e-01
-8.42e+00	1.00e+00	8.42e+00	1.19e-01
-1.99e+01 + 1.84e+00i	9.96e-01	2.00e+01	5.02e-02
-1.99e+01 - 1.84e+00i	9.96e-01	2.00e+01	5.02e-02
-4.78e+00 + 2.60e+01i	1.81e-01	2.64e+01	2.09e-01
-4.78e+00 - 2.60e+01i	1.81e-01	2.64e+01	2.09e-01
-3.02e+01	1.00e+00	3.02e+01	3.31e-02
-1.10e+02 + 2.97e+01i	9.65e-01	1.13e+02	9.13e-03
-1.10e+02 - 2.97e+01i	9.65e-01	1.13e+02	9.13e-03

Table 3.7: Closed Loop Poles : PI-PD based controller

Let us now compare the closed loop properties obtained by using PI-PD controller and dynamic output feedback controller.

	$\|\|S_o\|\|_\infty$	$\|\|T_o\|\|_\infty$	$\|\|S_i\|\|_\infty$	$\|\|T_i\|\|_\infty$	$\|\|KS_o\|\|_\infty$	$\|\|PS_i\|\|_\infty$
Dynamic Output feedback Controller	1.82	1.24	12.79	12.29	29.76	0.90
PI-PD controller	1.56	0.01	10.58	9.20	29.29	-9.85

Table 3.8: Attained Closed Loop Properties($||.||_\infty$ in db) for PI-PD and Dynamic Output Feedback Controller: NASA HiMAT

As shown in Table 3.8, the closed loop properties obtained using PI-PD controller is similar to the closed loop properties obtained by using Dynamic output feedback controller at the input loop breaking point. However, at the output loop breaking point, the dynamic output feedback controller gives good properties compared to the PI-PD controller. However the input disturbance attenuation is better in the PI-PD controller design.

Let us now compare the $|So1 - So2|$ and $|Si1 - Si2|$ plots where S_{o1} and S_{i1} corresponds to Dynamic output feedback controller and S_{o2} and S_{i2} corresponds to PI-PD controller as shown in Figure 3.17.

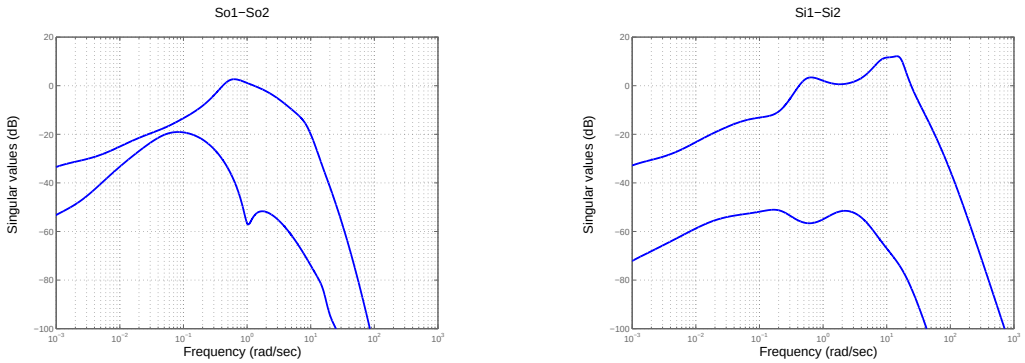

Figure 3.17: Comparison of $|S_{o1} - S_{o2}|$ and $|S_{i1} - S_{i2}|$: NASA-HiMAT

$|S_{o1} - S_{o2}|$ and $|S_{i1} - S_{i2}|$ have very low singular values at low frequencies i.e. the singular values are less than -20db below 0.01 rads/sec. This means that the PI-PD controller and Dynamic output feedback controller would give similar performances at both the loop breaking points if we operate at low frequencies.

In the following figures we compare the frequency domain and time domain plots of various closed loop properties for both PI-PD and dynamic output feedback controller based closed loop system for NASA-HiMAT.

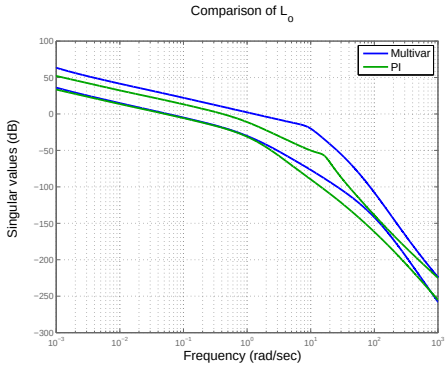

Figure 3.18: L_e : NASA HiMAT

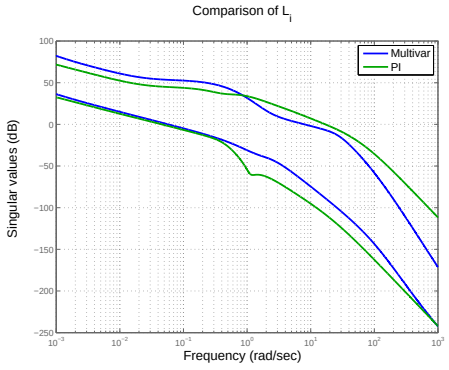

Figure 3.19: L_c : NASA HiMAT

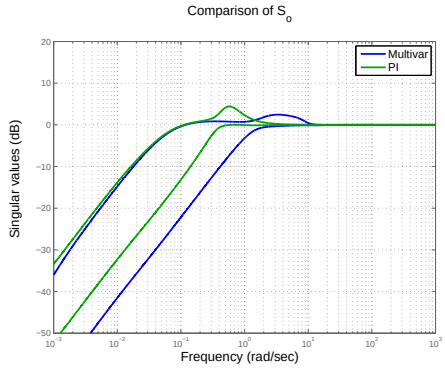

Figure 3.20: S_e : NASA HiMAT

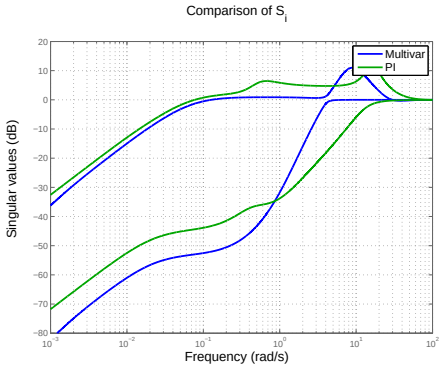

Figure 3.21: S_c : NASA HiMAT

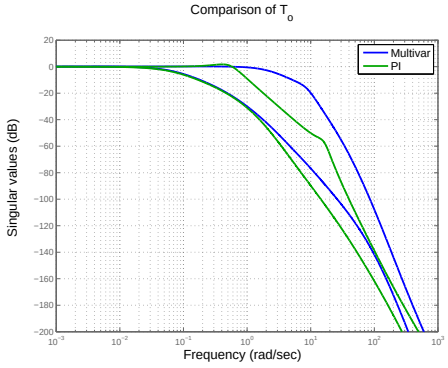

Figure 3.22: T_e : NASA HiMAT

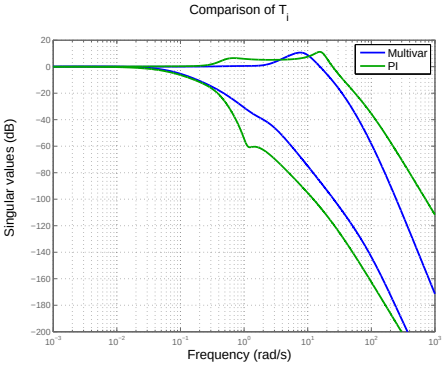

Figure 3.23: T_c : NASA HiMAT

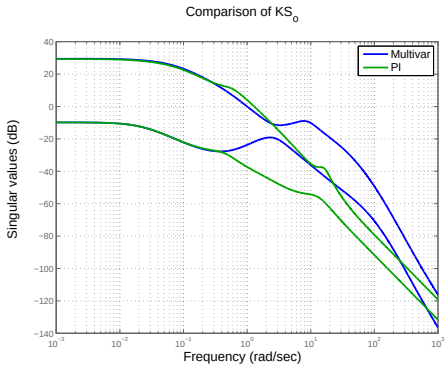

Figure 3.24: KS_e : NASA HiMAT

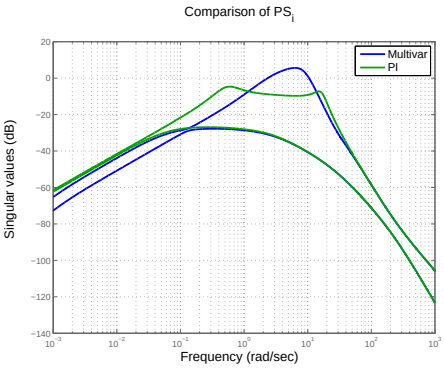

Figure 3.25: PS_c : NASA HiMAT

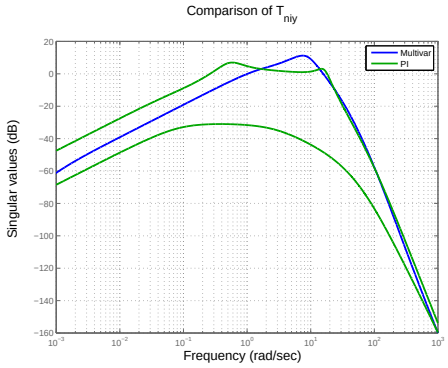

Figure 3.26: $T_{n_i \to y}$: NASA HiMAT

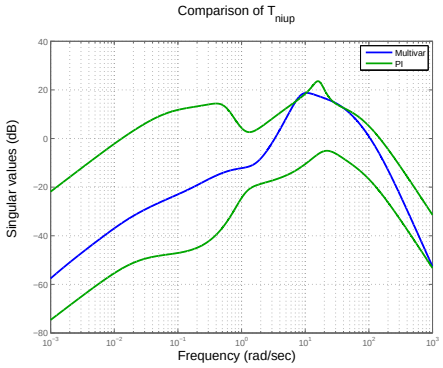

Figure 3.27: $T_{n_i \to u_p}$: NASA HiMAT

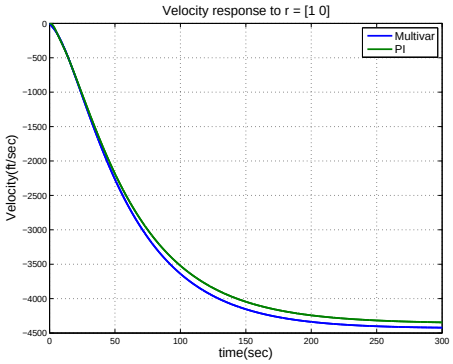

Figure 3.28: Velocity Response to $r = [1\ 0]$:HiMAT

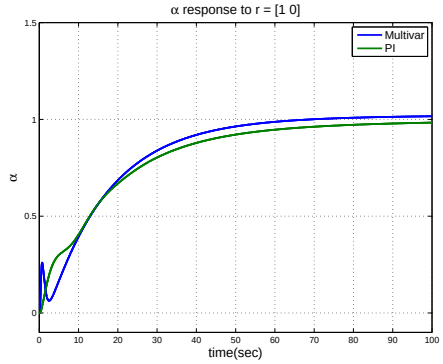

Figure 3.29: AOA Response to $r = [1\ 0]$:HiMAT

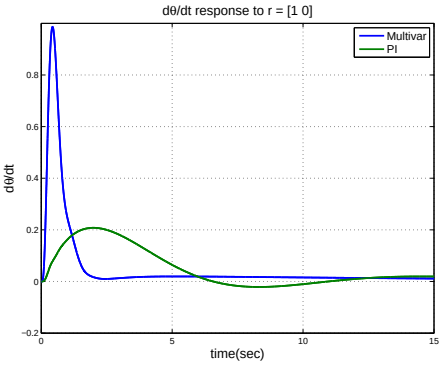

Figure 3.30: $\dot{\theta}$ Response to $r = [1\ 0]$:HiMAT

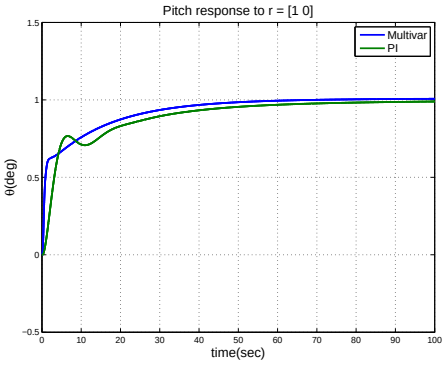

Figure 3.31: θ Response to $r = [1\ 0]$:HiMAT

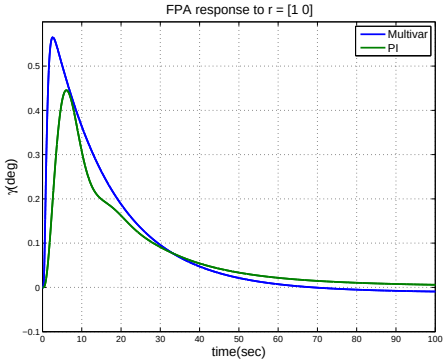

Figure 3.32: FPA Response to $r = [1\ 0]$:HiMAT

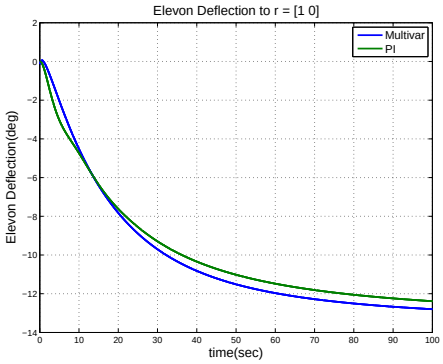

Figure 3.33: δ_e Response to $r = [1\ 0]$:HiMAT

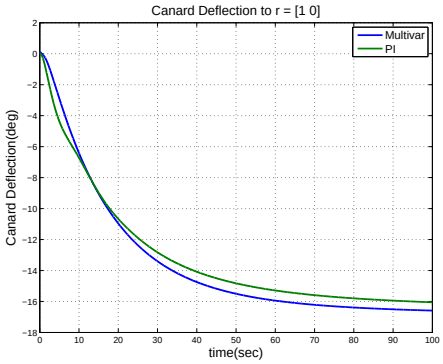

Figure 3.34: δ_c Response to $r = [1\ 0]$:HiMAT

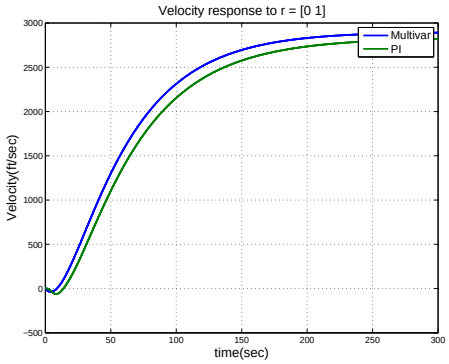

Figure 3.35: Velocity Response to $r = [0\ 1]$:HiMAT

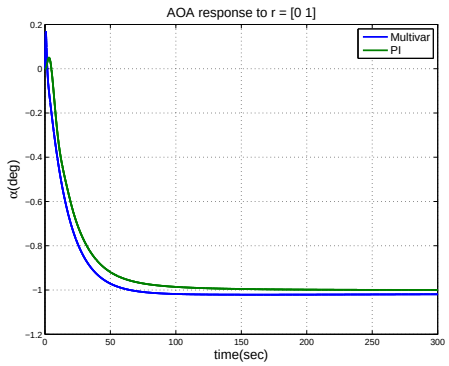

Figure 3.36: AOA Response to $r = [0\ 1]$:HiMAT

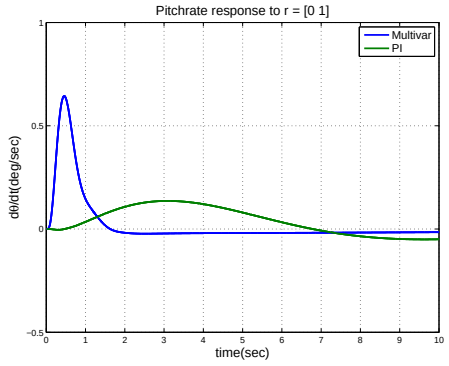

Figure 3.37: $\dot{\theta}$ Response to $r = [0\ 1]$:HiMAT

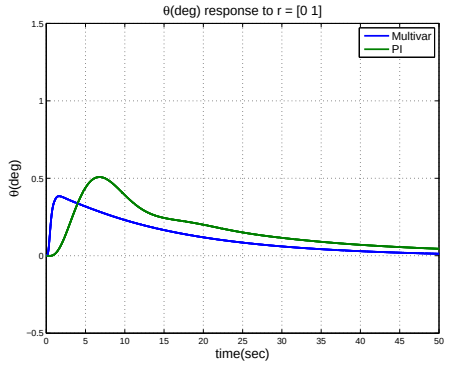

Figure 3.38: θ Response to $r = [0\ 1]$:HiMAT

3.6 Summary

After studying the closed loop properties, it is seen that the dynamic output feedback controller offers good properties at the output loop breaking point but bad properties at input loop breaking point. The PI-PD ($K_{o_{decentralize}}, K_{i_{decentralized}}$) controller also offers good properties at the output but bad properties at input loop breaking point.

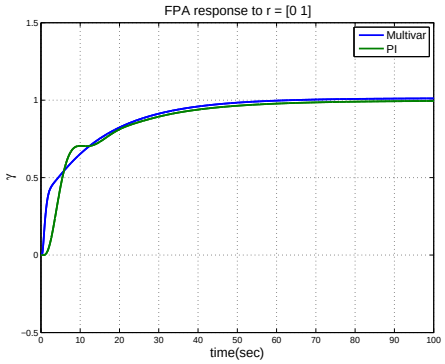

Figure 3.39: FPA Response to $r = [0\ 1]$:HiMAT

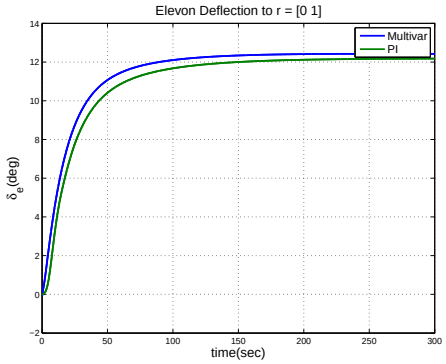

Figure 3.40: δ_e Response to $r = [0\ 1]$:HiMAT

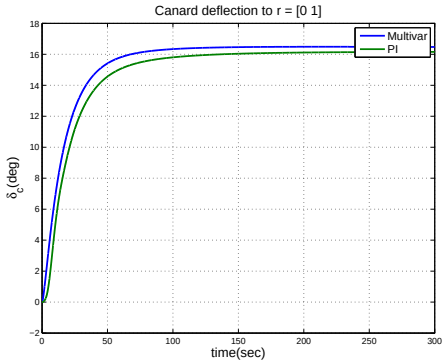

Figure 3.41: δ_c Response to $r = [0\ 1]$:HiMAT

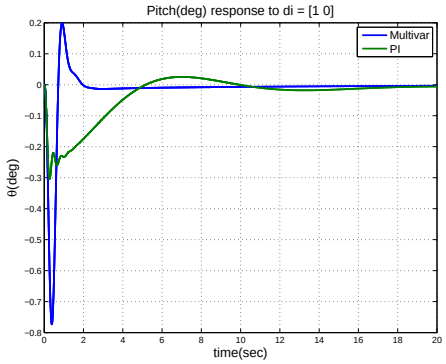

Figure 3.42: Pitch Response to $d_i = [1\ 0]$:HiMAT

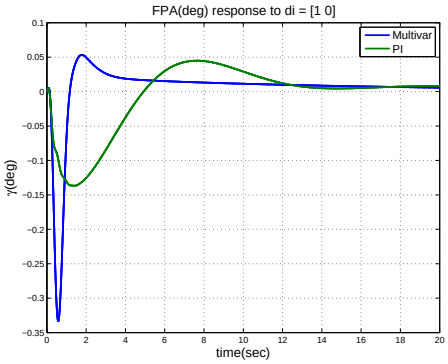

Figure 3.43: FPA Response to $d_i = [1\ 0]$:HiMAT

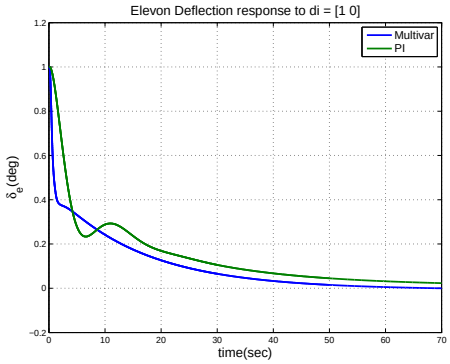

Figure 3.44: δ_e to $d_i = [1\ 0]$:HiMAT

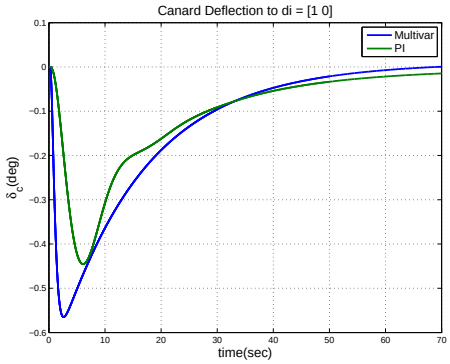

Figure 3.45: δ_c Response to $d_i = [1\ 0]$:HiMAT

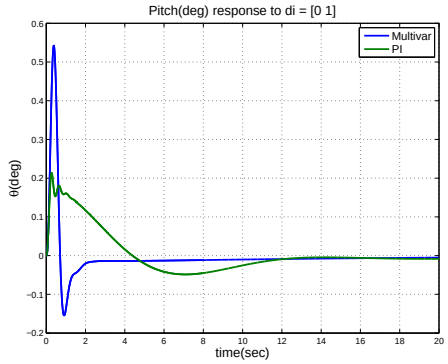

Figure 3.46: Pitch Response to $d_i = [0\ 1]$:HiMAT

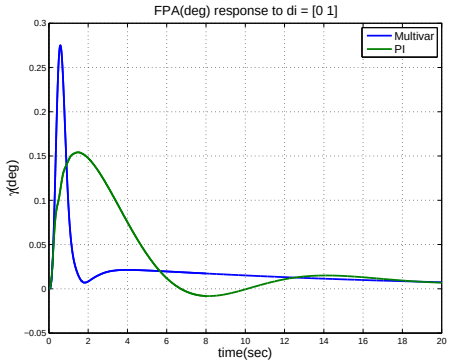

Figure 3.47: FPA Response to $d_i = [0\ 1]$:HiMAT

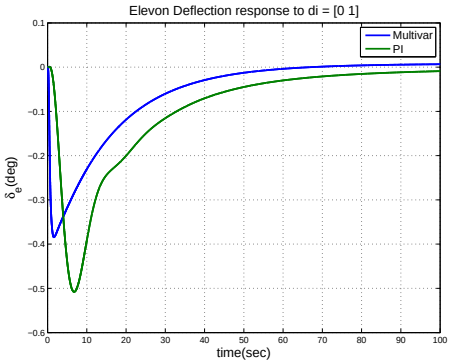

Figure 3.48: δ_e Response to $d_i = [0\ 1]$:HiMAT

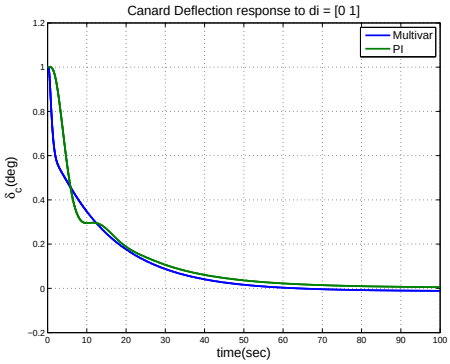

Figure 3.49: δ_c Response to $d_i = [0\ 1]$:HiMAT

Chapter 4

MCDONNEL DOUGLAS AV-8A HARRIER

4.1 Overview.

In this chapter, we briefly discuss the longitudinal dynamics of the AV-8A Harrier aircraft. In the following sections we design a dynamic output feedback controller using Linear Matrix Inequality. We also discuss the inner outer loop control structure and design a PI-PD controller for the longitudinal dynamics. Finally we attempt to design a PI-PD controller which would similar closed loop properties as the dynamic output feedback controller.

Background. The McDonnell Douglas(now Boeing) AV-8A Harrier is a single engine ground attack aircraft which is capable of vertical or short takeoff and landing. It was developed in the 1960s and formed the first generation of the Harrier series of aircrafts. It is powered by a single Pegasus turbofan engine mounted in the fuselage. The engine is fitted with four vectoring nozzles for directing the thrust generated(two for the bypass flow and two for the jet exhaust) and two air intakes. The aircraft also has several smaller reaction nozzles in the nose , tail and wingtips for the purpose of balancing during vertical flight. The aircraft is capable of forward flight like a fixed wing aircraft. It is also capable of doing VTOL and STOL manoeuvres where the lift and control surfaces are useless. The harrier also has two control elements namely the thrust vector and the reaction control system which is not found in conventional fixed-wing aircraft.

Figure 4.1: McDonnell Douglas AV-8A Harrier

4.2 AV-8A Harrier Longitudinal Dynamics

In this section, we examine the longitudinal dynamics for the AV-8A Harrier aircraft.

The TITO model for the longitudinal dynamics at the above flight conditions is as follows:

$$\dot{x} = Ax + Bu \tag{4.1}$$

$$y = Cx + Du \tag{4.2}$$

where

$$A = \begin{bmatrix} 0 & 1.0000 & 0 & 0 & 0 & 0 \\ -1.8370 & -1.8930 & 1.8370 & -0.0229 & 0.0062 & -7.1224 \\ 0.5295 & 0.0085 & -0.5295 & 0.0344 & 0.0002 & 0.0974 \\ -0.6021 & 0 & 0.0401 & -0.0621 & 0.0073 & -0.0452 \\ 0 & 0 & 0 & 0 & -1.9660 & 0 \\ 0 & 0 & 0 & 0 & 0 & -12.0000 \end{bmatrix}$$

$$B = \begin{bmatrix} 0 & 0 \\ 0 & 0 \\ 0 & 0 \\ 0 & 0 \\ 112.6518 & 0 \\ 0 & 12.0000 \end{bmatrix}$$

$$C = \begin{bmatrix} 0 & 0 & 1 & 0 & 0 & 0 \\ 0 & 0 & 0 & 1 & 0 & 0 \end{bmatrix}$$

$$D = \begin{bmatrix} 0 & 0 \\ 0 & 0 \end{bmatrix}$$

$$x = \begin{bmatrix} \theta & \text{Pitch angle} & \text{deg} \\ q & \text{Pitch rate} & \text{deg} \\ \gamma & \text{Flight path angle} & \text{deg} \\ v & \text{Velocity} & \text{ft/sec} \\ x_5 & \text{Stabilizer angle} & \text{deg} \\ x_6 & \text{Engine fan speed} & \text{ft/sec} \end{bmatrix}$$

$$u = \begin{bmatrix} \delta_s & \text{Stick input} \\ \delta_t & \text{Throttle} \end{bmatrix}$$

$$y = \begin{bmatrix} v & \text{Flight Path Angle} & \text{deg} \\ \gamma & \text{Velocity} & \text{deg} \end{bmatrix}$$

The aircraft's two control surfaces are as follows :

1. Stick input
2. Throttle

Poles and Zeros. The aircraft has stable phugoid modes at $s = -0.0236 \pm j0.0975$($\zeta = 0.235$,$w_n = 0.1$ rads/sec), stable short period modes at $s = -1.22 \pm j1.17$($\zeta = 0.722$,$w_n = 1.69$ rads/sec). It also has a transmission zero at $s = 5.5464$ and $s = -6.8290$.

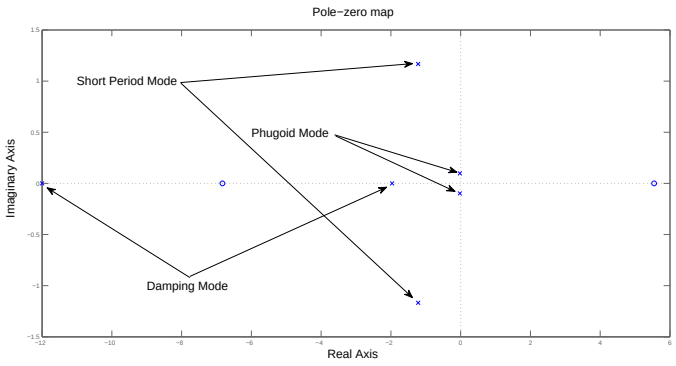

Figure 4.2: Visualization of Poles and Zeros for AV8A Longitudinal Dynamics

Transfer Function Matrix. The system transfer function matrix from u to y is given by

$$G(s) = C(sI - A)^{-1}B + D = \begin{bmatrix} G_{\delta_s \gamma} & G_{\delta_t \gamma} \\ G_{\delta_s v} & G_{\delta_t v} \end{bmatrix}$$

where

$$G_{\delta_s \gamma} = \frac{0.02253(s+0.1154)(s^2+3.366s+20.38)}{(s+1.966)(s^2+0.0472s+0.01007)(s^2+2.437s+2.848}$$

$$G_{\delta_t \gamma} = \frac{1.1689(s+6.753)(s-5.458)(s+0.02209)}{(s+1.966)(s^2+0.0472s+0.01007)(s^2+2.437s+2.848)}$$

$$G_{\delta_s v} = \frac{0.82749(s-0.1078)(s^2+2.531s+2.591)}{(s+1.966)(s^2+0.0472s+0.01007)(s^2+2.437s+2.848)}$$

$$G_{\delta_t v} = \frac{-0.5424(s+10.62)(s-8.763)(s+0.48)}{(s+1.966)(s^2+0.0472s+0.01007)(s^2+2.437s+2.848)}$$

The individual transfer functions show the presence of stable phugoid modes at $s = -0.0236 \pm j0.0975(\zeta = 0.235, w_n = 0.1$ rads/sec) and short period modes at $s = -1.22 \pm j1.17(\zeta = 0.722, w_n = 1.69$ rads/sec). The transfer functions also show the presence of right half plane zeros.

The frequency response bode plots for each of the 4 system transfer functions is given in Figure 4.3-4.6

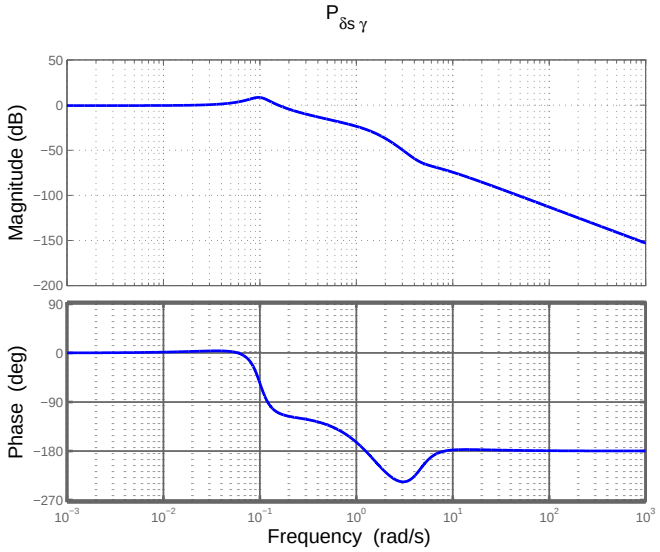

Figure 4.3: Frequency Response - δ_s to FPA

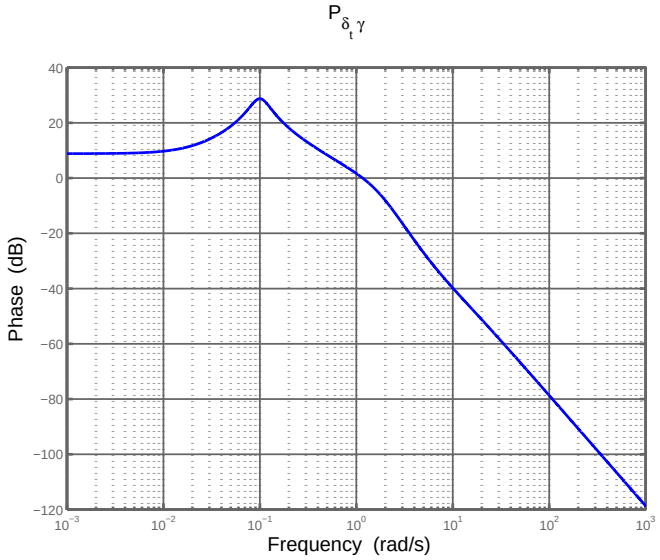

Figure 4.4: Frequency Response - δ_t to FPA

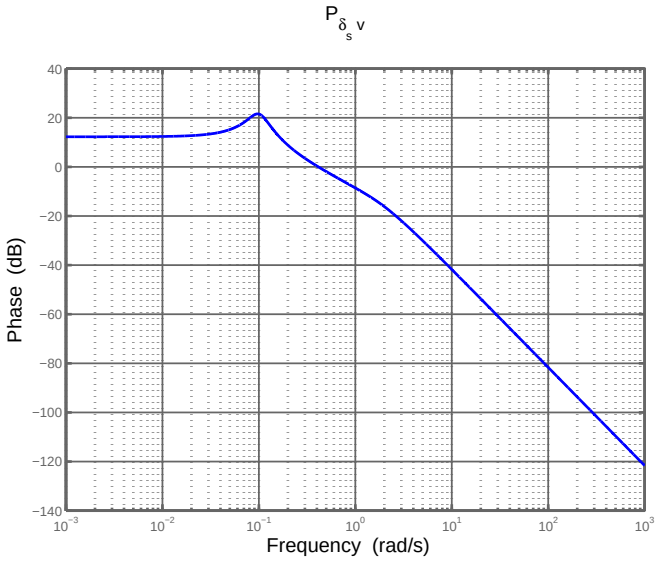

Figure 4.5: Frequency Response - δ_s to v

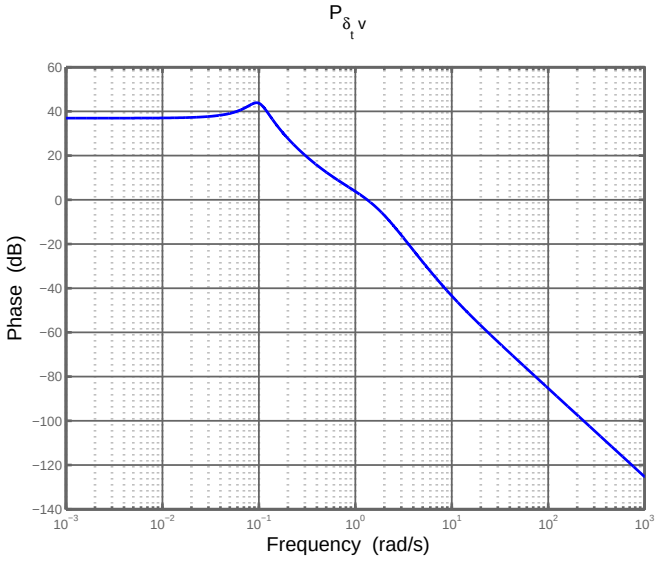

Figure 4.6: Frequency Response - δ_t to v

MIMO Frequency Response: Singular Values

The MIMO singular values for the plant transfer matrix from controls $u = [\delta_s \ \delta_t]$ to plant output $y = [FPA \ Vel]$ are plotted in Figure 4.7. The plot shows a peaking at 0.1 rads/sec due to the lightly damped phugoid mode at at $s = -0.0236 \pm j0.0975(\zeta = 0.235, w_n = 0.1$ rads/sec). In the plot, we notice that the minimum singular values of the plant corresponding to the δ_s channel are low and wide spread at low frequencies. Hence the resulting controller will have to compensate for the low plant gain in the δ_s channel. Thus we expect that significant stick input activity will be required in order to achieve a loop with desirable low frequency disturbance attenuation(e.g. $\sigma_{min}[PK] > 20$ db at low frequencies) and desirable low frequency command following.

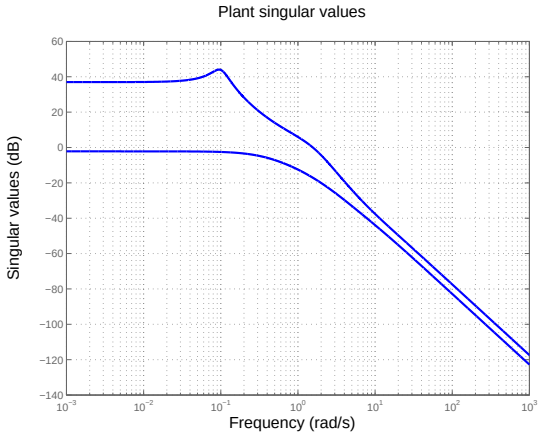

Figure 4.7: AV-8A Harrier Longitudinal Dynamics Singular Values MIMO Frequency Response

DC Gain Analysis. Singular Value Decomposition. While analyzing the AV-8A Harrier model at DC, we get the following matrix of DC gains:

$$\begin{bmatrix} \gamma \\ v \end{bmatrix} = \begin{bmatrix} 0.9400 & -2.766 \\ -4.0996 & 70.4110 \end{bmatrix} \begin{bmatrix} \delta_s \\ \delta_t \end{bmatrix}$$

A singular value decomposition at DC yields the following:

$$G(j0) = C(-A)^{-1}B + D = U\Sigma V^{\top} = \begin{bmatrix} 0.9400 & -2.766 \\ -4.0996 & 70.4110 \end{bmatrix}$$

$$U = \begin{bmatrix} -0.0399 & 0.9992 \\ 0.9992 & 0.0399 \end{bmatrix}; \Sigma = \begin{bmatrix} 70.5864 & 0 \\ 0 & 0.7770 \end{bmatrix}; V = \begin{bmatrix} -0.0586 & 0.9983 \\ 0.9983 & 0.0586 \end{bmatrix}$$

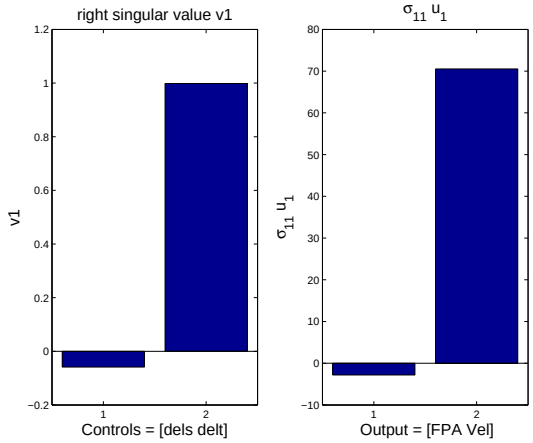

Figure 4.8: AV-8A Harrier SVD at DC for Longitudinal Dynamics $v_1 \rightarrow \sigma_1 u_1$

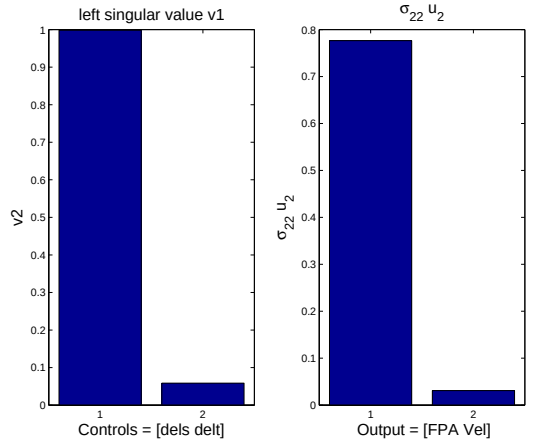

Figure 4.9: AV-8A Harrier SVD at DC for Longitudinal Dynamics $v_2 \rightarrow \sigma_2 u_2$

From the singular value decomposition, conclusions can be drawn about the steady state input output coupling.

1. Examination of the first columns of V,Σ and U shows that throttle has a greater impact on the velocity of the aircraft compared to the flight path angle .This may be visualized as shown in Figure 4.8. This analysis shows that throttle should be used as the primary control for maintaining steady velocity perturbations from equilibrium.

2. Examination of the second columns of V,Σ and U shows that stick input has a greater impact

on the flight path angle of the aircraft than the velocity of the aircraft. This may be visualized as shown in Figure 4.9. This analysis shows that stick input should be used as the primary control for maintaining steady flight path angle perturbations from equilibrium.

The Singular Value Decomposition at DC shows that AV8A longitudinal dynamics is sufficiently decoupled at DC

4.3 H_∞ Mixed Sensitivity Control System Design for AV-8A Harrier Longitudinal Dynamics

In this section , we consider the design of a control system for the longitudinal dynamics of AV-8A Harrier.

The TITO model for the longitudinal dynamics is as follows:

$$\dot{x} = Ax + Bu \tag{4.3}$$

$$y = Cx + Du \tag{4.4}$$

where

$$x = \begin{bmatrix} \theta & \text{Pitch angle} & \text{deg} \\ q & \text{Pitch rate} & \text{deg} \\ \gamma & \text{Flight path angle} & \text{deg} \\ v & \text{Velocity} & \text{ft/sec} \\ x_5 & \text{Stabilizer angle} & \text{deg} \\ x_6 & \text{Engine fan speed} & \text{ft/sec} \end{bmatrix}$$

$$u = \begin{bmatrix} \delta_s & \text{Stick input} \\ \delta_t & \text{Throttle} \end{bmatrix}$$

$$y = \begin{bmatrix} v & \text{Velocity} & \text{deg} \\ \gamma & \text{Flight path angle} & \text{deg} \end{bmatrix}$$

The aircraft is characterized by stable phugoid modes at $s = -0.0236 \pm j0.0975$($\zeta = 0.235$,$w_n =$ 0.1 rads/sec) and short period modes at $s = -1.22 \pm j1.17$($\zeta = 0.722$,$w_n = 1.69$ rads/sec).It also has a transmission zero at $s = 5.5464$ and $s = -6.8290$. The presence of RHP-zero at $s = 5.5464$ makes designing a control system for AV-8A tedious because RHP-zero puts an upper bound on the

acceptable closed loop bandwidth.

Bandwidth Design Specification. Based on the presence of RHP-zero at $s = 5.5464$, we sought an open loop bandwidth of about $\omega_B^* < 0.5z$ (Skogestad and Postlethwaite (2007),Page 186,235). We choose an open loop bandwidth of about 1 rad/sec.

H_∞ Dynamic Output Feedback Controller Design. We now design the dynamic output feedback controller keeping the above mentioned bandwidth constraints in mind. Let us consider the generalized plant of the following form:

$$\begin{cases} \dot{x} = Ax + B_1 u + B_2 w \\ z = C_1 x + D_{11} u + D_{12} w \\ y = C_2 x + D_{21} u + D_{22} w \end{cases}$$

where $u = [\delta_e \ \delta_t]^T$ is the input, $w = [r \ di]^T$ is the set of exogenous signals, $y = [\gamma \ v]^T$ is the measured output and z is an output vector related to the performance of the closed loop system.

Weighted H_∞ Mixed Sensitivity Problem The standard weighted H_∞ mixed sensitivity problem is to find a finite dimensional real-rational proper internally stabilizing controller K that satisfies: (Echols *et al.* (2015))

$$K = \arg\{ \min_{K \ stabilizing} \gamma | \begin{bmatrix} W_1 S_e \\ W_2 K S_e \\ W_3 T_e \end{bmatrix}_\infty < \gamma \} \tag{4.5}$$

where S is the sensitivity transfer function, T is the complementary sensitivity transfer function of the closed loop system and KS is the control action.

However we would use $w = [r \ d_i]$ as the set of exogenous signals in order to get good properties at both input and output loop breaking points.So we do a slightly modified weighted mixed sensitivity problem to find a finite dimensional real-rational proper internally stabilizing controller K that satisfies: (Echols *et al.* (2015))

$$K = \arg\{ \min_{K \ stabilizing} \gamma | \left\| \begin{bmatrix} W_1 S_e & W_1 P S_c \\ W_2 K S_e & W_2 T_c \\ W_3 T_e & W_3 P S_c \end{bmatrix} \right\|_\infty < \gamma \} \tag{4.6}$$

Finding a internally stabilizing controller K that minimizes γ can be translated into an LMI optimization problem as shown below(Gahinet *et al.* (1995),Scherer *et al.* (1997),Gahinet (1996),Boyd *et al.* (1993))

$$\begin{aligned} &\underset{\hat{A},\hat{B},\hat{C},\hat{D},X,Y}{\text{minimize}} \quad \gamma \\ &\text{s.t.} \quad \begin{bmatrix} AX + XA^T + B_2\hat{C} + (B_2\hat{C})^T & \hat{A}^T + (A + B_2\hat{D}C_2) & * & * \\ \hat{A} + (A + B_2\hat{D}C_2)^T & A^TY + YA + \hat{B}C + (\hat{B}C)^T & * & * \\ (B_1 + B_2\hat{D}D_{21})^T & (YB_1 + \hat{B}D_{21})^T & -\gamma I & * \\ C_1X + D_{12}\hat{C} & C_1 + D_{12}\hat{D}C_2 & D_{11} + D_{12}\hat{D}D_{21} & -\gamma I \end{bmatrix} < 0 \\ &\quad \begin{bmatrix} X & I \\ I & Y \end{bmatrix} > 0 \end{aligned}$$

After solving the optimization problem and obtaining the set of $\hat{A}$,$\hat{B}$,$\hat{C}$,$\hat{D}$,X,Y which minimizes γ, the dynamic output feedback controller is obtained as follows (Scherer *et al.* (1997)):

1. Find nonsingular matrices M,N which satisfies $MN^T = I - XY$

2. Construct the controller using

$$\begin{aligned} D_K &= \hat{D} \\ C_K &= (\hat{C} - D_K C_2 X) M^{-T} \\ B_K &= N^{-1}(\hat{B} - Y B_2 D_K) \\ A_K &= N^{-1}(\hat{A} - N B_K C_2 X - Y B_2 C_K M^T - Y(A + B_2 D_K C_2)X) M^{-T} \end{aligned} \tag{4.7}$$

Hinfinity design without Bilinear Transformation. Initially we design a controller using a straight forward H_∞ mixed sensitivity optimization without the use of Bilinear Transformation and without augmenting the plant.

Weighting functions.

$$W_1 = \begin{bmatrix} \frac{s/M_{s_1}+\omega_{b_1}}{s+\omega_{b_1}\epsilon} & 0 & 0 & 0 \\ 0 & \frac{s/M_{s_2}+\omega_{b_2}}{s+\omega_{b_2}\epsilon} & 0 & 0 \\ 0 & 0 & 7e-05 & 0 \\ 0 & 0 & 0 & 7e-05 \end{bmatrix}$$

$$W_2 = \begin{bmatrix} \frac{s+\omega_{bu_1}/M_{u_1}}{s\epsilon+\omega_{bu_1}\epsilon} & 0 \\ 0 & \frac{s+\omega_{bu_2}/M_{u_2}}{s\epsilon+\omega_{bu_2}} \end{bmatrix}$$

$$W_2 = \begin{bmatrix} \frac{s+\omega_{bc_1}/M_{y_1}}{s\epsilon+\omega_{bc_1}\epsilon} & 0 & 0 & 0 \\ 0 & \frac{s+\omega_{bc_2}/M_{y_2}}{s\epsilon+\omega_{bc_2}} & 0 & 0 \\ 0 & 0 & 7e-05 & 0 \\ 0 & 0 & 0 & 7e-05 \end{bmatrix}$$

Please note that the weighting functions W_1 and W_3 are 4×4 since both velocity and Flight path angle have been fed back in the inner loop. This concept has been explained in detail in the later sections.

	W1	W2	W3
M1	5	5	10
M2	5	5	10
ω_1	0.5	100	30
ω_2	0.5	100	30
ϵ_1	0.001	0.001	0.001
ϵ_2	0.001	0.001	0.001

Table 4.1: Weighting Function Parameters for AV-8A: Without Bilinear Transformation

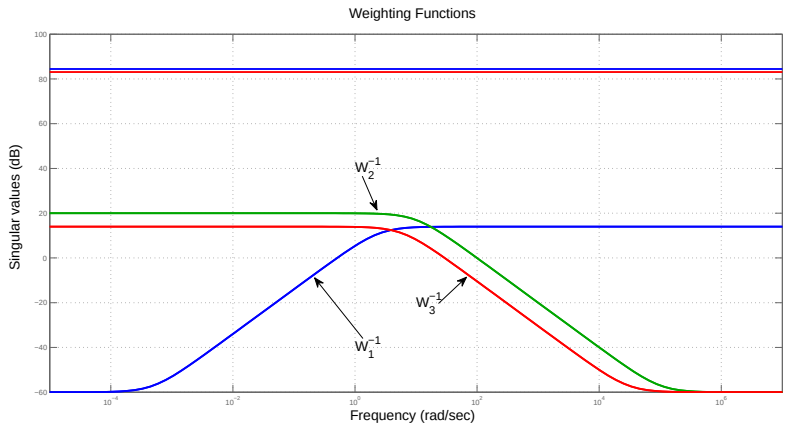

Figure 4.10: Weighting Functions for Mixed-Sensitivity H_∞ optimization

Closed loop poles. The closed loop poles that result from straight forward H_∞ optimization(without Bilinear Transformation) are as follows:

Pole	Damping	Frequency(rad/sec)
-2.36e-002 + 9.75e-002i	2.35e-001	1.00e-001
-2.36e-002 - 9.75e-002i	2.35e-001	1.00e-001
-2.02e+000	1.00e+000	2.02e+000
-2.01e+000 + 6.21e-001i	9.55e-001	2.10e+000
-2.01e+000 - 6.21e-001i	9.55e-001	2.10e+000
-2.36e+000	1.00e+000	2.36e+000
-1.87e+000 + 2.25e+000i	6.39e-001	2.92e+000
-1.87e+000 - 2.25e+000i	6.39e-001	2.92e+000
-6.30e+000	1.00e+000	6.30e+000
-1.05e+001 + 1.11e-001i	1.00e+000	1.05e+001
-1.05e+001 - 1.11e-001i	1.00e+000	1.05e+001
-1.18e+001	1.00e+000	1.18e+001

Table 4.2: Poles of AV-8A Closed Loop System : No Bilinear Transformation

The resulting minimum γ is

$$\gamma = 0.997 \tag{4.8}$$

The above design is unacceptable because of the presence of lightly damped poles($\zeta = 0.235$). This has resulted because the controller obtained from straight forward H_∞ mixed-sensitivity optimization has zeros which cancels out the poles associated with the lighty damped phugoid modes of the plant. This cancellation can be seen in Figure 4.11 where there is a bump(due to lightly damped phugoid mode poles) and a dip(due to zeros in the controller) in the singular value plots of plant and the controller K respectively at 0.1 rad/sec. There are several ways of circumventing this difficulty. One approach is to impose a minimum closed loop damping via a regional pole placement constraint. The second approach is to use Bilinear transformation which has been used in this thesis(Tsai *et al.* (1990),Folly (2007)).

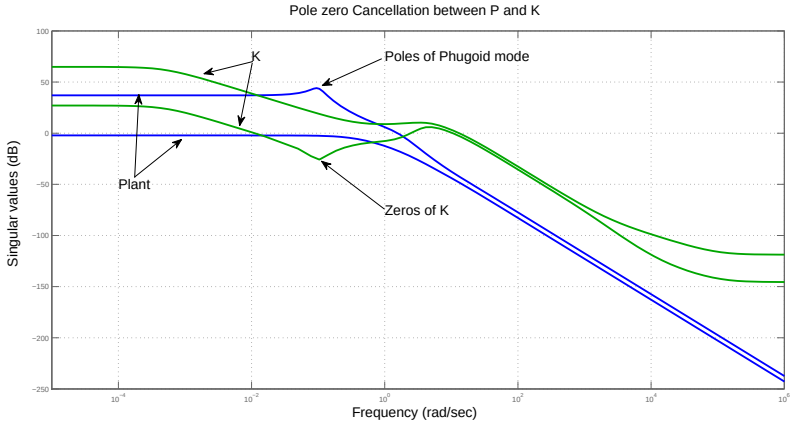

Figure 4.11: Pole-zero Cancellation Between P and K

Bilinear Transformation. The plant has lightly damped stable phugoid modes at $s = -0.0236 \pm j0.0975$($\zeta = 0.235$,$w_n = 0.1$ rads/sec). We use bilinear transformation to shift the lightly damped poles to the right half plane so that the controller obtained from H_∞ mixed-sensitivity optimization does not cancel out the lightly damped poles.

The following rules must be followed while selecting the parameters p_1 and p_2.

1. Parameter p_2 should be large($p_2 = -10^{20}$) so that the bilinear transformation merely becomes a rightward shifting transformation by $-p_1$ units.

2. Parameter p_1 should be chosen in such a way that all poles which must not be canceled by the resulting controller should be moved into the right half plane after the bilinear transformation has been applied.Typically p_1 should be less than the minimum of the real parts of the plant poles which needs to be moved to the right half plane. In our problem, we require $p_1 < -0.0236$.

3. Parameter p_1 affects the bandwidth of the open loop and closed loop system. The bandwidth(open loop and closed loop) increases as p_1 is decreased(i.e. making it more negative). As bandwidth increases, the peak of the KS singular value plot increases i.e. more control action results for step commands. Also, since AV-8A longitudinal dynamics has a RHP-zero which puts an upper bound on the acceptable bandwidth of the closed loop system, the selection of p_1 becomes important. Therefore p_1 should not be made too negative.

The bilinear transformation parameters selected are as follows:

$$p_1 = -0.1 \tag{4.9}$$

$$p_2 = -10^{20} \tag{4.10}$$

The selection results in

Transform:

$$s = \frac{\hat{s} + p_1}{\frac{\hat{s}}{p_2} + 1} = \frac{\hat{s} - 0.1}{\frac{\hat{s}}{-10^20} + 1} \approx \hat{s} - 0.1 \tag{4.11}$$

Inverse Transform:

$$\tilde{s} \approx s + 0.1 \tag{4.12}$$

The transform performs a rightward(destabilizing) shift to move the lightly damped poles to the right half plane. The inverse transform performs a stabilizing shift. It is used to transform the $\hat{K}$ corresponding to the transformed plant $\hat{P}$ to the original K corresponding to original plant P.

The selection of p_1 is based on our desire to pull the phugoid mode to a location that has a desirable damping i.e. $\zeta > 0.7$. The parameter p_1 moves the phugoid mode into the right half plane to $\hat{s} = -0.0236 \pm 0.0975i + 0.1 = 0.0764 \pm 0.0975i$. The open loop hamiltonian will have an eigenvalue at the reflection of this location i.e. at $\hat{s} = -0.0764 \pm 0.0975i$. The H_∞ design places a zero at this left half plane location. After applying inverse bilinear transformation , the final controller ends up with a zero at $s = -0.0764 \pm 0.0975i - 0.1 = -0.1764 \pm 0.0975i (\zeta = 0.875)$. Hence this zero pulls

the phugoid mode to a location that has a desirable damping i.e. $\zeta > 0.7$.

Disadvantages of Bilinear Transformation.

1. **Loss of Integral Action.** The H_∞ design method is performed on the transformed plant $\hat{P}$ with the original weighting functions. The resulting controller $\hat{K}$ is transformed back using inverse bilinear transformation. This results in the loss of integral action because the near integrators associated with $\hat{K}$(due to W1 selection) are shifted into the left half plane by $p_1 = 0.1$ units.

2. **Loss of closed loop frequency response shaping inequalities.** When bilinear transformation is used, the inequality $||T_{wz}||_{H_\infty} < \gamma$ does not hold for T_{wz} which consists of P,K and weighting functions W_1, W_2 and W_3. The inequality $||\hat{T}_{wz}||_{H_\infty} < \gamma$ holds for $\hat{T}_{wz}$ which consists of $\hat{P}$, $\hat{K}$ and original weighing functions W_1, W_2 and W_3. Hence weighting functions $W1, W2$ and $W3$ cannot be used to shape S,T and KS and they lose their physical significance.

Selection of Weighting functions

1. **Sensitivity Weighting.** A first order weighting function was selected for W1.

   (a) Initially we started with $\omega_{b_1} = \omega_{b_2} = 0.01$ rad/sec. This ensures that we are equally aggressive towards FPA steady state errors than Velocity steady state errors.

   (b) ϵ was chosen to be 0.003 so that we have adequate integral action to make $T_{d_o y}$ look small at low frequencies.

   (c) As the sensitivity bandwidth parameter ω_{b_i} is increased(decreased), the closed loop system bandwidth increases(decreases). For AV-8A Harrier longitudinal dynamics, presence on RHP zero puts an upper bound on the open loop bandwidth. Hence ω_{b_i} cannot be arbitrarily increased.

   (d) We selected $M_{s_1} = M_{s_2} = 7$ (16 db) to put an upper bound on the sensitivity peak.

2. **Control Sensitivity weighting.** Initially we choose W_2 to be a constant($W_2 = M_u$). This selection did not permit us to roll off KS at higher frequencies to attenuate the sensor noise. It also resulted in larger controls. Hence we select a first order dynamic W_2 as shown previously. This allows us to roll off KS at higher frequencies to ensure attenuation of sensor noise.

Table 4.3: Weighting Function Parameters for AV-8A

	W1	W2	W3
M1	7	0.1	2
M2	7	0.1	2
ω_1	0.01	10	20
ω_2	0.01	10	20
ϵ_1	0.003	0.01	0.009
ϵ_2	0.003	0.01	0.009

(a) We select $\omega_{b_{u1}} = \omega_{b_{u2}} = 10$ rad/sec. $\omega_{b_{u1}}$ and $\omega_{b_{u2}}$ are equal to ensure that we are equally aggressive to throttle action and stick input action.

(b) We select $\epsilon = 0.01$ to roll off the KS singular values at high frequencies to attenuate sensor noise.

(c) We select $M_{u_i} = 0.1$ to put an upper bound on the KS peak singular values.

3. **Complementary Sensitivity Weighting.** A first order dynamic weighting function was selected for W_3 as shown previously.

(a) We selected $\omega_{c_1} = \omega_{c_2} = 20$ rad/sec - one decade above our desired open loop unity gain crossover frequency of 2 rad/sec.

(b) We select $\epsilon = 0.001$ to roll off the singular values at high frequencies to attenuate the sensor noise.

(c) We select $M_{y_i} = 2(6$ db) to put an upper bound on the peaks so that the step responses have minimal overshoot.

The velocity and FPA output channel of the plant are augmented with integrators so as to ensure zero steady state error to a step reference input. The weighting function W_1 is designed to shape sensitivity at low frequencies and ensure that $||S||_\infty$ is below 8db. W_2 is chosen to shape KS_e such that $||KS||_\infty$ is not too high to prevent control signal saturation. W_3 is designed so as to ensure that $||T||_\infty$ is below 8 db and T rolls off at higher frequencies. A generalized plant is created using $w = [r\ d_i]$ as the set of exogenous signals so that we get good properties at both input and

output loop breaking points. Both velocity and FPA are fed back in the inner loop while designing the generalized plant.This serves as the inner loop feedback in a standard inner-outer feedback control architecture This controller architecture has been considered for designing the dynamic output feedback controller to ensure that the designer won't have to design an inner loop controller and an outer loop controller separately.γ is minimized by solving LMI using the software YALMIP. Inverse bilinear transformation is performed on the controller returned by the optimization to shift the controller to the left half plane so that it corresponds to the original untransformed plant. The integrators present at the output of the plant are shifted to the controller input. In other words, the controller is augmented with integrators at the input. The closed loop system is obtained using the final controller containing 4 inputs and 2 outputs and the original plant.

Closed loop pole(Good design). The closed loop poles that result from our second approach using bilinear transformation is as follows:

Pole	Damping	Frequency(rad/sec)
-1.79e-001 + 9.72e-002i	8.79e-001	2.03e-001
-1.79e-001 - 9.72e-002i	8.79e-001	2.03e-001
-1.95e+000 + 1.09e+000i	8.73e-001	2.24e+000
-1.95e+000 - 1.09e+000i	8.73e-001	2.24e+000
-3.24e+000	1.00e+000	3.24e+000
-2.00e+000 + 2.90e+000i	5.67e-001	3.53e+000
-2.00e+000 - 2.90e+000i	5.67e-001	3.53e+000
-1.25e+001	1.00e+000	1.25e+001
-1.79e+001 + 3.61e+000i	9.80e-001	1.83e+001
-1.79e+001 - 3.61e+000i	9.80e-001	1.83e+001
-2.03e+001	1.00e+000	2.03e+001
-5.94e+002	1.00e+000	5.94e+002
-2.00e+004	1.00e+000	2.00e+004
-2.01e+004	1.00e+000	2.01e+004

Table 4.4: Closed Loop Poles of AV8A using Bilinear Transformation

Closed loop zeros. The resulting closed loop transmission zeros are as follows.

Zeros	Damping	Frequency(rad/sec)
-1.36e+007	1.00e+000	1.36e+007
-8.03e+005	1.00e+000	8.03e+005
-1.23e+005	1.00e+000	1.23e+005
-2.01e+004 + 2.44e+001i	1.00e+000	2.01e+004
-2.01e+004 - 2.44e+001i	1.00e+000	2.01e+004
-2.00e+003 + 9.18e-001i	1.00e+000	2.00e+003
-2.00e+003 - 9.18e-001i	1.00e+000	2.00e+003
-6.83e+000	1.00e+000	6.83e+000
5.55e+000	-1.00e+000	5.55e+000
-1.65e-001 + 9.18e-002i	8.74e-001	1.89e-001
-1.65e-001 - 9.18e-002i	8.74e-001	1.89e-001

Table 4.5: Closed Loop Zeros of AV-8A Using Bilinear Transformation

The resulting minimum gamma for this design is

$$\gamma = 101.52 \tag{4.13}$$

4.4 Inner Outer Loop PI-PD Controller

In the subsection,we discuss the design methodology for Inner-Outer loop control design for the longitudinal control system. The inner outer loop structure in Figure 4.12 has been used to design a PI-PD controller.

where

1. Output vector: $y = [y1\ y2]^\top = [\gamma\ Velocity]^\top$
2. Control vector: $u = [u1\ u2]^\top = [\delta_s\ \delta_t]^\top$
3. State : $x_r = [\theta]$

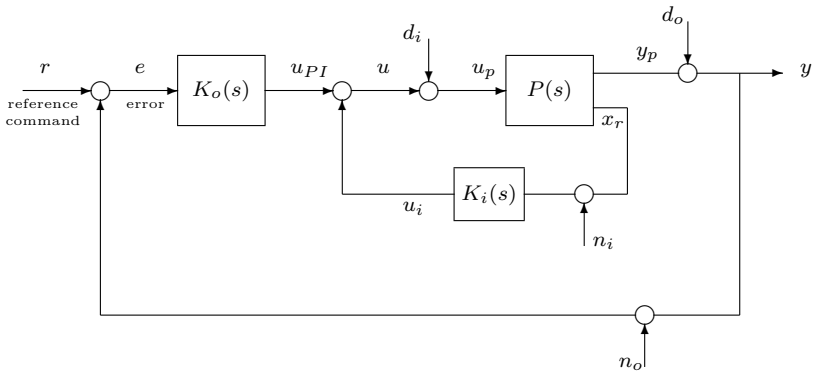

Figure 4.12: Inner Outer Feedback Loop :AV8A

Let us first design an inner-outer loop controller for the AV8A Harrier aircraft considering only the diagonal elements of the plant transfer function matrix i.e. $P_{\delta_s \to \gamma}$ and $P_{\delta_t \to v}$.

Let us consider the $(2,2)$ element of the plant transfer function matrix i.e. $P_{\delta_t \to v}$.

$$P_{\delta_t \to v} = \frac{-0.5424(s+10.62)(s-8.763)(s+0.48)}{(s+12)(s^2+0.0472s+0.01007)(s^2+2.437s+2.848)} \tag{4.14}$$

Initially let us assume that $P_{\delta_t \to v}$ does not need an inner-outer loop controller to have good closed loop properties.

Let us use only output feedback controller to stabilize $P_{\delta_t \to v}$.Let's assume $K_o = \frac{g_{o2}(s+z_{o2})}{s}$ where $g_{o2} > 0$, $z_{o2} > 0$. The rootlocus of $L = P_{\delta_t \to v} K_o$ where $K_o = \frac{0.4(s+0.01)}{s}$ is shown in Figure 4.13. It is seen that the closed loop system may be stable using only a PI controller but the closed loop poles would be very lightly damped. As we increase g_{o1}, the closed loop system become more lightly damped and eventually the closed loop system becomes unstable because the upward gain margin is very small as seen in Figure 4.14.

Pole	Damping	Frequency(rad/sec)	Time Constant(sec)
-9.67e-03	1.00e+00	9.67e-03	1.03e+02
-1.76e-01 + 7.38e-01i	2.32e-01	7.58e-01	5.69e+00
-1.76e-01 - 7.38e-01i	2.32e-01	7.58e-01	5.69e+00
-1.06e+00 + 5.74e-01i	8.79e-01	1.21e+00	9.44e-01
-1.06e+00 - 5.74e-01i	8.79e-01	1.21e+00	9.44e-01
-1.20e+01	1.00e+00	1.20e+01	8.33e-02

Table 4.6: Poles of $T = \frac{P_{\delta_t \to v} K_{o2}}{1 + P_{\delta_t \to v} K_{o2}}$ Using Output Feedback : AV8A

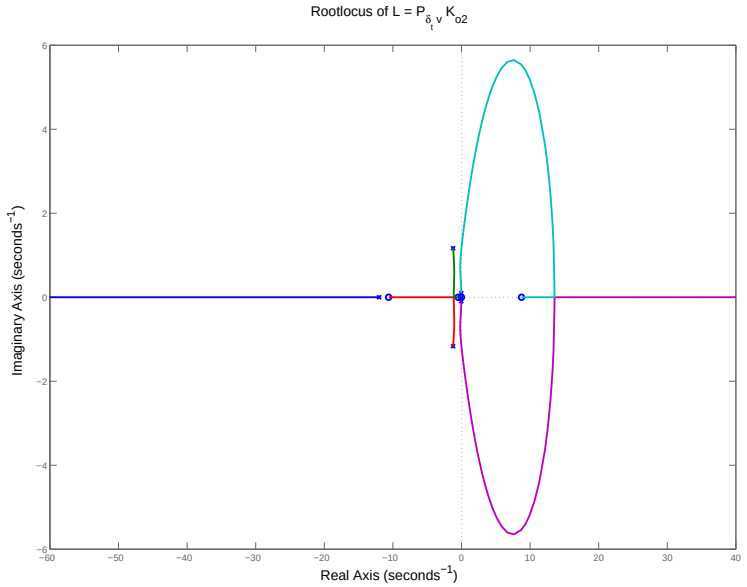

Figure 4.13: Rootlocus of $L = P_{\delta_t \to v} K_o$ Using PI controller :AV-8A

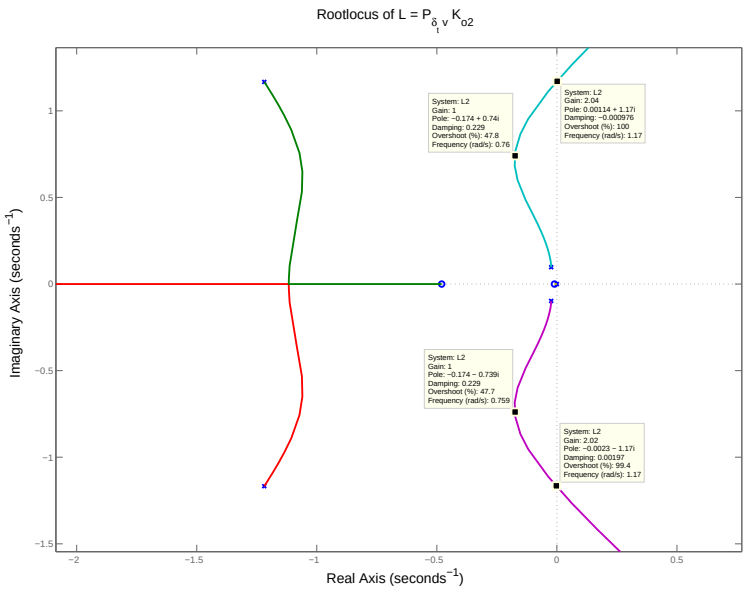

Figure 4.14: Rootlocus of $L = P_{\delta_t \to v} K_o$ using PI Controller Magnified at the Origin : AV-8A

Hence we use the inner-outer loop feedback control architecture in order to shift the lightly damped phugoid of $P_{\delta_t \to v}$ to a location with better damping using a PD controller in the inner loop to obtain $P_{mod} = \frac{L_{mod}}{1+L_{mod}}$ where $L_{mod} = P_{\delta_t \to v} K_{i1}$. This is followed by the stabilization of P_{mod} using a PI controller in the outer loop. The closed loop system architecture is shown in Figure 4.15 :

As seen in Figure 4.16 and Figure 4.17 , the inner loop with $K_{i1} = 0.25(s + 0.9)$ places the short period modes at the location $s = -0.974 \pm 1.39i$, $\zeta = 0.57$. The inner loop also places the phugoid modes at $s = -0.217 \pm 0.349i$, $\zeta = 0.528$.

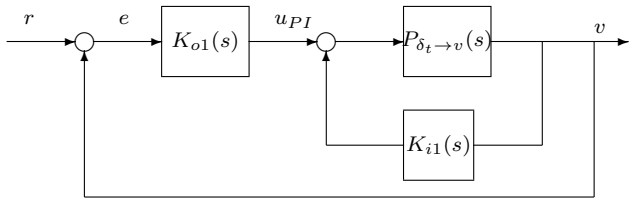

Figure 4.15: F8: Inner Outer Loop Structure for $P_{\delta_t \to v}(s)$

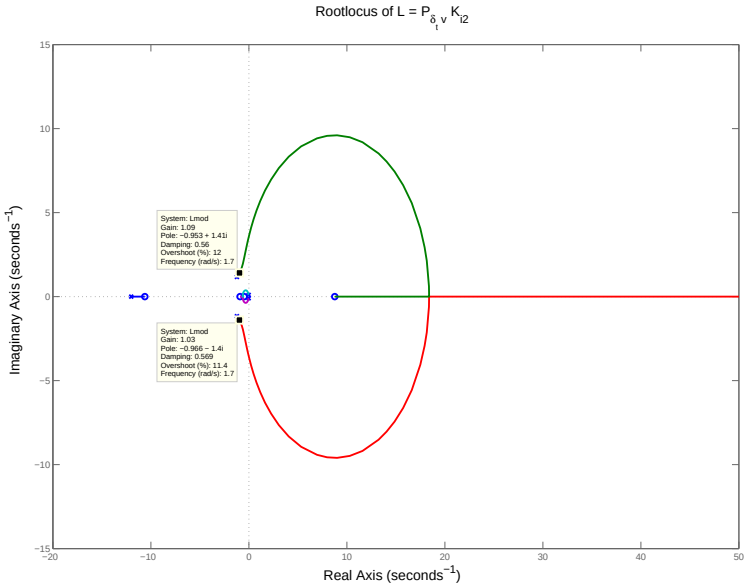

Figure 4.16: Rootlocus of $L_{mod} = P_{\delta_e \to \theta} K_i$ Using PD Controller

Let us use a PI controller to stabilize $L = P_{mod} K_{o2}$ where $P_{mod} = \frac{L_{mod}}{1+L_{mod}}$ and $L_{mod} = P_{\delta_t \to v} K_{i2}$. We select $K_{o2} = \frac{0.3(s+0.1)}{s}$. We should be careful while playing with the gain of the PI controller because the upward gain margin is finite. The rootlocus of $L = P_{mod} K_{o2}$ is as shown in Figure 4.18.

The poles of the closed loop system is as follows:

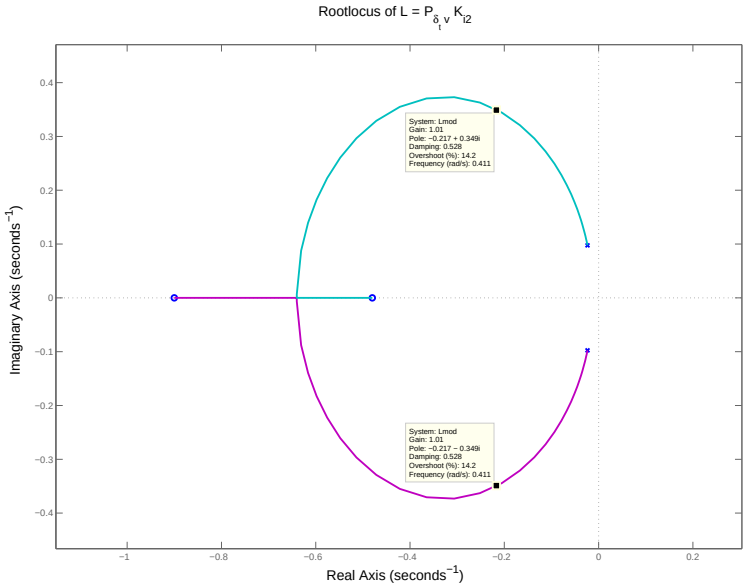

Figure 4.17: Rootlocus of $L_{mod} = P_{\delta_e \to \theta} K_i$ Magnified at Origin

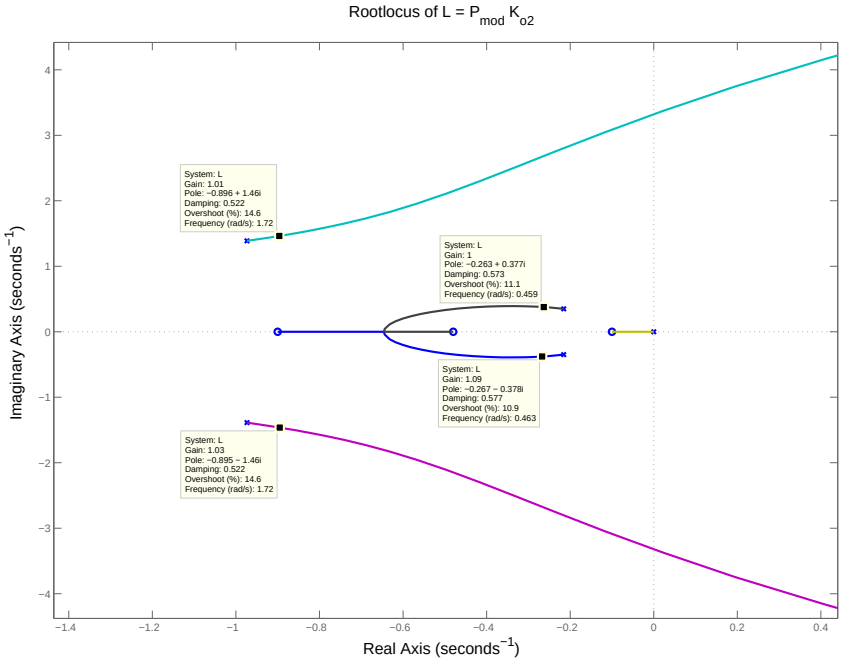

Figure 4.18: Rootlocus of $L = P_{mod} K_{o2}$ Magnified at Origin : AV-8A

Pole	Damping	Frequency(rad/sec)	Time constant(sec)
-2.20e-02	1.00e+00	2.20e-02	4.54e+01
-2.63e-01 + 3.77e-01i	5.72e-01	4.59e-01	3.80e+00
-2.63e-01 - 3.77e-01i	5.72e-01	4.59e-01	3.80e+00
-8.97e-01 + 1.46e+00i	5.23e-01	1.72e+00	1.11e+00
-8.97e-01 - 1.46e+00i	5.23e-01	1.72e+00	1.11e+00
-1.20e+01	1.00e+00	1.20e+01	8.36e-02
-2.00e+02 + 2.93e+00i	1.00e+00	2.00e+02	5.00e-03
-2.00e+02 - 2.93e+00i	1.00e+00	2.00e+02	5.00e-03

Table 4.7: Closed Loop Poles of $T = \frac{P_{mod}K_{o2}}{1+P_{mod}K_{o2}}$: AV-8A

Let us now stabilize $P_{\delta_s \to \gamma}$ using an inner-outer PI-PD controller.

$$P_{\delta_s \to \gamma} = \frac{0.02253(s + 0.1154)(s^2 + 3.366s + 20.38)}{(s + 1.966)(s^2 + 0.0472s + 0.01007)(s^2 + 2.437s + 2.848)} \tag{4.15}$$

To design the flight control system for FPA, let us consider the following inner-outer closed loop system in Figure 4.19.

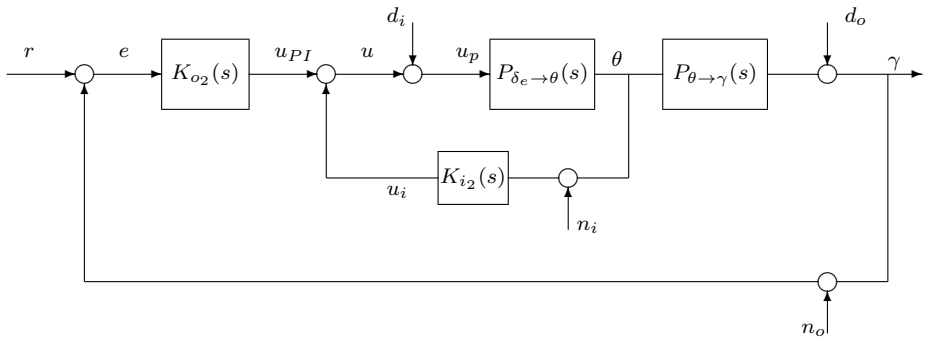

Figure 4.19: Inner Outer Feedback Loop for $P_{delta_e \to \gamma}$:AV8A

As a rule of thumb, we always consider the inner loop as a negative feedback loop. From the transfer function matrix of the plant we obtain

$$P_{\delta_s \to \theta}(s) = \frac{0.69844(s+0.3525)(s+0.2712)}{(s+1.966)(s^2+0.0472s+0.01007)(s^2+2.437s+2.848)} \tag{4.16}$$

$$P_{\theta \to \gamma}(s) = \frac{0.02253(s+0.1154)(s^2+3.366s+20.38)}{0.69844(s+0.3525)(s+0.2712)} \tag{4.17}$$

The inner loop is used to move the phugoid modes and short period modes to a location in the LHP with better damping so that the outer loop can stabilize the system and obtain a closed loop system with good properties.

Let us use $K_{i1} = 6(s+0.05)$ to shift the phugoid and the short period modes to better locations. As seen in Figure 4.20 and Figure 4.21 the poles of $T_{mod} = \frac{P_{\delta_s \to \theta}}{1+P_{\delta_s \to \theta} K_{i1}}$ have good damping.

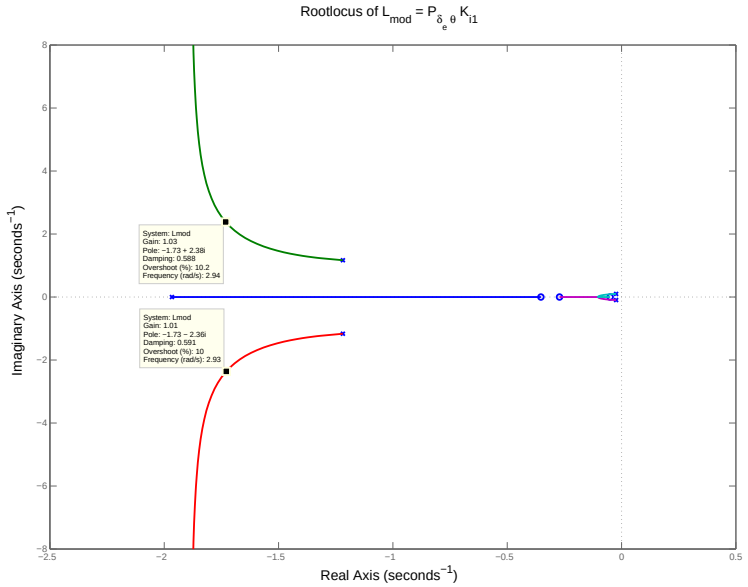

Figure 4.20: Rootlocus of $L_{mod} = P_{\delta_s \to \theta} K_{i1}$ Using PI Controller : AV-8A

Now we use the outer loop to stabilize P_{mod} where $P_{mod} = T_{mod} * P_{\theta \to \gamma}$.

$$P_{mod}(s) = \frac{0.022527(s^2+3.366s+20.38)}{(s+0.8972)(s+0.07149)(s^2+3.454s+8.508)} \tag{4.18}$$

Let us use $Ko1 = \frac{-0.1(s-0.1)}{s}$ to stabilize the system. The rootlocus of $L = P_{mod} K_{o1}$ is as shown in Figure 4.22. Hence $P_{\delta_s \to \gamma}$ is stabilized.

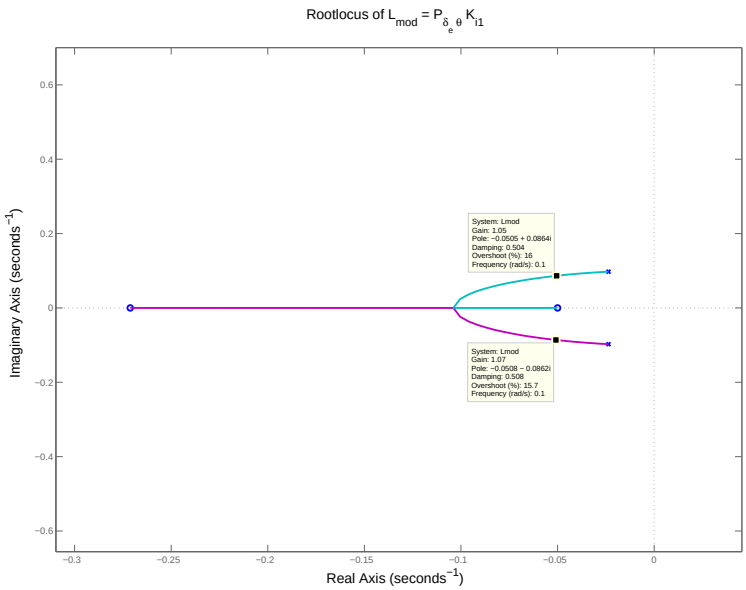

Figure 4.21: Rootlocus of $L_{mod} = P_{\delta_e \to \theta} K_{i1}$ Magnified at Origin : AV-8A

Pole	Damping	Frequency(rad/sec)	Time constant(sec)
-4.95e-02 + 8.69e-02i	4.95e-01	1.00e-01	2.02e+01
-4.95e-02 - 8.69e-02i	4.95e-01	1.00e-01	2.02e+01
-8.97e-01	1.00e+00	8.97e-01	1.11e+00
-1.73e+00 + 2.35e+00i	5.92e-01	2.92e+00	5.79e-01
-1.73e+00 - 2.35e+00i	5.92e-01	2.92e+00	5.79e-01

Table 4.8: Closed Loop Poles of $T_{mod} = \frac{P_{\delta_e \to \theta}}{1 + P_{\delta_e \to \theta} K_{i1}}$: AV-8A

Hence the decentralized controller obtained is as follows:

$$K_i(s) = \begin{bmatrix} 6(s+0.05) & 0 \\ 0 & 0.25(s+0.9) \end{bmatrix}$$

$$K_o(s) = \begin{bmatrix} \frac{-0.1(s-0.1)}{s} & 0 \\ 0 & \frac{0.3(s+0.1)}{s} \end{bmatrix} \tag{4.19}$$

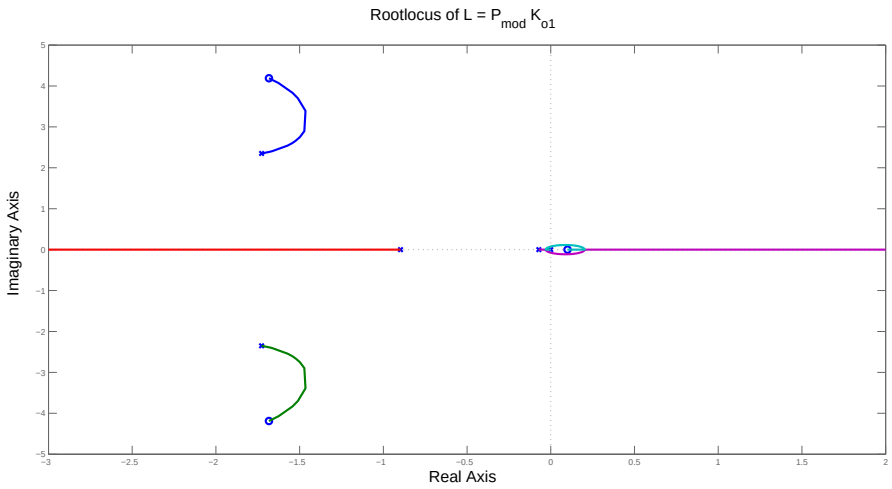

Figure 4.22: Rootlocus of $L = P_{mod}K_{o1}$

Pole	Damping	Frequency(rad/sec)
-1.13e-002	1.00e+000	1.13e-002
-5.28e-002	1.00e+000	5.28e-002
-9.06e-001	1.00e+000	9.06e-001
-1.73e+000 + 2.35e+000i	5.92e-001	2.92e+000
-1.73e+000 - 2.35e+000i	5.92e-001	2.92e+000

Table 4.9: Closed Loop Poles of $L = P_{mod}K_{o1}$: AV-8A

4.5 PI-PD Controller vs Dynamic Output Feedback Controller

In the section we try to obtain a PI-PD controller which best approximates the dynamic output feedback controller obtained in the previous section.

We have already designed a decentralized PI-PD controller which stabilizes the AV8A-Harrier plant provided only the diagonal elements are considered. The controller is as follows:

$$K_i(s) = \begin{bmatrix} 6(s+0.05) & 0 \\ 0 & 0.25(s+0.9) \end{bmatrix}$$
$$K_o(s) = \begin{bmatrix} \frac{-0.1(s-0.1)}{s} & 0 \\ 0 & \frac{0.3(s+0.1)}{s} \end{bmatrix} \tag{4.20}$$

This controller also stabilizes the centralized plant which means that the plant is sufficiently decoupled so that so that a decentralized controller which was designed for the decoupled system stabilizes the coupled system as well. Now, we do a exhaustive search in the neighborhood of the previously obtained g_{o1},z_{o1},g_{o2},z_{o2},g_{i1},z_{i1} parameters in order to obtain a PI-PD controller which best approximates the dynamic output feedback controller. While doing this search by brute force looping, we minimize $||S_{e1} - S_{e2}||_\infty$ (where S_{e1} corresponds to Output feedback controller and S_{e2} corresponds to PI-PD controler) in the low frequency range 0.0001 rads/sec to 0.01 rads/sec in order to ensure that we obtain the best PI-PD controller which gives us similar properties at the output loop breaking point when compared to the dynamic output feedback controller at low frequencies. We find the set of parameters of the controller which minimizes $||S_{e1} - S_{e2}||_\infty$.

After doing the optimization, we obtain the following PI-PD controller which minimizes $||S_{e1} - S_{e2}||_\infty$ in the range 0.0001 rads/sec to 0.01 rads/sec. The roll-off terms have been selected in a way so that the KS crossover frequency for the dynamic output feedback based closed loop system and the PI-PD based closed loop system is the same. This is done in order to ensure that we are in a position to compare two designs.

$$K_i(s) = \begin{bmatrix} 0.13(s-0.77)\left[\frac{4.8}{(s+4.8)}\right]^3 & 0 \\ 0 & 1.1(s-0.01)\left[\frac{4.8}{(s+4.8)}\right]^3 \end{bmatrix}$$
$$K_o(s) = \begin{bmatrix} \frac{-0.3(s-0.5)}{s}\left[\frac{30}{(s+30)}\right]^3 & 0 \\ 0 & \frac{1(s+0.06)}{s}\left[\frac{30}{(s+30)}\right]^3 \end{bmatrix} \tag{4.21}$$

The damping of the closed loop system using the PI-PD controller is as follows:

Pole	Damping	Frequency(rad/sec)	Time constant
-6.50e-02	1.00e+00	6.50e-02	1.54e+01
-1.29e-01 + 2.07e-01i	5.29e-01	2.44e-01	7.74e+00
-1.29e-01 - 2.07e-01i	5.29e-01	2.44e-01	7.74e+00
-9.99e-01 + 8.74e-01i	7.53e-01	1.33e+00	1.00e+00
-9.99e-01 - 8.74e-01i	7.53e-01	1.33e+00	1.00e+00
-2.41e+00	1.00e+00	2.41e+00	4.15e-01
-9.11e-01 + 2.24e+00i	3.77e-01	2.42e+00	1.10e+00
-9.11e-01 - 2.24e+00i	3.77e-01	2.42e+00	1.10e+00
-3.10e+00	1.00e+00	3.10e+00	3.23e-01
-5.35e+00 + 6.11e-01i	9.94e-01	5.38e+00	1.87e-01
-5.35e+00 - 6.11e-01i	9.94e-01	5.38e+00	1.87e-01
-5.78e+00 + 1.24e+00i	9.78e-01	5.92e+00	1.73e-01
-5.78e+00 - 1.24e+00i	9.78e-01	5.92e+00	1.73e-01
-1.34e+01	1.00e+00	1.34e+01	7.47e-02
-1.93e+01	1.00e+00	1.93e+01	5.18e-02
-2.66e+01 + 1.03e+01i	9.32e-01	2.85e+01	3.76e-02
-2.66e+01 - 1.03e+01i	9.32e-01	2.85e+01	3.76e-02
-3.40e+01 + 5.50e+00i	9.87e-01	3.45e+01	2.94e-02
-3.40e+01 - 5.50e+00i	9.87e-01	3.45e+01	2.94e-02
-3.93e+01	1.00e+00	3.93e+01	2.55e-02

Table 4.10: Closed Loop Poles : PI-PD Based Controller

Let us now compare the closed loop properties obtained by using PI-PD controller and dynamic output feedback controller.

As evident in Table 4.11, the dynamic output controller offers better closed loop properties than the PI-PD controller. The dynamic output controller also offers better input disturbance attenuation than the PI-PD controller.

	$\|\|S_e\|\|_\infty$	$\|\|T_e\|\|_\infty$	$\|\|S_c\|\|_\infty$	$\|\|T_c\|\|_\infty$	$\|\|KS_e\|\|_\infty$	$\|\|PS_c\|\|_\infty$
Dynamic Output feedback Controller	4.39	3.49	6.06	2.72	6.23	1.26
PI-PD controller	6.88	5.26	7.21	4.64	4.48	6.49

Table 4.11: Attained Closed Loop Properties for PI-PD and Dynamic Output Feedback Controller:AV-8A Harrier

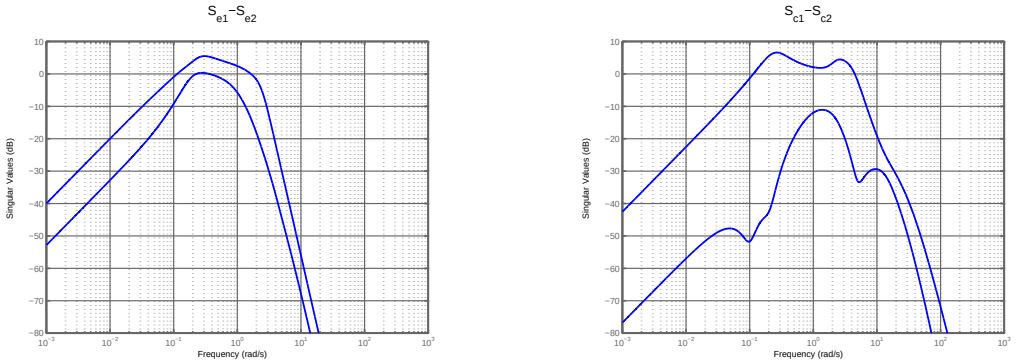

Figure 4.23: Comparison of $|S_{e1} - S_{e2}|$ and $|S_{c1} - S_{c2}|$ for AV-8A Harrier

Let us now compare the $|S_{e1} - S_{e2}|$ and $|S_{c1} - S_{c2}|$ plots where S_{e1} and S_{c1} corresponds to Dynamic output feedback controller and S_{e2} and S_{c2} corresponds to PI-PD controller as shown in Figure 4.23.

$|S_{e1} - S_{e2}|$ and $|S_{c1} - S_{c2}|$ have very low singular values at low frequencies. This means that the PI-PD controller and Dynamic output feedback controller would give similar performances at both the loop breaking points when operating at low frequencies.

The following are the plots showing the comparison of the frequency domain and time domain responses for the dynamic output feedback controller and PI-PD controller.

Frequency Domain Plots

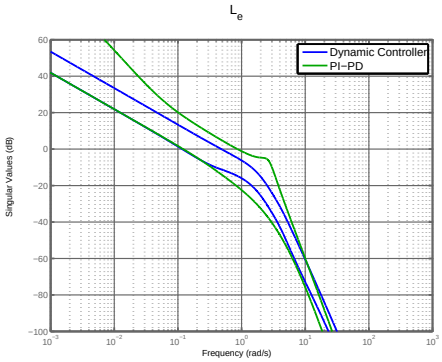

Figure 4.24: L_e : AV-8A

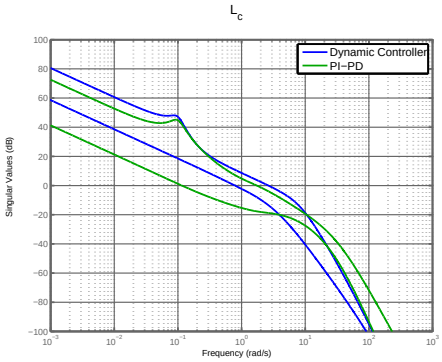

Figure 4.25: L_c : AV-8A

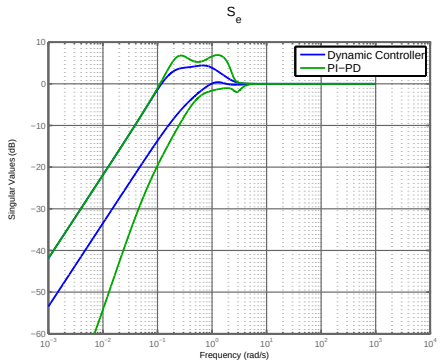

Figure 4.26: S_e : AV-8A

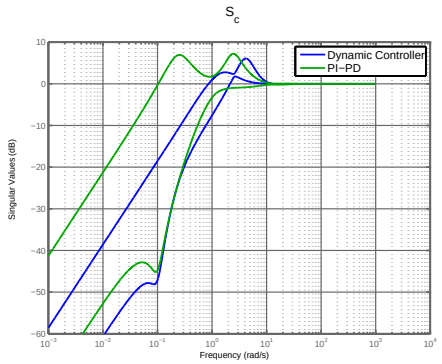

Figure 4.27: S_c : AV-8A

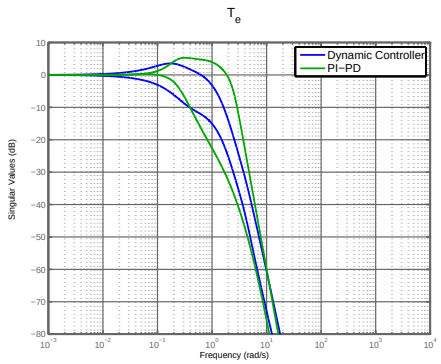

Figure 4.28: T_e : AV-8A

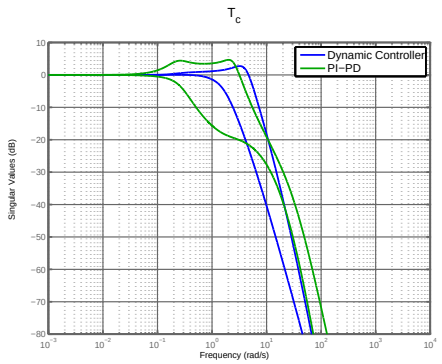

Figure 4.29: T_c : AV-8A

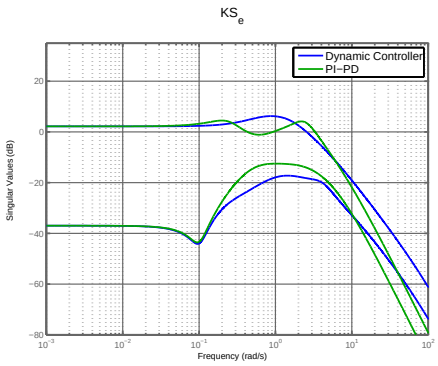

Figure 4.30: KS_e : AV-8A

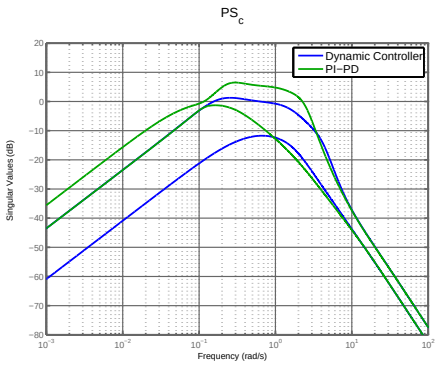

Figure 4.31: PS_c : AV-8A

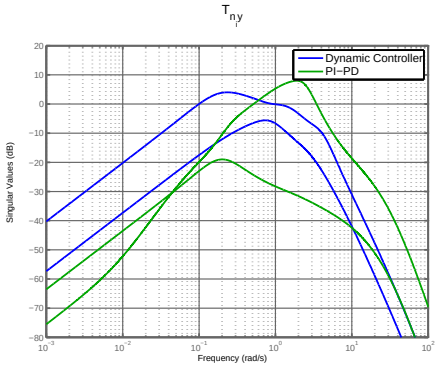

Figure 4.32: $T_{n_i \to y}$: AV-8A

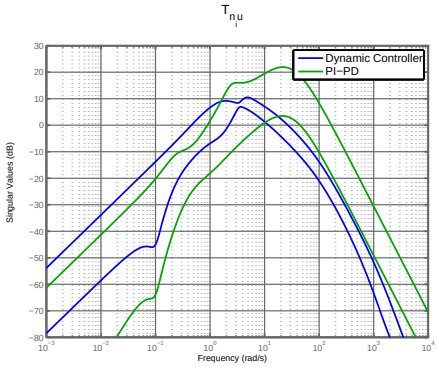

Figure 4.33: $T_{n_i \to y}$: AV-8A

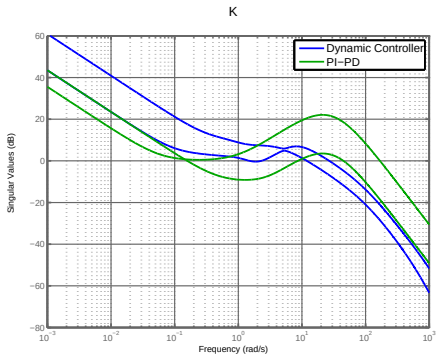

Figure 4.34: Controller Singular Values : AV-8A

Time Domain Plots

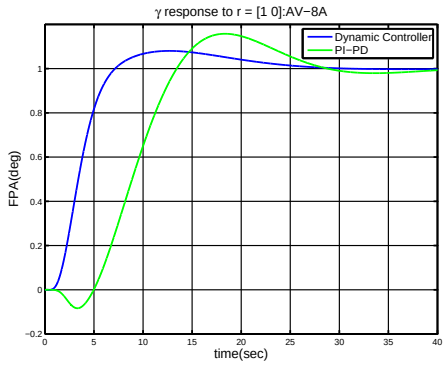

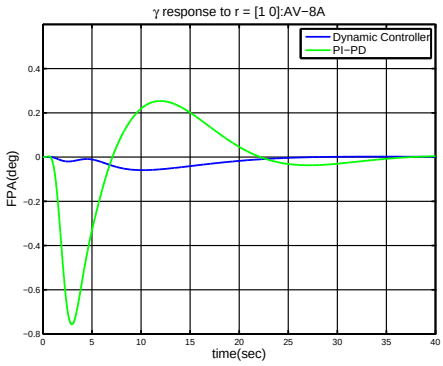

Figure 4.35: FPA Response to $r = [1\ 0]$: AV-8A Figure 4.36: FPA Response to $r = [0\ 1]$: AV-8A

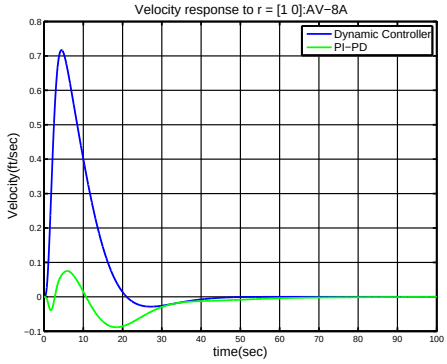

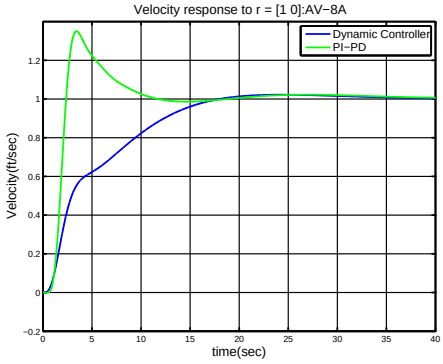

Figure 4.37: Velocity Response to $r = [1\ 0]$: AV-8A Figure 4.38: Velocity Response to $r = [0\ 1]$: AV-8A

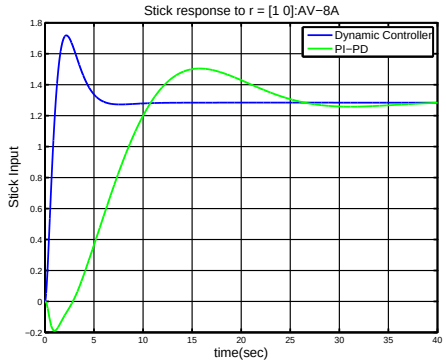

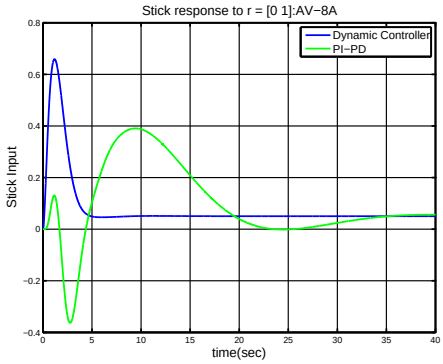

Figure 4.39: Stick Response to $r = [1\ 0]$: AV-8A Figure 4.40: Stick Response to $r = [0\ 1]$: AV-8A

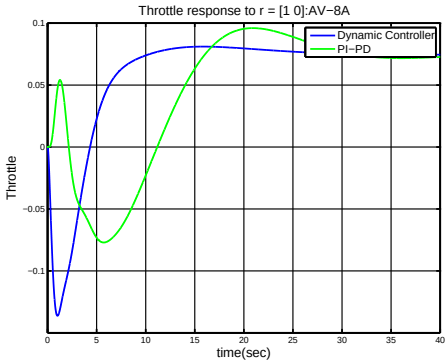

Figure 4.41: Throttle Response to $r = [1\ 0]$: AV-8A

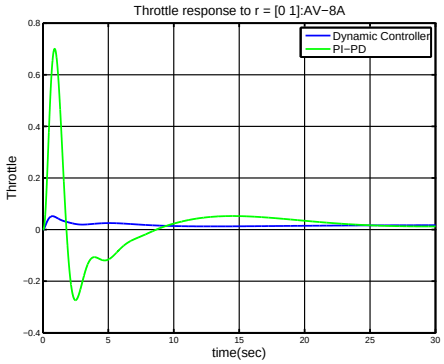

Figure 4.42: Throttle Response to $r = [0\ 1]$: AV-8A

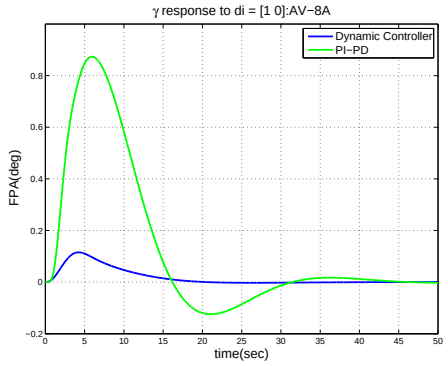

Figure 4.43: FPA Response to $d_i = [1\ 0]$: AV-8A

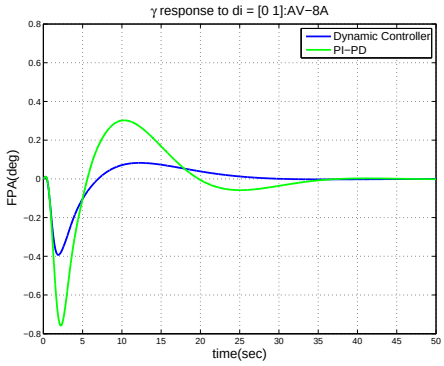

Figure 4.44: FPA Response to $d_i = [0\ 1]$: AV-8A

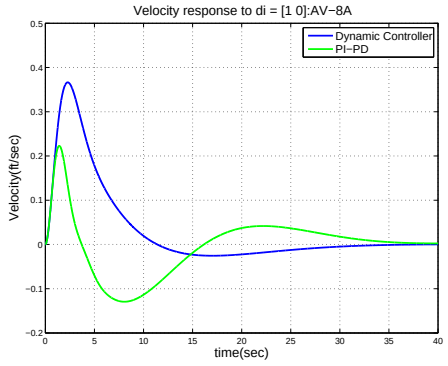

Figure 4.45: Velocity Response to $d_i = [1\ 0]$: AV-8A

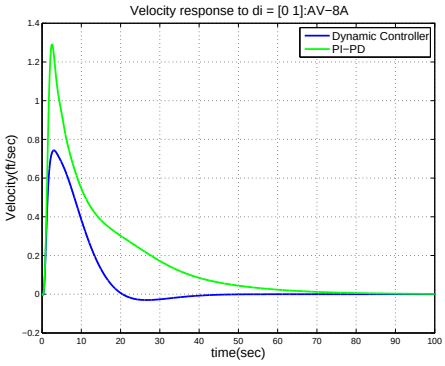

Figure 4.46: Velocity Response to $d_i = [0\ 1]$: AV-8A

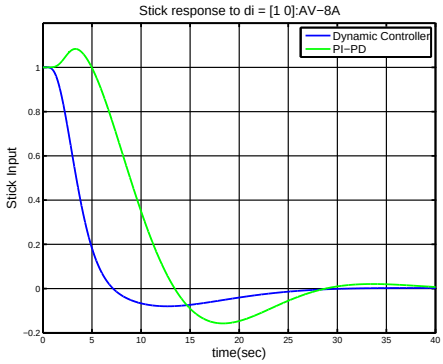

Figure 4.47: Stick Response to $d_i = [1\ 0]$: AV-8A

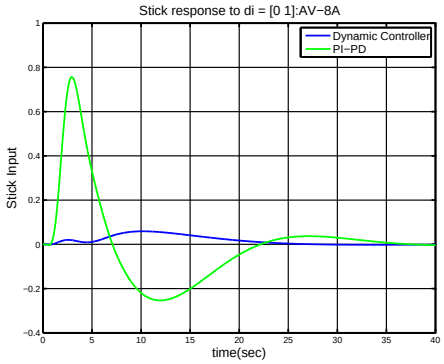

Figure 4.48: Stick Response to $d_i = [0\ 1]$: AV-8A

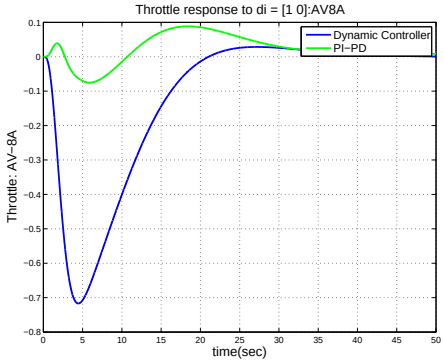

Figure 4.49: Throttle Response to $d_i = [1\ 0]$: AV-8A

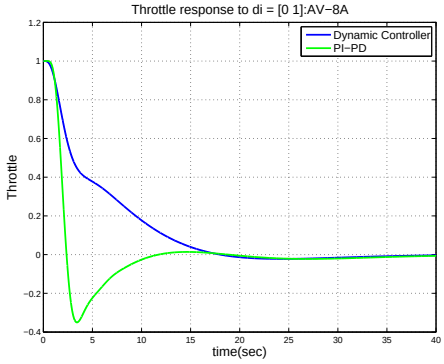

Figure 4.50: Throttle Response to $d_i = [0\ 1]$: AV-8A

4.6 Summary

After analyzing the closed loop properties, it is seen that the dynamic output feedback controller offers good properties at both the loop breaking points. The PI-PD ($K_{o_{decentralized}}, K_{i_{decentralized}}$) does not give as good properties at both the loop breaking points as a dynamic output feedback controller.

Chapter 5

VOUGHT F-8 CRUSADER

5.1 Overview.

In this chapter, we briefly discuss the longitudinal dynamics of the F8 aircraft. In the following sections we design a dynamic output feedback controller using Linear Matrix Inequality. We also discuss the inner outer loop control structure and design a PI-PD controller for the longitudinal dynamics. Finally we attempt to design a PI-PD controller which would similar closed loop properties as the dynamic output feedback controller.

Background. The Vought F-8 Crusader was a single-engine, supersonic, carrier-based air superiority jet aircraft built by Vought for the United States Navy and the Marine Corps. The F-8 was used by NASA as part of their digital "'fly-by wire" research program.The F-8 had a high-mounted wing which necessitated the use of a fuselage-mounted short and light landing gear which was unsual for a fighter aircraft. The most innovative aspect of the F-8 design was the variable-incidence wing which was pivoted by 7 deg out of the fuselage during takeoff and landing which increased the lift due to greater angle of attack without compromising forward visibility because the fuselage stayed level. The F-8 was the last aircraft designed by the Navy with guns as its primary weapon.

Figure 5.1: Vought F-8 Crusader

5.2 F8 Longitudinal Dynamics

In this section, we examine the longitudinal dynamics for the F8 aircraft.

Aircraft Characteristics. We examine the aircraft during a straight and level powered approach.The flight conditions are as follows:

1. Altitude of 20,000 ft (6095 meters)
2. Speed of Mach 0.9 (916.6 ft/sec)
3. Dynamic pressure 550 lbs/sq ft
4. Trim Pitch angle 2.25 deg
5. Trim Angle of Attack 2.25 deg
6. Trim Elevator Attack -2.65 deg

The aircraft is assumed to fly in the vertical plane with its wings level so that we can study its motion in the vertical plane, i.e. longitudinal dynamics. The important variables that characterize the plane are : horizontal velocity u of the airplane, the pitch angle theta, the pitch rate and the angle of attack alpha. The longitudinal motion of the aircraft is controlled by two aerodynamic control surfaces: the elevator which is located on the horizontal tail and the flaperons which are located on the wings. The longitudinal motion is also influenced by thurst generated by the engines. However, the thrust shall be considered to be constant. Hence we shall not consider it as a dynamic control variable.

The TITO model for the longitudinal dynamics at the above flight conditions is as follows:

$$\dot{x} = Ax + Bu \tag{5.1}$$

$$y = Cx + Du \tag{5.2}$$

where

$$A = \begin{bmatrix} 0 & 0 & 1.0000 & 0 \\ 1.5000 & -1.5000 & 0 & 0.0057 \\ -12.0000 & 12.0000 & -0.8000 & -0.0344 \\ -0.8524 & 0.2904 & 0 & -0.0140 \end{bmatrix}$$

$$B = \begin{bmatrix} 0 & 0 \\ 0.1600 & 0.6000 \\ -19.0000 & -2.5000 \\ -0.0115 & -0.0087 \end{bmatrix}$$

$$C = \begin{bmatrix} 1 & 0 & 0 & 0 \\ 0 & 1 & 0 & 0 \end{bmatrix}$$

$$D = \begin{bmatrix} 0 & 0 \\ 0 & 0 \end{bmatrix}$$

$$x = \begin{bmatrix} \theta & \text{perturbed pitch angle from trim} & \text{deg} \\ \gamma & \text{perturbed flight path angle from trim} & \text{deg} \\ q & \text{pitch rate} & \text{deg/sec} \\ v & \text{perturbation from horizontal speed} & \text{ft/sec} \end{bmatrix}$$

$$u = \begin{bmatrix} \delta_e & \text{Elevon deflection from trim} & \text{deg} \\ \delta_f & \text{Flaperon deflection from trim} & \text{deg} \end{bmatrix}$$

$$y = \begin{bmatrix} \theta & \text{Perturbed pitch angle from trim} & \text{deg} \\ \gamma & \text{Perturbed flight path angle from trim} & \text{deg} \end{bmatrix}$$

The aircraft's two control surfaces are as follows :

1. Elevator - Situated on the horizontal tail

2. Flaperon - Located on the wings

Poles and Zeros. The aircraft has stable phugoid modes at $s = -0.00577 \pm j0.0264(\zeta = 0.213, w_n = 0.027$ rads/sec), stable short period modes at $s = -1.15 \pm j3.45(\zeta = 0.317, w_n = 3.63$ rads/sec). It also has a transmission zero at $s = -0.0139$.

Transfer Function Matrix. The system transfer function matrix from u to y is given by

$$G(s) = C(sI - A)^{-1}B + D = \begin{bmatrix} G_{\delta_e\theta} & G_{\delta_f\theta} \\ G_{\delta_e\gamma} & G_{\delta_f\gamma} \end{bmatrix}$$

where

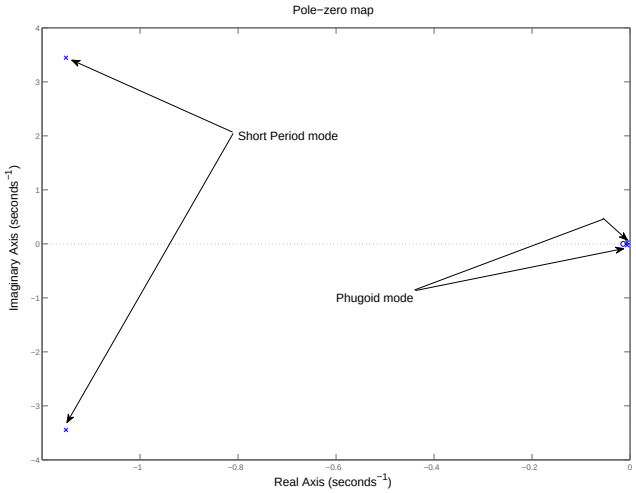

Figure 5.2: Visualization of Poles and Zeros for F8 Longitudinal Dynamics

$$G_{\delta_e\theta} = \frac{-19(s+1.4)(s+0.01287)}{(s^2+0.01155s+0.0007316)(s^2+2.302s+13.2)}$$

$$G_{\delta_f\theta} = \frac{0.16(s+13.3)(s-12.49)(s+0.01069)}{(s^2+0.01155s+0.0007316)(s^2+2.302s+13.2)}$$

$$G_{\delta_e\gamma} = \frac{-2.5(s-1.38)(s+0.01343)}{(s^2+0.01155s+0.0007316)(s^2+2.302s+13.2)}$$

$$G_{\delta_f\gamma} = \frac{0.6(s+0.0124)(s^2+0.8051s+5.751)}{(s^2+0.01155s+0.0007316)(s^2+2.302s+13.2)}$$

The individual transfer functions show the presence of stable phugoid modes at $s = -0.00577 \pm j0.0264(\zeta = 0.213, w_n = 0.027$ rads/sec) and short period modes at $s = -1.15 \pm j3.45(\zeta = 0.317, w_n = 3.63$ rads/sec).The transfer functions $G_{\delta_f\theta}$ and $G_{\delta_e\gamma}$ shows the presence of right half plane poles at $s = 12.49$ and $s = 1.38$. They are not transmission zeros but they make the F-8 difficult to control.

The frequency response bode plots for each of the 4 system transfer functions is given in Figure 5.3-5.6

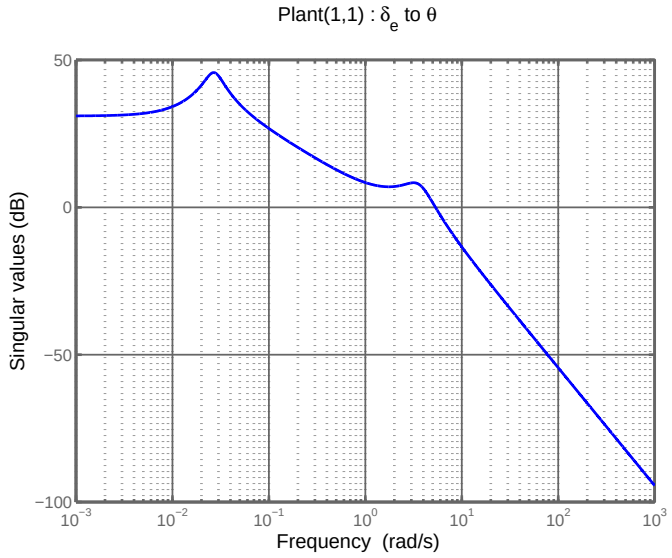

Figure 5.3: Frequency Response - δ_e to θ

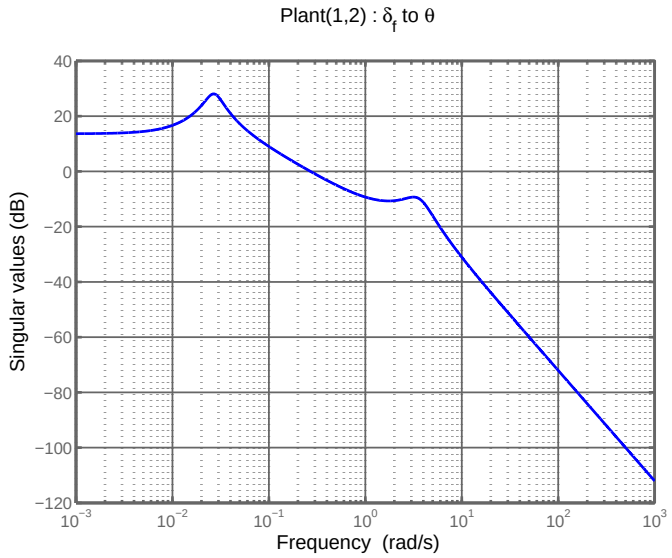

Figure 5.4: Frequency Response - δ_f to θ

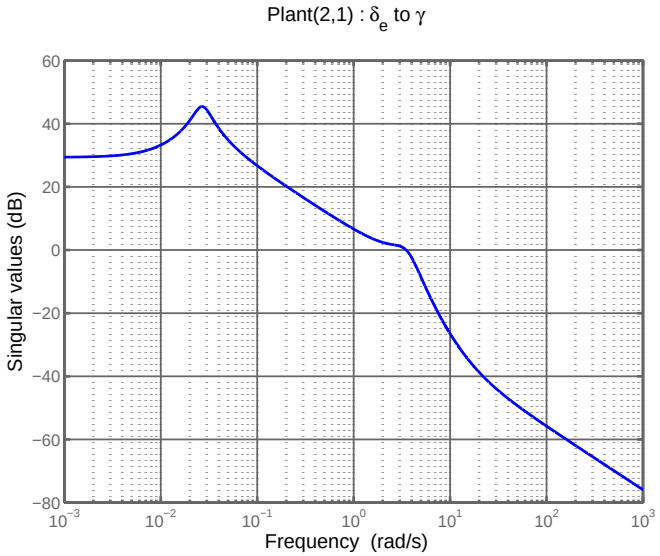

Figure 5.5: Frequency Response - δ_e to γ

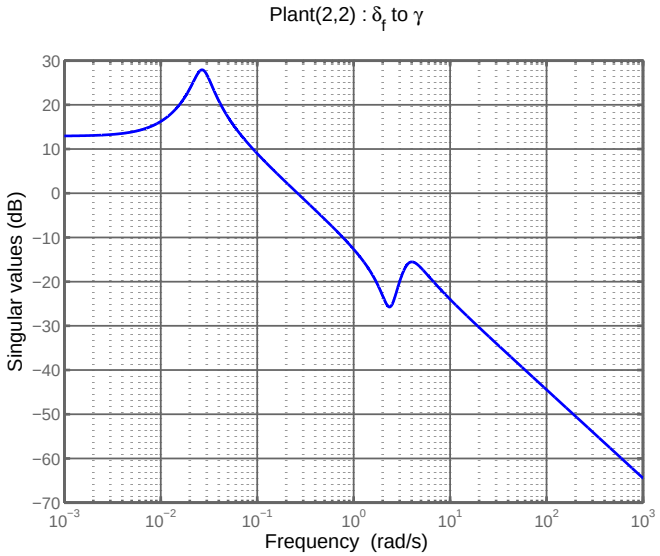

Figure 5.6: Frequency Response - δ_f to γ

MIMO Frequency Response: Singular Values

The MIMO singular values for the plant transfer matrix from controls $u = [\delta_e \ \delta_f]$ to plant output $y = [\theta \ \gamma]$ are plotted in Figure 5.7. The plot shows a peaking at 0.027 rads/sec and 3.63 rads/sec due to the lightly damped phugoid mode at $s = -0.00577 \pm j0.0264 (\zeta = 0.213, w_n = 0.027$ rads/sec) and

short period modes at $s = -1.15 \pm j3.45(\zeta = 0.317, w_n = 3.63$ rads/sec) respectively. In the plot, we notice that the minimum singular values of the plant corresponding to the δ_f channel are low and wide spread at low frequencies. Hence the resulting controller will have to compensate for the low plant gain in the δ_f channel. Thus we should expect significant flaperon activity to achieve a loop with desirable low frequency command following and good disturbance attenuation(e.g. $\sigma_{min}[PK] > 20$ db at low frequencies.

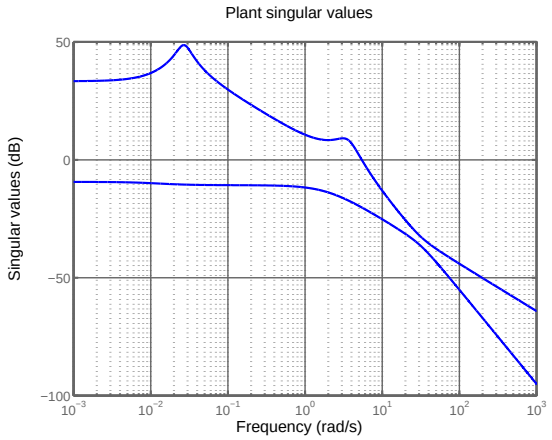

Figure 5.7: F8 Longitudinal Dynamics Singular Values MIMO Frequency Response

DC Gain Analysis. Singular Value Decomposition. While analyzing the F-8 model at DC, we get the following matrix of DC gains:

$$\begin{bmatrix} \theta \\ \gamma \end{bmatrix} = \begin{bmatrix} -35.4347 & 4.7950 \\ -29.4214 & 4.4283 \end{bmatrix} \begin{bmatrix} \delta_e \\ \delta_f \end{bmatrix}$$

A singular value decomposition at DC yields the following:

$$G(j0) = C(-A)^{-1}B + D = U\Sigma V^\top = \begin{bmatrix} -35.4347 & 4.7950 \\ -29.4214 & 4.4283 \end{bmatrix}$$

$$U = \begin{bmatrix} -0.7687 & -0.6396 \\ -0.6396 & 0.7687 \end{bmatrix}; \Sigma = \begin{bmatrix} 46.5158 & 0 \\ 0 & 0.3406 \end{bmatrix}; V = \begin{bmatrix} 0.9901 & 0.1401 \\ -0.1401 & 0.9901 \end{bmatrix}$$

From the singular value decomposition, conclusions can be drawn about the steady state input output coupling.

1. Examination of the first columns of V,Σ and U shows that elevator has a greater impact on the pitch angle of the aircraft compared to the flight path angle .This may be visualized as

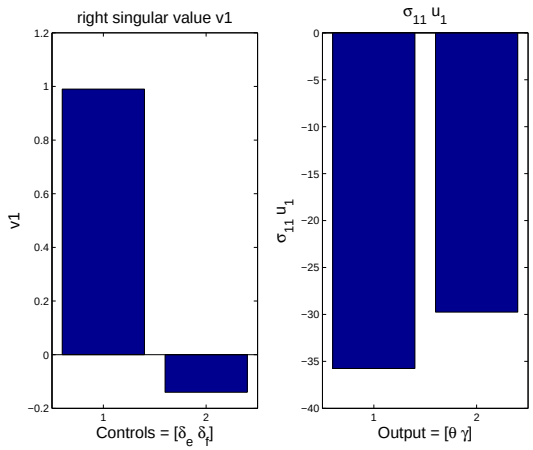

Figure 5.8: F8 SVD at DC for Longitudinal Dynamics $v_1 \rightarrow \sigma_1 u_1$

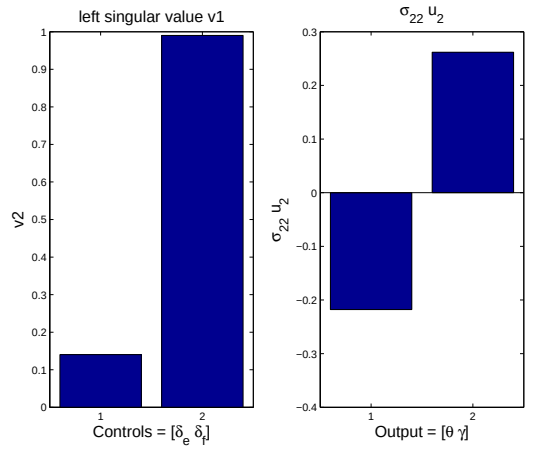

Figure 5.9: F8 SVD at DC for Longitudinal Dynamics $v_2 \rightarrow \sigma_2 u_2$

shown in Figure 5.8. This analysis shows that elevator should be used as the primary control for maintaining steady pitch angle perturbations from equilibrium.

2. Examination of the second columns of V,Σ and U shows that flaperon has a greater impact on the flight path angle of the aircraft than the pitch of the aircraft. This may be visualized as shown in Figure 5.9. This analysis shows that flaperon should be used as the primary control for maintaining steady flight path angle perturbations from equilibrium.

The Singular Value Decomposition at DC shows that the F8 is less coupled at DC.

5.3 H_∞ Mixed Sensitivity Control System Design for F-8 Longitudinal Dynamics

In this section , we consider the design of a dynamic output feedback control system for the longitudinal dynamics of F-8 aircraft.

The TITO model for the longitudinal dynamics at the above flight conditions is as follows:

$$\dot{x} = Ax + Bu \tag{5.3}$$

$$y = Cx + Du \tag{5.4}$$

where

$$x = \begin{bmatrix} \theta & \text{perturbed pitch angle from trim} & \text{deg} \\ \gamma & \text{perturbed flight path angle from trim} & \text{deg} \\ q & \text{pitch rate} & \text{deg/sec} \\ v & \text{perturbation from horizontal speed} & \text{ft/sec} \end{bmatrix}$$

$$u = \begin{bmatrix} \delta_e & \text{Elevon deflection from trim} & \text{deg} \\ \delta_f & \text{Flaperon deflection from trim} & \text{deg} \end{bmatrix}$$

$$y = \begin{bmatrix} \theta & \text{Perturbed pitch angle from trim} & \text{deg} \\ \gamma & \text{Perturbed flight path angle from trim} & \text{deg} \end{bmatrix}$$

Open Loop Bandwidth Design Specification. Since the F8 has no RHP zero or RHP pole, therefore there is no fundamental constraint on the bandwidth at the input and the output loop breaking point. However, there would always be unmodelelled high frequency acutater dynamics, high frequency parasitic dynamics or high frequency flexible modes which would put an upward bound on the bandwidth. Hence we shouldn't make our bandwidth very high so that these high frequency dynamics don't get excited. Let us choose an open loop bandwidth of 1 rads/sec.

H_∞ Dynamic Output Feedback Controller Design. We now design the dynamic output feedback controller keeping the above mentioned bandwidth constraints in mind. Let us consider the generalized plant of the following form:(Olalla *et al.* (2011),AbdelGhany and Bensenouci (2007))

$$\begin{cases} \dot{x} = Ax + B_1 u + B_2 w \\ z = C_1 x + D_{11} u + D_{12} w \\ y = C_2 x + D_{21} u + D_{22} w \end{cases}$$

where $u = [\delta_e \ \delta_f]^T$ is the input, $w = [r \ di]^T$ is the set of exogenous signals, $y = [\theta \ \gamma]^T$ is the measured output and z is an output vector related to the performance of the closed loop system.

Weighted H_∞ Mixed Sensitivity Problem The standard weighted H_∞ mixed sensitivity problem is to find a finite dimensional real-rational proper internally stabilizing controller K that satisfies (Scherer *et al.* (1997),Echols *et al.* (2015))

$$K = \arg\{ \min_{K \ stabilizing} \gamma | \left[\begin{array}{c} W_1 S_e \\ W_2 K S_e \\ W_3 T_e \end{array} \right]_\infty < \gamma \} \tag{5.5}$$

where S is the sensitivity transfer function, T is the complementary sensitivity transfer function of the closed loop system and KS is the control action.

However we would use $w = [r \ d_i]$ as the set of exogenous signals in order to get good properties at both input and output loop breaking points.So we do a slightly modified weighted mixed sensitivity problem to find a finite dimensional real-rational proper internally stabilizing controller K that satisfies(Echols *et al.* (2015)):

$$K = \arg\{ \min_{K \ stabilizing} \gamma | \left[\begin{array}{cc} W_1 S_e & W_1 P S_c \\ W_2 K S_e & W_2 T_c \\ W_3 T_e & W_3 P S_c \end{array} \right]_\infty < \gamma \} \tag{5.6}$$

Finding a internally stabilizing controller K that minimizes γ can be translated into an LMI optimization problem as shown below(Scherer *et al.* (1997)):

$$\underset{\hat{A},\hat{B},\hat{C},\hat{D},X,Y}{\text{minimize}} \quad \gamma$$

$$\text{s.t.} \quad \begin{bmatrix} AX + XA^T + B_2\hat{C} + (B_2\hat{C})^T & \hat{A}^T + (A + B_2\hat{D}C_2) & * & * \\ \hat{A} + (A + B_2\hat{D}C_2)^T & A^TY + YA + \hat{B}C + (\hat{B}C)^T & * & * \\ (B_1 + B_2\hat{D}D_{21})^T & (YB_1 + \hat{B}D_{21})^T & -\gamma I & * \\ C_1X + D_{12}\hat{C} & C_1 + D_{12}\hat{D}C_2 & D_{11} + D_{12}\hat{D}D_{21} & -\gamma I \end{bmatrix} < 0$$

$$\begin{bmatrix} X & I \\ I & Y \end{bmatrix} > 0$$

After solving the optimization problem and obtaining the set of $\hat{A}$,$\hat{B}$,$\hat{C}$,$\hat{D}$,X,Y which minimizes γ, the dynamic output feedback controller is obtained as follows(Scherer *et al.* (1997)):

1. Find nonsingular matrices M,N which satisfies $MN^T = I - XY$

2. Construct the controller using

$$\begin{aligned} D_K &= \hat{D} \\ C_K &= (\hat{C} - D_K C_2 X)M^{-T} \\ B_K &= N^{-1}(\hat{B} - YB_2D_K) \\ A_K &= N^{-1}(\hat{A} - NB_KC_2X - YB_2C_KM^T - Y(A + B_2D_KC_2)X)M^{-T} \end{aligned} \tag{5.7}$$

Structure of Weighting functions for H_∞ Mixed Sensitivity Optimization. The structure of weighting functions which has been used to do the above optimization is shown below:

$$W_1 = \begin{bmatrix} \frac{s/M_{s_1} + \omega_{b_1}}{s + \omega_{b_1}\epsilon} & 0 & 0 \\ 0 & \frac{s/M_{s_2} + \omega_{b_2}}{s + \omega_{b_2}\epsilon} & 0 \\ 0 & 0 & 7e-05 \end{bmatrix}$$

$$W_2 = \begin{bmatrix} \frac{s + \omega_{bu_1}/M_{u_1}}{s\epsilon + \omega_{bu_1}\epsilon} & 0 \\ 0 & \frac{s + \omega_{bu_2}/M_{u_2}}{s\epsilon + \omega_{bu_2}} \end{bmatrix}$$

$$W_2 = \begin{bmatrix} \frac{s + \omega_{bc_1}/M_{y_1}}{s\epsilon + \omega_{bc_1}\epsilon} & 0 & 0 \\ 0 & \frac{s + \omega_{bc_2}/M_{y_2}}{s\epsilon + \omega_{bc_2}} & 0 \\ 0 & 0 & 7e-05 \end{bmatrix}$$

Table 5.1: Weighting Function Parameters for F-8

	W1	W2	W3
M1	10	70	1
M2	10	70	1
ω_1	0.2	100	20
ω_2	0.2	100	20
ϵ_1	0.001	0.1	0.001
ϵ_2	0.001	0.1	0.001

While designing the dynamic output feedback controller, the controller architecture has been considered to imitate a classical inner-outer loop structure to ensure that the designer won't have to design an inner loop controller and outer loop controller separately. The controller architecture has been shown in Figure 5.10.

H_∞ Controller Synthesis

1. Augment the θ and γ output channels of the plant with integrators so as to ensure integral action at low frequencies which would lead to zero steady state error to a step reference input.

2. In order to prevent cancellation of the lightly damped phugoid modes and integrator states by the H_∞ controller synthesis methodology, use bilinear transformation(Tsai *et al.* (1990),Folly (2007)) to shift the system slightly to the right half plane. We use the following Bilinear transformation parameters for F8-longitudinal dynamics model.

   The bilinear transformation parameters for both NEOP and NENP model are selected are as follows:

$$p_1 = -0.0075 \tag{5.8}$$

$$p_2 = -10^{20} \tag{5.9}$$

   The selection results in

   Transform:

$$s = \frac{\hat{s} + p_1}{\frac{\hat{s}}{p_2} + 1} = \frac{\hat{s} - 0.0097}{\frac{\hat{s}}{-10^20} + 1} \approx \hat{s} - 0.0075 \tag{5.10}$$

Inverse Transform:

$$\tilde{s} \approx s + 0.0075 \tag{5.11}$$

3. Choose W1 to shape sensitivity transfer function to have good integral action at low frequencies and ensure that $||S||_\infty$ is below 8db. Choose W2 to shape the KS transfer function such that $||KS||_\infty$ is not too high which would prevent control signal saturation. Also ensure that KS rolls off at higher frequencies. Choose W3 so that $||T||_\infty$ is below 8 db and T rolls off at higher frequencies to ensure sensor noise attenuation at higher frequencies.

4. Create a generalized plant using $w = [r\ d_i]$ as the set of exogenous signals so that we get good properties at both input and output loop breaking points.

5. Minimize gamma by solving LMI as shown in Equation 5.3. We use YALMIP(Lofberg (2004),Löfberg (2008))for solving the LMI.

6. Obtain the controller from the parameters returned by the optimization. Do inverse bilinear transformation to shift the controller to the left half plane so that it corresponds to the original untransformed plant.

7. Shift the integrators from the plant output to the controller input. In other words, augment the controller at the input with integrators.

8. Feed the θ state into the controller as the 3rd input. This serves as the inner loop feedback as seen in a standard inner-outer feedback control architecture in Figure 5.10. Obtain the closed loop system using the final controller containing 3 inputs and 2 outputs and the original plant.

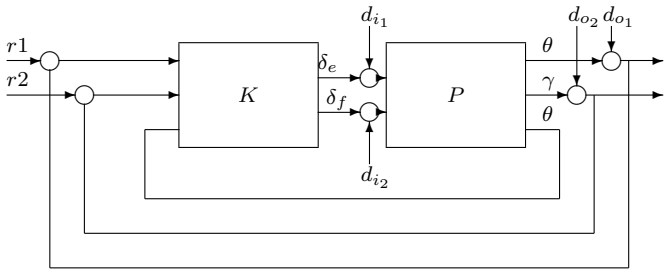

Figure 5.10: Topology of Dynamic Output Feedback Control System

After performing the optimization, the closed loop poles obtained are as follows:

Table 5.2: F8: Closed Loop Poles Using Dynamic Output Feedback

Pole	Damping	Frequency(rad/sec)	Time constant(sec)
-1.39e-02	1.00e+00	1.39e-02	7.19e+01
-1.39e-02	1.00e+00	1.39e-02	7.19e+01
-2.06e-01	1.00e+00	2.06e-01	4.85e+00
-3.14e-01	1.00e+00	3.14e-01	3.19e+00
-1.20e+00	1.00e+00	1.20e+00	8.31e-01
-1.58e+00 + 8.01e-01i	8.92e-01	1.77e+00	6.32e-01
-1.58e+00 - 8.01e-01i	8.92e-01	1.77e+00	6.32e-01
-1.25e+00 + 1.90e+00i	5.49e-01	2.28e+00	7.99e-01
-1.25e+00 - 1.90e+00i	5.49e-01	2.28e+00	7.99e-01
-2.59e+00 + 2.66e-01i	9.95e-01	2.60e+00	3.86e-01
-2.59e+00 - 2.66e-01i	9.95e-01	2.60e+00	3.86e-01
-1.50e+00 + 3.66e+00i	3.79e-01	3.95e+00	6.67e-01
-1.50e+00 - 3.66e+00i	3.79e-01	3.95e+00	6.67e-01
-1.07e+01 + 1.59e+01i	5.58e-01	1.92e+01	9.32e-02
-1.07e+01 - 1.59e+01i	5.58e-01	1.92e+01	9.32e-02
-2.00e+02 + 3.13e-02i	1.00e+00	2.00e+02	5.00e-03
-2.00e+02 - 3.13e-02i	1.00e+00	2.00e+02	5.00e-03
-2.00e+02 + 3.25e+00i	1.00e+00	2.00e+02	5.00e-03
-2.00e+02 - 3.25e+00i	1.00e+00	2.00e+02	5.00e-03
-3.25e+04	1.00e+00	3.25e+04	3.08e-05
-5.13e+04	1.00e+00	5.13e+04	1.95e-05
-6.05e+04	1.00e+00	6.05e+04	1.65e-05

5.4 Inner-Outer Loop Feedback Loop Control Design Methodology

In the section,we discuss the design methodology for Inner-Outer loop control design for the longitudinal control system.

where

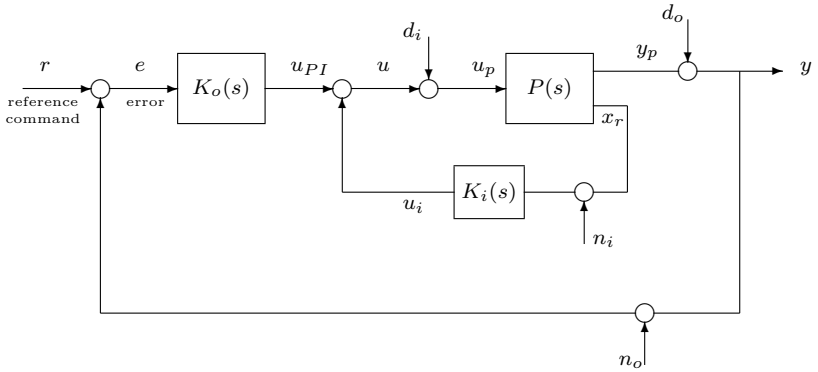

Figure 5.11: Inner Outer Feedback Loop

1. Output vector: $y = [y1\ y2]^\top = [\theta\ \gamma]^\top$
2. Control vector: $u = [u1\ u2]^\top = [\delta_e\ \delta_f]^\top$
3. State : $x_r = [\theta]$

Let us first design an inner-outer loop controller for the F8 aircraft considering only the diagonal elements of the plant transfer function matrix i.e. $P_{\delta_e \to \theta}$ and $P_{\delta_f \to \gamma}$.

Let us consider the $(1,1)$ element of the plant transfer function matrix i.e. $P_{\delta_e \to \theta}$.

$$P_{\delta_e \to \theta} = \frac{-19(s+1.4)(s+0.01287)}{(s^2+0.01155s+0.0007316)(s^2+2.302s+13.2)} \tag{5.12}$$

Initially let us assume that $P_{\delta_e \to \theta}$ does not need an inner-outer loop controller to be stabilized. Let us assume $Ko = \frac{-g_{o1}(s+z_{o1})}{s}$ where $g_{o1} > 0,\ z_{o1} > 0$. The rootlocus of $L = P_{\delta_e \to \theta} K_o$ where $K_o = \frac{-0.1(s+2)}{s}$ is shown in Figure 5.12. It is seen that the closed loop system may be stable using only a PI controller but the closed loop poles would be very lightly damped. As we increase g_{o1}, the closed loop system become more lightly damped.

Hence we use the inner-outer loop feedback control architecture in order to shift the lightly damped phugoid and short period modes of $P_{\delta_e \to \theta}$ to a location with better damping using a PD controller in the inner loop to obtain $P_{mod} = \frac{P_{\delta_e \to \theta}}{1+L_{mod}}$ where $L_{mod} = P_{\delta_e \to \theta} K_{i1}$. This is followed by

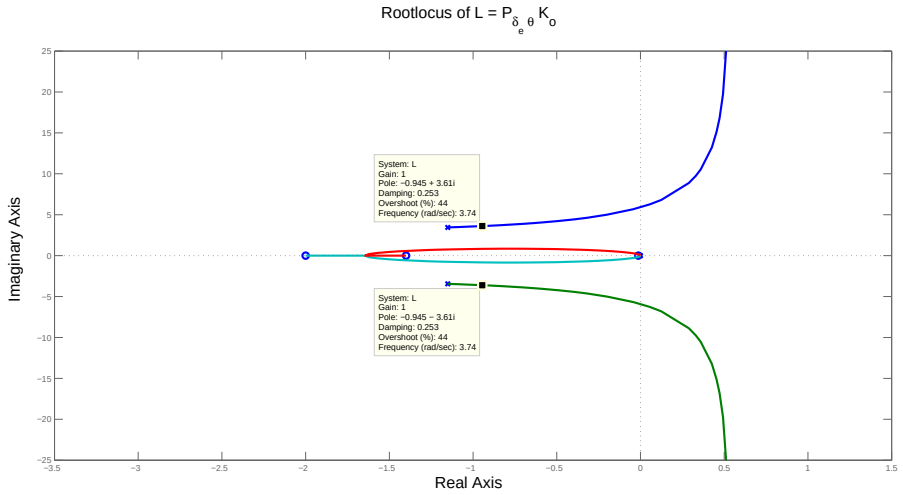

Figure 5.12: Rootlocus of $L = P_{\delta_e \to \theta} K_o$ using PI Controller :F8

the stabilization of P_{mod} using a PI controller in the outer loop. The closed loop system architecture is shown in Figure 5.13 :

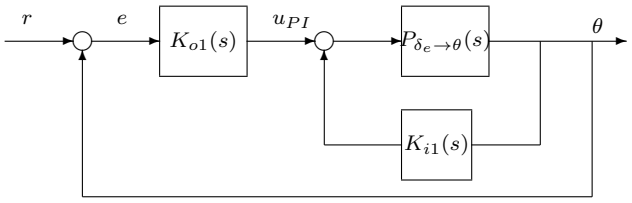

Figure 5.13: F8: Inner Outer Loop Structure for $P_{\delta_e \to \theta}(s)$

As seen in Figure 5.14 and Figure 5.15 , the inner loop with $K_{i1} = -0.3(s + 0.4)$ places the short period modes at the location $s = -3.93 \pm 2.62, \zeta = 0.832$. The inner loop also places the phugoid modes at $s = -0.139$ and $s = -0.0164$.

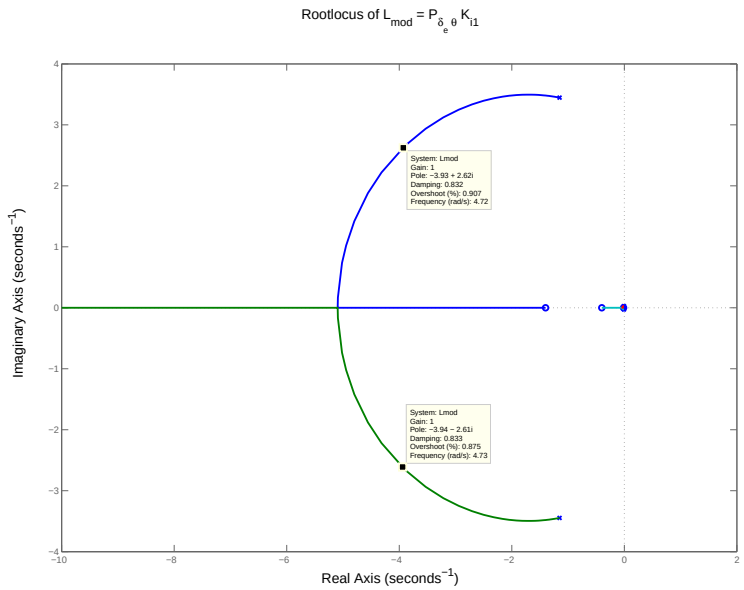

Figure 5.14: Rootlocus of $L_{mod} = P_{\delta_e \to \theta} K_i$ Using PD Controller : F8

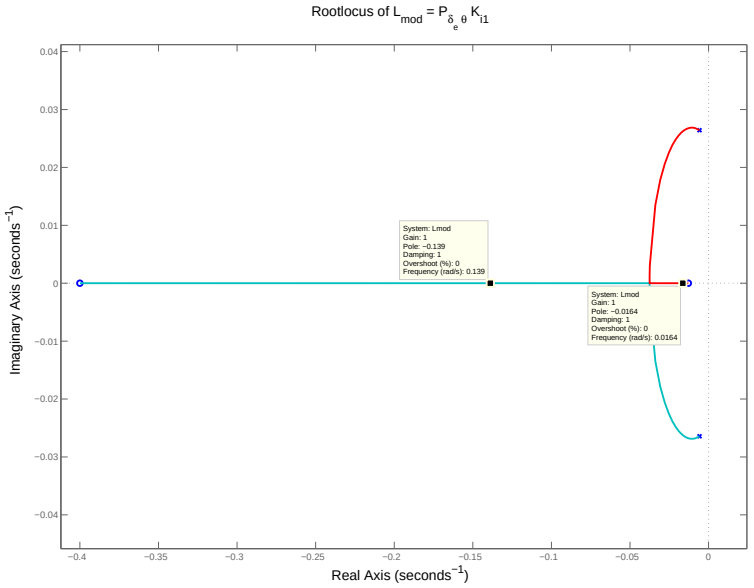

Figure 5.15: Rootlocus of $L_{mod} = P_{\delta_e \to \theta} K_i$ Magnified at Origin : F8

Now let us use an outer loop to stabilize $L = P_{mod} K_{o1}$ where $P_{mod} = \frac{P_{\delta_e \to \theta}}{1 + L_{mod}}$ and $L_{mod} = P_{\delta_e \to \theta} K_{i1}$. We select $K_{o1} = \frac{-2(s+1.5)}{s}$. The rootlocus of $L = P_{mod} K_{o1}$ is as shown in Figure 5.16.

$$P_{mod} = \frac{-19(s+1.4)}{(s+0.1385)(s^2+7.859s+22.34)} \tag{5.13}$$

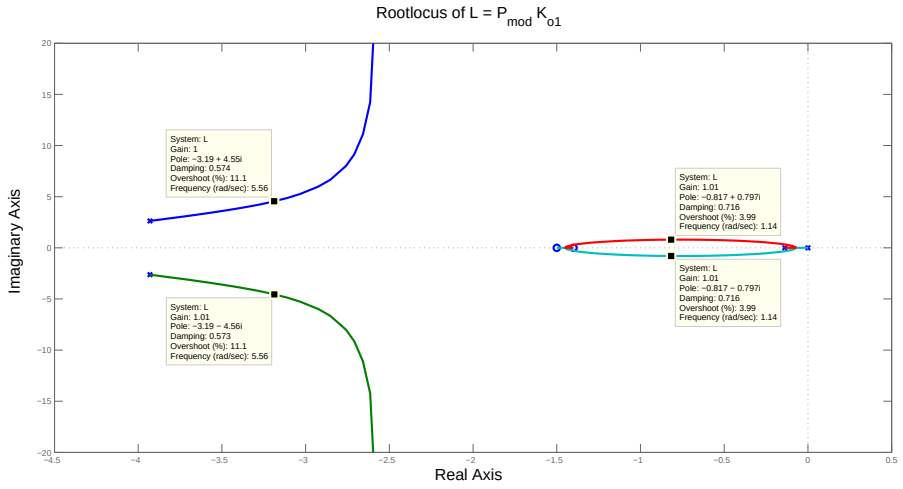

Figure 5.16: Rootlocus of $L = P_{mod}K_{o1}$: F8

The poles of the closed loop system is as follows:

Table 5.3: Closed Loop Poles of $T = \frac{P_{mod}K_{o1}}{1+P_{mod}K_{o1}}$ where $P_{mod} = \frac{P_{\delta_e \to \theta}}{1+P_{\delta_e \to \theta}K_{i1}}$: F8

Pole	Damping	Frequency(rad/sec)
-8.11e-001 + 7.99e-001i	7.12e-001	1.14e+000
-8.11e-001 - 7.99e-001i	7.12e-001	1.14e+000
-3.19e+000 + 4.54e+000i	5.74e-001	5.55e+000
-3.19e+000 - 4.54e+000i	5.74e-001	5.55e+000

Let us now consider the $(2,2)$ element of the plant transfer function matrix i.e. $P_{\delta_f \to \gamma}$.

$$P_{\delta_f \to \gamma} = \frac{0.6(s+0.0124)(s^2+0.8015s+5.751)}{(s^2+0.01155s+0.0007316)(s^2+2.302s+13.2)} \tag{5.14}$$

We can stabilize $P_{\delta_f \to \gamma}$ using only a PI controller. Let us select $K_{o2} = \frac{5(s+0.1)}{s}$. As seen in Figure 5.17 and Figure 5.18 we get closed loop poles with good damping.

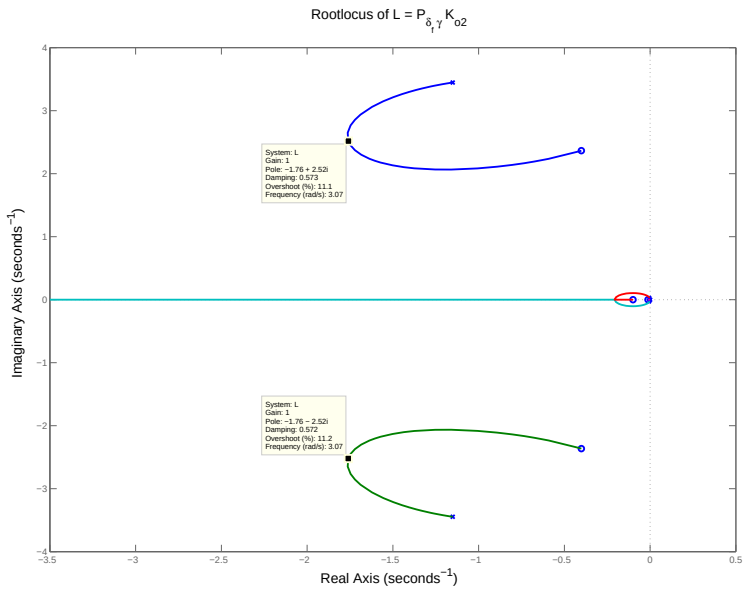

Figure 5.17: Rootlocus of $L = P_{\delta_f \to \gamma} K_{o2}$:F8

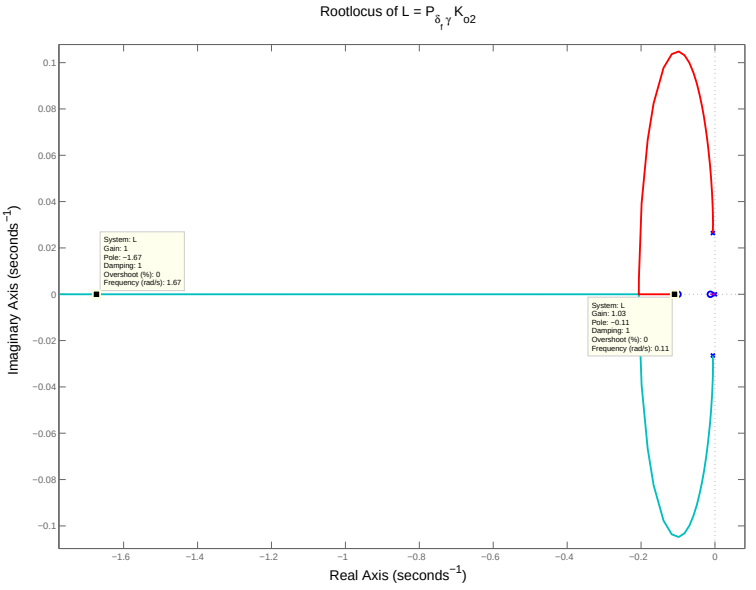

Figure 5.18: Rootlocus of $L = P_{\delta_f \to \gamma} K_{o2}$ Magnified at the Origin : F8

The poles of the closed loop system is as follows:

Table 5.4: Closed Loop Poles of $T = \frac{P_{\delta_f \to \gamma} K_{o2}}{1 + P_{\delta_f \to \gamma} K_{o2}}$: F8

Pole	Damping	Frequency(rad/sec)	Time constant(sec)
-1.23e-02	1.00e+00	1.23e-02	8.12e+01
-1.10e-01	1.00e+00	1.10e-01	9.10e+00
-1.67e+00	1.00e+00	1.67e+00	5.98e-01
-1.76e+00 + 2.52e+00i	5.72e-01	3.07e+00	5.68e-01
-1.76e+00 - 2.52e+00i	5.72e-01	3.07e+00	5.68e-01

5.5 PI-PD controller vs Dynamic Output Feedback Controller

In the section we try to obtain a PI-PD controller which best approximates the dynamic output feedback controller obtained in the previous sections.

In section we have obtained a decentralized PI-PD controller which stabilizes the F8 plant provided only the diagonal elements are considered. The controller obtained is as follows:

$$K_i(s) = \begin{bmatrix} -0.3(s+0.4) \\ 0 \end{bmatrix}$$
$$K_o(s) = \begin{bmatrix} \frac{-2(s+1.5)}{s} & 0 \\ 0 & \frac{5(s+0.1)}{s} \end{bmatrix} \tag{5.15}$$

This controller stabilizes the centralized plant but the closed loop poles are lightly damped. This however means that the plant is sufficiently decoupled so that a decentralized controller which was designed for the decoupled system stabilizes the coupled system as well. Now, we do a exhaustive search in the neighborhood of the previously obtained g_{o1},z_{o1},g_{o2},z_{o2},g_{i1},z_{i1} parameters in order to obtain a PI-PD controller which best approximates the dynamic output feedback controller. While doing this search by brute force looping, we minimize $||So1 - So2||_\infty$ (where So1 corresponds to Output feedback controller and So2 corresponds to PI-PD controler) in the low frequency range

0.0001 rads/sec to 0.01 rads/sec in order to ensure that we obtain the best PI-PD controller which gives us similar properties at the output loop breaking point when compared to the dynamic output feedback controller at low frequencies.

After doing the optimization, we obtain the following PI-PD controller which minimizes $||So1 - So2||_\infty$ in the range 0.0001 rads/sec to 0.01 rads/sec.The roll-off terms have been selected in a way so that the KS crossover frequency for the dynamic output feedback based closed loop system and the PI-PD based closed loop system is the same. This is done in order to ensure that we are in a position to compare two designs.

$$K_i(s) = \begin{bmatrix} -1(s+0.4)\left[\frac{50}{(s+50)}\right]^3 \\ 0 \end{bmatrix}$$
$$K_o(s) = \begin{bmatrix} \frac{-1.5(s+0.5)}{s}\left[\frac{5}{s+5}\right]^2 & 0 \\ 0 & \frac{1.5(s+0.9)}{s}\left[\frac{5}{s+5}\right]^2 \end{bmatrix} \tag{5.16}$$

The damping of the closed loop system using the PI-PD controller is as follows:

Table 5.5: Closed Loop Poles for F8 : PI-PD Based Controller

Pole	Damping	Frequency(rad/sec)	Time constant(sec)
-1.39e-02	1.00e+00	1.39e-02	7.17e+01
-3.07e-01	1.00e+00	3.07e-01	3.26e+00
-8.85e-01 + 7.49e-01i	7.63e-01	1.16e+00	1.13e+00
-8.85e-01 - 7.49e-01i	7.63e-01	1.16e+00	1.13e+00
-1.82e+00	1.00e+00	1.82e+00	5.50e-01
-2.20e+00 + 2.19e+00i	7.09e-01	3.10e+00	4.55e-01
-2.20e+00 - 2.19e+00i	7.09e-01	3.10e+00	4.55e-01
-6.78e+00	1.00e+00	6.78e+00	1.47e-01
-7.22e+00	1.00e+00	7.22e+00	1.38e-01
-5.91e+00 + 2.04e+01i	2.78e-01	2.13e+01	1.69e-01
-5.91e+00 - 2.04e+01i	2.78e-01	2.13e+01	1.69e-01
-6.91e+01 + 2.55e+01i	9.38e-01	7.37e+01	1.45e-02
-6.91e+01 - 2.55e+01i	9.38e-01	7.37e+01	1.45e-02

Let us now compare the closed loop properties obtained by using PI-PD controller and dynamic output feedback controller.

Table 5.6: Attained Closed Loop Properties for PI-PD and Dynamic Output Feedback Controller: F8

	$\|\|S_o\|\|_\infty$	$\|\|T_o\|\|_\infty$	$\|\|S_i\|\|_\infty$	$\|\|T_i\|\|_\infty$	$\|\|KS_o\|\|_\infty$	$\|\|PS_i\|\|_\infty$
Dynamic Output feedback Controller	7.41	4.07	6.03	3.79	13.17	6.017
PI-PD controller	3.91	3.18	7.25	4.74	10.61	-1.31

As shown in Table 5.6, the closed loop properties obtained using PI-PD controller is comparable to the closed loop properties obtained by using Dynamic output feedback controller.

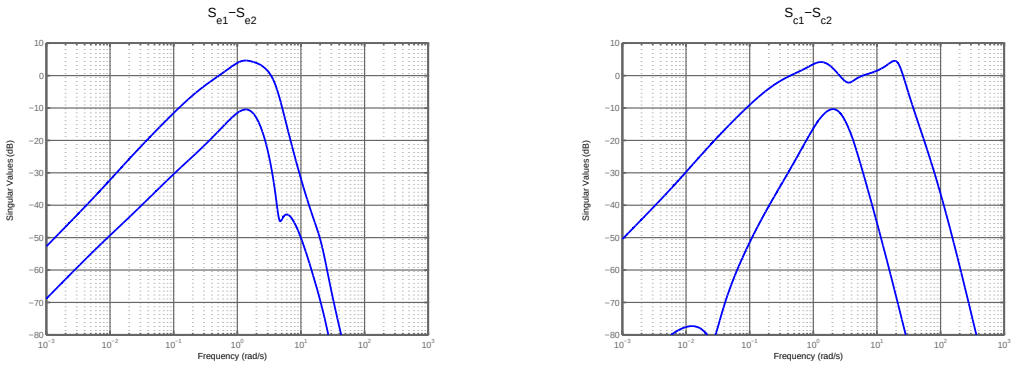

Figure 5.19: Comparison of $|S_{e1} - S_{e2}|$ and $|S_{c1} - S_{c2}|$: F8

Let us now compare the $|S_{e1} - S_{e2}|$ and $|S_{c1} - S_{c2}|$ plots where S_{e1} and S_{c1} corresponds to Dynamic output feedback controller and S_{e2} and S_{c2} corresponds to PI-PD controller as shown in Figure 5.19.

$|S_{e1} - S_{e2}|$ and $|S_{c1} - S_{c2}|$ have very low singular values at low frequencies. This means that the PI-PD controller and Dynamic output feedback controller would give similar performances at both the loop breaking points when we work at low frequencies. However the closed loop system has bad high frequency noise attenuation in the input channel when PI-PD controller is used as shown in Figure **??**. Any attempt at decreasing the crossover frequency of $T_{n_i \to u_p}$ leads to bad properties at the input loop breaking point.

Frequency Domain Plots

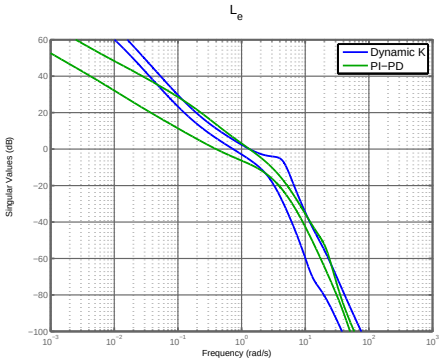

Figure 5.20: L_e : F8

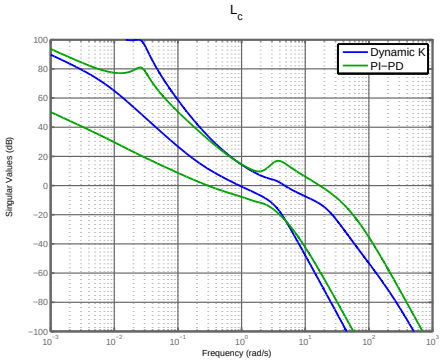

Figure 5.21: L_c : F8

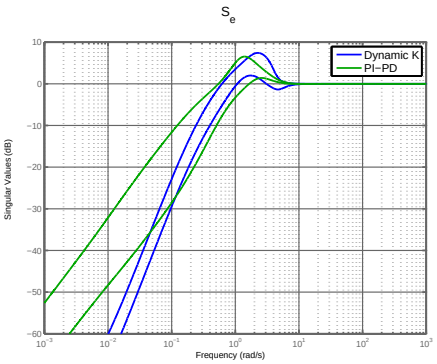

Figure 5.22: S_e : F8

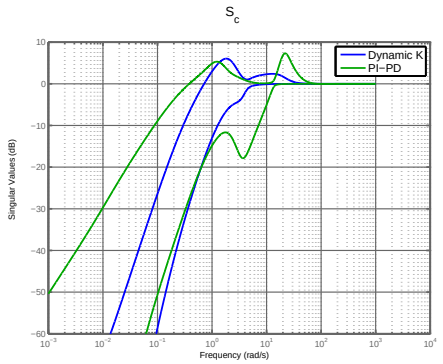

Figure 5.23: S_c : F8

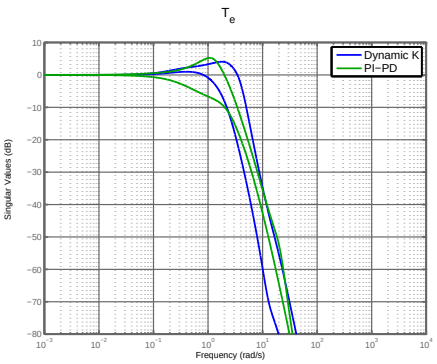

Figure 5.24: T_e : F8

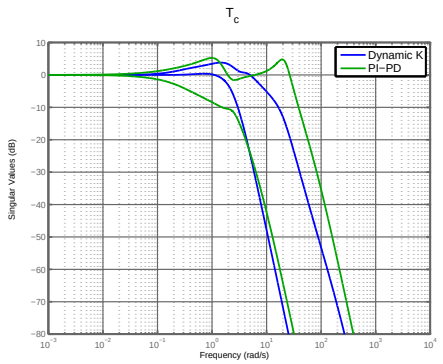

Figure 5.25: T_c : F8

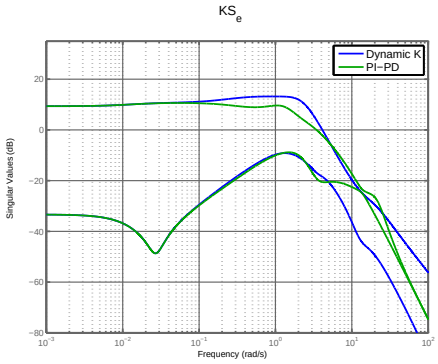

Figure 5.26: KS_e : F8

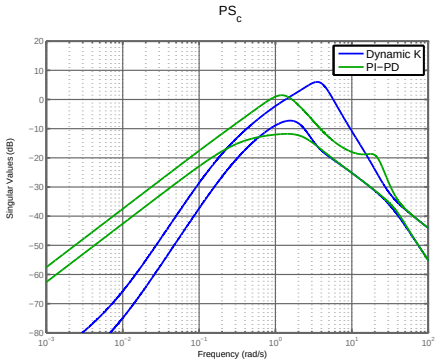

Figure 5.27: PS_c : F8

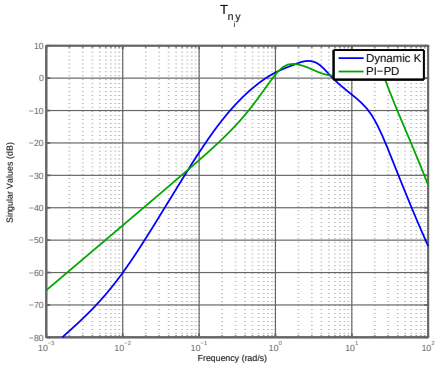

Figure 5.28: $T_{n_i \to y}$: F8

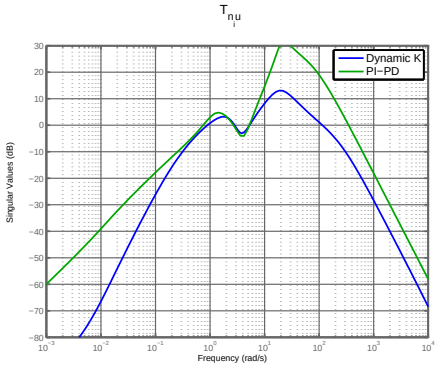

Figure 5.29: $T_{n_i \to y}$: F8

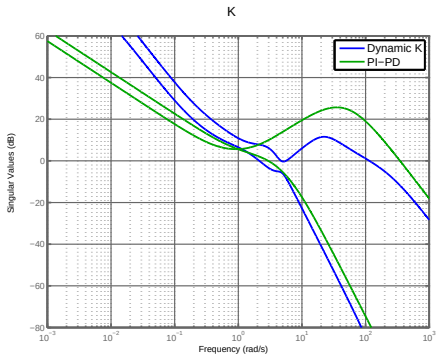

Figure 5.30: Controller Singular Values : F8

Time Domain Plots

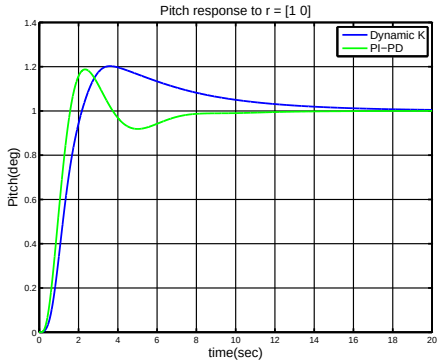

Figure 5.31: Pitch Response to $r = [1\ 0]$: F8

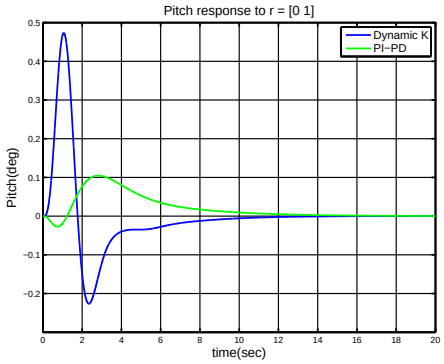

Figure 5.32: Pitch Response to $r = [0\ 1]$: F8

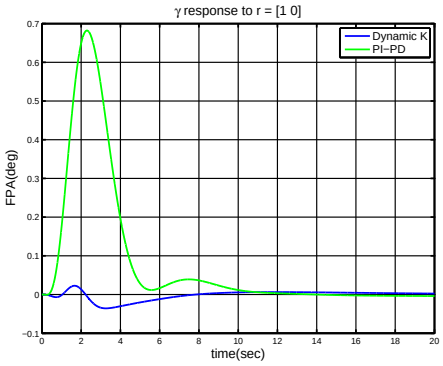

Figure 5.33: FPA Response to $r = [1\ 0]$: F8

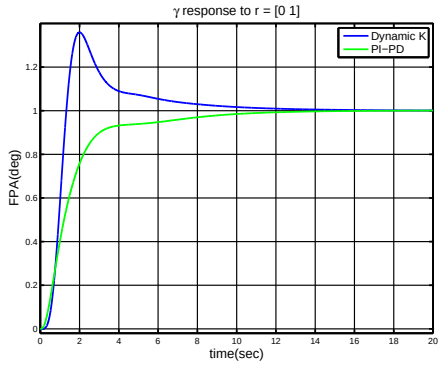

Figure 5.34: FPA Response to $r = [1\ 0]$: F8

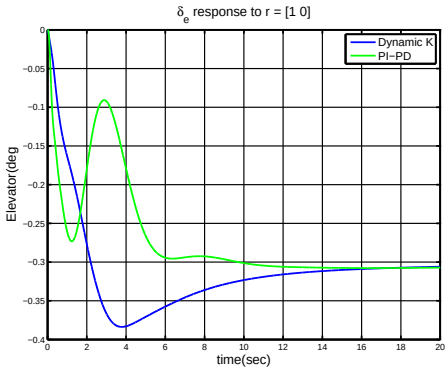

Figure 5.35: δ_e Response to $r = [1\ 0]$: F8

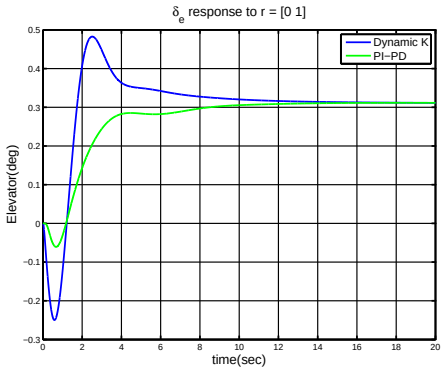

Figure 5.36: δ_e Response to $r = [0\ 1]$: F8

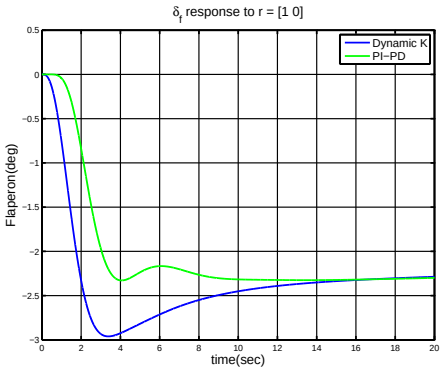

Figure 5.37: Flaperon Response to $r = [1\ 0]$: F8

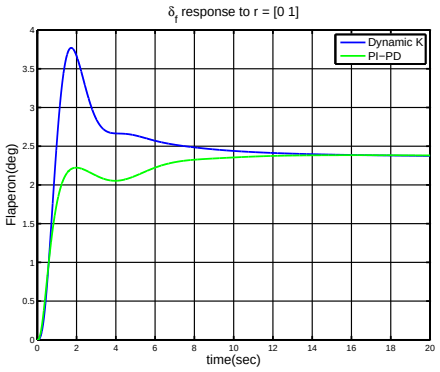

Figure 5.38: Flaperon Response to $r = [0\ 1]$: F8

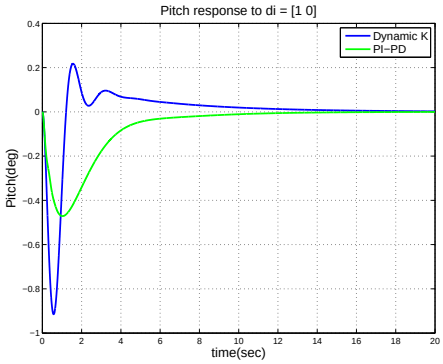

Figure 5.39: Pitch Response to $di = [1\ 0]$: F8

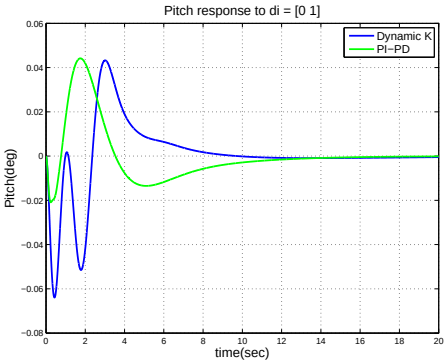

Figure 5.40: Pitch Response to $di = [0\ 1]$: F8

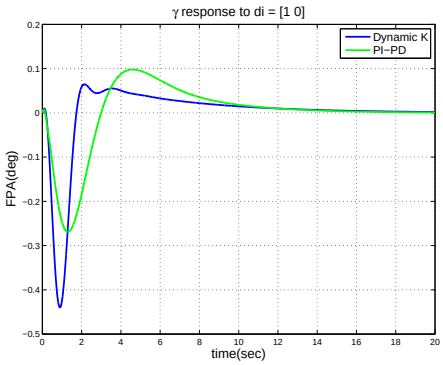

Figure 5.41: FPA Response to $di = [1\ 0]$: F8

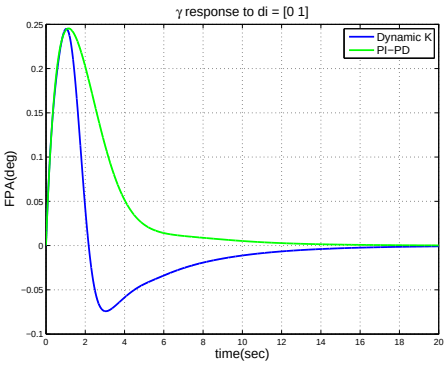

Figure 5.42: FPA Response to $di = [0\ 1]$: F8

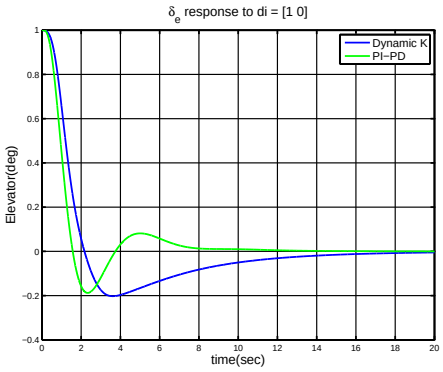

Figure 5.43: δ_e Response to $di = [1\ 0]$: F8

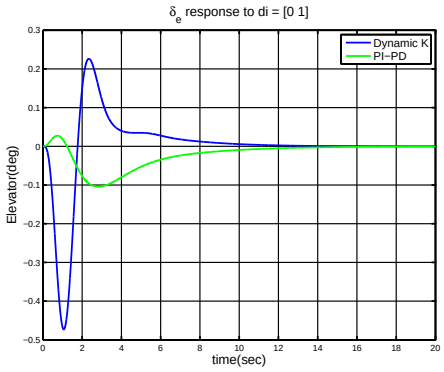

Figure 5.44: δ_e Response to $di = [0\ 1]$: F8

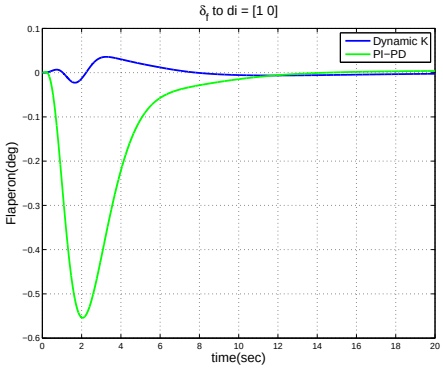

Figure 5.45: Flaperon Response to $di = [1\ 0]$: F8

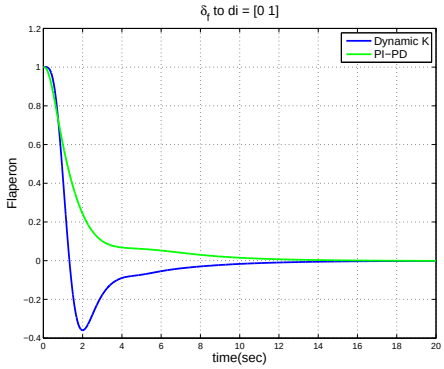

Figure 5.46: Flaperon Response to $di = [0\ 1]$: F8

5.6 Summary

After analyzing the closed loop properties, it is seen that the dynamic output feedback controller which has been designed using H_∞ non-standard mixed sensitivity techniques offers good closed loop properties at both the loop breaking points. The PI-PD($K_{o_{decentralized}}, K_{i_{decentralized}}$) controller offers better properties at the output and similar properties at the input. This shows that for a relatively decoupled minimum phase stable system, a PI-PD controller would offer good properties at both the loop breaking points. There is no need for a multivariable controller. However PI-PD controller has been designed using brute force enumeration. Hence it is time consuming. So in order to obtain a decent controller within a given amount of time, it might be appropriate to design a dynamic controller instead of a PI-PD controller.

Chapter 6

SUMMARY AND FUTURE DIRECTIONS

To summarize this thesis, decentralized and centralized controllers were designed for 4 different air crafts namely Hypersonic Aircraft, F-8, AV-8A and NASA-HiMAT. It was observed that design and control of complex vehicles requires sophisticated centralized(MIMO) control design methodologies. Decentralized(SISO) methods for designing a controller would be inadequate unless the plant is highly decoupled. It was also observed that full centralized PI-PD controllers would give an equally good performance as a centralized(MIMO) controller. However, it is time consuming to design a centralized PI-PD controller using exhaustive enumeration procedures. Therefore it is advantageous to design centralized(MIMO) controllers for controlling complex vehicles.

For the hypersonic aircraft, we have studied the design of dynamic output feedback controllers using Standard and Non-Standard Mixed Sensitivity Design on New Engine Old Plume and New Engine New Plume models of the Hypersonic aircraft. We have also designed 3 types of hierarchical PI-PD controllers and surgically inserted lead-lag networks to these controllers to improve the closed loop properties further. Decentralized Lead-lag networks were also designed for both the models of the Hypersonic Aircraft. The dynamic controller obtained using non-standard mixed sensitivity control gives better properties at the input loop breaking point as compared to the dynamic controller designed using standard mixed sensitivity. Both the controllers give good properties at the output loop breaking point. Hierarchical fully populated PI-PD controllers offers good properties at both loop breaking points but the design procedure is time consuming. Hence, there is a need for Multivariable Controller which can be designed in minimal time using LMI optimization but give an "'equilibrated design"'. For the NASA HiMAT, SISO decentralized PI-PD controller and multivariable controller give good properties at the error but bad properties at the input. Hence there is a need to explore generalized weighted mixed-sensitivity control methodology(Puttannaiah (2013)) to design a multivariable controller which could offers good properties at both loop breaking points. For AV-8A Harrier , the SISO decentralized PI-PD controller gives good properties at both loop breaking points but the multivariable controller is found to yield better performance.For F-8 Crusader, SISO decentralized ideas work really well performing comparably to the multivariable controllers examined.

Future work will emphasize more complex advanced control structures and methodologies like Hierarchical fully populated PID controllers and Hierarchical fully populated Lead-Lag controllers. It would also encompass integrated advanced vehicle design and control.

REFERENCES

AbdelGhany, A. and A. Bensenouci, "Robust output feedback control design using h/lmi and sa/lead-lag for an ann-adaptive power system stabilizer", in "Control & Automation, 2007. MED'07. Mediterranean Conference on", pp. 1–6 (IEEE, 2007).

Boyd, S., V. Balakrishnan, E. Feron and L. ElGhaoui, "Control system analysis and synthesis via linear matrix inequalities", in "American Control Conference, 1993", pp. 2147–2154 (IEEE, 1993).

Chavez, F. R. and D. K. Schmidt, "An integrated analytical aeropropulsive/aeroelastic model for the dynamic analysis of hypersonic vehicles", AIAA Paper 92-4567-CP pp. 551–563 (1992).

Chavez, F. R. and D. K. Schmidt, "Analytical aeropropulsive-aeroelastic hypersonic-vehicle model with dynamic analysis", Journal of Guidance, Control, and Dynamics **17**, 6, 1308–1319 (1994).

Dickeson, A. R., S. Sridharan, J. Benavides, D. Soloway, A. Kelkar and J. Vogel, "Decentralized control of an airbreathing scramjet-powered hypersonic vehicle", in "AIAA Conf. on Guidance, Navigation and Control, AIAA-2009", vol. 6281 (2009).

Dickeson, J. J., *Control Relevant Modeling and Design of Scramjet-Powered Hypersonic Vehicles* (2012).

Duan, G.-R. and H.-H. Yu, *LMIs in Control Systems: Analysis, Design and Applications* (CRC Press, 2013).

Echols, J. A., K. Puttannaiah, K. Mondal and A. A. Rodriguez, "Fundamental control system design issues for scramjet-powered hypersonic vehicles", (2015).

Folly, K., "A comparison of two methods for preventing pole-zero cancellation in h power system controller design", in "Power Tech, 2007 IEEE Lausanne", pp. 1266–1271 (IEEE, 2007).

Franklin, G. F., J. D. Powell and A. Emami-Naeini, "Feedback control of dynamics systems", Pretince Hall Inc (2006).

Freudenberg, J. and D. Looze, "Relations between properties of multivariable feedback systems at different loop-breaking points: Part ii", in "American Control Conference, 1986", pp. 771–777 (IEEE, 1986).

Gahinet, P., "Explicit controller formulas for lmi-based h synthesis", Automatica **32**, 7, 1007–1014 (1996).

Gahinet, P. and P. Apkarian, "Decentralized and fixed-structure h control in matlab", in "Decision and Control and European Control Conference (CDC-ECC), 2011 50th IEEE Conference on", pp. 8205–8210 (IEEE, 2011a).

Gahinet, P. and P. Apkarian, "Structured h synthesis in matlab", Proc. IFAC, Milan, Italy (2011b).

Gahinet, P., A. Nemirovskii, A. J. Laub and M. Chilali, "The lmi control toolbox user's guide", (1995).

Lofberg, J., "Yalmip: A toolbox for modeling and optimization in matlab", in "Computer Aided Control Systems Design, 2004 IEEE International Symposium on", pp. 284–289 (IEEE, 2004).

Löfberg, J., "Modeling and solving uncertain optimization problems in yalmip", in "Proceedings of the 17th IFAC World Congress", pp. 1337–1341 (2008).

Messner, W. C., M. D. Bedillion, L. Xia and D. C. Karns, "Lead and lag compensators with complex poles and zeros design formulas for modeling and loop shaping", Control Systems, IEEE **27**, 1, 44–54 (2007).

Ogata, K., *System dynamics*, vol. 3 (Prentice Hall Upper Saddle River, NJ, 1998).

Olalla, C., A. El Aroudi, I. Queinnec and R. Leyva, *LMI robust control of PWM converters: an output-feedback approach* (INTECH Open Access Publisher, 2011).

Puttannaiah, K., *H-Infinity Control Design Via Convex Optimization: Toward A Comprehensive Design Environment*, Ph.D. thesis, Arizona State University (2013).

Rodriguez, A. A., J. J. Dickeson, O. Cifdaloz, R. McCullen, J. Benavides, S. Sridharan, A. Kelkar, J. M. Vogel and D. Soloway, "Modeling and control of scramjet-powered hypersonic vehicles: challenges, trends, & tradeoffs", in "AIAA guidance, navigation and control conference and exhibit", vol. 6793 (2008).

Rodriguez, A. A., J. J. Dickeson, S. Sridharan, A. Korad, J. Khatri, J. Benavides, D. Soloway, A. Kelkar and J. Vogel, "Control-relevant modeling, analysis, and design for scramjet-powered hypersonic vehicles", in "Proceedings of the 16th AIAA/DLR/DGLR International Space Planes and Hypersonic Systems and Technologies Conference", (2009).

Saussié, D., Q. Barbès and C. Bérard, "Self-scheduled and structured h synthesis: a launch vehicle application.", in "American Control Conference (ACC), 2013", pp. 1590–1595 (IEEE, 2013).

Scherer, C., P. Gahinet and M. Chilali, "Multiobjective output-feedback control via lmi optimization", Automatic Control, IEEE Transactions on **42**, 7, 896–911 (1997).

Skogestad, S. and I. Postlethwaite, *Multivariable feedback control: analysis and design*, vol. 2 (Wiley New York, 2007).

Soloway, D., A. A. Rodriguez, J. J. Dickeson, O. Cifdaloz, J. Benavides, S. Sridharan, A. Kelkar and J. M. Vogel, "Constraint enforcement for scramjet-powered hypersonic vehicles with significant aero-elastic-propulsion interactions", in "American Control Conference, 2009. ACC'09.", pp. 3154–3159 (IEEE, 2009).

Sridharan, S., *Control Relevant Design of Scramjet-powered Hypersonic Vehicles with Aero-thermo-elastic-propulsive Effects and Uncertainty*, Ph.D. thesis, Arizona State University (2010).

Sridharan, S., J. J. Dickeson and A. A. Rodriguez, "Impact of plume modeling on the design and control for a class of air-breathing hypersonic vehicles", in "AIAA Conf. on Guidance, Navigation and Control, AIAA-2011", (2011).

Sridharan, S. and A. A. Rodriguez, "Performance based control-relevant design for scramjet-powered hyper sonic vehicles", in "AIAA Guidance, Navigation, and Control Conference", (2012).

Stein, G., "The practical, physical (and sometimes dangerous) consequences of control must be respected, and the underlying principles must be clearly and well taught.", IEEE Control Systems Magazine **272**, 1708/03 (2003).

Tsai, M., E. Geddes and I. Postlethwaite, "Pole-zero cancellations and closed-loop properties of an h mixed sensitivity design problem", in "Decision and Control, 1990., Proceedings of the 29th IEEE Conference on", pp. 1028–1029 (IEEE, 1990).

Yang, J., F. Hamelin, P. Apkarian and D. Sauter, "Mixed h-/h fault detection observer design for multi model systems via nonsmooth optimization approach", in "Control and Fault-Tolerant Systems (SysTol), 2013 Conference on", pp. 164–171 (IEEE, 2013).

APPENDIX A

INTRODUCTION TO LMI

A.1 General Form of LMI

A linear matrix inequality(LMI) is an inequality of the form (Duan and Yu (2013))

$$F(x) = F_0 + \sum_{i=1}^{m}(x_i F_i) > 0 \tag{A.1}$$

where $x \in R^m$ is the variable and the symmetric matrices $F_i = F_i^\top \in R^{n*n}, i = 0, 1..., m$, are given.The inequality symbol implies that $F(x)$ is positive definite. The inequality (1.1) is a strict inequality. We may also encounter non-strict inequality which is of the form

$$F(x) \geq 0 \tag{A.2}$$

The linear matrix inequality (1.1) defines a convex constraint on x i.e. the set $\{\ x|F(x) > 0\}$ of solutions of the LMI (1.1) is convex
The most general form of Linear Matrix Inequality is expressed as follows:

Let $Q \in S^n$,D,$E_i \in R^{m*n}$,$F_i \in R^{n*n}$,$i = 1, 2, ..., l$, then we can say that

$$L(X) = D'X + X'D + \sum_{i=1}^{l}(E_i'XF_i + F_i'X'E_i) + Q$$

is linear in matrix $X \in R^{m*n}$.We note that the matrix function L(X) is symmetric. Let us define the inequality

$$L(X) < 0 \tag{A.3}$$

Here are some properties related to LMIs.

Property 1.1 Let $A(x) = [A_{ij}(x)]_{q*p}$. Then $A(x) < 0$ is an LMI in vector x if and only if

$$A_{ij}(x), i = 1, 2, ..., q, j = 1, 2, ..., p$$

are linear in x.

Property 1.2 Let

$$A_i(x) < 0, i = 1, 2, ..., l$$

be a set of linear matrix functions in x. Then

1. $A_i < 0, i = 1, 2, ..., l$ are a set of LMIs in x if and only if

   $$diag(A_1(x), ..., A_l(x)) < 0$$

   is an LMI in x.

2. $A_i < 0, i = 1, 2, ..., l$, are a set of LMIs in x implies that

   $$\sum_{i=1}^{l} \alpha_i A_i(x) < 0$$

   is also an LMI in x where $\alpha_i \geq 0, i = 1, 2, ..., l$, are a set of real scalars which are not simultaneously zero.

A.2 Basic Examples Involving LMIs

In this section , a few basic examples have been presented which involves formulating the problem as an LMI. These examples would be used in the later chapters for proving various theorems(Duan and Yu (2013)).

A.2.1 Eigenvalue Minimization

Let us consider the problem of minimizing the maximal eigenvalue of a matrix that depends affinely on a variable.

Let $A_i \in R^{m*m}, i = 0, 1, 2, ..., n$, be a symmetric matrices, and define the matrix function

$$A(x) = A_0 + A_1x_1 + ... + A_nx_n \tag{A.4}$$

We have to find $x \in R^n$ to minimize

$$J(x) = \lambda_{max}(A(x))$$

This problem can be written in the form of an LMI as follows:
In order to convert this problem into an LMI, we prove the following lemma. **Lemma 1.1** Let M be a symmetric matrix. Then,

$$\lambda_{max}(M) \leq t \Leftrightarrow M - tI \leq 0 \tag{A.5}$$

Proof
For an arbitrary matrix M with eigenvector x and corresponding eigenvalue k, there holds

$$(M - tI)x = Mx - tx = (k - t)x$$

This states that for an arbitrary matrix M, there holds

$$\lambda(M - tI) = \lambda(M) - t.$$

Thus when M is symmtric, we have

$$\begin{aligned} \lambda_{max} \leq t &\Leftrightarrow \lambda_{max}(M - tI) \leq 0 \\ &\Leftrightarrow M - tI \leq 0. \end{aligned}$$

Applying this lemma to the matrix defined in (1.5) we finally have

$$\lambda_{max}(A(x)) \leq t \Leftrightarrow A(x) - tI \leq 0.$$

Conclusion 1.1
Problem 1.1 is equivalent to the following minimization problem

$$\begin{cases} min & \text{t} \\ s.t. & A(x) - tI \leq 0 \end{cases}$$

where $x_i, i = 1, 2, ..., n$, and $t > 0$, are the parameters to be optimized. In this way the eigenvalue minimization problem can be converted into an LMI problem.

A.2.2 Matrix Norm Minimization

The matrix norm minimization problem is a generalization of the eigenvalue minimization problem and uses the results of eigenvalue minimization problem.
Let $A_i \in R^{m*m}, i = 0, 1, 2, ..., n$, be a symmetric matrices, and define the matrix function

$$A(x) = A_0 + A_1x_1 + ... + A_nx_n \tag{A.6}$$

We have to find $x \in R^n$ to minimize

$$J(x) = \|A(x)\|_2$$

To convert the above problem into an LMI problem, the following result is needed which is a special case of the Schur complement lemma to be introduced later.

Lemma 1.2

Let A be a matrix and t be a positive scalar. Then,

$$A^\top A - t^2 I \le 0 \Leftrightarrow \begin{bmatrix} -tI & A \\ A^\top & -tI \end{bmatrix} \le 0 \tag{A.7}$$

Proof Let

$$Q = \begin{bmatrix} I & A \\ 0 & tI \end{bmatrix}$$

Then Q is nonsingular since $t > 0$. Please note that

$$Q^\top \begin{bmatrix} I & A \\ 0 & tI \end{bmatrix} Q = \begin{bmatrix} -tI & 0 \\ 0 & t(A^\top A - t^2 I) \end{bmatrix}$$

According to the definition of $\|A(x)\|_2$, we know that

$$\|A(x)\|_2 = (\lambda_{max}(A^\top A))^{1/2} \tag{A.8}$$

Using Lemma 1.1, we have ,for $t > 0$,

$$\begin{cases} \|A(x)\|_2 \le t \\ \Leftrightarrow \lambda_{max}(A^\top A) \le t^2 \\ \Leftrightarrow A^\top A - t^2 I \le 0 \\ \Leftrightarrow \begin{bmatrix} -tI & A \\ A^\top & -tI) \end{bmatrix} \le 0 \end{cases}$$

Hence we derive the following conclusion.

Conclusion 1.2

The aforementioned problem is equivalent to the following minimization problem using LMI

$$\begin{cases} min & \mathrm{t} \\ s.t. & \begin{bmatrix} -tI & A(x) \\ A^\top(x) & -tI \end{bmatrix} \le 0 \end{cases}$$

with $x_i, i = 1, 2, ..., n$, and t being parameters to be optimized.

A.2.3 Schur Stabilization

Schur stabilization corresponds to stability analysis of discrete-time linear systems. Let us consider the control of the following linear system

$$x(k+1) = Ax(k) + Bu(k)$$

where $x \in R^n$ is the state vector and $u \in R^r$ is the input vector. Let us consider the state feedback control law

$$u(k) = Kx(k),$$

then the closed-loop system is given by

$$x(k+1) = (A + BK)x(k)$$

We note that for an arbitrary matrix $M \in R^{n*n}$, there holds

$$|\lambda_i(A + BK)| \le \|A + BK\|_2, i = 1, 2, ..., n,$$

we have

$$|\lambda_i(M)| \leq \|M\|_2, i = 1, 2, ..., n,$$

We know that the closed loop system is stable in the discrete time sense if

$$\|A + BK\|_2 < 1$$

Motivated by the above statement, we have the following problem,
Let $A \in R^{n*n}$ and $B \in R^{n*r}$ and a scalar $0 < \gamma \leq 1$. We need to find a matrix $K \in R^{r*n}$ such that

$$\|A + BK\|_2 < \gamma. \tag{A.9}$$

We know that (1.9) is equivalent to

$$(A + BK)^\top (A + BK) < \gamma^2 I$$

Using Lemma 1.2 we can say that the above mentioned inequality is equivalent to

$$\begin{bmatrix} -\gamma I & (A + BK) \\ (A + BK)^\top & -\gamma I \end{bmatrix} < 0$$

Therefore, for finding a minimum γ which satisfies (1.5) we have the following optimization problem with LMI constraints with K and γ as parameters.

$$\begin{cases} min & \gamma \\ s.t. & \begin{bmatrix} -\gamma I & (A + BK) \\ (A + BK)^\top & -\gamma I \end{bmatrix} < 0 \\ \end{cases}$$

The following briefly summarizes the key notations which we will be using to present the theoretical results in this thesis. First. we present the key lemmas which would be used in designing the LMIs for various control system problems. Second, we would be presenting some notions of convex optimization. Lastly, we will describe the definitions of H_2 and H_∞ norms for a linear time invariant system(Duan and Yu (2013)).

A.3 Schur Complement Lemma

A.3.1 Schur Complements

In linear algebra, the Schur complement of a matrix block is defined as follows(Duan and Yu (2013)):
Consider the partitioned matrix

$$A = \begin{bmatrix} A_{11} & A_{12} \\ A_{21} & A_{22} \end{bmatrix} \tag{A.10}$$

When A_{11} is nonsingular,$A_{22} - A_{21}A_{11}^{-1}A_{12}$ is called the Schur complement of A_{11} denoted by $S_{ch}(A_{11})$

When A_{22} is nonsingular,$A_{11} - A_{12}A_{22}^{-1}A_{21}$ is called the Schur complement of A_{22} denoted by $S_{ch}(A_{22})$

For the partitioned matrix (2.1) the following holds true.

When A_{11} is nonsingular, then we can represent A as follows

$$A = \begin{bmatrix} A_{11} & 0 \\ 0 & A_{22} - A_{21}A_{11}^{-1}A_{12} \end{bmatrix} = \begin{bmatrix} A_{11} & 0 \\ 0 & S_{ch}(A_{11}) \end{bmatrix} \tag{A.11}$$

and therefore A is nonsingular if and only if $S_{ch}(A_{11})$ is nonsingular and

$$detA = detA_{11}detS_{ch}(A_{11}) \tag{A.12}$$

When A_{22} is nonsingular, then we can represent A as follows

$$A = \begin{bmatrix} A_{11} - A_{12}A_{22}^{-1}A_{21} & 0 \\ 0 & A_{22} \end{bmatrix} = \begin{bmatrix} S_{ch}(A_{22}) & 0 \\ 0 & A_{22} \end{bmatrix} \tag{A.13}$$

and therefore A is nonsingular if and only if $S_{ch}(A_{22})$ is nonsingular and

$$detA = detA_{22}detS_{ch}(A_{22}) \tag{A.14}$$

A.3.2 Matrix Inversion Lemma

For the partitioned matrix (2.1) the following conclusions hold true(Duan and Yu (2013)).

When A_{11} is nonsingular, A is nonsingular if and only if $S_{ch}(A_{11})$ is nonsingular and

$$A^{-1} = \begin{bmatrix} A_{11}^{-1} + A_{11}^{-1}A_{12}S_{ch}^{-1}(A_{11})A_{21}A_{11}^{-1} & -A_{11}^{-1}A_{12}S_{ch}^{-1}(A_{11} \\ -S_{ch}^{-1}(A_{11})A_{21}A_{11}^{-1} & S_{ch}^{-1}(A_{11}) \end{bmatrix} \tag{A.15}$$

When A_{22} is nonsingular, A is nonsingular if and only if $S_{ch}(A_{22})$ is nonsingular and

$$A^{-1} = \begin{bmatrix} S_{ch}^{-1}(A_{22}) & -S_{ch}^{-1}(A_{22})A_{12}A_{22}^{-1} \\ -A_{22}^{-1}A_{12}S_{ch}^{-1}(A_{22} & A_{22}^{-1} + A_{22}^{-1}A_{21}S_{ch}^{-1}(A_{22})A_{12}A_{22}^{-1} \end{bmatrix} \tag{A.16}$$

For the partitioned matrix (2.1), considering A_{11} and A_{22} to be nonsingular matrices, then the following also holds true

$$(A_{11} - A_{12}A_{22}^{-1}A_{21})^{-1} = A_{11}^{-1} + A_{11}^{-1}A_{12}(A_{22} - A_{21}A_{11}^{-1}A_{12})^{-1}A_{21}A_{11}^{-1} \tag{A.17}$$

$$(A_{22} - A_{21}A_{11}^{-1}A_{12})^{-1} = A_{22}^{-1} + A_{22}^{-1}A_{21}(A_{11} - A_{12}A_{22}^{-1}A_{21})^{-1}A_{12}A_{22}^{-1} \tag{A.18}$$

A.3.3 Schur Complement Lemma

The Schur complement lemma is a very well known lemma and it helps in converting a nonlinear matrix inequality into a LMI(Duan and Yu (2013)).
Let the partitioned matrix

$$A = \begin{bmatrix} A_{11} & A_{12} \\ A_{21} & A_{22} \end{bmatrix} \tag{A.19}$$

be symmetric. Then

A is positive definite if and only if A_{11} and $S_{ch}(A_{11})$ are both positive definite or A_{22} and $S_{ch}(A_{22})$ are both positive definite.

$$A > 0 \Leftrightarrow A_{11} > 0, S_{ch}(A_{11}) > 0 \Leftrightarrow A_{22} > 0, S_{ch}(A_{22}) > 0 \tag{A.20}$$

A is negative definite if and only if A_{11} and $S_{ch}(A_{11})$ are both negative definite or A_{22} and $S_{ch}(A_{22})$ are both negative definite.

$$A < 0 \Leftrightarrow A_{11} < 0, S_{ch}(A_{11}) < 0 \Leftrightarrow A_{22} < 0, S_{ch}(A_{22}) < 0 \tag{A.21}$$

The following statements are very important since it realizes the conversion from quadratic to linear inequalities. This conversion technique is based on Schur complement lemma and it would be used frequently in the thesis to design LMIs(Duan and Yu (2013)).
Let $A \in \mathbb{R}^{n*n}, B \in \mathbb{R}^{n*r}, C \in \mathbb{R}^{r*n}, Q \in \mathbb{S}^n, R \in \mathbb{S}^r$, and denote

$$\phi(P) = A^\top P + PA + (PB + C^\top)R^{-1}(B^\top P + C) + Q \tag{A.22}$$

and

$$\psi(P) = \begin{bmatrix} A^\top P + PA + Q & PB + C^\top \\ B^\top P + C & -R \end{bmatrix} \tag{A.23}$$

then

$$\phi(P) < 0 \Leftrightarrow \psi(P) < 0, if R > 0 \tag{A.24}$$

$$\phi(P) > 0 \Leftrightarrow \psi(P) < 0, if R < 0 \tag{A.25}$$

A.3.4 Elimination of Variables

This section provides some results related to the technique of Elimination of Variables which is used frequently while deducing a LMI(Duan and Yu (2013)).

There are two techniques related to the Elimination of Variables.

Let

$$Z = \begin{bmatrix} Z_{11} & Z_{12} \\ Z_{21} & Z_{22} \end{bmatrix}, Z_{11} \in \mathbb{R}^{n*n},$$

be symmetric. Then, there exists a symmetric matrix X such that

$$\begin{bmatrix} Z_{11} - X & Z_{12} & X \\ Z_{12}^\top & Z_{22} & 0 \\ X & 0 & -X \end{bmatrix} < 0 \tag{A.26}$$

if and only if

$$Z = \begin{bmatrix} Z_{11} & Z_{12} \\ Z_{12}^\top & Z_{22} \end{bmatrix} < 0 \tag{A.27}$$

Let $Z_{ij}, i = 1, 2, 3, j = i, ..., 3$, be given matrices of appropriate dimensions. Then,there exists a matrix Y such that

$$\begin{bmatrix} Z_{11} & Z_{12} & Z_{13} \\ Z_{12}^\top & Z_{22} & Z_{23} + Y^\top \\ Z_{13}^\top & Z_{23}^\top + Y & Z_{33} \end{bmatrix} < 0 \tag{A.28}$$

if and only if

$$\begin{bmatrix} Z_{11} & Z_{12} \\ Z_{12}^\top & Z_{22} \end{bmatrix} < 0, \ \begin{bmatrix} Z_{11} & Z_{13} \\ Z_{13}^\top & Z_{33} \end{bmatrix} < 0 \tag{A.29}$$

Such a matrix Y is given by

$$Y = Z_{13}^\top Z_{11}^{-1} Z_{12} - Z_{23}^\top \tag{A.30}$$

A.3.5 Reciprocal Projection Lemma

The reciprocal projection lemma is used for formulating the LMI for State feedback controller. The reciprocal projection lemma proof can be found at(Apkarian et al.,2000 ,Duan and Yu (2013)). For a given symmetric matrix $\psi \in \mathbb{S}^n$, there exists a matrix $S \in \mathbb{R}^{n*n}$ satisfying

$$\psi + S^\top + S < 0 \tag{A.31}$$

if and only if, for an arbitrarily fixed symmatric matrix $P \in \mathbb{S}^n$, there exists a matrix $W \in \mathbb{R}^{n*n}$ satisfying

$$\begin{bmatrix} \psi + P - (W^\top + W) & S^\top + W^\top \\ S + W & -P \end{bmatrix} < 0 \tag{A.32}$$

A.3.6 Trace of LMI

While deducing various control system design applications into LMIs, we may encounter a type of constraint which requires the trace of a matrix to be less than a given scalar quantity. The following statements provides a way of working with such a type of constraint(Duan and Yu (2013)).

Let $A(x) \in \mathbb{S}^m$ be a matix function in $\mathbb{R}^n$ and let γ be a positive scalar. Then the following statements hold true and are equivalent:

$\exists x \in \mathbb{R}^n$ such that $trace(A(x)) < \gamma$

$\exists x \in \mathbb{R}^n, Z \in \mathbb{S}^m$, such that $A(x) < Z$, while $trace(Z) < \gamma$

A.4 Hurwitz and Schur Stability

A.4.1 Hurwitz Stability

Let us consider a continious time linear system of the form

$$\dot{x}(t) = Ax(t) \tag{A.33}$$

This system is said to be stable if all the eigenvalues of matrix A have nonpositive real parts. We can also say that A is Hurwitz critically stable. If all the eigenvalues of A have negative real parts, then the linear system is asymptotically stable. We may say that matrix A is Hurwitz stable.

The system (2.24) is Hurwitz stable if and only if there exist a matrix $P \in \mathbb{S}^n$,such that

$$\begin{cases} P > 0 \\ A^\top P + PA < 0 \end{cases}$$

Using the aforementioned statements, we can convert the problem of checking the stability of a linear system into finding a symmetric matrix satisfying the pair of LMIs.

A.4.2 Schur Stability

The stability analysis problem for a discrete time system can be stated in a similar way using LMIs.

Let us consider the discrete-time linear system

$$x(k+1) = Ax(k) \tag{A.34}$$

To check the lyapunov stability of this system, we check the Schur stability of the matrix A which means that we check if all the eigenvalues of the matrix A are located within the unit circle of the complex plane.

The system is Schur stable if and only if there exists a matrix $P \in \mathbb{S}^n$, such that the following LMIs hold true.

$$\begin{cases} P > 0 \\ APA^\top - P < 0 \end{cases}$$

A.5 D-Stability

In this section, we formulate LMIs which helps us in enforcing constraints on the position of the closed loop poles so that satisfactory time response and closed loop damping may be achieved.We will also introduce the concept of $\mathbb{D}$-Stability and deduce LMI conditions for the $\mathbb{D}$-stability of a matrix with a given general $\mathbb{D}$ region(Duan and Yu (2013))

Let $\mathbb{D}$ be a subset of the complex plane which is symmetric about the real axis. Then a matrix $A \in \mathbb{R}^{n*n}$ is $\mathbb{D}$ stable if

$$\lambda_i(A) \in \mathbb{D}, i = 1, 2, ..., n \tag{A.35}$$

If there exists $L \in \mathbb{S}^m$ and $M \in \mathbb{R}^{m*m}$ such that $\mathbb{D}$ can be expressed as

$$\mathbb{D} = \left\{ z | z \in \mathbb{C}, L + zM + \bar{z}M^\top < 0 \right\} \tag{A.36}$$

then $\mathbb{D}$ is called an LMI region and

$$F_{\mathbb{D}}(s) = L + zM + \bar{z}M^\top$$

is called the characteristic function of the LMI region of $\mathbb{D}$. The LMI region is always convex and symmetric about the real axis.

Constraints on the closed loop poles to restrict them to a particular convex region, can be expressed in the form of an LMI. The following statements deduce the LMI for constraining the closed loop poles to a general LMI region.

Let $\mathbb{D}$ be an LMI region whose characteristic function is

$$F_{\mathbb{D}}(s) = L + zM + \bar{z}M^\top.$$

Then the matrix $A \in \mathbb{R}^{n*n}$ is $\mathbb{D}$-stable if and only if there exists a symmetric positive definite matrix P such that

$$L \otimes P + M \otimes (AP) + M^\top \otimes (AP)^\top < 0 \tag{A.37}$$

where $\otimes$ represents the Kronecker product.

Let us now use (2.28) and deduce LMIs to restrict the eigenvalues of A to a particular convex region. We consider three cases.

1. $\mathbb{D}_1 = \{x + yi | -\beta < x < \alpha < 0\}$

   Let us express $\mathbb{D}_1$ in the form of a LMI region of the form (2.27)

   $$\begin{aligned}
   \mathbb{D}_1 &= \{x + yi | -\beta < x < \alpha < 0\} \\
   &= \{z | -\beta < Re(z) < -\alpha\} \\
   &= \left\{z | -\beta < \tfrac{1}{2}(z + \bar{z}) < -\alpha\right\} \\
   &= \left\{z | -\beta - \tfrac{1}{2}(z + \bar{z}) < 0, \alpha + \tfrac{1}{2}(z + \bar{z}) < 0\right\} \\
   &= \left\{z | diag(\alpha, -\beta) + \tfrac{1}{2} diag(z, -z) + \tfrac{1}{2} diag(\bar{z}, -\bar{z}) < 0\right\}
   \end{aligned}$$

   Hence $\mathbb{D}_1$ is an LMI region with

   $$L = 2\begin{bmatrix} \alpha & 0 \\ 0 & \beta \end{bmatrix}, M = \begin{bmatrix} 1 & 0 \\ 0 & -1 \end{bmatrix}$$

   Using Kronecker product we obtain the following LMIs which serves as a constraint to place the eigenvalues of matrix A in region $\mathbb{D}_1$.

   The matrix $A \in \mathbb{R}^{n*n}$ is $\mathbb{D}_1$-stable if and only if there exists a matrix $P \in \mathbb{S}^n$ which satisfys the following constraints

   $$\begin{cases} P > 0 \\ A^\top P + PA + 2\alpha P < 0 \\ A^\top P + PA + 2\beta P > 0 \end{cases}$$

2. $\mathbb{D}_2 = \left\{x + yi | (x + q)^2 + y^2 < r^2\right\}$

   Let us express $\mathbb{D}_2$ in the form of a LMI region of the form (2.27)

   $$\begin{aligned}
   \mathbb{D}_2 &= \left\{x + yi | (x + q)^2 + y^2 < r^2\right\} \\
   &= \left\{x + yi | (x + yi + q)(x - yi + q) < r^2\right\} \\
   &= \left\{z | (z + q)(\bar{z} + q) < r^2\right\} \\
   &= \left\{ z | \begin{bmatrix} -r & z + q \\ \bar{z} + q & -r \end{bmatrix} < 0 \right\} \\
   &= \left\{ z | \begin{bmatrix} -r & q \\ q & r \end{bmatrix} + z \begin{bmatrix} 0 & 1 \\ 0 & 0 \end{bmatrix} + \bar{z} \begin{bmatrix} 0 & 1 \\ 0 & 0 \end{bmatrix}^\top < 0 \right\}
   \end{aligned}$$

   Hence $\mathbb{D}_2$ is an LMI region with

$$L = \begin{bmatrix} -r & q \\ q & -r \end{bmatrix}, M = \begin{bmatrix} 0 & 1 \\ 0 & 0 \end{bmatrix}$$

Using Kronecker product we obtain the following LMIs which serves as a constraint to place the eigenvalues of matrix A in region $\mathbb{D}_2$.

The matrix $A \in \mathbb{R}^{n*n}$ is $\mathbb{D}_2$-stable if and only if there exists a matrix $P \in \mathbb{S}^n$ which satisfys the following constraints

$$\begin{cases} P > 0 \\ \begin{bmatrix} -rP & qP + AP \\ qP + PA^\top & -rP \end{bmatrix} < 0 \end{cases}$$

3. $\mathbb{D}_3 = \{x + yi| \mid y \mid < -xtan(\theta)\}$ with $0 < \theta < \pi/2$

Let us express $\mathbb{D}_3$ in the form of a LMI region of the form (2.27)

$$\begin{array}{rcl} \mathbb{D}_3 & = & \{x + yi| \mid y \mid < -xtan(\theta)\} \\ & = & \left\{x + yi | y^2 < x^2 tan^2(\theta), xtan(\theta) < 0\right\} \\ & = & \left\{x + yi | y^2 cos^2(\theta) < x^2 sin^2(\theta), xsin(\theta) < 0\right\} \\ & = & \left\{x + yi | \begin{bmatrix} xsin(\theta) & iycos(\theta) \\ -iycos(\theta) & xsin(\theta) \end{bmatrix} < 0\right\} \\ & = & \left\{z | \begin{bmatrix} (z + \bar{z})sin(\theta) & (z - \bar{z})cos(\theta) \\ (-z + \bar{z})cos(\theta) & (z + \bar{z})sin(\theta) \end{bmatrix} < 0\right\} \end{array}$$

Hence $\mathbb{D}_3$ is an LMI region with

$$L = \begin{bmatrix} 0 & 0 \\ 0 & 0 \end{bmatrix}, M = \begin{bmatrix} sin(\theta) & cos(\theta) \\ -cos(\theta) & sin(\theta) \end{bmatrix}$$

Using Kronecker product we obtain the following LMIs which serves as a constraint to place the eigenvalues of matrix A in region $\mathbb{D}_3$.

The matrix $A \in \mathbb{R}^{n*n}$ is $\mathbb{D}_3$-stable if and only if there exists a matrix $P \in \mathbb{S}^n$ which satisfys the following constraints

$$\begin{cases} P > 0 \\ \begin{bmatrix} (AP + PA^\top)sin(\theta) & (AP - PA^\top)cos(\theta) \\ (PA^\top - AP)cos(\theta) & (AP + PA^\top)sin(\theta) \end{bmatrix} < 0 \end{cases}$$

A.6 H_∞/H_2 Index

A.6.1 H_∞ Norm

In this section we explain the H_∞ norm and the H_2 norm of rational matrices. We also present LMI conditions for these norms to be bounded.

The H_∞ norm of a rational matrix is an extension of the spectral norm of a constant matrix A which is defined as

$$\|A\|_2 = (\lambda_{max}(AA^\top))^{1/2} = \sigma_{max}(A)$$

Let $P(s)$ be a rational matrix. Then the H_∞ norm is defined as

$$\|P\|_\infty = \sup_w \{\sigma_{max}(P(jw))\}$$

If $P(s)$ does not have poles in the closed right half complex plane. Then

$$\|P\|_\infty = \sup_w \{\sigma_{max}(P(jw))|Re(s) > 0\}$$

A.6.2 H_2 Norm

Suppose $P(s)$ is a matrix such that

$$\int_{-\infty}^{\infty} G(jw)G^H(jw)\,\mathrm{d}w < \infty \mathrm{rm}$$

Then the H_2 norm of $G(s)$ is defined as

$$\|G(s)\|_\infty = trace\left(\frac{1}{2\pi}\int_{-\infty}^{\infty} G(jw)G^H(jw)\,\mathrm{d}w\right)^{\frac{1}{2}} \tag{A.38}$$

Let us consider the following transfer function in control systems context.

$$G(s) = C(sI - A)^{-1}B + D \tag{A.39}$$

To find the H_2 norm of this matrix function , we need to use the following results.

Let $A, Q \in \mathbb{R}^{n*n}$, and A be stable, Q be positive semi-definite, then the following lyapunov equation

$$A^\top P + PA = -Q$$

has a unique positive definite solution which is expressed as

$$P = \int_0^{\infty} G(jw)G^H(jw)\,\mathrm{d}w$$

Based on this result we can state the following result. Let $G(s)$ be defined as 2.30. Then

1. $\|G(s)\|_2$ exists if and only if A is stable and $D = 0$
2. When A is stable and $D = 0$, then the following holds

   $\|G(s)\|_2^2 = trace(CXC^\top)$
   with $X > 0$ being the unique solution of the lyapunov equation defined as

   $$AX + XA^\top + BB^\top = 0 \tag{A.40}$$

   or
   $\|G(s)\|_2^2 = trace(B^\top XB)$
   with $Y > 0$ being the unique solution of the lyapunov equation defined as

   $$A^\top Y + YA + C^\top C = 0 \tag{A.41}$$

A.6.3 LMI for H_∞ index

Let us define a system as given below

$$\begin{cases} \dot{x} = Ax + Bw \\ y = Cx + Du \end{cases}$$

where x is the state vector, y is the output vector and w is the disturbance vector. Then we have

$$y(s) = G(s)w(s)$$

where

$$G(s) = C(sI - A)^{-1}B + D \tag{A.42}$$

Now we consider the H_∞ norm of $G(s)$ to be bounded by a given level γ i.e.

$$\|G(s)\|_\infty < \gamma \tag{A.43}$$

where gamma is the level of attenuation of disturbance in the system.
Now we present the LMI conditions for (2.34) to be valid.

Let G(s) be given by (2.33). Then $\|G(s)\|_\infty < \gamma$ if and only if there exists a symmetric positive definite matrix P such that one of the following two inequalities holds. In other words, $G(s)$ is bounded-real if and only if there exists a matrix P ¿ 0 satisfying one of the following LMI conditions(Duan and Yu (2013)).

$$\begin{bmatrix} A^\top P + PA & PB & C^\top \\ B^\top P & -\gamma I & D^\top \\ C & D & -\gamma I \end{bmatrix} < 0 \tag{A.44}$$

$$\begin{bmatrix} A^\top P + PA + C^\top C & PB + C^\top D \\ B^\top P + D^\top C & D^\top D - \gamma^2 I \end{bmatrix} < 0 \tag{A.45}$$

In control system applications, we are interested in finding the minimal γ which satisfies $\|G(s)\|_\infty < \gamma$. This problem can be converted into a minimization problem with LMI constraints(Duan and Yu (2013)).

$$\begin{cases} min \quad \gamma \\ s.t \quad P > 0 \\ \begin{bmatrix} A^\top P + PA & PB & C^\top \\ B^\top P & -\gamma I & D^\top \\ C & D & -\gamma \end{bmatrix} < 0 \end{cases}$$

or

$$\begin{cases} min \quad \gamma \\ s.t \quad P > 0 \\ \begin{bmatrix} A^\top P + PA + C^\top C & PB + C^\top D \\ B^\top P + D^\top C & D^\top D - \gamma^2 I \end{bmatrix} < 0 \end{cases}$$

A.6.4 LMI for H_2 index

Now we consider the H_2 norm of $G(s)$ to be bounded by a given level γ i.e.

$$\|G(s)\|_2 < \gamma \tag{A.46}$$

Let us consider $A \in \mathbb{R}^{n*n}$,$B \in \mathbb{R}^{n*r}$,$C \in \mathbb{R}^{m*n}$ and $\gamma > 0$. Then $\|G(s)\|_2 < \gamma$ holds if and only if one of the following statements holds true(Duan and Yu (2013)).

1. $\exists X > 0$,s.t.
$$AX + XA^\top + BB^\top < 0, trace(CXC^\top) < \gamma^2 \tag{A.47}$$
2. $\exists Y > 0$,s.t.
$$A^\top Y + YA + C^\top C < 0, trace(B^\top YB) < \gamma^2 \tag{A.48}$$

In control system applications, we are interested in finding the minimal γ which satisfies $\|G(s)\|_2 < \gamma$. This problem can be converted into a minimization problem with LMI constraints(Duan and Yu (2013)).

$$\begin{cases} min & \gamma \\ s.t & AX + XA^\top + BB^\top < 0 \\ & trace(CXC^\top) < \gamma \\ & X > 0 \end{cases}$$

or

$$\begin{cases} min & \gamma \\ s.t & A^\top Y + YA + C^\top C < 0 \\ & trace(B^\top YB) < \gamma \\ & Y > 0 \end{cases}$$

A.7 Anaysis of Properties

A.7.1 Hurwitz Stabilizability and Detectability

Let us define a system

$$\begin{cases} \dot{x} = Ax + Bu \\ y = Cx + Du \end{cases}$$

Then this system or the matrix pair (A, B) is said to be Hurwitz stabilizable if there exists some matrix K such that A+BK is Hurwitz stable(Duan and Yu (2013)).
We now present some LMI conditions for Hurwitz stabilizability.

The matrix pair (A, B) is Hurwitz stabilizable if and only if one of the following conditions hold

There exists a symmetric positive definite matrix P such that

$$(A + BK)P + P(A + BK)^\top < 0 \tag{A.49}$$

Let W = KP, then we obtain the following LMI from (2.40)

$$AP + PA^\top + BW + W^\top B^\top < 0 \tag{A.50}$$

There exists a symmetric positive definite matrix P such that

$$AP + PA^\top < \gamma BB^\top \tag{A.51}$$

for some scalar $\gamma > 0$

Hurwitz detectability is the dual concept of Hurwitz Stabilizability. The matrix pair (A, C) is said to be Hurwitz detectable if there exists some matrix L such that $A+LC$ is Hurwitz stable(Duan and Yu (2013)).
We now present some LMI conditions for Hurwitz detectability.

The matrix pair (A, B) is Hurwitz detectable if and only if one of the following conditions hold

There exists a symmetric positive definite matrix P such that

$$(A + LC)^\top P + P(A + LC) < 0 \tag{A.52}$$

Let $W^\top = PL$, then we obtain the following LMI from (2.43)

$$A^\top P + PA + C^\top W + W^\top C < 0 \tag{A.53}$$

There exists a symmetric positive definite matrix P such that

$$A^\top P + PA < \gamma C^\top C \tag{A.54}$$

for some scalar $\gamma > 0$

APPENDIX B

TRADEOFFS AND LIMITATIONS OF PERFORMANCE

In this chapter, some fundamental limitations imposed by RHP-poles and RHP zeros have been mentioned. Some algebraic and analytic constraints on Sensitivity and Complementary Sensitivity has been covered in brief. Various design tradeoffs which are a consequence of unstable RHP-poles, non-minimum phase zeros and bandwidth limitations have also been mentioned in the chapter.

We know that $S = (I + L)^{-1}$ and $T = L(I + L)^{-1}$ leads to

$$S + T = I \tag{B.1}$$

We want S to be small to ensure good command following and good disturbance attenuation. We also want T to be small to ensure good sensor noise attenuation. However both these conditions can't be achieved simultaneously. S(jw) and T(jw) cannot be both small at the same frequency. Hence there is a trade-off at each frequency between properties such as sensitivity reduction, disturbance attenuation governed by $|S(jw)|$ and sensor noise reduction and robustness to high frequency uncertainty governed by $|T(jw)|$.

B.1 The Waterbed Effect

In this subsection, we would talk about a trade-off between sensitivity reduction and sensitivity increase that must be performed when

L(s) has at least two or more poles than zeros(first waterbed formula)

L(s) has a RHP-zero(second waterbed formula)

The term "Waterbed" has been used since the trade-off between sensitivity reduction and sensitivity increase is similar to sitting on a waterbed in which if we push it down at one point, this will reduce the water level locally but this would result in an increase in water level at some other region in the bed(Skogestad and Postlethwaite (2007))

First waterbed formula

The first waterbed formula is related to the Bode sensitivity integral coined by Bode. It says that if L(s) has N_p RHP-poles at locations p_i, then assuming that the feedback system is stable, the sensitivity function must satisfy(Skogestad and Postlethwaite (2007))

$$\int_0^\infty \log|S(jw)|dw = \pi . \sum_{i=1}^{N_p} Re(p_i) \tag{B.2}$$

where $Re(p_i)$ denotes real part of p_i

This means that area of sensitivity increase($\log|S|$ positive) is greater than the area of sensitivity decrease($\log|S|$ negative) by an amount of $\pi . \sum_{i=1}^{N_p} Re(p_i)$. Thus we may observe peaking in the sensitivity bode plot. This peaking may be decreased if the increase in area occurs over a large frequency range i.e. if $|S(jw)| = 1 + \delta$ for $\omega \in [\omega_1, \omega_2]$ where the interval $[\omega_1, \omega_2]$ is sufficiently large.

For a stable plant, the bode sensitivity integral reduces to

$$\int_0^\infty \log|S(jw)|dw = 0 \tag{B.3}$$

This means that the area of sensitivity reduction($\log|S(jw)|$ negative) is equal to the area of sensitivity increase($\log|S(jw)|$ positive). Hence if we try to increase the bandwidth of S (pushing down on S at low frequencies), then we would expect that the sensitivity bode plot would have a larger peak.(Stein (2003)),(Skogestad and Postlethwaite (2007))

The first waterbed formula may also be explained by using Nyquist plots. Let us consider the open loop transfer function L(s) which has at least two or more poles than zeros. Let $L(s) = \frac{3}{(s+1)^2}$.

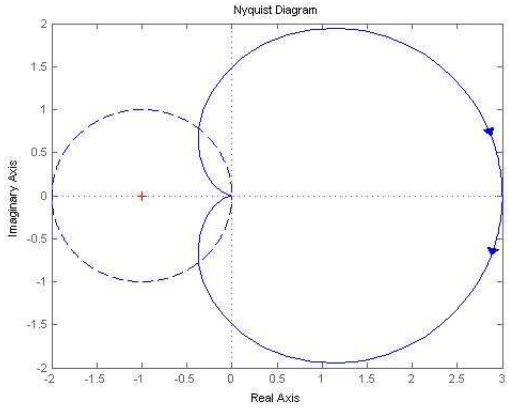

Figure B.1: Nyquist plot of $L(s) = \frac{3}{(s+1)^2}$

As shown in Figure B.1, the Nyquist plot enters the unit circle at some frequencies. Hence at these frequencies $|1 + L|$ is less than 1. So $S = (1 + L)^{-1}$ is greater than one at these frequencies. In practice L(s) would always have at least two or more poles than zeros at high frequencies due to unmodelled actuator dynamics. Hence there will always exist a frequency range where $|S| > 1$.

Second waterbed formula

The presence of RHP-zeros in the open loop transfer function always implies that the $||S||_\infty > 1$. To illustrate this, let us consider a non-minimum phase open loop transfer function $L(s) = \frac{1}{1+s}\frac{1-s}{1+s}$ and the minimum phase counterpart $L_m(s) = \frac{1}{1+s}$.(Skogestad and Postlethwaite (2007))

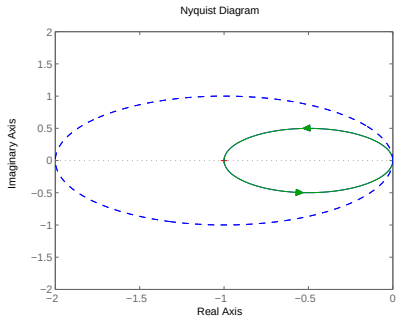

Figure B.2: Nyquist plot of $L(s) = \frac{1}{1+s}\frac{1-s}{1+s}$

In the Figure B.2 we see that the additional phase lag contributed by the RHP-zero and the extra pole causes the Nyquist plot to enter the unit circle. Hence 1+L is less than one at some frequencies or $S = (I + L)^{-1}$ is larger than 1.

Second waterbed formula states that if L(s) has N_p RHP-poles and a single real RHP-zero z or a complex pair of zero $z = x \pm y$, then for closed-loop stability, the sensitivity function must satisfy (Skogestad and Postlethwaite (2007))

$$\int_0^\infty \log|S(jw)|w(z,w)dw = \pi.\log\prod_{n=1}^{N_p}|\frac{p_i+z}{p_i-z}| \tag{B.4}$$

where if the zero is real

$$w(z,w) = \frac{2z}{z^2+w^2} = \frac{2}{z}\frac{1}{1+(\frac{w}{z})^2} \tag{B.5}$$

and if the zero pair is complex i.e. $z = x \pm jy$

$$w(z,w) = \frac{x}{x^2 + (y-w)^2} + \frac{x}{x^2 + (y+w)^2} \tag{B.6}$$

The weight w(z,w) limits the contribution of $\log|S|$ to sensitivity integral at frequencies $w > z$. Hence the waterbed is finite in this case and the tradeoff between S less than 1 and S greater than 1 is done over a limited frequency range. To illustrate this, let us consider $L_1(jw) = \frac{2}{s(s+1)}$ and $L_2(jw) = L_1(jw)\frac{-s+5}{s+5}$.

The following is the bodeplot of S_1 where $L_1 = \frac{2}{s(s+1)}$ and S_2 where $L_2(jw) = L_1(jw)\frac{-s+5}{s+5}$.

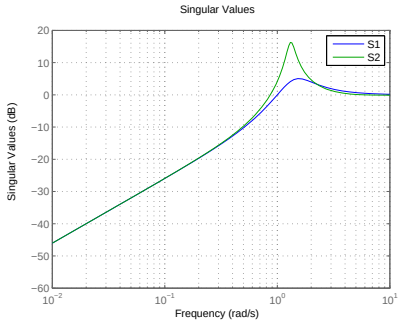

Figure B.3: Bode plot of $L_1 = \frac{2}{s(s+1)}$ and $L_2 = L_1\frac{-s+5}{s+5}$

As shown in Figure B.3 , the area of $\log S$ is almost the same for S_1 and S_2 below the 0 db line. However the frequency range in which $\log S_2$ contributes positively to the area of $\log S$ is limited due to the presence of RHP-zero. Hence, in order to ensure that the area of $\log S(jw)$ above the 0 db line is the same for both cases, there must be peaking in $S_2(jw)$. Hence we can clearly see the effect of a RHP-zero in the open loop transfer function.

B.2 Bounds on Peaks

In this subsection, we present bounds on the H_∞ norm on the weighted sensitivity($w_1 S$) and weighted complementary sensitivity($w_2 T$) (Skogestad and Postlethwaite (2007)).

Sensitivity peak. For closed loop stability, for each RHP-zero z of G(s), the sensitivity transfer function must satisfy

$$\|w_1 S\|_\infty \geq |w_1(z)|.\prod_{i=1}^{N_p} \frac{|z+p_i|}{|z-p_i|} \tag{B.7}$$

where p_i denotes the N_p RHP-poles of G(s). If G(s) has no RHP-poles, the bound simplifies to

$$\|w_1 S\|_\infty \geq |w_1(z)| \tag{B.8}$$

Without a weight the bound simplifies to

$$\|S\|_\infty \geq \prod_{i=1}^{N_p} \frac{|z+p_i|}{|z-p_i|} \tag{B.9}$$

Complementary Sensitivity peak. For each RHP pole p of G(s), the complementary sensitivity function must satisfy

$$\|w_2 T\|_\infty \geq |w_2(p)|.\prod_{j=1}^{N_z} \frac{|z_j+p|}{|z_j-p|} \tag{B.10}$$

where z_j denote the N_z RHP zeros of G(s). If G(s) has no RHP-zeros, then the bound simplifies to

$$\|w_2 T\|_\infty \geq |w_2(p)| \tag{B.11}$$

Without a weight the bound simplifies to

$$\|T\|_\infty \geq \prod_{j=1}^{N_z} \frac{|z_j + p|}{|z_j - p|} \tag{B.12}$$

From these bounds we note that

S is primarily limited by RHP-zeros. The bound $|w_1 S| \geq |w_1(z)|$ shows that we need to take into consideration the RHP-zeros while shaping S.

T is primarily limited by RHP-poles. The bound $|w_2 T| \geq |w_2(p)|$ shows that we need to take into consideration the RHP-poles while shaping T.

If the RHP-zero and RHP-pole are located close to each other, then $\|H\|_\infty$ of S and T are large.

B.3 Tradeoff Between Undershoot and Settling Time

RHP-zeros pose a fundamental constraint on the achievable output performance. The presence of a RHP-zero in the plant causes an undershoot in the step response of the system. If we define undershoot(y_{us}) as the negative peak value of the step response of the system with y_f as the final steady state value of the output then for a plant with RHP-zero $z(z > 0)$, the following lower bound on the closed loop undershoot holds (Skogestad and Postlethwaite (2007),Page 184).

$$|y_{us}| \geq |y_f| \frac{1 - \eta}{e^{zt_s} - 1} \tag{B.13}$$

where t_s is the settling time and $\eta(\eta = 0.05)$ is the corresponding level for the settling time. The above equation shows that as the settling time is reduced(BW increased), the system with RHP-zeros will show larger undershoot in the step response.

To show the trade-off between undershoot and settling time, we consider the plant

$$P(s) = \tfrac{z-s}{z+s}, z = 2$$

Let us consider the controller

$$K(s) = g\tfrac{s+4}{s}(\tfrac{100}{s+100})^2$$

The step response of the closed loop system and the sensitivity are plotted for $g = 0.1, 0.3, 0.5$ as shown in Figure B.5 and Figure B.4 .

As shown in Figure B.4 and Figure B.5 , we note that as the gain increases,the settling time decreases but the undershoot and the peak of Sensitivity bode plot increases. Thus we need to do a tradeoff between settling time and undershoot.The figures also show that the closed loop properties deteriorate as the Bandwidth increases which means that RHP-zero poses a fundamental constraint i.e. an upper bound on the BW of the system at the error.

B.4 Relation Between Overshoot and Settling Time

A stable feedback system with a RHP-pole has an overshoot in the closed loop step response y(t). If we consider y_{os} as the positive peak value of the step response of the system with y_f as the final steady state value of the output then for a plant with RHP-pole $p(p > 0)$ and r be the reference, then the following lower bound on the closed loop overshoot holds(Skogestad and Postlethwaite (2007),Page 193).

$$y_{os} \geq y_f \frac{(pt_r - 1)e^{pt_r} + 1}{pt_r} + r \geq y_f \frac{pt_r}{2} + r \tag{B.14}$$

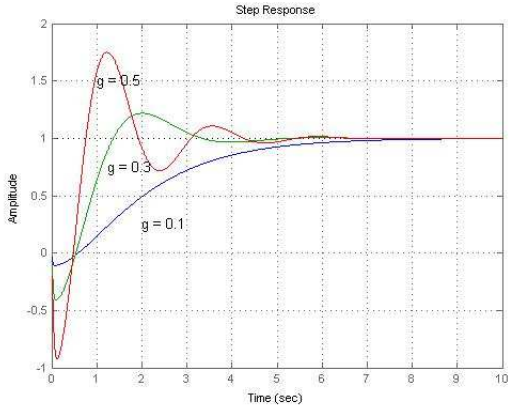

Figure B.4: Variation of Step response

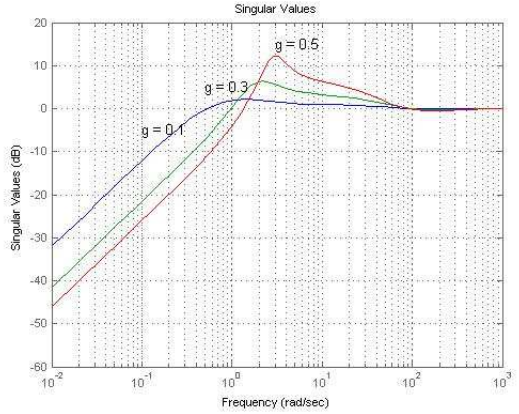

Figure B.5: Variation of Sensitivity

From the above equation, we can infer that the overshoot in the closed loop step response increases as the rise time increases(BW decreases).

To show the trade-off between overshoot and settling time, we consider the plant

$$P(s) = \frac{1}{s-z}, z = 1$$

Let us consider the controller

$$K(s) = g\left(\frac{s+1}{s}\right)$$

The step response of the closed loop system and the sensitivity are plotted for $g = 1.5, 2, 3$ as shown in Figure B.6 and Figure B.7.

As shown in Figure B.6 and Figure B.7 , we note that as the gain decreases,the settling time increases and the overshoot and the peak of Sensitivity bode plot increases. The figures also show that the closed loop properties deteriorate as the Bandwidth decreases which means that RHP-pole poses a fundamental constraint i.e. an lower bound on the BW of the system at the control.

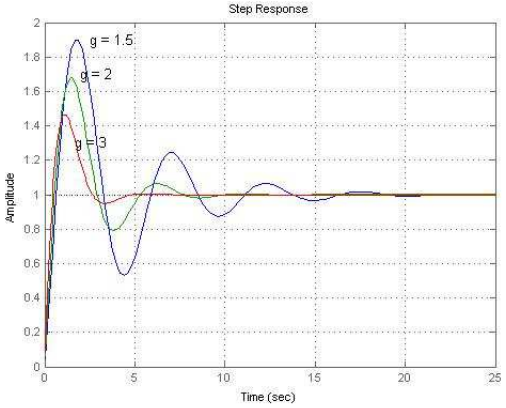

Figure B.6: Variation of Step response

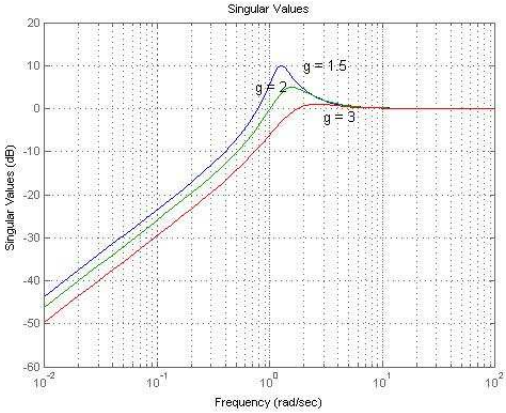

Figure B.7: Variation of Complementary Sensitivity

APPENDIX C

RAW DATA

C.1 Synthesis of Dynamic Output Feedback LMI

The following proof can be found in Scherer *et al.* (1997).
Let us consider the generalized plant given by the state equations

$$\begin{cases} \dot{x} = Ax + B_1 u + B_2 w \\ z = C_1 x + D_{11} u + D_{12} w \\ y = C_2 x + D_{21} u + D_{22} w \end{cases}$$

where $u \in \mathbb{R}^{n_u}$ is the control input, w is the vector of exogneous inputs (reference signals, disturbance signals ,sensor noise), $y \in \mathbb{R}^{n_y}$ is the measured output and z is an output vector related to the performance of the closed loop system.

Let us consider the dynamic output-feedback control law $u = Ky$. Let our dynamic output feedback controller be of the form

$$\begin{cases} \dot{x_k} = A_k x_k + B_k y \\ u = C_k x_k + D_k y \end{cases}$$

Let T denote the closed loop system from w to z for the control law $u = Ky$. Let us express T as

$$\begin{cases} \dot{x_{cl}} = \mathbb{A} x_{cl} + \mathbb{B} w \\ z = \mathbb{C} x_{cl} + \mathbb{D} w \end{cases}$$

where

$$\left[\begin{array}{c|c} \mathbb{A} & \mathbb{B} \\ \hline \mathbb{C} & \mathbb{D} \end{array}\right] = \left[\begin{array}{cc|c} A + B_2 D_K C_2 & B_2 C_K & B_1 + B_2 D_K D_{21} \\ B_K C_2 & A_K & B_K D_{21} \\ \hline C_1 + D_{12} D_K C_2 & D_{12} C_K & D_{11} + D_{12} D_K D_{21} \end{array}\right] \tag{C.1}$$

Let $||T||_\infty$ denote the H_∞ norm of the closed loop transfer function matrix T from w to z. According to the Bounded Real Lemma, $\mathbb{A}$ is stable and $||T||_\infty < \gamma$ if and only if there exists a symmetric matrix P such that

$$\begin{bmatrix} \mathbb{A}^T P + P\mathbb{A} & P\mathbb{B} & \mathbb{C}^T \\ \mathbb{B}^T P & -\gamma I & \mathbb{D}^T \\ \mathbb{C} & \mathbb{D} & -\gamma I \end{bmatrix} < 0, P > 0 \tag{C.2}$$

The substitution of $\mathbb{A}$,$\mathbb{B}$,$\mathbb{C}$ and $\mathbb{D}$ in Equation C.2 leads to the formation of Bilinear Matrix Inequality(BMI) which is no longer convex. Hence we propose the following change of variables:

Let n be the number of states of the plant and let k be the order of the controller. Let us partition P and P^{-1} as

$$P = \begin{bmatrix} Y & N \\ N^T & * \end{bmatrix}, P^{-1} = \begin{bmatrix} X & M \\ M^T & * \end{bmatrix} \tag{C.3}$$

where X and Y are $n \times n$ and symmetric. From $PP^{-1} = I$ we infer that

$$P\Pi_1 = \Pi_2 \tag{C.4}$$

where

$$\begin{aligned} \Pi_1 &= \begin{bmatrix} X & I \\ M_T & 0 \end{bmatrix} \\ \Pi_2 &= \begin{bmatrix} I & Y \\ 0 & N^T \end{bmatrix} \\ MN^T &= I - XY \end{aligned} \tag{C.5}$$

Let us define the change of controller variables as follows:

$$\begin{aligned} \hat{A} &= NA_KM^T + NB_KC_2X + YB_2C_KM^T + Y(A + B_2D_KC_2)X \\ \hat{B} &= NB_K + YBD_K \\ \hat{C} &= C_KM^T + D_KCX \\ \hat{D} &= D_K \end{aligned} \tag{C.6}$$

The variables $\hat{A}$,$\hat{B}$ and $\hat{C}$ have dimensions $n \times n$,$n \times n_u$ and $n_y \times n$. After obtaining M and N matrices having full row rank and obtaining the $\hat{A}$,$\hat{B}$,$\hat{C}$,$\hat{D}$,X and Y by solving the LMI, we can compute the output feedback controller matrices A_K,B_K,C_K and D_K.

Please note the following identities which have been derived from Equation C.3, C.4 and C.5.

$$\begin{aligned} \Pi_1^TP\mathbb{A}\Pi_1 &= \Pi_2^TP\mathbb{A}\Pi_1 = \begin{bmatrix} AX + B_2\hat{C} & A + B_2\hat{D}C_2 \\ \hat{A} & YA + \hat{B}C_2 \end{bmatrix} \\ \Pi_1^TPB_1 &= \Pi_2^TB_1 = \begin{bmatrix} B_1 + B_2\hat{D}D_{21} \\ YB_1 + \hat{B}D_{21} \end{bmatrix} \qquad C_1\Pi_1 = \begin{bmatrix} C_1X + D_{12}\hat{C} & C_1 + D_{12}\hat{D}C_2 \end{bmatrix} \\ \Pi_1^TP\Pi_1 &= \Pi_1^T\Pi_2 = \begin{bmatrix} X & I \\ I & Y \end{bmatrix} \end{aligned} \tag{C.7}$$

We would use these identities to derive the Dynamic Output feedback LMI from Equation C.2 using suitable congruence transformation. Let us apply congruence transformation on Equation C.2 using diag(Π_1,I).

$$\begin{bmatrix} \Pi_1^T & 0 & 0 \\ 0 & I & 0 \\ 0 & 0 & I \end{bmatrix} \begin{bmatrix} \mathbb{A}^TP + P\mathbb{A} & P\mathbb{B} & \mathbb{C}^T \\ \mathbb{B}^TP & -\gamma I & \mathbb{D}^T \\ \mathbb{C} & \mathbb{D} & -\gamma I \end{bmatrix} \begin{bmatrix} \Pi_1 & 0 & 0 \\ 0 & I & 0 \\ 0 & 0 & I \end{bmatrix} < 0 \tag{C.8}$$

After substituting the value of $\mathbb{A}$,$\mathbb{B}$,$\mathbb{C}$and $\mathbb{D}$ from Equation C.1 into Equation C.8, we obtain the following LMI.

$$\begin{bmatrix} AX + XA^T + B_2\hat{C} + (B_2\hat{C})^T & \hat{A}^T + (A + B_2\hat{D}C_2) & * & * \\ \hat{A} + (A + B_2\hat{D}C_2)^T & A^TY + YA + \hat{B}C + (\hat{B}C)^T & * & * \\ (B_1 + B_2\hat{D}D_{21})^T & (YB_1 + \hat{B}D_{21})^T & -\gamma I & * \\ C_1X + D_{12}\hat{C} & C_1 + D_{12}\hat{D}C_2 & D_{11} + D_{12}\hat{D}D_{21} & -\gamma I \end{bmatrix} < 0 \tag{C.9}$$

Also since $P > 0$, applying congruence transformation leads to the following inequality :

$$\Pi_1^TP\Pi_1 = \begin{bmatrix} X & I \\ I & Y \end{bmatrix} > 0 \tag{C.10}$$

Hence the dynamic output feedback controller can be obtained by solving the following optimization problem:

$$\underset{\hat{A},\hat{B},\hat{C},\hat{D},X,Y}{\text{minimize}} \quad \gamma$$

$$\text{s.t.} \quad \begin{bmatrix} AX + XA^T + B_2\hat{C} + (B_2\hat{C})^T & \hat{A}^T + (A + B_2\hat{D}C_2) & * & * \\ \hat{A} + (A + B_2\hat{D}C_2)^T & A^TY + YA + \hat{B}C + (\hat{B}C)^T & * & * \\ (B_1 + B_2\hat{D}D_{21})^T & (YB_1 + \hat{B}D_{21})^T & -\gamma I & * \\ C_1X + D_{12}\hat{C} & C_1 + D_{12}\hat{D}C_2 & D_{11} + D_{12}\hat{D}D_{21} & -\gamma I \end{bmatrix} < 0$$

$$\begin{bmatrix} X & I \\ I & Y \end{bmatrix} > 0$$

After solving the optimization problem and obtaining the set of $\hat{A}$,$\hat{B}$,$\hat{C}$,$\hat{D}$,X,Y which minimizes γ, the dynamic output feedback controller is obtained as follows:

Find nonsingular matrices M,N which satisfies $MN^T = I - XY$

Construct the controller using

$$\begin{aligned} D_K &= \hat{D} \\ C_K &= (\hat{C} - D_K C_2 X)M^{-T} \\ B_K &= N^{-1}(\hat{B} - YB_2D_K) \\ A_K &= N^{-1}(\hat{A} - NB_KC_2X - YB_2C_KM^T - Y(A + B_2D_KC_2)X)M^{-T} \end{aligned} \tag{C.11}$$

APPENDIX D

MATLAB CODE

D.1 Vought F-8 Crusader

```
%F8 Aircraft
clc;
clear all;
close all;
wvec = logspace(-3,3,10000);
s = tf('s');
%%
Aorg = [ -0.8  -0.0006  -12      0
         0    -0.014   -16.64 -32.2
         1    -0.0001  -1.5     0
         1     0        0       0 ];

Borg = [ -19     -2.5
         -0.66  -0.5
         -0.16  -0.6
         0       0  ];

Corg = [ 0   0    0    1
         0   0   -1    1 ];

Dorg = 0*ones(size(Corg)*[1 0]', size(Borg)*[0 1]');

%**************************************************************************
%
% FACTS ON SCALING: Scaling affects the shape of singular value plots.
%                   It does not alter pole locations, zero locations.
%                   It does alter directionality information.
%
%
% Scaling Matrices
%
%  unew = su uold
%  xnew = sx xold
%  ynew = sy yold
%
%
% New Control Variables
%     unew =  [ delta_e, elevator deflection from trim (deg)
%               delta_f, flaperon deflection (deg) ]
%
%
% New State Variables
%      xnew  = [ theta, perturbed pitch angle from trim (deg)
%                gamma, perturbed flight path angle from trim (deg)
%                    q, pitch rate (deg/sec)
%                    u, perturbation from horizontal speed (ft/sec)  ]
%
%
% New Output Variables
%      ynew = [ theta, perturbed pitch angle from trim (deg)
%               gamma, perturbed flight path angle from trim (deg) ]

r2d = 180/pi;
su = diag( [r2d, r2d] );

sx = [ 0     0   0     r2d
       0     0  -r2d   r2d
       r2d   0   0     0
       0     1   0     0];

sy =  diag([ r2d, r2d ]) ;
```

```
%
% Scaled Linear Dynamics
%
Aorg = sx*Aorg*inv(sx);
Borg = sx*Borg*inv(su);
Corg1 = sy*Corg*inv(sx);
Dorg1 = sy*Dorg*inv(su);

% Corg = [Corg1 ; 1 0 0 0;0 0 1 0];
Corg = [Corg1 ; 1 0 0 0 ];
% Dorg = [Dorg1; 0 0;0 0];
Dorg = [Dorg1; 0 0];
P_ss = ss(Aorg,Borg,Corg1,Dorg1);

%%Outputing all states

% Augmenting with integrators

A = blkdiag(Aorg,zeros(size(Corg1,1)));
A(end-size(Corg1,1)+1:end,1:size(Corg1,2)) = Corg1;
B = [Borg;zeros(size(Corg1,1),size(Borg,2))];
C = [zeros(2,4) eye(2)];
C = [C;1 0 0 0 0 0];

D = [Dorg];

P_aug = ss(A,B,C,D);


%% BILINEAR TRANSFORMATION FOR HINF CONTROL SYSTEM DESIGN ( ASK Dr.Rodriguez)

%
% damp(P_ss)
%
%         Eigenvalue            Damping     Freq. (rad/s)
%
%  -5.77e-003 + 2.64e-002i     2.13e-001      2.70e-002
%  -5.77e-003 - 2.64e-002i     2.13e-001      2.70e-002
%  -1.15e+000 + 3.45e+000i     3.17e-001      3.63e+000
%  -1.15e+000 - 3.45e+000i     3.17e-001      3.63e+000


%
%
p2 = -1e20; p1 = -0.0075; %-0.5                                          % Bilinear transformation parameters
                                                                         % When p2 is large, the transformation essenti
                                                                         % implements a shift to right by -p1 units
                                                                         % - making the plant look more unstable
[Atp,Btp,Ctp,Dtp] = bilin(A,B,C,D,1,'Sft_jw',[p2 p1]);     % Obtain ssr for transformed plant
P_transformed     = ss(Atp,Btp,Ctp,Dtp);                                 % Form Transformed plant P_transformed

%% Weighting functions

%W1
m = [0.2];
for i = 1:1:length(m)

% W1

k1 = 1;
M1 =  10 ;% Affects overshoot
M2 =  10 ;% Affects overshoot
wb1  =  0.2 ;% Affects overshoot
wb11 =  0.2 ;% Affects overshoot
eps11 = 0.001 ; % 0.001;
eps12 = 0.001 ; % 0.001;
w11  = [(tf([(1/M1)^(1/k1) wb1],[1 wb1*(eps11)^(1/k1)]))^(1/k1)];
w12  = [(tf([(1/M2)^(1/k1) wb11],[1 wb11*(eps12)^(1/k1)]))^(1/k1)];
W1 = blkdiag(w11,w12,6e-05);
[aw1,bw1,cw1,dw1] = ssdata(W1);
```

```
%W2

k2 = 1;
M21  = 70  ; % [0.1 - 0.5] good !!
M22  = 70  ;
wb21 =  100 ;    % 100
wb22 =  100 ;    % 100
eps21 = 0.1; % 0.1
eps22 = 0.1; % 0.1
w21 = [(tf([1 wb21/(M21)^(1/k2)],[(eps21)^(1/k2) wb21]))^(1/k2)];
w22 = [(tf([1 wb22/(M22)^(1/k2)],[(eps22)^(1/k2) wb22]))^(1/k2)];
W2 = blkdiag(w21,w22);
[aw2,bw2,cw2,dw2] = ssdata(W2);

%W3

k3 =  1 ;
M31  = 1 ;  %1
M32  = 1 ;  %1
wb31 = 20 ;  %20
wb32 = 20 ;  %20
eps31 = 0.001;  % 0.001
eps32 = 0.001 ; % 0.001
w31 = [(tf([1 wb31/(M31)^(1/k3)],[(eps31)^(1/k2) wb31]))^(1/k3)];
w32 = [(tf([1 wb32/(M32)^(1/k3)],[(eps32)^(1/k2) wb32]))^(1/k3)];
W3 = blkdiag(w31,w32,7e-05);
[aw3,bw3,cw3,dw3] = ssdata(W3);

ss_W1 = ss(aw1,bw1,cw1,dw1);
ss_W2 = ss(aw2,bw2,cw2,dw2);
ss_W3 = ss(aw3,bw3,cw3,dw3);

%% OUTPUT r and di
%
[A ,B ,C ,D]  = ssdata(P_transformed);
[A1,B1,C1,D1] = ssdata(W1);
[A2,B2,C2,D2] = ssdata(W2);
[A3,B3,C3,D3] = ssdata(W3);

Ap = [          A              ,  zeros(size(A,1),size(A1,2)) , zeros(size(A,1),size(A2,2))
, zeros(size(A,1),size(A3,2)) ;
              B1*C             ,             A1              , zeros(size(A1,1),size(A2,2)) , zeros(size(A
      zeros(size(A2,1),size(A,2)),  zeros(size(A2,1),size(A1,2)),            A2
, zeros(size(A2,1),size(A3,2));
              B3*C             ,  zeros(size(A3,1),size(A1,2)), zeros(size(A3,1),size(A2,2)) ,
A3              ];

Bp1 = [zeros(size(A,1),size(B1,2)) ,            B             ;
              -B1                ,            B1*D          ;
       zeros(size(B2,1),size(B1,2)),            B2            ;
       zeros(size(B3,1),size(B1,2)),            B3*D         ];

Bp2 = [ B    ;
        B1*D ;
        B2   ;
        B3*D];

Cp1 = [          D1*C             ,              C1             , zeros(size(C1,1),size(C2,2))
, zeros(size(C1,1),size(C3,2));
        zeros(size(C2,1),size(A,2)) , zeros(size(C2,1),size(C1,2)) ,            C2
, zeros(size(C2,1),size(C3,2));
                 D3*C              , zeros(size(C3,1),size(C1,2)) , zeros(size(C3,1),size(C2,2))
,         C3                ];

Cp2 = [           C               , zeros(size(C,1),size(C1,2))  , zeros(size(C,1),size(C2,2))
, zeros(size(C,1),size(C3,2))];

Dp11 = [          -D1                ,            D1*D               ;
        zeros(size(D2,1),size(D1,2)) , zeros(size(D2,1),size(D,2))    ;
        zeros(size(D3,1),size(D1,2)) ,            D3*D              ];

Dp12 = [  D1*D ;
```

```
          D2   ;
          D3*D];

Dp21 = [-eye(size(C,1),size(D1,2))  ,              D  ];

Dp22 = [D];

P_weights = ss(Ap,[Bp1 Bp2],[Cp1;Cp2],[Dp11 Dp12;Dp21 Dp22]);


%% Decision variables for controller modelling

Y1 = sdpvar(size(Ap,1),size(Ap,1));
X1 = sdpvar(size(Ap,1),size(Ap,1));
An = sdpvar(size(Ap,1),size(Ap,1),'full');
Bn = sdpvar(size(Ap,1),size(Cp2,1));
Cn = sdpvar(size(Bp2,2),size(Ap,1));
Dn = sdpvar(size(Bp2,2),size(Cp2,1));
gamma = sdpvar(1);
eps = 10^-6 ;  %5

%% LMI

Matrix1=[Ap*Y1+Y1*Ap'+Bp2*Cn+Cn'*Bp2' , [Ap'+An+[Bp2*Dn*Cp2]']'      , Bp1+Bp2*Dn*Dp21    , [Cp1*Y1+Dp12*Cn]'
;
          Ap'+An+[Bp2*Dn*Cp2]'       , X1*Ap+Ap'*X1+Bn*Cp2+Cp2'*Bn' , X1*Bp1+Bn*Dp21     , [Cp1+Dp12*Dn*Cp2]'
;
            [Bp1+Bp2*Dn*Dp21]'       ,  [X1*Bp1+Bn*Dp21]'           , -gamma*eye(size(Bp1,2))
, [Dp11+Dp12*Dn*Dp21]' ;
             Cp1*Y1+Dp12*Cn          ,  Cp1+Dp12*Dn*Cp2             ,  Dp11+Dp12*Dn*Dp21 , -gamma*eye(size(Dp
];

Matrix2 = [        Y1       , eye(size(Ap,1)) ;
           eye(size(Ap,1)) ,       X1        ];

Constraint1 = [Matrix1 <= -eps*eye(size(Matrix1))];
Constraint2 = [Matrix2 >=  eps*eye(size(Matrix2))];

Constraint_total=[Constraint1,Constraint2];
Objective = gamma;
sol = solvesdp(Constraint_total,Objective);


Y1 = double(Y1);
X1 = double(X1);
An = double(An);
Bn = double(Bn);
Cn = double(Cn);
Dn = double(Dn);

N = X1 ;
M = inv(X1)-Y1;

%% Controller structure with augmentation
Dk = Dn ;
Ck = (Cn - Dk*Cp2*Y1)*inv(M)';
Bk = N\(Bn-X1*Bp2*Dk) ;
Ak = N\(An - N*Bk*Cp2*Y1 - X1*Bp2*Ck*M' -X1*(Ap + Bp2*Dk*Cp2)*Y1)*inv(M)';
[Ak,Bk,Ck,Dk] =  bilin(Ak,Bk,Ck,Dk,-1,'S_ftjw',[p2 p1]);
K = ss(Ak,Bk,Ck,Dk);
integrator = [1/s 0 0 ; 0 1/s 0 ; 0 0 1 ];
K1 = K*integrator ;

K1 = series(K1,200^2/(s+200)^2);

Mi1 = [1 0 0 0];

[Lo1,Li1,So1,Si1,To1,Ti1,KS1,PS1,Tniy1,Tniu1]=f_CLMapInnerOuter_BigK(P_ss,-K1,Mi1);
  if (isstable(To1))
    fprintf('\n');
    fprintf('So1 =  %f , ',mag2db(norm(So1,inf)));
    fprintf('To1 =  %f , ',mag2db(norm(To1,inf)));
```

```
    fprintf('Si1 =  %f , ',mag2db(norm(Si1,inf)));
    fprintf('Ti1 =  %f , ',mag2db(norm(Ti1,inf)));
    fprintf('KS1 =  %f , ',mag2db(norm(KS1,inf)));
    fprintf('PS1 =  %f , ',mag2db(norm(PS1,inf)));
    fprintf('\n');

  end

end


%}
%% PID
%
% gi1_vec = [-0.6];%[-0.6]; %gi2 decreases,
% zi1_vec = [0.4];%[0.4];
% go1_vec = [-0.5];%[-0.8]; % go1 decreases,
% zo1_vec = [0.3];%[0.4];% zo1 increases,                    S
% go2_vec = [1.5];%[1.5];%0.7  go2 increase, S
% zo2_vec = [0.4];%[0.5];% zo2 increase,

gi1_vec = [-1];%[-0.6]; %gi2 decreases,
zi1_vec = [0.4];%[0.4];
go1_vec = [-1.5];%[-0.8]; % go1 decreases,
zo1_vec = [0.5];%[0.4];% zo1 increases,                   S
go2_vec = [1.5];%[1.5];%0.7  go2 increase, S
zo2_vec = [0.9];%[0.5];% zo2 increase,


%%
min = inf;

        for kkk = 1:length(gi1_vec)
           for lll = 1:length(zi1_vec)
              for mmm=1:length(go1_vec)
                 for nnn = 1:length(zo1_vec)
                    for ooo = 1:length(go2_vec)
                       for ppp = 1:length(zo2_vec)

gi1 = gi1_vec(kkk);
zi1 = zi1_vec(lll);
go1 = go1_vec(mmm);
zo1 = zo1_vec(nnn);
go2 = go2_vec(ooo);
zo2 = zo2_vec(ppp);

%% Controllers

Ki=[gi1*(s+zi1) ; 0];
Ko=[go1*(s+zo1)/s 0; 0 go2*(s+zo2)/s];
for m = [50] %50
    for n = [3] %3
Ki2=series(Ki,m^n/(s+m)^n); %50,3

Ko2=series(Ko,blkdiag(5^2/(s+5)^2,5^2/(s+5)^2)); % 5,3

K2 = [Ko2,Ki2];

Mi2=[1 0 0 0]; % feedback pitch in inner-loop

[Lo2,Li2,So2,Si2,To2,Ti2,KS2,PS2,Tniy2,Tniu2]=f_CLMapInnerOuter(P_ss,Ki2,Ko2,Mi2);

  if (isstable(To2))

%  a = stepinfo(To1(1,1));
%  b = stepinfo(To1(2,2));

%%
%     fprintf('\n');
%     fprintf('So1 =  %f , ',mag2db(norm(So1,inf)));
%     fprintf('To1 =  %f , ',mag2db(norm(To1,inf)));
%     fprintf('Si1 =  %f , ',mag2db(norm(Si1,inf)));
```

```
%     fprintf('Ti1 =  %f , ',mag2db(norm(Ti1,inf)));
%     fprintf('KS1 =  %f , ',mag2db(norm(KS1,inf)));
%     fprintf('PS1 =  %f , ',mag2db(norm(PS1,inf)));
    fprintf('\n');
    fprintf('So2 =  %f , ',mag2db(norm(So2,inf)));
    fprintf('To2 =  %f , ',mag2db(norm(To2,inf)));
    fprintf('Si2 =  %f , ',mag2db(norm(Si2,inf)));
    fprintf('Ti2 =  %f , ',mag2db(norm(Ti2,inf)));
    fprintf('KS2 =  %f , ',mag2db(norm(KS2,inf)));
    fprintf('PS2 =  %f , ',mag2db(norm(PS2,inf)));
    fprintf('\n');

  end
                       end

                    end



end
end
end
          end
        end
        end
```

D.2 AV-8A Harrier

```
clc;
close all;
clear all;

wvec=logspace(-3,3,10000);
s=tf('s');
%% Longitudinal dynamics of AV-8A Harrier Aircraft at a medium speed flight
%% condition

% Controls  : 1) dels (Stick input)
%             2) delt (throttle)

% States :  1) Pitch angle
%           2) Pitch rate
%           3) Flight path angle
%           4) Velocity
%           5) Stabilizer angle
%           6) Engine fan speed

% Output    1) Flight path angle
%           2) Velocity

A = [   0       1      0       0      0       0    ;
    -1.8370 -1.8930  1.8370 -0.0004 0.0062 -0.1243 ;
     0.5295  0.0085 -0.5295  0.0006 0.0002  0.0017 ;
    -34.5000    0    2.3000 -0.0621 0.4209 -0.0452 ;
        0       0      0       0   -1.9660    0    ;
        0       0      0       0      0   -12.0000];

B = [ 0      0;
      0      0;
      0      0;
      0      0;
      1.9660 0;
      0   12.0000];

C   = [ 57.3  0   0   0   0   0;
          0 57.3  0   0   0   0;
          0   0  57.3 0   0   0;
          0   0   0   1   0   0;
          0   0   0   0  57.3 0;
```

```
          0   0   0   0   0   1];

D = zeros(6,2);

P = ss(A,B,C,D);

Sx = [ 57.3  0   0   0   0   0;
         0 57.3  0   0   0   0;
         0   0  57.3 0   0   0;
         0   0   0   1   0   0;
         0   0   0   0  57.3 0;
         0   0   0   0   0   1];

% Converting radians to degrees

Aorg        = Sx*A*inv(Sx);
Borg        = Sx*B;
Corg        = C*inv(Sx);
Dorg        = D;

%Selecting only velocity and flight path angle as the output
Corg1 = Corg([3 4],:);
Dorg1 = zeros(2,2);
P_ss = ss(Aorg,Borg,Corg1,Dorg1);

% Corg2 = Corg(1,:);

Corg_new = [Corg1 ; 1 0 0 0 0 0;0 0 0 1 0 0];
Dorg_new = zeros(4,2);
P_new = ss(Aorg,Borg,Corg_new,Dorg_new);

%% Augmenting with integrator

A = blkdiag(Aorg,zeros(size(Corg1,1)));
A(end-size(Corg1,1)+1:end,1:size(Corg1,2)) = Corg1;
B = [Borg;zeros(size(Corg1,1),size(Borg,2))];
C = [zeros(2,6) eye(2)];
C = [C ; 1 0 0 0 0 0 0 0;0 0 0 1 0 0 0 0];
D = zeros(4,2);

P_aug = ss(A,B,C,D);

%% BILINEAR TRANSFORMATION FOR HINF CONTROL SYSTEM DESIGN

%         Eigenvalue            Damping     Freq. (rad/s)

%  -2.36e-002 + 9.75e-002i     2.35e-001      1.00e-001
%  -2.36e-002 - 9.75e-002i     2.35e-001      1.00e-001
%  -1.22e+000 + 1.17e+000i     7.22e-001      1.69e+000
%  -1.22e+000 - 1.17e+000i     7.22e-001      1.69e+000
%  -1.97e+000                  1.00e+000      1.97e+000
%  -1.20e+001                  1.00e+000      1.20e+001

p2 = -1e20; p1 = -0.1; %0.5                                          % Bilinear transformation parameters
                                                                  % When p2 is large, the transformation essenti
                                                                  % implements a shift to right by -p1 units
                                                                  % - making the plant look more unstable
[Atp,Btp,Ctp,Dtp] = bilin(A,B,C,D,1,'Sft_jw',[p2 p1]);     % Obtain ssr for transformed plant
P_transformed     = ss(Atp,Btp,Ctp,Dtp);                     % Form Transformed plant P_transformed

%% Weighting functions
% q = [1 2.5 5];%[ 5:-1:1 0.9:-0.1:0.1 0.09:-0.01:0.01];
q = [1];
for j = 1:length(q)

color = ['b' 'g' 'r'];
%
k1 = 1;
k2 = 1 ;
M11 =  1;     % 1
M12 =  1;    % 1
wb1  = 0.01;  % 0.01
```

```
wb2 =  0.01;  % 0.01
eps1 = 0.003; % 0.003
eps2 = 0.003; % 0.003
w11  = [(tf([(1/M11)^(1/k1) wb1],[1 wb1*(eps1)^(1/k1)]))^(1/k1)];
w12  = [(tf([(1/M12)^(1/k2) wb2],[1 wb2*(eps2)^(1/k2)]))^(1/k2)];

W1 = blkdiag(w11,w12,6e-05,7e-05);
[aw1,bw1,cw1,dw1] = ssdata(W1);

%W2

k2 = 1;
M21  = 0.3; % 0.3
M22  = 0.015; % 0.015
wb21 = 3; %3
wb22 = 3; %3
eps21 = 0.01; %0.01
eps22 = 0.01; %0.01
w21 = [(tf([1 wb21/(M21)^(1/k2)],[(eps21)^(1/k2) wb21]))^(1/k2)];
w22 = [(tf([1 wb22/(M22)^(1/k2)],[(eps22)^(1/k2) wb22]))^(1/k2)];
W2 = blkdiag(w21,w22);
[aw2,bw2,cw2,dw2] = ssdata(W2);

%W3

k3 =  1  ;
M3  = 2  ; % 2
wb3 = 20 ;  % 20
 eps3 = 0.009; % 0.009
w3 = [(tf([1 wb3/(M3)^(1/k3)],[(eps3)^(1/k2) wb3]))^(1/k3)];
W3 = blkdiag(w3,w3,7e-05,6e-05);
[aw3,bw3,cw3,dw3] = ssdata(W3);

ss_W1 = ss(aw1,bw1,cw1,dw1);
ss_W2 = ss(aw2,bw2,cw2,dw2);
ss_W3 = ss(aw3,bw3,cw3,dw3);

%}

%% OUTPUT r and di

[A ,B ,C ,D]  = ssdata(P_transformed);
[A1,B1,C1,D1] = ssdata(W1);
[A2,B2,C2,D2] = ssdata(W2);
[A3,B3,C3,D3] = ssdata(W3);

Ap = [           A               ,  zeros(size(A,1),size(A1,2)) , zeros(size(A,1),size(A2,2))
, zeros(size(A,1),size(A3,2)) ;
               B1*C              ,              A1              , zeros(size(A1,1),size(A2,2)) , zeros(size(A
      zeros(size(A2,1),size(A,2)),  zeros(size(A2,1),size(A1,2)),            A2
, zeros(size(A2,1),size(A3,2));
               B3*C              ,  zeros(size(A3,1),size(A1,2)), zeros(size(A3,1),size(A2,2)) ,
A3               ];

Bp1 = [zeros(size(A,1),size(B1,2)) ,             B              ;
                -B1               ,             B1*D           ;
        zeros(size(B2,1),size(B1,2)),            B2             ;
        zeros(size(B3,1),size(B1,2)),            B3*D          ];

Bp2 = [ B    ;
        B1*D ;
        B2   ;
        B3*D];

Cp1 = [           D1*C             ,              C1             , zeros(size(C1,1),size(C2,2))
, zeros(size(C1,1),size(C3,2));
        zeros(size(C2,1),size(A,2)) , zeros(size(C2,1),size(C1,2)) ,            C2
, zeros(size(C2,1),size(C3,2));
                 D3*C              , zeros(size(C3,1),size(C1,2)) , zeros(size(C3,1),size(C2,2))
,         C3                ];

Cp2 = [           C                , zeros(size(C,1),size(C1,2))  , zeros(size(C,1),size(C2,2))
```

```
, zeros(size(C,1),size(C3,2))];

Dp11 = [          -D1                 ,            D1*D                ;
        zeros(size(D2,1),size(D1,2)) , zeros(size(D2,1),size(D,2))    ;
        zeros(size(D3,1),size(D1,2)) ,            D3*D               ];

Dp12 = [  D1*D ;
          D2   ;
          D3*D];

Dp21 = [-eye(size(C,1),size(D1,2))  ,              D  ];

Dp22 = [D];

P_weights = ss(Ap,[Bp1 Bp2],[Cp1;Cp2],[Dp11 Dp12;Dp21 Dp22]);

%}

%% Decision variables for LMI

Y1 = sdpvar(size(Ap,1),size(Ap,1));
X1 = sdpvar(size(Ap,1),size(Ap,1));
An = sdpvar(size(Ap,1),size(Ap,1),'full');
Bn = sdpvar(size(Ap,1),size(Cp2,1));
Cn = sdpvar(size(Bp2,2),size(Ap,1));
Dn = sdpvar(size(Bp2,2),size(Cp2,1));
gamma = sdpvar(1);
eps = 10^-3 ;  %5

%% LMI

Matrix1=[Ap*Y1+Y1*Ap'+Bp2*Cn+Cn'*Bp2' , [Ap'+An+[Bp2*Dn*Cp2]']'      , Bp1+Bp2*Dn*Dp21    , [Cp1*Y1+Dp12*Cn]'
;
          Ap'+An+[Bp2*Dn*Cp2]'       , X1*Ap+Ap'*X1+Bn*Cp2+Cp2'*Bn' , X1*Bp1+Bn*Dp21     , [Cp1+Dp12*Dn*Cp2]'
;
            [Bp1+Bp2*Dn*Dp21]'       ,  [X1*Bp1+Bn*Dp21]'           , -gamma*eye(size(Bp1,2))
, [Dp11+Dp12*Dn*Dp21]' ;
             Cp1*Y1+Dp12*Cn          ,  Cp1+Dp12*Dn*Cp2             ,  Dp11+Dp12*Dn*Dp21 , -gamma*eye(size(Dp
];

Matrix2 = [        Y1       , eye(size(Ap,1)) ;
           eye(size(Ap,1)) ,       X1        ];

Constraint1 = [Matrix1 <= -eps*eye(size(Matrix1))];
Constraint2 = [Matrix2 >=  eps*eye(size(Matrix2))];

Constraint_total=[Constraint1,Constraint2];
Objective = gamma;
sol = solvesdp(Constraint_total,Objective)
gamma

Y1 = double(Y1);
X1 = double(X1);
An = double(An);
Bn = double(Bn);
Cn = double(Cn);
Dn = double(Dn);

N = X1 ;
M = inv(X1)-Y1;

%% Controller structure with augmentation
Dk = Dn ;
Ck = (Cn - Dk*Cp2*Y1)*inv(M)';
Bk = N\(Bn-X1*Bp2*Dk) ;
Ak = N\(An - N*Bk*Cp2*Y1 - X1*Bp2*Ck*M' -X1*(Ap + Bp2*Dk*Cp2)*Y1)*inv(M)';
[Ak,Bk,Ck,Dk] =  bilin(Ak,Bk,Ck,Dk,-1,'S_ftjw',[p2 p1]);
K = ss(Ak,Bk,Ck,Dk);

integrator = [1/s 0 0 0 ;0 1/s 0 0;0 0 1 0;0 0 0 1];
K = K*integrator;
```

```
K = series(K,50^2/(s+50)^2);

Mi1=[1 0 0 0 0 0;0 0 0 1 0 0]; % feedback pitch in inner-loop

K1 = -K;
%% closed loop system

[Ap, Bp, Cp, Dp] = ssdata(P_ss);
[Ak, Bk, Ck, Dk] = ssdata(-K);
Bo = Bk(:,1:size(Cp,1));
Bi = Bk(:,(size(Cp,1)+1):end);
Do = Dk(:,1:size(Cp,1));
Di = Dk(:,(size(Cp,1)+1):end);
Q = inv(eye(size(Dp,1),size(Dp,1))+Dp*Do);
M = Mi1;

Acl = [Ap-Bp*Do*Q*Cp+Bp*Do*Q*Dp*Di*M-Bp*Di*M , Bp*Ck-Bp*Do*Q*Dp*Ck   ;
       Bo*Q*Dp*Di*M-Bo*Q*Cp-Bi*M             , Ak - Bo*Q*Dp*Ck      ];

Bcl = [Bp*Do*Q , Bp-Bp*Do*Q*Dp , Bp*Do*Q*Dp*Di-Bp*Di , -Bp*Do*Q ;
       Bo*Q    , -Bo*Q*Dp      , Bo*Q*Dp*Di-Bi       , -Bo*Q   ];


%To
C_To = [Cp-Dp*Do*Q*Cp+Dp*Do*Q*Dp*Di*M-Dp*Di*M , Dp*Ck-Dp*Do*Q*Dp*Ck ];
B_To = [Bp*Do*Q ; Bo*Q];
D_To = Dp*Do*Q ;
To1 = (ss(Acl,B_To,C_To,D_To));

%So
B_So = To1.b;
C_So = -To1.c;
D_So = eye(size(Dp,1),size(Dp,1))-Dp*Do*Q;
So1 = (ss(Acl,B_So,C_So,D_So));

%KS
B_KS = To1.b;
C_KS = [-Do*Q*Cp+Do*Q*Dp*Di*M-Di*M , Ck-Do*Q*Dp*Ck];
D_KS = Do*Q;
KS1 = (ss(Acl,B_KS,C_KS,D_KS));

%Si
B_Si = [Bp-Bp*Do*Q*Dp  ;
          -Bo*Q*Dp     ];
C_Si = KS1.c ;
D_Si = eye(size(Do,1),size(Do,1))-Do*Q*Dp;
Si1 = (ss(Acl,B_Si,C_Si,D_Si));

%Ti
B_Ti = Si1.b;
C_Ti = KS1.c;
D_Ti = -Do*Q*Dp;
Ti1 = (ss(Acl,B_Ti,C_Ti,D_Ti));

%PS
B_PS = Si1.b;
C_PS = To1.c;
D_PS = Dp-Dp*Do*Q*Dp;
PS1 = (ss(Acl,B_PS,C_PS,D_PS));

%Tniy
B_Tniy = [Bp*Do*Q*Dp*Di-Bp*Di ;
           Bo*Q*Dp*Di-Bi      ];
C_Tniy = To1.c;
D_Tniy = -Dp*Di+Dp*Do*Q*Dp*Di ;
Tniy1 = (ss(Acl,B_Tniy,C_Tniy,D_Tniy));

%Tniu
B_Tniu = Tniy1.b;
C_Tniu = KS1.c;
D_Tniu = Do*Q*Dp*Di-Di;
Tniu1 = (ss(Acl,B_Tniu,C_Tniu,D_Tniu));
```

```
%Lo
A_Lo = [Ap-Bp*Di*M , Bp*Ck ;
        -Bi*M      , Ak    ];
B_Lo = [Bp*Do ; Bo];
C_Lo = [Cp-Dp*Di*M , Dp*Ck];
D_Lo = Dp*Do;
Lo1 = (ss(A_Lo,B_Lo,C_Lo,D_Lo));

%Li
A_Li = [Ap         , zeros(size(Ap,1),size(Ak,2))  ;
        -Bo*Cp-Bi*M , Ak                          ];
B_Li = [Bp ; -Bo*Dp];
C_Li = [-Do*Cp-Di*M Ck];
D_Li = -Do*Dp;
Li1 = (ss(A_Li,B_Li,C_Li,D_Li));

%% PID
%

gi1_vec = [0.01]; % gi1 increases,So1-So2 increases(slightly),Si1-Si2 increases(slightly),So decreases, Si in

zi1_vec = [0.4];% zi1 increases, So1-So2 increases(slightly),Si1-Si2 increases(slightly),So increases,Si incr

go1_vec = [-0.2]; %-0.2% go1 increases,So1-So2 increases,Si1-Si2 decreases,So1 increases,Si1 increases,Dampin

zo1_vec = [-1];    %-1% [-1];zo1 decreases,
                   % So1-So2 decreases till -1 then increases...
                   % Si1-Si2 decreases
                   % So increases,
                   % Si increases
                   % Damping improves till
                   % -1 then worsens

gi2_vec = [0.15]; %****

zi2_vec = [0.6];

go2_vec = [0.4];%0.3919;go2 increases, So1-So2 decreases, Si1-Si2 decreases,So increases,Si increases,Damping

zo2_vec = [0.06]; %zo2 increases,So1-So2 decreases,Si1-Si2 decreases,So increases,Si increases,Damping worsen


min = inf;
for iii=1:length(gi1_vec)
    for jjj=1:length(zi1_vec)
        for kkk =1:length(go1_vec)
            for lll = 1:length(zo1_vec)
                for mmm = 1:length(go2_vec)
                    for nnn = 1:length(zo2_vec)
                        for ooo = 1:length(gi2_vec)
                            for ppp = 1:length(zi2_vec)


gi1 = gi1_vec(iii);
zi1 = zi1_vec(jjj);
go1 = go1_vec(kkk);
zo1 = zo1_vec(lll);
go2 = go2_vec(mmm);
zo2 = zo2_vec(nnn);
gi2 = gi2_vec(ooo);
zi2 = zi2_vec(ppp);

Mi2=[1 0 0 0 0 0;0 0 0 1 0 0]; % feedback pitch in inner-loop

s=tf('s');
Ki=[gi1*(s+zi1) 0; 0 gi2*(s+zi2)];
Ko=[go1*(s+zo1)/s 0; 0 go2*(s+zo2)/s];

% Roll off
s=tf('s');
for m = [10]
```

```
    for n = [2]
        for o = [50]
            for p = [2]
Ki2=series(Ki,10^2/(s+10)^2);  % 10,2
Ko2=series(Ko,o^p/(s+o)^p); % 100,2
K2=[Ko2 Ki2];

[Lo2,Li2,So2,Si2,To2,Ti2,KS2,PS2,Tniy2,Tniu2]=f_CLMapInnerOuter(P_ss,Ki2,Ko2,Mi2);

end
                        end
                    end
                end
            end
        end
    end
end
end
end
end
    end
end
end
```

D.3 NASA HiMAT

```
%NASA hiMAT

% Control inputs:   1)Elevon Deflection
%                   2)Canard deflection

% Measured outputs: 1)angle of attack (alpha)
%                   2)Pitch angle(theta)
% 6 states :
%                   1)Velocity
%                   2)alpha
%                   3)thetadot
%                   4)attitude(theta)
%                   5)Canard control actuater dynamics
%                   6)Elevon control actuator dynamics

clc;
close all;
clear all;
s = tf('s');
wvec = logspace(-3,3,10000);

%% Plant

Aorg =[-2.2567e-02  -3.6617e+01  -1.8897e+01  -3.2090e+01   3.2509e+00  -7.6257e-01 ;
       9.2572e-05  -1.8997e+00   9.8312e-01  -7.2562e-04  -1.7080e-01  -4.9652e-03 ;
       1.2338e-02   1.1720e+01  -2.6316e+00   8.7582e-04  -3.1604e+01   2.2396e+01 ;
                0            0   1.0000e+00            0            0            0 ;
                0            0            0            0  -3.0000e+01            0 ;
                0            0            0            0            0  -3.0000e+01];

Borg =[0     0;
       0     0;
       0     0;
       0     0;
      30     0;
       0    30];

Corg1 = [0    0     0      1     0     0 ;
         0   -1     0      1     0     0];

Corg = [Corg1 ;0 0 0 1 0 0]; %feeding back thetadot for Inner loop controller

Dorg = [0     0 ;
```

```
        0     0 ;
        0     0 ];

Dorg1 = [0 0;0 0];

P_ss = ss(Aorg,Borg,Corg1,Dorg1);

%% Augmenting the plant with integrators and feeding back thetadot

A = blkdiag(Aorg,zeros(size(Corg1,1)));
A(end-size(Corg1,1)+1:end,1:size(Corg1,2)) = Corg1;
B = [Borg;zeros(size(Corg1,1),size(Borg,2))];
C = [zeros(2,6) eye(2)];
C = [C ;0 0 0 1 0 0 0 0];
D = Dorg;

P_aug = ss(A,B,C,D);

%% BILINEAR TRANSFORMATION FOR HINF CONTROL SYSTEM DESIGN

%

 %NO NEED FOR BILINEAR TRANSFORMATION
 % REASON :

%  damp(P_ss)
%
%         Eigenvalue            Damping     Freq. (rad/s)
%
%  -2.58e-001                  1.00e+000      2.58e-001
%   6.90e-001 + 2.49e-001i    -9.41e-001      7.33e-001
%   6.90e-001 - 2.49e-001i    -9.41e-001      7.33e-001
%  -5.68e+000                  1.00e+000      5.68e+000
%  -3.00e+001                  1.00e+000      3.00e+001
%  -3.00e+001                  1.00e+000      3.00e+001

p = [-0.05];
for j = 1:1:length(p)

p2 = -1e20; p1 = p(j);    %0.01                              % Bilinear transformation parameters
                                                             % When p2 is large, the transformation essenti
                                                             % implements a shift to right by -p1 units
                                                             % - making the plant look more unstable

[Atp,Btp,Ctp,Dtp] = bilin(A,B,C,D,1,'Sft_jw',[p2 p1]);     % Obtain ssr for transformed plant
P_transformed     = ss(Atp,Btp,Ctp,Dtp);                     % Form

%% Weighting functions

%W1

m = [0.01];% 500:50:1000];

for i  = 1:1:length(m)
k1 = 1;
Ms1 = 1; % 5
Ms2 = 1; % 5
wb1  = 1; % 1
wb2  = 1; % 1
eps1 = 0.005; %0.01
eps2 = 0.005; %0.01
w1  = [(tf([(1/Ms1)^(1/k1) wb1],[1 wb1*(eps1)^(1/k1)]))^(1/k1)];
w2  = [(tf([(1/Ms2)^(1/k1) wb2],[1 wb2*(eps2)^(1/k1)]))^(1/k1)];
W1 = blkdiag(w1,w2,6e-05);
[aw1,bw1,cw1,dw1] = ssdata(W1);

%W2

k2 = 1;
Mu1  = 2;Mu2 = 2; % 5
wbu1 = 750; % 450
wbu2 = 750; % 450
```

```
eps =  0.01; %0.009
w21 = [(tf([1 wbu1/(Mu1)^(1/k2)],[(eps)^(1/k2) wbu1]))^(1/k2)];
w22 = [(tf([1 wbu2/(Mu2)^(1/k2)],[(eps)^(1/k2) wbu2]))^(1/k2)];
W2 = blkdiag(w21,w22);
[aw2,bw2,cw2,dw2] = ssdata(W2);

%W3

k3 =  1  ; %1
My  = 5  ; %5
wbc = 20 ; % 20
eps = 0.01 ; %0.05
w3 = [(tf([1 wbc/(My)^(1/k3)],[(eps)^(1/k2) wbc]))^(1/k3)];
W3 = blkdiag(w3,w3,7e-05);
[aw3,bw3,cw3,dw3] = ssdata(W3);

ss_W1 = ss(aw1,bw1,cw1,dw1);
ss_W2 = ss(aw2,bw2,cw2,dw2);
ss_W3 = ss(aw3,bw3,cw3,dw3);

%% Exogenous signal w = [ r di]

[A ,B ,C ,D]  = ssdata(P_transformed);
[A1,B1,C1,D1] = ssdata(W1);
[A2,B2,C2,D2] = ssdata(W2);
[A3,B3,C3,D3] = ssdata(W3);

Ap = [          A               ,  zeros(size(A,1),size(A1,2)) , zeros(size(A,1),size(A2,2))
, zeros(size(A,1),size(A3,2)) ;
               B1*C             ,             A1               , zeros(size(A1,1),size(A2,2)) , zeros(size(A
      zeros(size(A2,1),size(A,2)),  zeros(size(A2,1),size(A1,2)),            A2
, zeros(size(A2,1),size(A3,2));
               B3*C             ,  zeros(size(A3,1),size(A1,2)), zeros(size(A3,1),size(A2,2)) ,
A3               ];

Bp1 = [zeros(size(A,1),size(B1,2)) ,             B              ;
               -B1                 ,             B1*D           ;
       zeros(size(B2,1),size(B1,2)),             B2             ;
       zeros(size(B3,1),size(B1,2)),             B3*D          ];

Bp2 = [ B    ;
        B1*D ;
        B2   ;
        B3*D];

Cp1 = [          D1*C              ,              C1              , zeros(size(C1,1),size(C2,2))
, zeros(size(C1,1),size(C3,2));
        zeros(size(C2,1),size(A,2)) , zeros(size(C2,1),size(C1,2)) ,            C2
, zeros(size(C2,1),size(C3,2));
               D3*C               , zeros(size(C3,1),size(C1,2)) , zeros(size(C3,1),size(C2,2))
,         C3                ];

Cp2 = [           C                , zeros(size(C,1),size(C1,2))  , zeros(size(C,1),size(C2,2))
, zeros(size(C,1),size(C3,2))];

Dp11 = [          -D1                ,            D1*D               ;
        zeros(size(D2,1),size(D1,2)) , zeros(size(D2,1),size(D,2))    ;
        zeros(size(D3,1),size(D1,2)) ,            D3*D               ];

Dp12 = [  D1*D ;
          D2   ;
          D3*D];

Dp21 = [-eye(size(C,1),size(D1,2))  ,              D  ];

Dp22 = [D];

P_weights = ss(Ap,[Bp1 Bp2],[Cp1;Cp2],[Dp11 Dp12;Dp21 Dp22]);

%% Decision variables for LMI

Y1 = sdpvar(size(Ap,1),size(Ap,1));
```

```
X1 = sdpvar(size(Ap,1),size(Ap,1));
An = sdpvar(size(Ap,1),size(Ap,1),'full');
Bn = sdpvar(size(Ap,1),size(Cp2,1));
Cn = sdpvar(size(Bp2,2),size(Ap,1));
Dn = sdpvar(size(Bp2,2),size(Cp2,1));
gamma = sdpvar(1);
eps = 1e-5 ;  %5

%% LMI

Matrix1=[Ap*Y1+Y1*Ap'+Bp2*Cn+Cn'*Bp2' , [Ap'+An+[Bp2*Dn*Cp2]']'      , Bp1+Bp2*Dn*Dp21    , [Cp1*Y1+Dp12*Cn]'
;
          Ap'+An+[Bp2*Dn*Cp2]'       , X1*Ap+Ap'*X1+Bn*Cp2+Cp2'*Bn' , X1*Bp1+Bn*Dp21     , [Cp1+Dp12*Dn*Cp2]'
;
            [Bp1+Bp2*Dn*Dp21]'       ,  [X1*Bp1+Bn*Dp21]'           , -gamma*eye(size(Bp1,2))
, [Dp11+Dp12*Dn*Dp21]' ;
             Cp1*Y1+Dp12*Cn          ,  Cp1+Dp12*Dn*Cp2             ,  Dp11+Dp12*Dn*Dp21 , -gamma*eye(size(Dp
];

Matrix2 = [        Y1       , eye(size(Ap,1)) ;
           eye(size(Ap,1)) ,       X1        ];

Constraint1 = [Matrix1 <= -eps*eye(size(Matrix1))];
Constraint2 = [Matrix2 >=  eps*eye(size(Matrix2))];

Constraint_total=[Constraint1,Constraint2];
Objective = gamma;
sol = solvesdp(Constraint_total,Objective);


Y1 = double(Y1);
X1 = double(X1);
An = double(An);
Bn = double(Bn);
Cn = double(Cn);
Dn = double(Dn);

N = X1 ;
M = inv(X1)-Y1;

%% Controller structure with augmentation
Dk = Dn ;
Ck = (Cn - Dk*Cp2*Y1)*inv(M)';
Bk = N\(Bn-X1*Bp2*Dk) ;
Ak = N\(An - N*Bk*Cp2*Y1 - X1*Bp2*Ck*M' -X1*(Ap + Bp2*Dk*Cp2)*Y1)*inv(M)';
[ak1,bk1,ck1,dk1] =  bilin(Ak,Bk,Ck,Dk,-1,'S_ftjw',[p2 p1]);
K1 = ss(Ak,Bk,Ck,Dk);
integrator = [1/s 0 0;0 1/s 0;0 0 1];
K2 = K1*integrator ;

K3 = series(K2,(100^2/(s+100)^2));
Mi1 = [0 0 0 1 0 0];

[Lo1,Li1,So1,Si1,To1,Ti1,KS1,PS1,Tniy1,Tniu1]=f_CLMapInnerOuter_BigK(P_ss,-K3,Mi1);

a = stepinfo(To1(1,1));
b = stepinfo(To1(2,2));

if isstable(To1)
% damp(To1)

  fprintf('\n');
    fprintf('So1Peak =  %f , ',mag2db(norm(So1,inf)));
    fprintf('To1Peak =  %f , ',mag2db(norm(To1,inf)));
    fprintf('Si1Peak =  %f , ',mag2db(norm(Si1,inf)));
    fprintf('Ti1Peak =  %f , ',mag2db(norm(Ti1,inf)));
    fprintf('PSpeak = %f , ',mag2db(norm(PS1,inf)))
    fprintf('KSpeak = %f , ',mag2db(norm(KS1,inf)))
    fprintf('parameter = %f ',i);
    fprintf('\n');
    fprintf('StepTo11peak = %f , ',a.Overshoot);
```

```
    fprintf('StepTo22peak = %f , ',b.Overshoot);
      fprintf('\n');


end
end
end

%}

 %%  PI-PD

 %

% gi1_vec = [-1.0346];
% gi2_vec = [-0.16972];
% gi3_vec = [0.75038];
% gi4_vec = [0.1353];
% go1_vec = [-0.99907];
% zo1_vec = [0.2433];
% go2_vec = [0.1353];
% zo2_vec = [6.856];

% gi1_vec = [-1.0346];
% gi2_vec = [-0.16972];
% gi3_vec = [0.75038];
% gi4_vec = [0.1353];
% go1_vec = [-0.99907];
% zo1_vec = [0.2433];
% go2_vec = [0.1353];
% zo2_vec = [6.856];

gi1_vec = [-0.45];
gi2_vec = [-0.3];
gi3_vec = [0.09];%[-0.1];
gi4_vec = [5.5];%[1.8];
go1_vec = [-1.1]; %
zo1_vec = [0.4];%
go2_vec = [-0.3];%
zo2_vec = [-5];



min = inf;
%%

        for iii= 1:length(gi1_vec)
            for jjj = 1:length(gi2_vec)
                for kkk = 1:length(gi3_vec)
                    for lll = 1:length(gi4_vec)
                for mmm =1:length(go1_vec)
                    for nnn = 1:length(zo1_vec)
                       for ooo = 1:length(go2_vec)
                          for ppp = 1:length(zo2_vec)



%%

gi1 = gi1_vec(iii);
gi2 = gi2_vec(jjj);
gi3 = gi3_vec(kkk);
gi4 = gi4_vec(lll);
go1 = go1_vec(mmm);
zo1 = zo1_vec(nnn);
go2 = go2_vec(ooo);
zo2 = zo2_vec(ppp);

%% Controllers
s=tf('s');
Ki2=[gi1 gi2 ;
     gi3 gi4];
```

```
Ko2=[go1*(s+zo1)/s 0; 0 go2*(s+zo2)/s];
Ki2=series(Ki2,70^2/(s+70)^2);%70,2
Ko2=series(Ko2,blkdiag(4^2/(s+4)^2,50^2/(s+50)^2)); %1,2

K2 = [Ko2 Ki2];
Mi2=[0 0 1 0 0 0;
     0 0 0 1 0 0]; % feedback pitch in inner-loop

[Lo2,Li2,So2,Si2,To2,Ti2,KS2,PS2,Tniy2,Tniu2]=f_CLMapInnerOuter(P_ss,Ki2,Ko2,Mi2);
%%


   if (isstable(To2))
% while(n < min)



    fprintf('\n');
    fprintf('So1Peak =  %f , ',mag2db(norm(So1,inf)));
    fprintf('To1Peak =  %f , ',mag2db(norm(To1,inf)));
    fprintf('Si1Peak =  %f , ',mag2db(norm(Si1,inf)));
    fprintf('Ti1Peak =  %f , ',mag2db(norm(Ti1,inf)));
    fprintf('KS1Peak =  %f , ',mag2db(norm(KS1,inf)));
    fprintf('PS1Peak =  %f , ',mag2db(norm(PS1,inf)));
    fprintf('\n');
    fprintf('So2Peak =  %f , ',mag2db(norm(So2,inf)));
    fprintf('To2Peak =  %f , ',mag2db(norm(To2,inf)));
    fprintf('Si2Peak =  %f , ',mag2db(norm(Si2,inf)));
    fprintf('Ti2Peak =  %f , ',mag2db(norm(Ti2,inf)));
    fprintf('KS2Peak =  %f , ',mag2db(norm(KS2,inf)));
    fprintf('PS2Peak =  %f , ',mag2db(norm(PS2,inf)));
    fprintf('\n');

   end
                          end
                       end
                    end
                end
                    end
                end
            end
        end
```

D.4 New Engine Old Plume

```
close all; clear all;clc;
s = tf('s');
wvec = logspace(-3,3,10000);

%% NEW ENGINE OLD PLUME
%
Aorg = [
-0.00161983452436639    -0.000173653118186216   9.85221125198869e-09    -0.000383285547441667
-0.000153334284598949   -6.40990402063117e-07   -0.000517647827164931   0   -0.000246189995128958
0
0.0174436232266518  -0.0952505742413470 -2.45973545620615e-06   0.0952505742413470  -0.0473740081521685 0.000
-0.0333718434315429 0   -0.0954009317216059 0
1.77986936072073    -11.7204708121079   -0.00182586605258989    11.7204708121079    -6.51667947017910
-0.0499188708626610 -20.8953256566930   0   -10.6317565947130   0
0   0   1   0   0   0   0   0   0   0
0   0   0   0   0   1   0   0   0   0
96.6858565835592    -175.176839832411   0   175.176839832411    -486.360518917941   -0.790307353781827
-62.7375115982431   0   -194.060730791534   0
0   0   0   0   0   0   0   1   0   0
7.24340636721254    -1.71987412949226   0   1.71987412949226    -3.78805277857882   0   -2328.68432267708
-1.91361201729023   -1.92565360634944   0
0   0   0   0   0   0   0   0   0   1
-29.6855826478488   -8.31276945317075   0   8.31276945317075    6.16367497142926    0   1.59220472539801
0   -8995.50484452050   -3.79649083015465 ];
```

```
Borg = [
0.0659511726422028  -0.000642964403131860
0.106326843669806   0.0175428125197014
27.5975073455364    -9.48877384602615
0   0
0   0
-20.2860969693575   39.6819134079967
0   0
177.216008339087    -25.3583618231909
0   0
-95.7318231087356   -4.29758487599550 ];
%}

Corg1 =[
1   0   0   0   0   0   0   0   0   0
0   1   0   0   0   0   0   0   0   0 ];

Corg  = [Corg1;0 0 0 1 zeros(1,6)];

Dorg = [0  0
        0  0
        0  0];
Dorg1 = [0 0 ;
         0 0];

P_ss = ss(Aorg,Borg,Corg1,Dorg1);

P_new = ss(Aorg,Borg,Corg,Dorg);

[A,B,C,D] = ssdata(P_new);

%% Hinf controller using LMI

%

% Augment Plant with integrators

A = Aorg;B = Borg;C = Corg1;D = Dorg;

A = blkdiag(A,zeros(size(C,1)));
A(end-size(C,1)+1:end,1:size(C,2)) = C;
B = [B;zeros(size(C,1),size(B,2))];
C = [zeros(2,10) eye(2)];
C = [C ; zeros(1,3) 1 zeros(1,8)];

P_aug = ss(A,B,C,[]);

% Bilinear transformation

p = [-0.0097]; %-0.0097
m = 0.25;%[0.01 0.05 0.25 0.275 0.3]
w = [1];

for k = 1:1:length(p)

p1 = p(k)  ;  %-0.0097
p2 = -1e20 ;
[Atp,Btp,Ctp,Dtp] = bilin(A,B,C,D,1,'Sft_jw',[p2 p1]);

P_transformed = ss(Atp,Btp,Ctp,Dtp);

% Weights at output for hinflmi and augw
for i = 1:1:length(m)
  for j = 1:1:length(w)

% NEOP with flexible mode cancellation
%
k1 = 1;
M1 = 7  ; % 5 % Affects overshoot
M2 = 7  ; % 5 % Affects overshoot
wb1  = 0.8 ;  % 0.8 Affects overshoot
```

```
wb11 = 0.8 ;  % 0.8 Affects overshoot
eps11 = 0.5 ; % 0.3;
eps12 = 0.5 ; % 0.3;
w11  = [(tf([(1/M1)^(1/k1) wb1],[1 wb1*(eps11)^(1/k1)]))^(1/k1)];
w12  = [(tf([(1/M2)^(1/k1) wb11],[1 wb11*(eps12)^(1/k1)]))^(1/k1)];
W1 = blkdiag(w11,w12,6e-05);
[aw1,bw1,cw1,dw1] = ssdata(W1);

%W2

k2 = 1;
M21  = 0.07 ;  % 0.07 [0.1 - 0.5] good !!
M22  = 0.07 ;  % 0.07
wb21 =  200 ;    % 200
wb22 =  200 ;    % 200
eps21 = 0.0001; % 0.0001
eps22 = 0.0001; % 0.0001
w21 = [(tf([1 wb21/(M21)^(1/k2)],[(eps21)^(1/k2) wb21]))^(1/k2)];
w22 = [(tf([1 wb22/(M22)^(1/k2)],[(eps22)^(1/k2) wb22]))^(1/k2)];
W2 = blkdiag(w21,w22);
[aw2,bw2,cw2,dw2] = ssdata(W2);

%W3

k3 =  1 ;
M31  = 5 ;  %5
M32  = 5 ;  %5
wb31 = 50 ;  %50
wb32 = 50 ;  %50
eps31 = 0.001;  % 0.001
eps32 = 0.001 ; % 0.001
w31 = [(tf([1 wb31/(M31)^(1/k3)],[(eps31)^(1/k2) wb31]))^(1/k3)];
w32 = [(tf([1 wb32/(M32)^(1/k3)],[(eps32)^(1/k2) wb32]))^(1/k3)];
W3 = blkdiag(w31,w32,7e-05);
[aw3,bw3,cw3,dw3] = ssdata(W3);


% r and di : w = [r di]


[A ,B ,C ,D]  = ssdata(P_transformed);
[A1,B1,C1,D1] = ssdata(W1);
[A2,B2,C2,D2] = ssdata(W2);
[A3,B3,C3,D3] = ssdata(W3);

Ap = [          A              ,  zeros(size(A,1),size(A1,2)) , zeros(size(A,1),size(A2,2))
, zeros(size(A,1),size(A3,2)) ;
              B1*C             ,             A1              , zeros(size(A1,1),size(A2,2)) , zeros(size(A
      zeros(size(A2,1),size(A,2)),  zeros(size(A2,1),size(A1,2)),            A2
, zeros(size(A2,1),size(A3,2));
              B3*C             ,  zeros(size(A3,1),size(A1,2)), zeros(size(A3,1),size(A2,2)) ,
A3              ];

Bp1 = [zeros(size(A,1),size(B1,2)) ,            B             ;
              -B1                ,            B1*D          ;
       zeros(size(B2,1),size(B1,2)),           B2            ;
       zeros(size(B3,1),size(B1,2)),           B3*D         ];

Bp2 = [ B    ;
        B1*D ;
        B2   ;
        B3*D];

Cp1 = [          D1*C             ,             C1             , zeros(size(C1,1),size(C2,2)) , zeros(siz
        zeros(size(C2,1),size(A,2)) , zeros(size(C2,1),size(C1,2)) ,            C2
, zeros(size(C2,1),size(C3,2));
                 D3*C             , zeros(size(C3,1),size(C1,2)) , zeros(size(C3,1),size(C2,2))
,         C3                ];

Cp2 = [           C               , zeros(size(C,1),size(C1,2))  , zeros(size(C,1),size(C2,2))
, zeros(size(C,1),size(C3,2))];
```

```
Dp11 = [          -D1                 ,            D1*D              ;
        zeros(size(D2,1),size(D1,2)) ,             D2               ;
        zeros(size(D3,1),size(D1,2)) ,            D3*D              ];

Dp12 = [  D1*D;
          D2  ;
         D3*D];
Dp21 = [-eye(size(C,1),size(D1,2))  ,              D  ];
Dp22 = [D];

P_weights = ss(Ap,[Bp1 Bp2],[Cp1;Cp2],[Dp11 Dp12;Dp21 Dp22]);

Y1 = sdpvar(size(Ap,1),size(Ap,1));
X1 = sdpvar(size(Ap,1),size(Ap,1));
An = sdpvar(size(Ap,1),size(Ap,1),'full');
Bn = sdpvar(size(Ap,1),size(Cp2,1));
Cn = sdpvar(size(Bp2,2),size(Ap,1));
Dn = sdpvar(size(Bp2,2),size(Cp2,1));
gamma1 = sdpvar(1);
eps = 10^-13 ; %13

Matrix1=[Ap*Y1+Y1*Ap'+Bp2*Cn+Cn'*Bp2' , [An+[Ap+Bp2*Dn*Cp2]']'      , Bp1+Bp2*Dn*Dp21
, [Cp1*Y1+Dp12*Cn]'    ;
          An+[Ap+Bp2*Dn*Cp2]'        , X1*Ap+Ap'*X1+Bn*Cp2+Cp2'*Bn' , X1*Bp1+Bn*Dp21
, [Cp1+Dp12*Dn*Cp2]'   ;
            [Bp1+Bp2*Dn*Dp21]'        ,  [X1*Bp1+Bn*Dp21]'           , -gamma1*eye(size(Bp1,2))
, [Dp11+Dp12*Dn*Dp21]' ;
             Cp1*Y1+Dp12*Cn           ,  Cp1+Dp12*Dn*Cp2             ,  Dp11+Dp12*Dn*Dp21
, -gamma1*eye(size(Dp11,1))       ];



Matrix2 = [        Y1       , eye(size(Ap,1))  ;
           eye(size(Ap,1)) ,       X1        ];

Constraint1 = [Matrix1 <= -eps*eye(size(Matrix1))];
Constraint2 = [Matrix2 >=  eps*eye(size(Matrix2))];
Constraint3 = [Y1 >= eps*eye(size(Y1,1))];
Constraint4 = [X1 >= eps*eye(size(X1,1))];

Constraint_total=[Constraint1,Constraint2,Constraint3,Constraint4];
Objective = gamma1;
solvesdp(Constraint_total,Objective)

Y1 = double(Y1);
X1 = double(X1);
An = double(An);
Bn = double(Bn);
Cn = double(Cn);
Dn = double(Dn);
gamma1 = double(gamma1);

N = X1 ;
M = inv(X1)-Y1;

Dk = Dn ;
Ck = (Cn - Dk*Cp2*Y1)*inv(M)';
Bk = N\(Bn-X1*Bp2*Dk) ;
Ak = N\(An - N*Bk*Cp2*Y1 - X1*Bp2*Ck*M' -X1*(Ap + Bp2*Dk*Cp2)*Y1)*inv(M)';

[ak1,bk1,ck1,dk1] =  bilin(Ak,Bk,Ck,Dk,-1,'S_ftjw',[p2 p1]);
K = ss(ak1,bk1,ck1,dk1);

integrator = [1/s 0 0;0 1/s 0;0 0 1];
K1 = K*integrator ;

K3 = series(K1,140^2/(s+140)^2); % 60 , 3

Mi1=[zeros(1,3) 1 zeros(1,6)]; % feedback pitch in inner-loop

[Lo1,Li1,So1,Si1,To1,Ti1,KS1,PS1,Tniy1,Tniu1]=f_CLMapInnerOuter_BigK(P_ss,-K3,Mi1);
a11 = stepinfo(To1(1,1));
```

```
a12 = stepinfo(To1(2,2));

  end
end
end

%}
%%

% Ko decentralized Ki decentralized

%

gi1_vec = [0];
zi1_vec = [0];
gi2_vec = [-0.8]; %-0.8 % decrease peak increas
zi2_vec = [5];    %5         increase peak decrease
go11_vec = [1.25];    %1.75
zo11_vec = [0.04];   %0.06
go12_vec = [0];
zo12_vec = [0];
go21_vec = [0];
zo21_vec = [0];
go22_vec = [-9.5];  % -11
zo22_vec = [0.07]; % 0.07

% gi1_vec = [0];
% zi1_vec = [0];
% gi2_vec = [-1.5];  % -0.7 % decrease peak increas
% zi2_vec = [6];     % 3         increase peak decrease
% go11_vec = [1];  % 1.5
% zo11_vec = [0.02]; % 0.06
% go12_vec = [0];
% zo12_vec = [0];
% go21_vec = [0];
% zo21_vec = [0];
% go22_vec = [-1.5];   % -6
% zo22_vec = [0.1]; % 0.12

min = inf;
for iii=1:length(zi2_vec)
    for jjj=1:length(gi2_vec)
        for kkk = 1:length(zi1_vec)
            for lll = 1:length(gi1_vec)
               for mmm =1:length(go11_vec)
                  for nnn = 1:length(zo11_vec)
                     for ooo = 1:length(go12_vec)
                        for ppp = 1:length(zo12_vec)
                            for qqq = 1:length(go21_vec)
                                for rrr = 1:length(zo21_vec)
                                    for sss = 1:length(go22_vec)
                                        for ttt = 1:length(zo22_vec)



zi2 = zi2_vec(iii);
gi2 = gi2_vec(jjj);
zi1 = zi1_vec(kkk);
gi1 = gi1_vec(lll);
go11 = go11_vec(mmm);
zo11 = zo11_vec(nnn);
go12 = go12_vec(ooo);
zo12 = zo12_vec(ppp);
go21 = go21_vec(qqq);
zo21 = zo21_vec(rrr);
go22 = go22_vec(sss);
zo22 = zo22_vec(ttt);


Mi2=[zeros(1,3) 1 zeros(1,6)];

s=tf('s');
```

```
Ki=[gi1*(s+zi1) ; gi2*(s+zi2)];
Ko=[go11*(s+zo11)/s go12*(s+zo12)/s; go21*(s+zo21)/s go22*(s+zo22)/s];

m = [45]; n = [3]; o = [1.3];p = [3]; %45,3,1.5,3

for i = 1:1:length(m)
for j = 1:1:length(n)
for k = 1:1:length(o)
for l = 1:1:length(p)
s=tf('s');
Ki2=series(Ki,m(i)^n(j)/(s+m(i))^n(j));
Ko2=series(Ko,o(k)^p(l)/(s+o(k))^p(l));
K2=[Ko2 Ki2];

[Lo2,Li2,So2,Si2,To2,Ti2,KS2,PS2,Tniy2,Tniu2]=f_CLMapInnerOuter(P_ss,Ki2,Ko2,Mi2);
a21 = stepinfo(To2(1,1));
a22 = stepinfo(To2(2,2));
end
end
end
end
                                        end
                                    end
                                end
                            end
                        end
                    end
                end
            end
        end
    end
end


% Ko decentralized Ki theta centralized

%

gi1_vec = [0.3889];%[0.3 0.4 0.5 0.6 0.7];
zi1_vec = [4.018 ]; %4.018
gi2_vec = [0.059];  % 0.059 %decrease peak increas
zi2_vec = [10.73];  % 10.73         increase peak decrease
go11_vec = [-3];    % -3
zo11_vec = [0.077];   % 0.077
go12_vec = [0];
zo12_vec = [0];
go21_vec = [0];
zo21_vec = [0];
go22_vec = [2.5];  % 3
zo22_vec = [0.045]; % 0.045
col_vec = ['b' 'g' 'r'];

min = inf;
for iii=1:length(zi2_vec)
    for jjj=1:length(gi2_vec)
        for kkk = 1:length(zi1_vec)
            for lll = 1:length(gi1_vec)
               for mmm =1:length(go11_vec)
                  for nnn = 1:length(zo11_vec)
                     for ooo = 1:length(go12_vec)
                        for ppp = 1:length(zo12_vec)
                            for qqq = 1:length(go21_vec)
                                for rrr = 1:length(zo21_vec)
                                    for sss = 1:length(go22_vec)
                                        for ttt = 1:length(zo22_vec)



zi2 = zi2_vec(iii);
gi2 = gi2_vec(jjj);
zi1 = zi1_vec(kkk);
```

```
gi1 = gi1_vec(lll);
go11 = go11_vec(mmm);
zo11 = zo11_vec(nnn);
go12 = go12_vec(ooo);
zo12 = zo12_vec(ppp);
go21 = go21_vec(qqq);
zo21 = zo21_vec(rrr);
go22 = go22_vec(sss);
zo22 = zo22_vec(ttt);


Mi3=[zeros(1,3) 1 zeros(1,6)];

s=tf('s');
Ki=[gi1*(s+zi1) ; gi2*(s+zi2)];
Ko=[go11*(s+zo11)/s go12*(s+zo12)/s; go21*(s+zo21)/s go22*(s+zo22)/s];

m = [50]; n = [3]; o = [1.6];p = [3]; %50,3,1.5,3

for i = 1:1:length(m)
for j = 1:1:length(n)
for k = 1:1:length(o)
for l = 1:1:length(p)
s=tf('s');
Ki3=series(Ki,m(i)^n(j)/(s+m(i))^n(j));
Ko3=series(Ko,o(k)^p(l)/(s+o(k))^p(l));
K3=[Ko3 Ki3];

[Lo3,Li3,So3,Si3,To3,Ti3,KS3,PS3,Tniy3,Tniu3]=f_CLMapInnerOuter(P_ss,Ki3,Ko3,Mi3);
a31 = stepinfo(To3(1,1));
a32 = stepinfo(To3(2,2));


end
end
end
end
                                        end
                                    end
                                end
                            end
                        end
                    end
                end
            end
        end
    end
end

%}

% Ko centralized Ki theta centralized

%

gi1_vec = 0.25;%[0.25 0.35 0.45 0.55] ; % 0.1756 Li BW [0.25 0.35 0.45 0.55]

zi1_vec = [3.25];                       % 3.25 Li BW

gi2_vec = [-0.1];                    % -0.1 Li BW

zi2_vec = [4.715];          % 4.715

go11_vec = [0.1974] ;                    % 0.1974

zo11_vec = [-0.194];                     % -0.194  no change

go12_vec = [2.6];                     % 0.1

zo12_vec = [0.1];                      % 0.1
```

```
go21_vec = [3.5];                      % 3.5 affects KS , tsett of vel

zo21_vec = [0.075];                     % 0.075 affects KS , tsett of vel

go22_vec = [0.4835];                     % 0.4835 no change

zo22_vec = [-0.0574];    % -0.0574 no change

min = inf;
for iii=1:length(zi2_vec)
    for jjj=1:length(gi2_vec)
        for kkk = 1:length(zi1_vec)
            for lll = 1:length(gi1_vec)
               for mmm =1:length(go11_vec)
                  for nnn = 1:length(zo11_vec)
                     for ooo = 1:length(go12_vec)
                        for ppp = 1:length(zo12_vec)
                            for qqq = 1:length(go21_vec)
                                for rrr = 1:length(zo21_vec)
                                    for sss = 1:length(go22_vec)
                                        for ttt = 1:length(zo22_vec)



zi2 = zi2_vec(iii);
gi2 = gi2_vec(jjj);
zi1 = zi1_vec(kkk);
gi1 = gi1_vec(lll);
go11 = go11_vec(mmm);
zo11 = zo11_vec(nnn);
go12 = go12_vec(ooo);
zo12 = zo12_vec(ppp);
go21 = go21_vec(qqq);
zo21 = zo21_vec(rrr);
go22 = go22_vec(sss);
zo22 = zo22_vec(ttt);


Mi4=[zeros(1,3) 1 zeros(1,6)];

s=tf('s');
Ki=[gi1*(s+zi1) ; gi2*(s+zi2)];
Ko=[go11*(s+zo11)/s go12*(s+zo12)/s; go21*(s+zo21)/s go22*(s+zo22)/s];

m = [60]; n = [3]; o = [1.7];p = [3];


for i = 1:1:length(m)
for j = 1:1:length(n)
for k = 1:1:length(o)
for l = 1:1:length(p)
s=tf('s');
Ki4=series(Ki,m(i)^n(j)/(s+m(i))^n(j));
Ko4=series(Ko,o(k)^p(l)/(s+o(k))^p(l));
K4=[Ko4 Ki4];

[Lo4,Li4,So4,Si4,To4,Ti4,KS4,PS4,Tniy4,Tniu4]=f_CLMapInnerOuter(P_ss,Ki4,Ko4,Mi4);
a41 = stepinfo(To4(1,1));
a42 = stepinfo(To4(2,2));

end
end
end
end
                                        end
                                    end
                                end
                            end
                        end
                    end
                end
            end
        end
    end
```

```
            end
        end
    end
end
```

D.5 New Engine New Plume

```
close all;
clear all;
clc;
s = tf('s');
wvec = logspace(-3,3,10000);

%% NEW ENGINE NEW PLUME
%
Aorg = [
-0.000765493197068893   -0.000619189572893596   9.98098364723372e-09    6.22509072657125e-05    -0.0004957179
0.0398256071163982  -0.106750102119458  -2.46681854898512e-06   0.106750102119458   -0.0565053547573918 0.000
-8.13713435624790   -6.48745781627056   -0.00182676880431733    6.48745781627056    -2.69343551595363   -0.04
0   0   1   0   0   0   0   0   0   0
0   0   0   0   0   1   0   0   0   0
97.7307242797890    -175.419307332950   0   175.419307332950    -486.465384423634   -0.790307353781827  -62.4
0   0   0   0   0   0   0   1   0   0
6.82432124669712    -1.57125267814757   0   1.57125267814757    -3.71600254756222   0   -2328.83881300339   -
0   0   0   0   0   0   0   0   0   1
-29.7382596677102   -8.28953904356666   0   8.28953904356666    6.18686985587133    0   1.57849738968707    0

Borg = [
0.0712759693723950  -0.000654310307661334
0.241985299802785   0.0176611650172086
-34.6487159397153   -9.55146419597720
0   0
0   0
-20.2978430934309   39.9550972872018
0   0
176.090260268325    -25.5329374689752
0   0
-94.9585209610859   -4.32717092161711 ];

%}

Corg1 =[
1   0   0   0   0   0   0   0   0   0
0   1   0   0   0   0   0   0   0   0 ];

Corg  = [Corg1;0 0 0 1 zeros(1,6)];

Dorg = [0  0
        0  0
        0  0];
Dorg1 = [0 0 ;
         0 0];

P_ss = ss(Aorg,Borg,Corg1,Dorg1);

P_new = ss(Aorg,Borg,Corg,Dorg);

[A,B,C,D] = ssdata(P_new);

%% Hinf controller using LMI

%

% Augment Plant with integrators

A = Aorg;B = Borg;C = Corg1;D = Dorg;

A = blkdiag(A,zeros(size(C,1)));
A(end-size(C,1)+1:end,1:size(C,2)) = C;
```

```
B = [B;zeros(size(C,1),size(B,2))];
C = [zeros(2,10) eye(2)];
C = [C ; zeros(1,3) 1 zeros(1,8)];

P_aug = ss(A,B,C,[]);

% Bilinear transformation

p = [-0.0097]; %-0.0097
m = 0.25;%[0.01 0.05 0.25 0.275 0.3]
w = [1];

for k = 1:1:length(p)

p1 = p(k)  ;  %-0.0097
p2 = -1e20 ;
[Atp,Btp,Ctp,Dtp] = bilin(A,B,C,D,1,'Sft_jw',[p2 p1]);

P_transformed = ss(Atp,Btp,Ctp,Dtp);

% Weights at output for hinflmi and augw
for i = 1:1:length(m)
  for j = 1:1:length(w)

% NENP with flexible mode cancellation
%
k1 = 1;
M1 = 10  ; %1 % Affects overshoot               3
M2 = 10  ; %1 % Affects overshoot
wb1  = 2; % 2 Affects overshoot
wb11 = 2; % 2 Affects overshoot
eps11 = 0.25 ;% 0.07 ;
eps12 = 0.25 ;%  ;
w11  = [(tf([(1/M1)^(1/k1) wb1],[1 wb1*(eps11)^(1/k1)]))^(1/k1)];
w12  = [(tf([(1/M2)^(1/k1) wb11],[1 wb11*(eps12)^(1/k1)]))^(1/k1)];
W1 = blkdiag(w11,w12,6e-05);
[aw1,bw1,cw1,dw1] = ssdata(W1);

%W2

k2 = 1;
M21  = 0.09 ;  % 0.03 0.03 [0.1 - 0.5] good !!
M22  = 0.09 ;  % 0.03 0.03
wb21 =  300;    % 200 300
wb22 =  300;    % 200 300
eps21 = 0.0001; % 0.0001
eps22 = 0.0001; % 0.0001
w21 = [(tf([1 wb21/(M21)^(1/k2)],[(eps21)^(1/k2) wb21]))^(1/k2)];
w22 = [(tf([1 wb22/(M22)^(1/k2)],[(eps22)^(1/k2) wb22]))^(1/k2)];
W2 = blkdiag(w21,w22);
[aw2,bw2,cw2,dw2] = ssdata(W2);

%W3

k3 =  1 ;
M31  = 6 ;  %5
M32  = 6 ;  %5
wb31 = 50 ;  %50
wb32 = 50 ;  %50
eps31 = 0.001 ; % 0.001
eps32 = 0.001 ; % 0.001
w31 = [(tf([1 wb31/(M31)^(1/k3)],[(eps31)^(1/k2) wb31]))^(1/k3)];
w32 = [(tf([1 wb32/(M32)^(1/k3)],[(eps32)^(1/k2) wb32]))^(1/k3)];
W3 = blkdiag(w31,w32,7e-05);
[aw3,bw3,cw3,dw3] = ssdata(W3);


% r and di : w = [r di]


[A ,B ,C ,D]  = ssdata(P_transformed);
[A1,B1,C1,D1] = ssdata(W1);
```

```
[A2,B2,C2,D2] = ssdata(W2);
[A3,B3,C3,D3] = ssdata(W3);

Ap = [          A              ,  zeros(size(A,1),size(A1,2)) , zeros(size(A,1),size(A2,2))
, zeros(size(A,1),size(A3,2)) ;
               B1*C             ,             A1              , zeros(size(A1,1),size(A2,2)) , zeros(size(A
     zeros(size(A2,1),size(A,2)),  zeros(size(A2,1),size(A1,2)),           A2
, zeros(size(A2,1),size(A3,2));
               B3*C             ,  zeros(size(A3,1),size(A1,2)), zeros(size(A3,1),size(A2,2)) ,
A3               ];

Bp1 = [zeros(size(A,1),size(B1,2)) ,            B             ;
               -B1                ,            B1*D          ;
       zeros(size(B2,1),size(B1,2)),            B2            ;
       zeros(size(B3,1),size(B1,2)),            B3*D         ];

Bp2 = [ B    ;
        B1*D ;
        B2   ;
        B3*D];

Cp1 = [          D1*C             ,              C1             , zeros(size(C1,1),size(C2,2)) , zeros(siz
        zeros(size(C2,1),size(A,2)) , zeros(size(C2,1),size(C1,2)) ,            C2
, zeros(size(C2,1),size(C3,2));
               D3*C               , zeros(size(C3,1),size(C1,2)) , zeros(size(C3,1),size(C2,2))
,         C3               ];

Cp2 = [           C               , zeros(size(C,1),size(C1,2))  , zeros(size(C,1),size(C2,2))
, zeros(size(C,1),size(C3,2))];

Dp11 = [          -D1              ,            D1*D             ;
        zeros(size(D2,1),size(D1,2)) ,             D2             ;
        zeros(size(D3,1),size(D1,2)) ,            D3*D            ];

Dp12 = [  D1*D;
          D2  ;
         D3*D];
Dp21 = [-eye(size(C,1),size(D1,2))  ,             D  ];
Dp22 = [D];

P_weights = ss(Ap,[Bp1 Bp2],[Cp1;Cp2],[Dp11 Dp12;Dp21 Dp22]);

Y1 = sdpvar(size(Ap,1),size(Ap,1));
X1 = sdpvar(size(Ap,1),size(Ap,1));
An = sdpvar(size(Ap,1),size(Ap,1),'full');
Bn = sdpvar(size(Ap,1),size(Cp2,1));
Cn = sdpvar(size(Bp2,2),size(Ap,1));
Dn = sdpvar(size(Bp2,2),size(Cp2,1));
gamma1 = sdpvar(1);
eps = 10^-13 ; %13

Matrix1=[Ap*Y1+Y1*Ap'+Bp2*Cn+Cn'*Bp2' , [An+[Ap+Bp2*Dn*Cp2]']'      , Bp1+Bp2*Dn*Dp21
, [Cp1*Y1+Dp12*Cn]'    ;
          An+[Ap+Bp2*Dn*Cp2]'        , X1*Ap+Ap'*X1+Bn*Cp2+Cp2'*Bn' , X1*Bp1+Bn*Dp21
, [Cp1+Dp12*Dn*Cp2]'   ;
            [Bp1+Bp2*Dn*Dp21]'        ,  [X1*Bp1+Bn*Dp21]'           , -gamma1*eye(size(Bp1,2))
, [Dp11+Dp12*Dn*Dp21]' ;
             Cp1*Y1+Dp12*Cn           ,  Cp1+Dp12*Dn*Cp2             ,  Dp11+Dp12*Dn*Dp21
, -gamma1*eye(size(Dp11,1))       ];



Matrix2 = [        Y1       , eye(size(Ap,1))  ;
           eye(size(Ap,1)) ,       X1        ];

Constraint1 = [Matrix1 <= -eps*eye(size(Matrix1))];
Constraint2 = [Matrix2 >=  eps*eye(size(Matrix2))];
Constraint3 = [Y1 >= eps*eye(size(Y1,1))];
Constraint4 = [X1 >= eps*eye(size(X1,1))];

Constraint_total=[Constraint1,Constraint2,Constraint3,Constraint4];
Objective = gamma1;
```

```
solvesdp(Constraint_total,Objective)

Y1 = double(Y1);
X1 = double(X1);
An = double(An);
Bn = double(Bn);
Cn = double(Cn);
Dn = double(Dn);
gamma1 = double(gamma1);

N = X1 ;
M = inv(X1)-Y1;

Dk = Dn ;
Ck = (Cn - Dk*Cp2*Y1)*inv(M)';
Bk = N\(Bn-X1*Bp2*Dk) ;
Ak = N\(An - N*Bk*Cp2*Y1 - X1*Bp2*Ck*M' -X1*(Ap + Bp2*Dk*Cp2)*Y1)*inv(M)';

[ak1,bk1,ck1,dk1] =  bilin(Ak,Bk,Ck,Dk,-1,'S_ftjw',[p2 p1]);
K = ss(ak1,bk1,ck1,dk1);

integrator = [1/s 0 0;0 1/s 0;0 0 1];
K1 = K*integrator ;

K3 = series(K1,130^2/(s+130)^2); % 60 , 3

Mi1=[zeros(1,3) 1 zeros(1,6)]; % feedback pitch in inner-loop

[Lo1,Li1,So1,Si1,To1,Ti1,KS1,PS1,Tniy1,Tniu1]=f_CLMapInnerOuter_BigK(P_ss,-K3,Mi1);
a11 = stepinfo(To1(1,1));
a12 = stepinfo(To1(2,2));

  end
end
end

%}
%%

% Ko decentralized Ki decentralized

%

gi1_vec = [0];
zi1_vec = [0];
gi2_vec = [-0.7]; % -0.85   -0.7% decrease peak increas
zi2_vec = [3];     % 5    3     increase peak decrease
go11_vec = [1.5];    % 2   1.5
zo11_vec = [0.06]; % 0.06    0.06
go12_vec = [0];
zo12_vec = [0];
go21_vec = [0];
zo21_vec = [0];
go22_vec = [-6];   % -6 -2.5
zo22_vec = [0.12]; % 0.12

min = inf;
for iii=1:length(zi2_vec)
    for jjj=1:length(gi2_vec)
        for kkk = 1:length(zi1_vec)
            for lll = 1:length(gi1_vec)
               for mmm =1:length(go11_vec)
                  for nnn = 1:length(zo11_vec)
                     for ooo = 1:length(go12_vec)
                        for ppp = 1:length(zo12_vec)
                            for qqq = 1:length(go21_vec)
                                for rrr = 1:length(zo21_vec)
                                    for sss = 1:length(go22_vec)
                                        for ttt = 1:length(zo22_vec)
```

```
zi2 = zi2_vec(iii);
gi2 = gi2_vec(jjj);
zi1 = zi1_vec(kkk);
gi1 = gi1_vec(lll);
go11 = go11_vec(mmm);
zo11 = zo11_vec(nnn);
go12 = go12_vec(ooo);
zo12 = zo12_vec(ppp);
go21 = go21_vec(qqq);
zo21 = zo21_vec(rrr);
go22 = go22_vec(sss);
zo22 = zo22_vec(ttt);


Mi2=[zeros(1,3) 1 zeros(1,6)];

s=tf('s');
Ki=[gi1*(s+zi1) ; gi2*(s+zi2)];
Ko=[go11*(s+zo11)/s go12*(s+zo12)/s; go21*(s+zo21)/s go22*(s+zo22)/s];

m = [35]; n = [3]; o = [2];p = [3];

for i = 1:1:length(m)
for j = 1:1:length(n)
for k = 1:1:length(o)
for l = 1:1:length(p)
s=tf('s');
Ki2=series(Ki,m(i)^n(j)/(s+m(i))^n(j));
Ko2=series(Ko,o(k)^p(l)/(s+o(k))^p(l));
K2=[Ko2 Ki2];

[Lo2,Li2,So2,Si2,To2,Ti2,KS2,PS2,Tniy2,Tniu2]=f_CLMapInnerOuter(P_ss,Ki2,Ko2,Mi2);
a21 = stepinfo(To2(1,1));
a22 = stepinfo(To2(2,2));

end
end
end
end
                                        end
                                    end
                                end
                            end
                        end
                    end
                end
            end
        end
    end
end

%}

% Ko decentralized Ki theta centralized

%

gi1_vec = [-0.3 -0.4 -0.5 -0.6 -0.7];%[-0.38]; % -0.5
zi1_vec = [1.5];     % 1.5
gi2_vec = [-0.08]; % -0.08 % decrease peak increas
zi2_vec = [14];    % 14    % increase peak decrease
go11_vec = [4];    % 4
zo11_vec = [0.06];   %0.06
go12_vec = [0];
zo12_vec = [0];
go21_vec = [0];
zo21_vec = [0];
go22_vec = [-5];  % -3
zo22_vec = [0.1]; % 0.3
col_vec = ['b' 'g' 'r'];
```

```
min = inf;
for iii=1:length(zi2_vec)
    for jjj=1:length(gi2_vec)
        for kkk = 1:length(zi1_vec)
            for lll = 1:length(gi1_vec)
               for mmm =1:length(go11_vec)
                  for nnn = 1:length(zo11_vec)
                     for ooo = 1:length(go12_vec)
                        for ppp = 1:length(zo12_vec)
                            for qqq = 1:length(go21_vec)
                                for rrr = 1:length(zo21_vec)
                                    for sss = 1:length(go22_vec)
                                        for ttt = 1:length(zo22_vec)



zi2 = zi2_vec(iii);
gi2 = gi2_vec(jjj);
zi1 = zi1_vec(kkk);
gi1 = gi1_vec(lll);
go11 = go11_vec(mmm);
zo11 = zo11_vec(nnn);
go12 = go12_vec(ooo);
zo12 = zo12_vec(ppp);
go21 = go21_vec(qqq);
zo21 = zo21_vec(rrr);
go22 = go22_vec(sss);
zo22 = zo22_vec(ttt);


Mi3=[zeros(1,3) 1 zeros(1,6)];

s=tf('s');
Ki=[gi1*(s+zi1) ; gi2*(s+zi2)];
Ko=[go11*(s+zo11)/s go12*(s+zo12)/s; go21*(s+zo21)/s go22*(s+zo22)/s];

m = [45]; n = [3]; o = [3];p = [3]; %60,3,1.5,3

for i = 1:1:length(m)
for j = 1:1:length(n)
for k = 1:1:length(o)
for l = 1:1:length(p)
s=tf('s');
Ki3=series(Ki,m(i)^n(j)/(s+m(i))^n(j));
Ko3=series(Ko,o(k)^p(l)/(s+o(k))^p(l));
K3=[Ko3 Ki3];

[Lo3,Li3,So3,Si3,To3,Ti3,KS3,PS3,Tniy3,Tniu3]=f_CLMapInnerOuter(P_ss,Ki3,Ko3,Mi3);
a31 = stepinfo(To3(1,1));
a32 = stepinfo(To3(2,2));

end
end
end
end
                                        end
                                    end
                                end
                            end
                        end
                    end
                end
            end
        end
    end
end

%}

% Ko centralized Ki theta centralized
```

```
%

gi1_vec = [-0.3];%-0.2 -0.3 -0.4 -0.5 -0.7] ; % -0.14719 [-0.2 -0.3 -0.4 -0.5 -0.7]Input prop( flex) best
zi1_vec = [2];   % 2
gi2_vec = [-0.05]; % -0.05 So peak is affected
zi2_vec = [1.6]; % 1.6 zi2 decreases : So1-So2 decreases(slightly),Si1-Si2 increases(slightly), damping worse
go11_vec = [2 ] ; % 3
zo11_vec = [-0.01]; %  -0.00358 no change
go12_vec = [-1.2];  % -1.3 output Lo
zo12_vec = [0.26];   %0.26  %output Lo best
go21_vec = [-5];  % -5
zo21_vec = [0.08];  %0.02 changed to 0.08 to improve  input & output prop
go22_vec = [-0.2];  %-0.20114 no change
zo22_vec = [0.37];    % no change

min = inf;
for iii=1:length(zi2_vec)
    for jjj=1:length(gi2_vec)
        for kkk = 1:length(zi1_vec)
            for lll = 1:length(gi1_vec)
               for mmm =1:length(go11_vec)
                  for nnn = 1:length(zo11_vec)
                     for ooo = 1:length(go12_vec)
                        for ppp = 1:length(zo12_vec)
                            for qqq = 1:length(go21_vec)
                                for rrr = 1:length(zo21_vec)
                                    for sss = 1:length(go22_vec)
                                        for ttt = 1:length(zo22_vec)



zi2 = zi2_vec(iii);
gi2 = gi2_vec(jjj);
zi1 = zi1_vec(kkk);
gi1 = gi1_vec(lll);
go11 = go11_vec(mmm);
zo11 = zo11_vec(nnn);
go12 = go12_vec(ooo);
zo12 = zo12_vec(ppp);
go21 = go21_vec(qqq);
zo21 = zo21_vec(rrr);
go22 = go22_vec(sss);
zo22 = zo22_vec(ttt);


Mi4=[zeros(1,3) 1 zeros(1,6)];

s=tf('s');
Ki=[gi1*(s+zi1) ; gi2*(s+zi2)];
Ko=[go11*(s+zo11)/s go12*(s+zo12)/s; go21*(s+zo21)/s go22*(s+zo22)/s];

m = [45]; n = [3]; o = [3];p = [3];


for i = 1:1:length(m)
for j = 1:1:length(n)
for k = 1:1:length(o)
for l = 1:1:length(p)
s=tf('s');
Ki4=series(Ki,m(i)^n(j)/(s+m(i))^n(j));
Ko4=series(Ko,o(k)^p(l)/(s+o(k))^p(l));
K4=[Ko4 Ki4];

[Lo4,Li4,So4,Si4,To4,Ti4,KS4,PS4,Tniy4,Tniu4]=f_CLMapInnerOuter(P_ss,Ki4,Ko4,Mi4);
a41 = stepinfo(To4(1,1));
a42 = stepinfo(To4(2,2));

end
end
end
end
                                        end
```

```
                                        end
                                    end
                                end
                            end
                        end
                    end
                end
            end
        end
    end
end
```